NOVEL PLANT NUCLEAR ENVELOPE-ASSOCIATED COILED-COIL PROTEINS

Vidya Pawar Menon

A thesis submitted in partial fulfilment of the requirements of Oxford Brookes University for the degree of Doctor of Philosophy

April 2015

Abstract

The nuclear envelope (NE) is a double lipid bilayer enclosing the eukaryotic genome. The metazoan nucleoskeleton includes the peripheral lamina and the internal nucleoskeleton. The lamina is composed of a network of intermediate filament (IF) proteins called lamins, as well as lamin- and/or chromatin-binding inner nuclear membrane (INM) proteins. The components of the metazoan lamina lack sequence homologues in plants. There is however evidence of a network of nuclear filamentous proteins underlying the NE. This study aims to characterise a novel family of NE-associated proteins (NEAP) in the model plant, *Arabidopsis thaliana*.

The family consists of four proteins, AtNEAP1-4 conserved in plants restricted to the angiosperm clade. Their expression is ubiquitous with up-regulation in embryo, inflorescence and guard cells. NEAP protein structure consists of extensive coiled-coil (CC) domains, followed by a nuclear localisation signal (NLS) and a C-terminal transmembrane (TM) domain. Confocal microscopy shows that fluorescent protein tagged NEAP proteins localise to the nuclear periphery as part of highly immobilised stable complexes. Domain deletion mutants confirm the presence of functional NLS and TM domains, while their CC nature causes insolubility under high ionic salt and Triton X-100 conditions similar to other IF-like proteins. AtNEAP2 and AtNEAP3 interact with themselves as well as with AtNEAP1 and each other. NEAP proteins also interact with the classical and mid-SUN domain families. NEAP proteins also cause mis-localisation of the plant nuclear matrix constituent protein 1 from the nuclear periphery to the nucleoplasm. An *A. thaliana* cDNA library screen identified a basic leucine zipper transcription factor (TF), AtbZIP18 as a novel interactor of AtNEAP1. This is a first description of a chromatin-binding protein partner of the plant INM.

Single and double NEAP knockout and knockdown mutants analysed displayed various defects in nuclear size, shape and positioning in different tissues. Therefore NEAP proteins appear to be involved in regulating nuclear morphology in plants. Thus as novel nuclear IF-like proteins that interact with a chromatin binding TF and have functions in regulating nuclear morphology, NEAP proteins are putative components of the plant lamina anchored at the INM.

Acknowledgements

I would like to thank my supervisors, Professor David Evans and Dr. Katja Graumann for everything they have done for me during the course of this PhD. Right from the beginning, David and Katja's passion for nuclear envelope research was highly infectious and their meticulous attention to detail inspired me to attain a higher standard with my work. I am very grateful to David for always being around as a mentor to advice and guide through any obstacles and to happily organise meetings despite his busy schedule. I am also very grateful to Katja for first starting me up in the laboratory, and then providing unending support throughout my PhD as a supervisor and a friend. I cannot thank you enough David and Katja, for being a great source of personal support always looking after my welfare and wellbeing.

I would also like to thank Professor Christophe Tatout and Dr. Emmanuel Vanrobays for organising my month long research in Blaise Pascal University, Clermont Ferrand, France. I am very grateful to Manu for his help with the yeast two hybrid experiments in the laboratory and for plenty of good wine and cheese. I would also like to thank Dr. Sylvette Tourmente for a great time and amazing road trips during my stay in Clermont.

I would also like to thank all ex-members of the nuclear envelope group, including Dr. Carla Galinha, Frances Tolmie and Dr. Sarah Smith. I would like to thank Dr. John Runions for training me to use the confocal microscopes and providing help and guidance with my FRAP and FRET analysis. I would also like to thank Professor Chris Hawes for his help during the yearly assessments and advice and suggestions for future work. I would also like to thank all current and ex- members in the S208a and S209a offices of the collective Plant Cell Biology group for their help, advice and support on several occasions during my PhD. I would specially like to thank Alessandra Rocchetti, Anish Senan, Frances Tolmie, Katja Graumann, Samantha Barry and Sarah Smith for their support, company and friendship as well as some memorable nights out.

Most importantly I would like to thank my family and friends, without their support I wouldn't be at the point that I am at today. I cannot thank enough my husband Sharad Menon, for being there for me and supporting me to take up and finish this PhD. You were always a constant source of motivation when the chips were down and a reminder about looking at the bigger picture. I would also like to thank my friends Abhijit, Sarjil and Shraddha for keeping me de-stressed outside of work. I would like to thank my parents and my parents-in-law for their continuous support and patience during the course of my PhD and for bearing with my absence on several important family occasions. मम्मी आणि पप्पा, तुम्ही दिलेली प्रेरणा व आशिर्वाद या शिवाय मी हे पूर्ण करू शकले नसते. So thank you very much.

Contents

List of figures

List of tables

Abbreviations

aa	Amino acid
ABRC	Arabidopsis biological resource centre
apFRET	Acceptor photo-bleaching fluorescence resonance energy transfer
53BP1	p53 binding protein
BAF	Barrier to autointegration factor
BLAST	Basic Local Alignment Search Tool
BY2	*N. tabacum* bright yellow 2 cell line
bZIP	Basic-leucine zipper
C	Carboxy terminus
CC	Coiled-coil
cDNA	Complementary DNA
CDS	Coding DNA sequence
CFP	Cyan fluorescent protein
CMV	Cauliflower mosaic virus
CRWN	Crowded nuclei
Cub	C-terminal ubiquitin
δTIP	Delta tonoplast instrisic protein.
DAS	Dense Alignment Surface
DNA	Deoxyribonucleic Acid
DTT	Dithiothreitol
EDTA	Ethylene diamine tetra acetic acid
E_F	FRET efficiency
ER	Endoplasmic reticulum
FG	Phenylalanine–glycine
FP	Fluorescent protein
FPP	Filament-like plant protein
FRAP	Fluorescence recovery after photo-bleaching
gDNA	Genomic DNA
GDP	Guanosine di phosphate
GFP	Green fluorescent protein
GTP	Guanosine tri phosphate

HEAT	Huntingtin, elongation factor 3, protein phosphatase 2A and PI3-kinase TOR1
HP1	Heterochromatin protein 1
IF	Intermediate filaments
INM	Inner nuclear membrane
KASH	Klarsicht ANC1 SYNE-1 homology
KD	Knockdown
KO	Knockout
LAP	Lamina associated polypeptides
LBR	Lamin B receptor
LEM	LAP 1 and 2, emerin, man
LINC	Little nuclei
LINC	Linker of Nucleoskeleton Cytoskeleton complex
MAF	MAR binding filament-like protein
MAR	DNA matrix attachment regions
mlp	Myosin-like proteins1 and 2
MS	Murashige and Skoog
MYTH	Membrane yeast two hybrid
N	Amino terminal
NE	Nuclear envelope
NE81	Nuclear envelope 81, *D. discoideum* lamin like protein
NEAP	Nuclear envelope associated proteins
NES	Nuclear export signal
NIF	Nuclear intermediate filament
NLS	Nuclear localisation signal
NMCP	Nuclear matrix constituent protein
NPC	Nuclear pore complex
NUA	Nuclear pore anchor
Nub	N-terminal ubiquitin
NUP	Nuclear peripheral
Nup	Nucleoporin
ONM	Outer nuclear membrane
Opt	Osteopotentia
PBS	Phosphate-buffered saline

PCNA	Proliferating cell nuclear antigen
PNER	Peri-nuclear endoplasmic reticulum
qRT-PCR	Quantitative reverse transcriptase – polymerase chain reaction
Ran	Ras-related nuclear GTPase
RanGAP	Ran GTPase activating protein
Rb	Retinoblastoma protein
ROI	Region of interest
SDS	Sodium dodecyl sulfate
PAGE	Polyacrylamide gel electrophoresis
SEM	Standard error of mean
SINE	SUN domain interacting NE
SUN	Sad1/UNC84 domain
$T_{1/2}$	Half time of recovery
TAE	Tris acetate EDTA buffer
TAIR	The Arabidopsis information resource
TCA	Trichloroacetic acid
T-DNA	Transfer-DNA
TF	Transcription factor
TIK	Toll interleukin-resistance domain and a KASH domain
TM	Transmembrane domain
tpr	Translocated promoter region
UTR	Untranslated region
WIT	WPP interacting tail anchored
WPP	Tryptophan proline proline
WT	Wild type
YEB	Yeast extract broth
YFP	Yellow fluorescent protein
YNB	Yeast nitrogen base

Chapter 1

Introduction

Chapter 1

Introduction

The nuclear envelope (NE) is an evolutionary hallmark of eukaryotic organisms. It presents a physical barrier comprising a double lipid bilayer between the cytoplasm and the nuclear interior. The outer nuclear membrane (ONM) is separated from the inner nuclear membrane (INM) by a 50 nm wide lumen called the periplasmic space (Callan and Tomlin 1950, Cohen et al. 2002, Fiserova et al. 2009). The ONM is connected to the peri-nuclear endoplasmic reticulum (PNER); as well as to the INM at the pore membrane (see figure 1). Two adjacent pore membranes hold a nuclear pore complex (NPC), which is a selective bi-directional transport channel. The NPC's are critical to excluding cytosolic metabolic processes from the nucleus while allowing restricted transport of proteins (Fahrenkrog et al. 2004, Hetzer et al. 2005, Tran et al. 2014). They also facilitate export of synthesized RNA and ribosomes to the cytoplasm and control macromolecular trafficking across the NE (Gorlich and Kutay 1999). Thus while maintaining a separation of compartments, the nucleus is intricately connected to the rest of the cell both via the NPC's and the PNER. On the cytoplasmic side, the ONM also attaches the nucleus to the cytoskeleton through Linker of Nucleoskeleton Cytoskeleton (LINC) complexes, which have an important role in nuclear positioning inside the cell as well as movement in response to developmental or environmental stimuli (Ciska and Moreno Diaz de la Espina 2014).

The inclusion of genetic material within a membranous structure has aided the evolution of higher complexity and multi-cellularity of life. The NE not only protects but also holds the complex eukaryotic genome in place and regulates its function. Underlying the metazoan INM is a filamentous lattice called the lamina. The lamina forms the main structural skeleton of the nucleus; tethers chromatin to the INM and NPC's and is essential for maintaining integrity of the nucleus. This tethering impacts important nuclear functions like DNA replication and repair, gene expression and silencing, and RNA maturation and splicing.

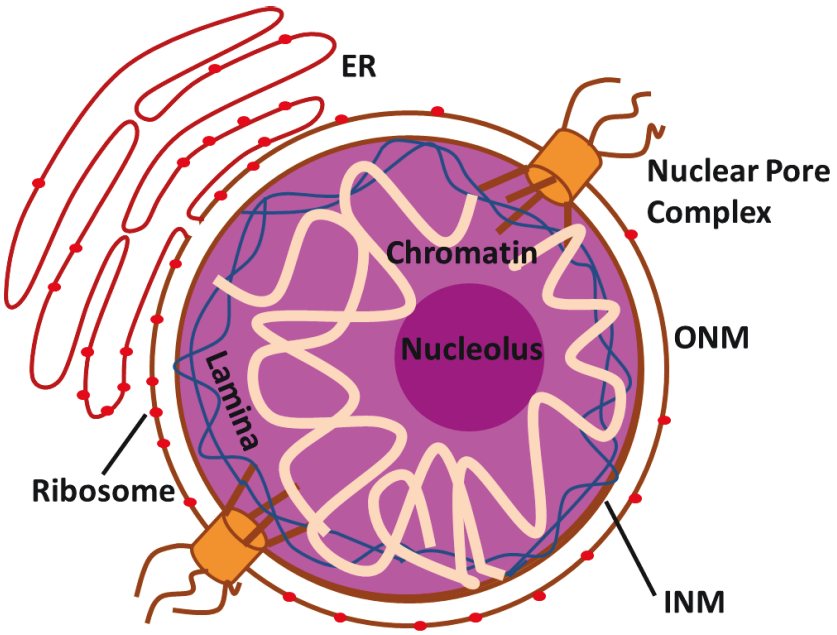

Figure 1.1: Schematic representation of the structural components of the NE in metazoans. The cartoon shows the ONM is continuous with the endoplasmic reticulum (ER) and covered with ribosomes. The NPC spans the NE and the fibrous lamina lies under the INM while tethering the heterochromatin to the INM and the NPC. The plant NE is also known to be in similar in structure to metazoans.

The work described in this thesis involves a previously unknown family of proteins in *Arabidopsis thaliana* (L.) Heynh named, nuclear envelope associated proteins (NEAP). This study tests the hypothesis that the NEAP proteins are structural components of the *A. thaliana* nuclear lamina. This chapter provides a brief introduction to the NE, and compares the protein components of its three central domains important for nuclear morphology, namely the two membranes, the nuclear lamina and the NPC in opisthokonts and plants. It also summarises approaches that have advanced understanding of the plant lamina, and aims to identify gaps in current knowledge while comparing the two systems.

1.1 The NE membranes

Most plant and opisthokont nuclei are round or oval in shape. As in opisthokonts, plant chromosomes occupy discrete territories organised into NE tethered heterochromatin and the centrally localised euchromatin (Cremer et al. 2006, Cheung and Reddy 2012). NE membranes surround the nucleus, an approximately 10 μm diameter structure. Plant NEs are structurally similar to their opisthokont counterparts. The NE is continuous with the PNER allowing

diffusion of proteins between the ER lumen and the periplasmic space (Franke et al. 1981, Voeltz et al. 2002). The ONM is decorated with ribosomes similar to rough ER and also have a common subset of proteins (Newport and Forbes 1987, Gerace and Burke 1988). Although the ONM and the PNER share lipid and lumen continuity, their junction points (diameter 2-30 nm) restrict protein transport, which are then selectively retained via their specialised domains at the NE leading to specific enrichment of proteins unique to the INM and ONM respectively (Staehelin 1997, Wilhelmsen et al. 2006).

The klarsicht ANC1 SYNE-1 homology (KASH) domain proteins are ONM-specific proteins found in opisthokonts (Starr and Fischer 2005, Wilhelmsen et al. 2006). The KASH domain is essential for their retention and localisation at the ONM. While plant ONM proteins lack the conserved opisthokont KASH domain, they have been shown to contain alternative plant-specific domains performing characteristic KASH-like functions (Zhou et al. 2012a, Zhou et al. 2014). The amino (N)- terminal cytoplasmic domains of KASH domain proteins interact with all types of cytoskeletal components like filamentous actin, microtubules and intermediate filaments (IF), impacting regulation of nuclear movement and intracellular force transmission as demonstrated in several vertebrate species (Meyerzon et al. 2009a, Zhang et al. 2009, Fridolfsson et al. 2010, Luxton et al. 2010, Morgan et al. 2011). Plant nuclei have been shown to associate with myosin motors and move along actin (Nagai 1993, Skalamera and Heath 1998, Tamura et al. 2013, Zhou et al. 2014).

KASH domain proteins also interact with centrosomes and spindle pole bodies in animals and yeast respectively (Starr and Fischer 2005, Wilhelmsen et al. 2006). Plants lack centrosomes, and the plant ONM substitutes their role as a microtubule organising centre for microtubule nucleation and spindle formation during cell division (Shimamura et al. 2004).

The KASH domain of ONM proteins interacts with the Sad1/UNC84 (SUN) domain of INM proteins highly conserved in opisthokonts and plants. The INM SUN domain proteins also interact either directly or indirectly with nucleoskeleton proteins, called lamins in metazoans as well as with chromatin, thus connecting the nucleoskeleton to the cytoskeleton (Guttinger et al. 2009, Starr and Fridolfsson 2010). Plants genomes are devoid of homologues of

lamins and lamin binding INM proteins (except SUN domain proteins) that form the metazoan nucleoskeleton. Electron microscopy images however clearly show a filamentous lattice lacing the INM along with several connection points with the INM, NPCs and chromatin (Fiserova et al. 2009). Thus plants must have an alternative structural nucleoskeleton probably performing functions very similar to the metazoan lamina (described in section 1.3).

The SUN-KASH interaction is a highly conserved feature spanning the NE and forms the backbone of the cytoskeleton-nucleoskeleton bridging complex in animals, plants and fungi (Crisp et al. 2006, Evans et al. 2014, Zhou et al. 2014). These complexes play an important role in maintaining nuclear shape, size and integrity as well as co-ordinating chromatin movement in response to forces originating in the cytoskeleton (Meyerzon et al. 2009b, Fridolfsson et al. 2010, Fridolfsson and Starr 2010, Starr and Fridolfsson 2010).

1.1.1 SUN domain proteins

SUN domain proteins are a family of INM proteins broadly conserved in eukaryotes including opisthokonts and plants (Fridkin et al. 2004, Haque et al. 2006, Graumann et al. 2010, Murphy et al. 2010, Friederichs et al. 2012). The nomenclature of the SUN domain originates from a conserved region in the carboxy (C) terminus of *Caenorhabditis elegans* (Maupas) UNC-84 protein homologous to *Schizosaccharomyces pombe* (Lindner) protein, Sad1 (Malone et al. 1999). Both *S. pombe* and *Saccharomyces cerevisiae* (Maupas) have a single SUN domain protein, whereas *Drosophila melanogaster* (Meigen) and *C. elegans* have two homologues. Mammalian species including *Homo sapiens* (L.) and *Mus musculus* (L.) show five homologues of the C-terminal SUN domain proteins (Hiraoka and Dernburg 2009).

Although the structure of opisthokont SUN domain proteins is highly variable, importantly they have regions with not only conserved structure but also function. The C-terminal SUN domain is located in the periplasmic space of the NE, where it interacts with the KASH domain (Crisp et al. 2006). Additionally, SUN domain proteins contain at least one transmembrane (TM) domain and one or more self-polymerising coiled-coil (CC) regions, placed between the SUN and TM domains, also localised in the periplasmic space (Malone et al.

1999, Starr 2009). On their N-terminus they also contain the lesser conserved nuclear localisation signals (NLS) and lamin binding domains localised in the nucleoplasm (Lee et al. 2002, Fridkin et al. 2004, Haque et al. 2006, Tapley et al. 2011).

SUN domain proteins are also conserved across plant species with homologues in moss, algae, as well as mono and dicots (Graumann et al. 2010, Murphy et al. 2010, Graumann and Evans 2011). Additionally, a new family of proteins has been identified containing a SUN domain at the centre of the protein, rather than its classical C-terminal positioning (Murphy et al. 2010).

1.1.2 Classical SUN domain proteins in plants

Based on the widely studied canonical nature of the C-terminal SUN domain, its constituent proteins have been termed the classical SUN domain family in various plant literature. As stated earlier, classical SUN domain proteins are highly conserved in the viridiplantae lineage, including algae and moss, as well as higher plants like *A. thaliana*, *Zea mays* (L.) and *Oryza sativa* (L.) (Moriguchi et al. 2005, Graumann et al. 2010, Murphy et al. 2010, Graumann and Evans 2011).

Two classical SUN domain proteins containing 430-480 amino acid (aa) residues have been described in both *A. thaliana* and Z. mays (Graumann and Evans 2010, Murphy et al. 2010). They are similar in size to yeast SUN domain proteins, but smaller than their metazoan forms. They are however largely similar in structure, particularly a C-terminal SUN domain and a CC domain, both in the periplasmic space, a TM domain spanning across to the nucleoplasm and a nucleoplasmic N-terminal NLS (Graumann et al. 2010, Murphy et al. 2010). The absence of lamin binding domains in plant SUN domain proteins is hardly surprising with the lack of plant lamins. However, there is evidence for interaction of SUN domain proteins with alternative components of the plant nucleoskeleton, which is described in section 1.2.5 (Graumann 2014). The importance of the NLS and the CC domains in NE targeting of *A. thaliana* SUN domain proteins has been shown by non-NE localisation of deletion mutants (Graumann et al. 2010). In metazoan systems, SUN domain proteins are translocated across the NPC's by various

chaperoning mechanism that often make each other redundant (Gardner et al. 2011, Tapley et al. 2011). For example, more than one NLS of the *C. elegans* SUN domain protein, UNC84 is responsible for targeting it independently to the INM via the Ras-related nuclear GTPase (Ran) dependent importin pathway which has been described in detail in section 1.3.2 (Tapley et al. 2011).

When first described, *A. thaliana* and rice SUN domain proteins were suggested to localise at the phragmoplast and mitotic spindle (Van Damme et al. 2004, Moriguchi et al. 2005). Fluorescent protein (FP) tagged AtSUN1 and AtSUN2 localise to the NE in interphase in stably expressing *A. thaliana* plants. Electron microscopy studies reveal them to be closely associated with the INM (Graumann et al. 2010). In the mitotic prophase, AtSUN1 and AtSUN2 accumulate at the NE; post break down they associate with mitotic ER membranes and rapidly aggregate around chromatin during post mitotic NE reassembly, suggesting a role in chromatin organisation (Graumann and Evans 2011, Friederichs et al. 2012). NE localisation of C-terminal SUN domain proteins is also confirmed in maize interphase and meiotic prophase nuclei (Murphy et al. 2014). Similarly in yeast, both the *S. pombe* and *S. cerevisiae* SUN domain proteins localise to the INM and spindle pole bodies (Bupp et al. 2007, Tran et al. 2014). *A. thaliana* SUN1 and SUN2 interact with each other forming homo- and hetero- polymers, similar to human SUN domain proteins (Graumann et al. 2010, Zhou et al. 2012b, Graumann et al. 2014).

1.1.3 Novel mid-SUN domain proteins in plants

Apart from the classical SUN domain proteins, a new class of proteins have been identified in plants with the conserved SUN domain at the centre of the protein, as opposed to being C-terminal (Murphy et al. 2010). In addition to the central SUN domain, they contain a TM domain at their N-terminus, followed by a highly conserved domain of unknown function, one or more CC domains, and two adjacently placed TM domains on their C-terminus (Murphy et al. 2010). Significantly larger in size than their classical counterparts, three homologues have been described in maize as well as *A. thaliana* (Murphy et al. 2010). In maize, SUN3 and SUN4 are ubiquitously expressed but SUN5 is pollen specific (Murphy et al. 2010). In *A. thaliana*, SUN3 and SUN4 are expressed in all

tissues, while SUN5 is up-regulated in pollen, anther and endosperm tissues (Graumann et al. 2014). Unlike maize mid-SUN domain proteins which are predominantly NE localised, *A. thaliana* SUN3 and SUN4 localise to the NE as well as the ER (Murphy et al. 2010). In *A. thaliana*, SUN3 and SUN4 both interact with SUN1 and SUN2, while SUN5 does not. SUN3 also interacts with SUN4. SUN5 interacts with itself and with SUN3. The CC domain of SUN1 and SUN2 are important for this interaction (Graumann et al. 2014).

Homologues of mid-SUN domain proteins are found across the opisthokonta domain including mammals, flies, worms and yeast (Murphy et al. 2010). The mouse mid-SUN domain protein, osteopotentia (Opt), localises to the rough ER, plays an important role in its integrity and expansion (Sohaskey et al. 2010). It's yeast orthologue, *S. cerevisiae* SLP1 localises to cortical and PNER and plays an important role in localisation of C-terminal SUN domain protein, Mps3 at the NE (Friederichs et al. 2012).

1.1.4 The KASH domain family

KASH domain proteins, as described in section 1.1, are ONM-specific and highly conserved in vertebrates and yeast. The characteristic KASH domain that defines the family interacts with the SUN domain, an interaction indispensable for the ONM localisation of KASH domain proteins (Crisp et al. 2006). The KASH domain is made up of two subdomains; comprising a TM domain and a stretch of 6-30 aa in the periplasmic space (Starr and Fridolfsson 2010). The periplasmic portion of the KASH domain ends in a conserved PPPX motif, that docks inside one of the three pockets created by the SUN trimer (Razafsky and Hodzic 2009, Sosa et al. 2012). The penultimate proline on the PPPX motif is essential for this binding and is highly conserved (Razafsky and Hodzic 2009).

The N-terminal domains of KASH proteins remain in the cytoplasm establishing nuclear anchorage to the cytoskeleton (Starr and Fridolfsson 2010). The cytoplasmic N-termini of metazoan KASH domain proteins called Nesprins, contain the characteristic spectrin repeats placed adjacently to the KASH domain (Rajgor and Shanahan 2013). Nesprin1, approximately 1000 kDa in size contains 74 spectrin repeats. Nesprin2 is smaller, approximately 800 kDa, and contains 56 spectrin repeats. Nesprin3 and Nesprin4 are considerably

smaller, approximately 110kDa and 42kDa, with only 8 and 1 spectrin repeats respectively (Rajgor and Shanahan 2013). Nesprin1 and Nesprin2 bind filamentous actin via calponin homology (CH) domains at their extreme N-terminus (Zhang et al. 2002, Taranum et al. 2012). Nesprin3 and Nesprin4 lack the CH domains, but instead bind IFs and microtubules via plectin/vimentin and kinesin respectively (Wilhelmsen et al. 2005, Roux et al. 2009, Taranum et al. 2012). Although varied in structure, the N-termini of KASH domain proteins perform overlapping functions of associating with different elements of the cytoskeleton in nematodes, flies and mammals, suggesting functional homology across species (Wilhelmsen et al. 2006, Technau and Roth 2008, Minn et al. 2009, Zhang et al. 2009).

In summary, the metazoan KASH domain proteins have highly varied N-terminal domains as well as sequentially varied TM domains as part of the KASH domain. The conserved PPPX motif of the metazoan KASH domain is missing in plants, which has prolonged the search for plant KASH domain proteins. In recent years, three families of plant-specific KASH proteins have been successfully identified in *A. thaliana* (Zhou et al. 2012a, Graumann et al. 2014, Zhou et al. 2014).

1.1.5 Plant KASH domain proteins

In *A. thaliana,* tryptophan proline proline (WPP) domain interacting proteins (WIP) have been confirmed as plant-specific KASH domain proteins (Zhou et al. 2012a). They do not contain the conserved PPPX motif of the opisthokont KASH domain; instead they have a plant-wide conserved VVPT motif, containing the conserved penultimate proline indispensable for interaction with the SUN domain in metazoans. The VVPT KASH motif interacts with the SUN domain and is essential for the ONM targeting of the constituent proteins (Zhou et al. 2012a).

A. thaliana WIP and WPP interacting tail anchored (WIT) proteins target plant specific Ran GTPase activating protein (RanGAP1) to the plant NE (Xu et al. 2007). RanGAP aids Ran in hydrolysis of GTP to GDP driving diverse cellular processes including nuclear transport, mitotic spindle assembly and post-mitotic NE reassembly (Xu et al. 2007).

WIP1, 2 and 3 interact with SUN domain proteins, an interaction vital for the NE targeting of WIP proteins (Zhou et al. 2012a). WIP1 also interacts with SUN3 *in planta*, specifically its KASH domain interacts with SUN3, SUN4 and SUN5 (Graumann et al. 2014). WIP proteins also interact with WIT proteins (Zhou et al. 2012a). Whether the ONM WIT proteins also interact with SUN domain proteins is yet to be ascertained. Interestingly, WIT1 and 2 interact with myosin XI-i which not only interacts with actin, but has also been shown to affect nuclear morphology and movement (Tamura et al. 2013). Thus plant WIP proteins fulfil all the criteria of KASH proteins, namely, TM domain mediated ONM localisation, SUN domain binding essential for NE targeting and cytoskeleton association, as well as an additional feature of mid-SUN interaction.

Using highly conserved features of the XXPT motif of *A. thaliana* WIP proteins, a recent study identified 10 new families of putative KASH proteins in plants (Zhou et al. 2014). Four *A. thaliana* proteins localised to the NE, interact with the SUN domain of SUN domain proteins and were named SUN domain interacting NE (SINE) proteins 1 to 4. The *Medicago trunculata* (Gaertn.) protein SINE5 also localises to the NE and interacts with the SUN domain. The KASH domain and the XXPT motif mediate the SUN domain interaction which is critical to ONM localisation of SINE proteins. SINE1 associates with F-actin and is important for anchorage and positioning of guard cell nuclei in the leaf epidermis. SINE2 plays an important role in innate immunity and contributes to plant resistance against filamentous pathogens (Zhou et al. 2014).

In a recent study, a novel plant KASH protein has been identified as an interactor of SUN1 and SUN2 (Graumann et al. 2014). It contains a toll interleukin-resistance domain and a KASH domain, after which it is named TIK. TIK has the metazoan KASH-characteristic PPPX motif, followed by a conserved C-terminal TM domain. TIK protein forms dimers with itself via its KASH domain. Additionally, TIK not only interacts with SUN1 and SUN2 but also SUN3, SUN4 and SUN5, and the KASH domain is essential for this interaction. TIK is suggested to localise at the NE and is expressed at low levels in all tissues but up-regulated in roots (Graumann et al. 2014).

1.1.6 SUN-KASH bridges of the NE

The ultrastructure of SUN-KASH bridges is revealed in micrographs of the NE showing connections between structural proteins of the nucleoskeleton and cytoskeleton spanning the two nuclear membranes both in animal and plant systems (Franke et al. 1981, Fiserova et al. 2009). Protein crystallisation studies have shown that the CC domains of human SUN2 protein oligomerise to form a trimeric complex creating three pockets for KASH binding (Sosa et al. 2012, Zhou et al. 2012b). Interestingly, the C-terminal KASH motif critical for SUN domain interaction, PPPX sits inside the KASH pocket (Sosa et al. 2012). The flexibility of the hexameric complex is further augmented by disulphide bridging of cysteine residues on either side of the SUN-KASH protomer, as well as oligomerisation of KASH protein (Sosa et al. 2012, Rajgor and Shanahan 2013).

The fundamental function of SUN-KASH bridges is connecting the nucleoskeleton to the cytoskeleton. This function in turn governs characteristics like nuclear shape, size, anchoring and co-ordinated nuclear movement with cytoplasmic forces. Mammalian KASH proteins regulate nuclear size (Lu et al. 2012). SUN and KASH mutant neurons show failure of nuclear migration, leading to defective nucleokinesis in mice (Zhang et al. 2009). KASH proteins Syne1 and 2 are important for nuclear anchorage and organisation in mice skeletal muscle cells (Zhang et al. 2007). Drosophila SUN and KASH domain proteins are important for nuclear migration in eye development, as well as nuclear spacing in skeletal muscle cells (Apel et al. 2000, Kracklauer et al. 2007, Elhanany-Tamir et al. 2012). KASH proteins in *C. elegans*, UNC83 is important for nuclear migration and ANC1 is responsible for nuclear anchorage (McGee et al. 2006, Fridolfsson et al. 2010). Several studies have shown aberrant metazoan SUN domain proteins to cause defects in nuclear migration and positioning (Sulston and Horvitz 1981, Goshima et al. 1999, Starr and Han 2005, Lombardi et al. 2011).

SUN-KASH bridges also connect chromatin to the cytoskeleton. Several opisthokont SUN domain proteins anchor telomeres playing an important role in telomere maintenance and chromosome movement (Ding et al. 2007, Hiraoka and Dernburg 2009). Along with telomeres; the *S. pombe* SUN domain protein

also tethers centromeres (Hou et al. 2012). KASH mutant mice show a severe chromosome pairing defect in meiosis and also fail to repair double strand breaks (Horn et al. 2013). SUN-KASH complexes recruit centrosomes that mediate homologous pairing, recombination and repair, and segregation of chromosomes in meiosis (Fridkin et al. 2009, Hiraoka and Dernburg 2009, Starr and Fridolfsson 2010, Woglar and Jantsch 2014). Several mammalian proteins have been described to have a role in the anchoring of SUN-KASH bridges. These include lamin A, Samp1 and emerin which anchor the LINC complex to the lamina in somatic cells and TERB1 which is involved in its chromosomal anchoring in meiotic cells (Chang et al. 2015). Opisthokont SUN-KASH bridges also function in processes like gene regulation, apoptosis, cell signalling and mechanotransduction of extracellular physical stimuli to the nucleus (Luxton and Starr 2014).

1.1.7 Plant SUN-KASH complexes

In plants, both mid-SUN and C-terminal SUN domain proteins interact with plant-specific KASH domain families, WIP, SINE and TIK to constitute the SUN-KASH bridging complexes. SUN-KASH bridges in plants have been shown to have functions of maintaining nuclear morphology similar to those in opisthokont systems. Double mutant *sun1 sun2* transfer (T)-DNA lines show aberrant nuclear shape, wherein their typically elongated nuclei in root hair and epidermal cells are abnormally rounded (Oda and Fukuda 2011). A triple mutation for *sun3 sun4 sun5* in *A. thaliana* is embryo lethal. While a *sun3* mutant line showed rounded nuclei, a *sun4 sun5* double mutant showed significantly smaller nuclei (Graumann et al. 2014). Triple knockout *wip1 wip2 wip3* nuclei are atypically rounded similar to the *sun4 sun5* double knockout, suggesting common functions in maintaining nuclear shape (Zhou et al. 2012a). Mature epidermal cells deficient in myosin XI-i, which connects plant SUN-KASH bridges to the actin cytoskeleton, have smaller nuclei (Tamura et al. 2013). While the *tik* mutant line shows shorter roots compared to wild type (WT), their root nuclei are significantly smaller than WT (Graumann et al. 2014). The shared roles of plant SUN and KASH domain proteins in maintaining

nuclear morphology characteristics like shape and size are indicative of their common functions as components of the SUN-KASH bridging complex.

Plant nuclei move in a number of circumstances, including in response to light and fungal infection, and are known to involve an actin rather than a microtubule based system (Nagai 1993, Skalamera and Heath 1998). Motor protein myosin XI-i anchors plant nuclei to F-actin via the WIT-WIP complex and moves them along actin cables in the cytoplasm (Tamura et al. 2013). SINE1 also associates with F-actin and is essential for nuclear anchorage and positioning. Thus both SINE and WIP based complexes actively participate in nuclear anchorage, movement and positioning in plants.

Along with well-known functions of SUN-KASH bridges in opisthokonts, plant specific SUN-WIP complexes also have unique functions at the plant NE. The specialised role of the WIT-WIP complex in anchoring RanGAP to the NE has previously been described in section 1.1.5, which is different from metazoans where specific NPC components act as RanGAP anchors. Thus plant SUN-WIP bridges function in maintaining a RanGTP gradient across the NE to facilitate nucleo-cytoplasmic transport (Zhou et al. 2012a).

Plant SUN-KASH bridges have also been implicated in chromatin regulation. SUN1 and SUN2 accumulate at the NE in the mitotic prophase; post NE break down they associate with mitotic ER membranes and rapidly aggregate around chromatin during post mitotic NE reassembly (Graumann and Evans 2011). In meiosis, SUN mutants show impaired telomere tethering at the NE as well as defective chromosome pairing and recombination (Murphy et al. 2010). An *A. thaliana sun1 sun2* double mutant showed severe meiotic defects causing reduction in fertility (Varas et al. 2015). In the same study, SUN1 and SUN2 have been suggested to be involved in telomere attachment and movement in pollen mother cells (Varas et al. 2015).

1.2 The lamina

The nuclear lamina is a meshwork of filamentous proteins at the nuclear periphery that forms an important component of the nucleoskeleton in metazoans (Burke and Stewart 2013). The lamina is seen attached to the INM

and the NPCs and interweaved over condensed chromatin (Fawcett 1966, Goldberg et al. 2008a). Several studies have indicated that the nuclear lamina is conserved in eukaryotes including metazoans as well as previously debated plants, fungi and unicellular protozoans (Fiserova et al. 2009, Goldberg et al. 2008a, Ciska and Moreno 2014). As part of the nucleoskeleton, the lamina provides mechanical support and connects chromatin to the cytoskeleton by associating with the SUN-KASH bridges of the NE which control nuclear morphology and movement (Burke and Stewart 2013). The lamina tethers epigenetically silent heterochromatin and also plays an important role in maintaining chromatin integrity, chromatin organisation as well as gene silencing and transcription regulation (Reddy and Singh 2008, Peric-Hupkes and van Steensel 2010).

In somatic cells, the lamina appears dense and its structure is difficult to resolve (Fawcett 1966, Goldberg et al. 2008a). The lamina in a *Xenopus leavis* (Daudin) oocyte nucleus is relatively simple and made up of a single type of lamin III filaments (Goldberg et al. 2008a, b). The 8-10 nm diameter filaments of lamin III are arranged in parallel and separated by a distance of ~15 nm. The separated filaments are interconnected by ~5 nm filaments giving the structure an appearance of a second perpendicular network. However the smaller connecting filaments do not show continuity, instead they individually criss-cross the parallel filaments at regular intervals (Goldberg et al. 2008a, b). When lamins B1 and B2 are over-expressed in the oocyte nucleus, it triggers formation of membrane extensions and assembly of filaments on these overgrown membranes. The filaments formed by lamins B1 and B2 are similar to those of lamin III, except they appear less ordered with less prominent cross connections (Goldberg et al. 2008b). Overexpression of lamin A does not cause membrane overgrowth, instead lamin A bundles over the existing oocyte lamina. These 15nm diameter filaments run parallel and form layers that pile over the endogenous network at different angles (Goldberg 2008b). In tobacco BY2 cells, the nuclear lamina structure is organised similar to the endogenous lamina of the X. leavis oocyte (Fiserova et al. 2009).

1.2.1 Lamins

In metazoans, the lamina is composed of type V IF proteins called lamins and lamin binding proteins (Burke and Stewart 2013). Lamin proteins oligomerise to form overlapping filaments while lamin-binding proteins mediate association with the INM and/or chromatin (Simon and Wilson 2013).

Lamins have a typical IF structure comprising a central alpha helical CC rod domain between non-helical head and tail domains. The rod domain is flanked on both ends by conserved cyclin-dependant kinase 1 (CDK1) phosphorylation sites. The tail domain contains an NLS and two conserved domains including an immunoglobulin-like β fold and a C-terminal CaaX motif (C: cysteine; a: aliphatic residues; X: any aa) (Dechat et al. 2010).

Lamins are classified as A and B type. In mammals a single gene (*LMNA* in humans) encodes all four A-type lamin protein isoforms including lamin A, lamin C, lamin C2 and laminAΔ10. A-type lamins are developmentally regulated and differentially expressed in varied tissues. Two genes *LMNB1* and *LMNB2* encode three B-type lamins B1, B2 and B3 in humans. B-type lamins are indispensable for nuclear stability; at least one B-type lamin is present in all cells throughout development (Dechat et al. 2010).

Lamin A, lamin B1 and lamin B2 are synthesized in the cytoplasm as prelamins, where the cysteine residue of the CaaX motif is farnesylated, followed by its carboxy methylalation post proteolytic cleavage of the aaX (Nigg 1992). Farnesylated lamins are then trafficked into the nucleus and incorporated in the nuclear lamina. Once incorporated in the lamina the farnesylated C-terminus of pre-lamin A is cropped to form mature lamin A (Dechat et al. 2010). B-type lamins on the other hand remain permanently farnesylated staying attached to the INM at all times (Dechat et al. 2010). Lamins are also targets of other post-translational modifications like phosphorylation and sumoylation (Zhang and Sarge 2008, Kuga et al. 2010).

A-type lamins form a thick network, stretching up to 100nm deep into the nucleoplasm (Kaufmann et al. 2011). On the other hand, the fibrillar network formed by B-type lamins remains at the nuclear periphery closely associated to the INM via their hydrophobic farnesyl residues (Jung et al. 2013). All A and B

type lamins interact with each other *in vitro*. However *in vivo,* lamins A and B preferentially self-polymerise to form separate networks, which are capable of interaction with each other (Goldberg et al. 2008b). During assembly of lamina filaments, first the CC domains oligomerise to form lamin homodimers (Aebi et al. 1986, Sugimoto et al. 2001, Solovei et al. 2013). Individual homomers assemble in a head to tail fashion into units that then laterally associate in an anti-parallel conformation to form a protofilament (Wang and Higgins 2013). Further lateral association of protofilaments gives rise to the approximately 10nm IF like structure of lamins (Hirota et al. 2005, Ben-Harush et al. 2009, Burke and Stewart 2013, Solovei et al. 2013).

The lamin protein family is conserved in all studied metazoan species; however, there are no homologues in plants, yeast or protozoans (Meier 2007). Instead, in the absence of lamins other structural proteins successfully assemble filamentous networks very similar in nature to the metazoan lamina (Ciska and Moreno Diaz de la Espina 2014).

1.2.2 Lamin binding proteins

The metazoan lamina is anchored to the NE by lamin binding proteins including INM integral proteins, NPC and nucleoskeleton components (Simon and Wilson, 2013). A total of 54 binding partners have been identified for A-type lamins, whereas about 25 proteins have been shown to bind B-type lamins (Davidson and Lammerding 2014).

Metazoan lamins interact with nuclear structural proteins like F-actin, titin and non-KASH nesprin isoforms; nesprin1α and nesprin2 (Zastrow et al. 2006). Lamin A also interacts with nucleoporins Nup153 and Nup88 (Smythe et al. 2000, Lussi et al. 2011). Most INM proteins bind either A, B or both lamin filaments (Gruenbaum et al. 2005, Wilson and Foisner 2010). These include the C-terminal SUN domain proteins, lamina associated polypeptides (LAP) 1 and 2, emerin, man (LEM) domain proteins and the lamin B receptor (LBR) (Worman et al. 1988, Wilson and Foisner 2010). LEM domain proteins are INM integral components of the lamina known to bind Barrier to autointegration factor (BAF), a chromatin binding protein enriched at the NE (Berk et al. 2013). The BAF-LEM interaction is highly conserved in metazoans (Margalit et al.

2007b). BAF also binds A-type lamins (Margalit et al. 2007a). Lamins bind directly to a number of transcription and regulatory factors (Wilson and Foisner 2010, Simon and Wilson 2013). The LBR has eight TM domains spanning the INM and an N-terminus containing a lamin B binding domain as well as a chromatin binding region (Olins et al. 2010). Lamins and LBR also bind the Proliferating Cell Nuclear Antigen (PCNA) involved in DNA repair and replication (Shumaker et al. 2008). Apart from SUN domain proteins, plants lack homologues to all INM integral lamin-binding proteins.

1.2.3 Lamin-chromatin interaction

The lamina tethers chromatin at the INM and regulates its organisation and function via chromatin-binding partners including structural proteins, transcription factors (TF) and signalling molecules. Lamins bind histones, proteins that fold and package chromatin and Heterochromatin Protein 1 (HP1), involved in heterochromatin assembly and gene silencing (Okada et al. 2005, Dechat et al. 2010). In drosophila, lamin DM0 binds JIL1 kinase which phosphorylates histone H3 and is essential for organisation of the lamina and chromatin (Bao et al. 2005). The tumour suppressor Retinoblastoma protein (Rb) also associates with A-type lamins (Nitta et al. 2006, Simon and Wilson 2013). A-type lamins are involved in the tumour suppressor p53 binding protein (53BP1) stabilisation and telomere maintenance both essential for genome integrity (Gonzalez-Suarez et al. 2009).

1.2.4 The protozoan lamina

Although the lamina is conserved across metazoan and protozoan kingdoms, the lamin protein family is confined to vertebrate and invertebrate species. The *Dictyostelium discoideum* (Raper) NE81 is the first lamin like protein identified in unicellular organisms (Kruger et al. 2012). NE81 is an 81kDa protein co-purified from isolated centrosomes. Although it does not share sequence homology with lamins, they share several structural features. Similar to lamins, NE81 contains the central CC rod domain, a CDK1 phosphorylation site on the N-terminal border of the rod domain, an NLS, and a C-terminal CaaX motif. Also as in case of lamins, NE81 is associated with the INM and the CaaX motif and its related

post-translational modifications are essential for its targeting (Batsios et al. 2012, Kruger et al. 2012). NE81 homologues are not found in other protozoans and are limited to the class *D. discoideum*.

A second protozoan lamina constituent, nuclear peripheral (NUP) 1 protein has also been identified in *Trypanosoma brucei* (Plimmer & Bradford, 1899) with homologues restricted within the trypanosomatid order (DuBois et al. 2012). NUP1 is a large 400kDa CC protein localised to net-like structures at the nuclear periphery. Unlike NE81, NUP1 has very few structural similarities to lamins which are limited to the presence of CC domains and a functional NLS. Functional similarity of NUP1 to lamins is demonstrated by its role in *T. brucei* chromatin organisation and gene regulation (DuBois et al. 2012). The fact that NE81 structure is highly similar to the lamins unlike NUP1 correlates with the nature of the evolutionary relationship between dictyostelia, trypanosoma and metazoans. In phylogenetic order, dictyostelia are placed between the lamin rich metazoans and the lamin devoid protozoans (Kruger et al. 2012). Additionally a CC NPC component, Nup92 has been related to chromosome segregation and mitotic spindle assembly and suggested to be a functional analogue of the metazoan translocated promoter region (tpr) protein with similar functions (described in section 1.3.3) (Holden et al. 2014). As in trypanosomatids, the plant lamina has evolved a separate set of CC proteins unrelated to lamins, but similar in their function.

1.2.5 The plant lamina

The metazoan lamina is a well-studied entity with respect to its structural components, lamins and their binding partners. One of the reasons for the greater understanding and interest in the animal lamina, are a host of developmental and ageing related human diseases called nuclear envelopathies and laminopathies, caused by single gene mutations of lamina associated proteins (Cau et al. 2014, Hatch and Hetzer 2014). The absence of lamin proteins from the plant lamina has meant that knowledge about the plant lamina has been slower to emerge. However the plant lamina has been successfully visualised using electron microscopy, and various studies have adopted multiple approaches to identify the components of the plant lamina

(McNulty and Saunders 1992, Minguez and Moreno Diaz de la Espina 1993, Masuda et al. 1997, Blumenthal et al. 2004, Fiserova et al. 2009). This section aims to summarise all current information about the plant lamina and discuss approaches responsible for successful identification of its constituent proteins.

Electron microscopy studies have revealed a meshwork of proteins underlying the INM in *Allium cepa* (L.) and *Nicotiana tabacum* (L.) cells (Minguez and Moreno Diaz de la Espina 1993, Fiserova et al. 2009). The plant lamina, observed in *N. tabacum* and *Pisum sativum* (L.) nuclei, is made up of two types of filaments, one 10-13 nm and another 5-8 nm in thickness (Li and Roux 1992, Blumenthal et al. 2004, Fiserova et al. 2009).

Several immunological studies have used antibodies against metazoan lamin and IF proteins, to screen plant nuclear extracts for identification of plant-specific filamentous proteins (McNulty and Saunders 1992, Minguez and Moreno Diaz de la Espina 1993, Masuda et al. 1997). A *Daucus carota* nuclear matrix constituent protein, NMCP1 localises to the nucleoplasmic periphery and binds the mitotic spindle (Masuda et al. 1997). NMCP1, a 134 kDa protein, is larger than metazoan lamins. Similar to lamins, it has a large central CC domain and a putative NLS in its tail domain (Masuda et al. 1997). NMCP1 was the first member of the large NMCP protein family found to be highly conserved in land plants.

1.2.6 Contribution of the NMCP family to the plant lamina

The NMCP family is highly conserved in plants, but absent from fungi and metazoans. Ciska et al (2013) analysed 31 plant species and found two species of unicellular algae, *Volvox carteri* (F.Stein) and *Chlamydomonas reinhardtii* (P.A.Dang) lacked homologues to the NMCP family (Ciska et al. 2013). The NMCP family is classified into two types, NMCP type1 and NMCP2 in flowering plants. The sequenced plant kingdom has a total of 71 NMCP genes, with a minimum of 2 genes in all species (Ciska et al. 2013).

In *A. thaliana*, four homologues have been identified and named as LINC1-4, in recognition of their phenotype having little nuclei (Dittmer et al. 2007). However owing to confusion with the nomenclature of the Linker of Nucleoskeleton

Cytoskeleton (LINC) complex, the authors renamed the LINC proteins as CRWN for their phenotype of crowded nuclei (Wang et al. 2013). Current literature, however, utilises LINC, CRWN and NMCP interchangeably to denote the same family of nuclear matrix proteins in a variety of plant species. LINC1 belongs to the NMCP type 1 group whereas LINC2, LINC3 and LINC4 belong the NMCP type 2 group.

The NMCP protein family is tripartite in structure similar to lamins. Their structure comprises a central CC rod domain highly conserved in the NMCP family (Ciska and Moreno Diaz de la Espina 2014). There are highly conserved segments within the CC domain, including its N- and C-terminal ends that have been suggested to take part in head to tail assembly of lamin filaments (Kapinos et al. 2010). The rod domain is flanked by N- terminal head and C- terminal tail domains, both containing a CDK1 phosphorylation site each. The tail domain also contains a conserved NLS and a highly conserved C-terminus (Ciska et al. 2013). All characteristics described so far show extensive similarity to lamin structure. On the other hand, the NMCP CC region is almost twice in size as the lamin rod domain; and the NMCP tail domain lacks the immunoglobulin fold and the CaaX motif of lamins (Ciska and Moreno Diaz de la Espina 2014).

In onion root meristem, NMCP1 antibody localises to the nuclear periphery and associates with the peripheral lamina, proximal to condensed chromatin and to a lesser extent to the internal nucleoskeleton (Ciska et al. 2013). 35S promoter driven gDNA-FP fusions of LINC1 and LINC2 localise mainly to the nuclear periphery and nucleoplasm respectively in *A. thaliana* root epidermal and meristematic nuclei (Dittmer et al. 2007). Under the native promoter, LINC1-green FP (GFP) was highly expressed in meristematic tissues, but not differentiated root hair and epidermal cells (Dittmer et al. 2007). In another independent study, Sakamoto and Takagi (2013) identified LINC1 and LINC4 by mass spectrometry analysis from the nuclear lamina fractions prepared from *A. thaliana* leaf protoplasts (Sakamoto and Takagi 2013). They also found LINC1 and 4 mainly localised to the NE, and LINC2 and 3 to the nucleoplasm in leaf and root epidermal cells (Sakamoto and Takagi 2013). Similarly in rice, carrot and celery, NMCP homologues have been shown to localise to the nucleoplasmic periphery (Masuda et al. 1997, Moriguchi et al. 2005, Kimura et

al. 2010). NMCP1 is expressed at higher levels in onion root meristem compared to mature root cells, thus NMCP1 expression is developmentally regulated (Ciska et al. 2013). In celery and *A. thaliana*, NMCP proteins are also differentially regulated during cell division performing separate functions (Sakamoto and Takagi 2013). In celery, NMCP1 is interspersed within the mitotic spindle in the metaphase, associates with the surface of segregating chromosomes in anaphase and reorganises around the reforming NE in telophase (Kimura et al., 2010). NMCP2 on the other hand, is dispersed in the mitotic cytoplasm until late anaphase, and re-associates around chromosomes at the end of telophase (Kimura et al., 2010). Similarly during pro-metaphase to anaphase in *A. thaliana* root apical meristem cells LINC2, LINC3 and LINC4 diffuse to the cytoplasm, while LINC1 associates with the condensing chromatin (Sakamoto and Takagi, 2013). During late telophase, LINC1 starts dissociating from chromatin and localises to the newly formed NE, whereas LINC2, 3 and 4 are imported to the nucleus and associate to the chromatin surface (Sakamoto and Takagi, 2013). Thus LINC proteins are suggested to be important for chromatin organisation and segregation. The *linc1 linc2* double mutant also showed changes in chromosome architecture compared to the WT, a decrease in number of chromocentres, the signs of epigenetically silent centromeric and heterochromatin regions accompanied by increased nuclear density (Dittmer et al. 2007). Wang et al. (2013) also showed that LINC4 was essential for organisation of chromocentres in interphase nuclei. Smaller *linc4* mutant nuclei had reduced number of chromocentres whereas larger endopolyploid *linc4* mutant nuclei showed higher chromocentre numbers (Wang et al. 2013). Further, centromeric and 5S RNA repeats failed to localise typically to chromocentre regions indicating aberrant chromatin organisation (Wang et al. 2013).

As stated earlier, the plant lamina lacks lamins and lamin binding INM proteins like the LEM domain proteins and LBR (Rose et al. 2004). However, lamin binding metazoan SUN domain proteins are conserved and have homologues in plants (Graumann et al. 2010, Murphy et al. 2010, Oda and Fukuda 2011). A recent study has shown that *A. thaliana* LINC1 is anchored to the NE by SUN domain proteins; wherein multiple points of evidence prove that the N-terminus

of SUN1 and SUN2 is essential for this interaction (Graumann 2014). A novel INM protein KAKU4 has been identified which interacts with LINC1 and LINC4, and plays an important role in nuclear morphology (Goto et al. 2014, Tamura et al. 2015).

The plant lamina associates with SUN-KASH bridges and also contributes to similar functions of maintaining nuclear morphology. *Linc1 linc2* double mutant plants are smaller compared to WT or single mutant plants. The single *linc1* and *linc2* as well as the double mutant show reduced nuclear size and a homogenous increase in roundedness in leaf epidermal and pavement cells, root epidermal, cortex and root hairs and anther filament cells (Dittmer et al. 2007). Nuclear area in *linc1*, *linc4* and their *linc1 linc4* double mutant was significantly smaller compared to WT, and to *linc2*, *linc3* and the *linc2 linc3* double mutant. All mutants, showed an increase in nuclear roundedness in leaf and root epidermal cells except *linc3*, which had significantly rounded nuclei in root epidermal cells but not leaf cells (Sakamoto and Takagi 2013). Similar results were shown by Wang et al. (2013) where single mutant *linc1, linc4* and double mutant *linc1 linc2*, *linc1 linc3* and *linc1 linc4* but not single *linc2* and *linc3* mutants showed smaller nuclei (Wang et al. 2013). The study also showed increased sphericity of *linc4* mutant nuclei as well as their aberrant nuclear margins and thin protrusions extending from their nuclear envelopes (Wang et al. 2013). Thus LINC1 belonging the NMCP type 1 group appears to have non-overlapping chromosomal localisation as well as nuclear morphology functions with LINC2, LINC3 and LINC4 belonging to the NMCP type 2 group (Tamura et al. 2015). Several *kaku4* mutant plants also show smaller and spherical nuclei compared to WT (Goto et al. 2014). LINC1 and KAKU4 overexpression independent of each other leads to nuclear membrane overgrowth and deformation (Goto et al. 2014). LINC mutant plants, similar to lamin deficient mutants, show phenotypes related to defects in nuclear shape, size and chromatin architecture, thus associating them with function of the nucleoskeleton-cytoskeleton complex.

1.2.7 Other putative components of the plant lamina

Using antibodies to various metazoan lamina components, several candidate plant lamina proteins have been successfully identified. Plant nuclear IF (NIF) proteins of 54, 60 and 65 kDa have been identified from pea and onion nuclear matrices and shown to assemble into 6-12 nm thick filaments (McNulty and Saunders 1992, Minguez and Moreno Diaz de la Espina 1993, Blumenthal et al. 2004). Similarly metazoan spectrin antibodies have identified plant spectrin-like proteins associated with pea and onion nuclear matrices (De Ruijter et al. 2000, Perez-Munive and Moreno Diaz de la Espina 2011). Plant nuclear spectrin-like proteins localise at the nuclear periphery, chromatin and nucleolus and associate with nuclear actin and IFs (Perez-Munive and Moreno Diaz de la Espina 2011). However the aa sequences of these plant NIF and spectrin-like proteins remain elusive.

Lamins bind to DNA Matrix Attachment Regions (MAR); a MAR binding Filament-like protein MAF1 was identified in *Solanum lycopersicum* (L.) and *P. sativum* (Meier et al. 1996, Blumenthal et al. 2004). A yeast two hybrid screen identified a *S. lycopersicum* CC filament-like plant protein (FPP) as MAF1 interactor (Gindullis et al. 1999). The FPP protein has seven homologues in *A. thaliana* that need characterisation. A nuclear ankyrin like protein is suggested to be a nuclear matrix protein in rice, but needs further characterisation (Moriguchi et al. 2005).

Nuclear actin can form microfilaments in the plant nucleus, and has been suggested to contribute to the nucleoskeleton. Three actin-binding plant nuclear proteins - profilin, actin depolarising factor and nuclear myosin1 have been suggested as candidate matrix-associated proteins (Kandasamy et al. 2002, Ruzicka et al. 2007, Cruz et al. 2008).

1.3 The NPC

NPCs are large multi-protein complexes that function as bidirectional transport channels at the NE. NPCs are a conserved feature of metazoan, plant, yeast and protozoan NEs. The nuclear pore co-evolved with the NE, and the majority of NPC components are conserved in the last common eukaryotic ancestor

(DeGrasse et al. 2009). The partition of RNA maturation and protein translation on either side of the NE presents a barrier for mRNA export to the cytoplasm and import of nuclear proteins across the NE. The evolution of the NPC has fulfilled this essential function of regulating nucleo-cytoplasmic transport across the NE.

1.3.1 Structure and components of the NPC

In plants the NPC is approximately 100MDa which is closer in size to the 120 MDa vertebrate NPC and larger than yeast, which is 50 MDa (Tamura and Hara-Nishimura 2013). The ultrastructure of the NPC is highly conserved in vertebrates, plants and yeast (Allen and Douglas 1989, Goldberg and Allen 1996, Fiserova et al. 2009). The NPC forms a cylindrical channel of eightfold radial symmetry. It has an average outer diameter of 110-120 nm in vertebrates, about 105 nm in plants and 95 nm in yeast (Kiseleva et al. 2004, Fiserova et al. 2009). The vertebrate NPC is composed of three sub-assemblies, a central pore with an inner diameter of about 50 nm, eight filaments extending into the cytoplasm and eight nuclear filaments connected by a ring like structure to form the nuclear basket (Arlucea et al. 1998). In metazoans as well as plants, NPCs in dividing cells have a bigger channel diameter compared to quiescent cells in which NPCs have a smaller pore diameter and contains filaments extending from its base (Goldberg and Allen 1996, Kiseleva et al. 2001, Fiserova et al. 2009).

The NPC is a multimeric complex of about 30 glycoproteins called nucleoporins (Nup). Unlike other NE protein components, Nup proteins are highly conserved among vertebrates, yeast and plants, suggesting their evolution was an indispensable part of formation of the nucleus and happened very early compared to NE proteins belonging to other domain (DeGrasse et al. 2009). Nups are classified into three groups, including phenylalanine–glycine (FG) repeat-containing, scaffold Nups and TM Nups. The FG domain contains multiple unfolded FG-rich peptides that are binding sites for several transporter-cargo molecules (Denning et al. 2003). Thus the FG Nups constituting a third of NPC mass, are important in nucleo-cytoplasmic transport.

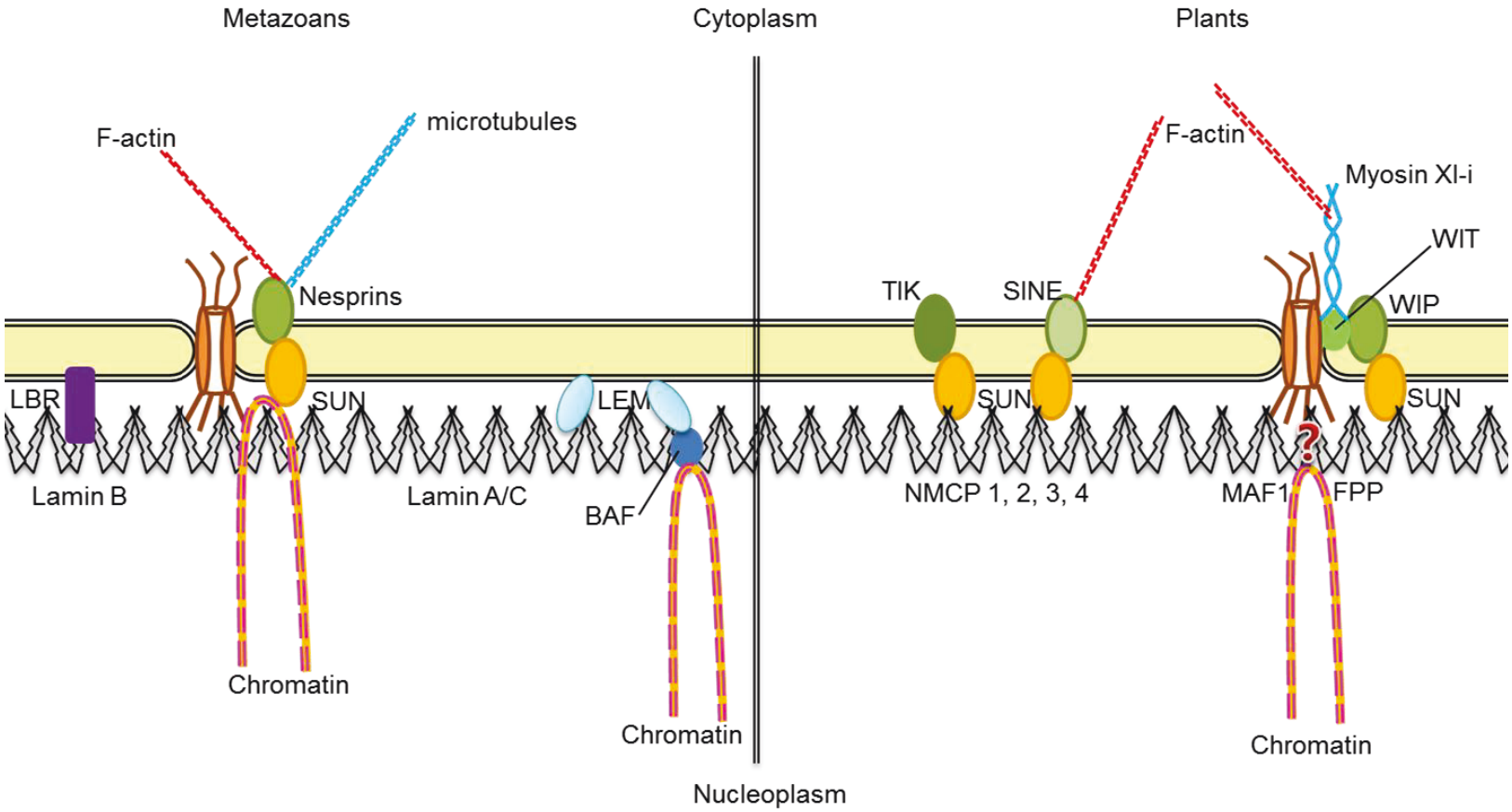

Figure 1.2: Protein components of the metazoan and plant NE. SUN domain proteins are conserved in both kingdoms. Nesprins, the metazoan KASH proteins have extensive cytoskeletal binding domains. Plant KASH proteins (WIP, SINE and TIK) bind SUN domain proteins. WIP binds WIT, which associates with the tail of myosin XI-i (described in section 1.1.5). SINE proteins also interact with F-actin. The lamins, LEM domain proteins, BAF and LBR form components of the metazoan lamina, SUN proteins and BAF associate with chromatin in metazoans. The NMCP proteins form part of the lamina in plants (described in section 1.2.6). MAF1 and FPP proteins have been suggested to be associated with the plant lamina (section 1.2.7).

The inner ring of the NPC constitutes the scaffold Nups while the outer ring that is attached to the equatorial plane of the NE is made up of membrane Nups.

Plant Nups share sequence similarity with both vertebrate and yeast Nups. However, until a proteomic study identified 30 Nups in *A. thaliana*, only 8 plant Nups had previously been described (Tamura et al. 2010). This study showed that sequences of plant Nups are more similar to vertebrates than yeast. Plants contain a sequence homologue to the vertebrate pore domain component, gp210 which anchors NPCs to the membrane and is not found in yeast. Similarly vertebrate WD-repeat Nups, Aladin and Nup43 have homologues in plants but not yeast, and have been suggested to be important for multiprotein assembly (Tamura et al. 2010). However, higher plants lack homologues to seven vertebrate proteins, Nup358, Nup188, Nup153, Nup45, Nup37, NDC1, and Pom121 (Figure 1.3). Nup358 anchors RanGAP to the NE, a function substituted by the WIT-WIP complexes in plants (Xu et al. 2007, Hutten et al. 2008).

1.3.2 Nucleo-cytoplasmic transport

The NPC is a bi-directional transport channel guarding the movement of molecules in and out of the nucleus. Molecules less than 40 kDa or 5nm diameters diffuse freely across the central channel of the NPC (Mohr et al. 2009). Larger molecules are shuttled across the NPC channel by cargo receptor molecules called karyopherins in an energy-dependent manner. The NPC is capable of transporting cargo as big as about 39nm in diameter as in case of intact ribosomal subunits and viral capsids (Pante and Kann 2002). Messenger ribo-nucleoprotein complexes which are larger than 50nm in diameter are also efficiently transported across the NPC following their rearrangement in smaller ~25 nm structures (Daneholt 2001). Cargo is selected for transport on the basis of its ability to bind FG repeat containing Nups either directly or via karyopherins (Tran et al. 2014).

Karyopherins contain the tandem HEAT (Huntingtin, elongation factor 3, protein phosphatase 2A and PI3-kinase TOR1) repeats which bind cargo, Ran and the FG Nups (Macara 2001, Harel and Forbes 2004). Karyopherin-cargo binding is mediated by the presence of NLS and nuclear export signals (NES) on cargo

molecules (Tran et al. 2014). Karyopherins are classified as importins and exportins depending on the direction of transport. The directionality of transport is determined by a gradient of the two hydrolysed states of Ran maintained across the NE; Ran GDP on the cytoplasmic side and Ran GTP on the nucleoplasmic side (Tamura and Hara-Nishimura 2014). NLS containing cargo binds importin α in the absence of Ran GTP in the cytoplasm, which forms a trimeric complex with importin β (Wozniak et al. 1998, Chook and Blobel 2001). Importin β binds FG repeat domains of NUPs allowing transport of the complex to the nucleoplasm, where RanGTP binds to the complex causing release of the cargo into the nucleus. The Importin α/β-RanGTP complex is recycled back to the cytoplasm where RanGTP is hydrolysed re-allowing binding of cargo. On the other hand, exportins bind NESs on export cargo in the presence of RanGTP in the nucleoplasm (Azuma and Dasso 2000, Macara 2001, Smith et al. 2002, Quimby and Dasso 2003, Weis 2003). Similar to importin β, by binding FG NUPs exportins translocate the exportin-cargo-RanGTP complex to the cytoplasm and release the cargo post GTP hydrolysis in a cyclical manner (Rose and Meier 2001).

1.3.3 NPC association with nucleoskeleton-cytoskeleton bridges

The functions of NPCs are not limited to cargo trafficking, they also perform important roles in nuclear morphology, chromatin architecture and gene regulation by associating with nucleoskeleton-cytoskeleton bridges of the NE. Similar to metazoans, NPCs in plants are seen distributed non randomly into rows on the NE surface (Aaronson and Blobel 1975, Goldberg and Allen 1996, Maeshima et al. 2006). Metazoan NPCs are interconnected and form immobile arrays associated with the nuclear lamina (Goldberg and Allen 1996, Daigle et al. 2001). In *C. elegans*, the nuclear lamina is important for spatial distribution of NPCs on the NE (Liu et al. 2000). Lamin mutant NEs in drosophila show defective NPC distribution leading to abnormal clustering of NPCs (Lenz-Bohme et al. 1997). These functions are mediated by a nuclear basket protein, Nup153 which interacts with the lamina and participates in NPC anchoring and distribution (Smythe et al. 2000, Walther et al. 2001). In mammals, SUN1

interacts with NPCs and is also important for NPC distribution at the NE (Liu et al. 2007).

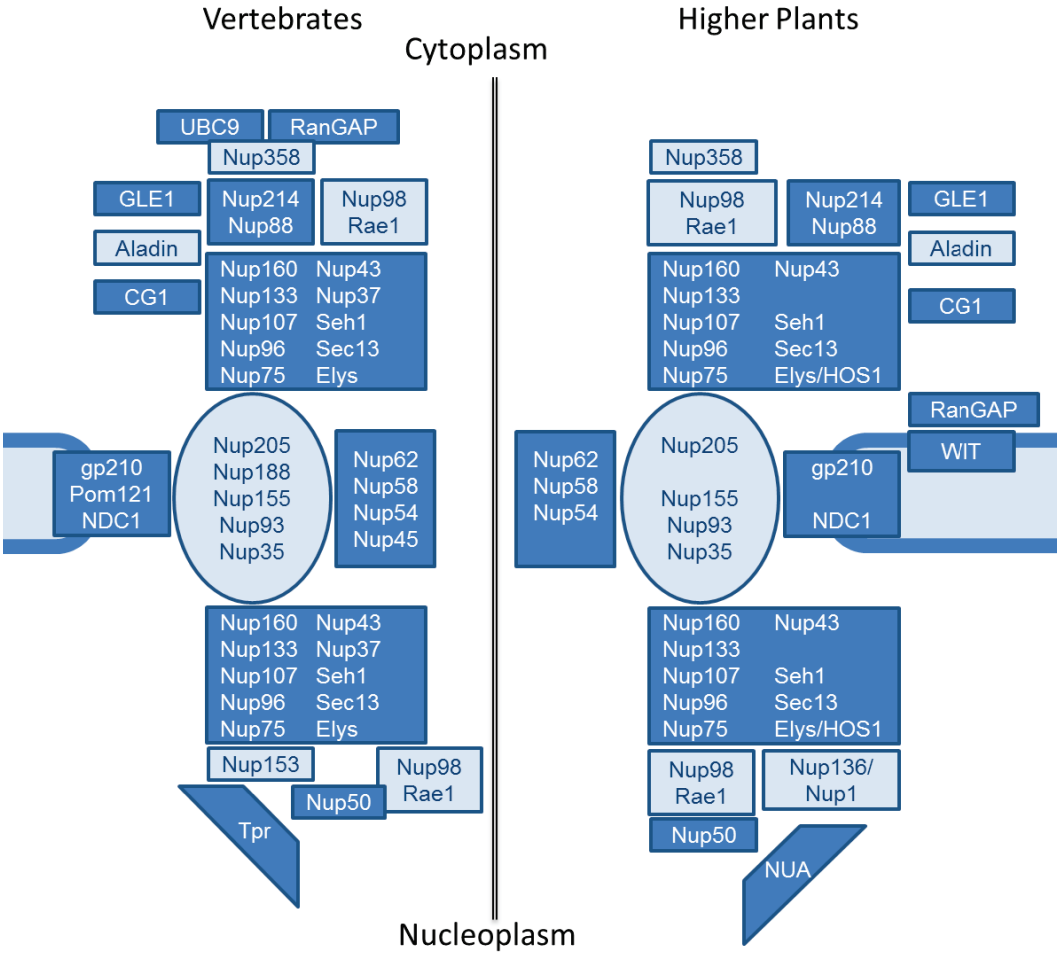

Figure 1.3: Comparison of protein components of plant and vertebrate NPCs adapted from Zhou et al. 2013. Proteins belonging to sub-complexes are grouped in the different shapes and placed according to their localisation at the NPC.

Similar to metazoans, nucleoplasmic rings of the NPC in plants are seen attached to the filamentous lamina network (Fiserova et al. 2009). Filamentous proteins of the nuclear pore basket, mammalian translocated promoter region (tpr) and its yeast homologues, myosin-like proteins1 and 2 (mlp) function in interaction with chromatin and the mitotic spindle, as well as gene silencing (Niepel et al. 2005, Vinciguerra et al. 2005, Nakano et al. 2010). The *A. thaliana* homologue of tpr/mlp proteins, nuclear pore anchor (NUA) has also been implicated in mitotic spindle assembly (Ding et al. 2012).

A plant specific nucleoporin, Nup136 has been implicated in defects in nuclear morphology, pollen development and flowering time (Tamura et al. 2010).

Nup136 mutant nuclei were significantly more circular than WT nuclei whereas Nup136 overexpressing nuclei were highly elongated compared to WT nuclei (Tamura et al. 2010, Tamura and Hara-Nishimura 2011). Thus Nup136 has been suggested to be the functional analogue of the metazoan Nup153. Nup160 and Nup88 have also been shown to have functions in maintaining normal nuclear morphology (Tamura et al. 2015). Although these suggest association of Nup136, Nup160 and Nup188 with the nuclear lamina, they havenot yet been shown to interact directly or indirectly with proteins of the plant lamina or INM.

1.4 Aims

This research focusses on characterisation of a novel family of NEAP proteins in *A. thaliana*. Some members of this family have been described previously; first to be described were AtNEAP1 encoded by At3g05830 and AtNEAP2 encoded by At5g26770 (Lu 2011). AtNEAP1 was first identified in a Bioinformatics screen for KASH-like proteins, containing CC regions, an NLS and a TM domain (Graumann, unpublished). AtNEAP2 was identified due to its 72% sequence similarity and AtNEAP3 encoded by At1g09470 was identified to have 50% sequence similarity to AtNEAP1 (Graumann, unpublished). AtNEAP1 localises to the NE, and was co-localised with AtSUN1 in transient expressing tobacco leaf epidermal cells (Lu 2011). This study also found that despite a predicted TM domain, AtNEAP1 was not intrinsic to NE membranes and was isolated from the soluble fraction in a TritonX-110 membrane protein segregating assay (Lu 2011). AtNEAP1 localisation at the NE however, remains unexplained in the absence of an active TM domain. Whether AtNEAP1 is a plant KASH protein and has any interaction partners at the NE is not known. Knowledge about the NEAP family is limited, with little or no indication of its function *in planta*. The aims of this study were to characterise the NEAP family and elucidate its functions. Several approaches were implemented towards fulfilment of this goal.

Firstly, a bioinformatics based analysis of protein sequences of family members was performed with the aim of understanding evolutionary relationships and phylogeny of the protein family within sequenced plant and non-plant genomes.

Predictions of features like the CC, NLS and TM domains were made in order to explore putative protein functions. Further conserved regions of these predicted domains were deleted from NEAP proteins to probe the hypothesis of those predictions.

The second aim was to study protein expression *in planta* and confirm its NE localisation within the cell. Protein expression arrays containing NEAP cDNA clusters were analysed to examine NEAP expression in plant tissues at different stages of development. In order to verify their NE association, localisation of FP tagged AtNEAP proteins was undertaken in stable and transient expression systems in *Nicotiana benthamiana* (Domin) using confocal microscopy. The strength of their membrane association was tested using a confocal microscopy technique fluorescence recovery after photo-bleaching (FRAP), described in Chapter 2 (section 2.5.2).

The third objective was to study interaction of AtNEAP proteins with other NE proteins; this was done using a confocal microscopy technique acceptor photo-bleaching fluorescence resonance energy transfer (apFRET) and a split-ubiquitin membrane based yeast two hybrid (MYTH) assay. Both techniques are described in Chapter 2 (sections 2.5.3 and 2.6). An *A. thaliana* cDNA library was screened using the MYTH assay, with the goal of identification of novel NEAP interacting partners (Chapter 2, section 2.6.3).

To achieve the final aim of understanding NEAP function *in planta,* NEAP mutants were analysed to identify changes in phenotype and morphology. *A. thaliana* plants with single NEAP mutations were characterised and crossed to generate double, triple and quadruple mutants in order to tackle functional redundancy within the family (T-DNA mutants are described in Chapter 2, table 2.2).

Chapter 2

Materials and Methods

Chapter 2

Materials and Methods

Most plastic consumables were sourced from Fisher Scientific (Loughborough, UK), Greiner Bio-One (San Diego, US), Sigma (Dorset, UK) and SLS (Hessle, UK) unless otherwise stated.

2.1.1 Bacterial strains

All cloning was performed in *Esherichia coli* using the chemically competent high efficiency strain DH5α called NEB 5α (NEB, Hitchin, UK). The DB3.1 strain of *E.coli*, was used to propagate empty gateway entry plasmids containing the lethal *ccdB* gene (Bernard and Couturier 1992). Chemically competent *Agrobacterium tumefaciens* strain GV3101 was used for sub cloning of binary vectors, followed by plant transformation. The GV3101 strain was resistant to rifampamycin and gentamycin (see table 2.1 for all antibiotic concentrations used in this study.

Table 2.1: List of antibiotics and concentrations used in bacterial and plant media.

Antibiotic	Concentration (µg/mL)
Basta	10
Gentamycin	10
Hygromycin B	50
Kanamycin	100
Rifampamycin	25
Spectinomycin	50
Sulphadiazine	7.5

2.1.2 Bacterial growth and media

The *E.coli* strains were grown in Lysogeny broth (LB) medium (10 g/L Bacto-tryptone, 5 g/L yeast extract, 10 g/L Sodium chloride in distilled water (DW) pH 7.5 ± 1% w/v agar) as broth in shaking cultures overnight or on agar plates (9 cm diameter) as solid colonies at 37°C for 24 hours. *A. tumefaciens* were grown in yeast extract broth (YEB) medium (5 g/L tryptone, 1 g/L yeast extract, 5 g/L

nutrient broth, 5 g/L sucrose, 0.49 g/L MgSO4·7H2O in DW pH 7.2 ± 1% w/v agar) as broth in shaking cultures over night or on agar plates (9 cm diameter) as solid colonies for 48 hours, both at 28°C. Glycerol stabs of *E.coli* and *A. tumefaciens* were prepared by mixing cell cultures with 100% glycerol in a 1:1 ratio for long term storage at -80C.

2.1.3 *E. coli* transformation

A tube containing 50 µL NEB5α competent *E. coli* cells were thawed on ice for 10 minutes. 1-5 µl of 1 pg - 100 ng plasmid DNA was added to the cells and mixed by flicking the tube 5 times and was left on ice for 30 minutes. Cells were heat shocked at 42°C for 1 minute and placed immediately on ice for 5 minutes. Cells were then suspended in 950 µl of SOC medium (NEB) and placed in an incubator shaking at 250 rpm for 1 hour at 37°C. The required selection plates were allowed to warm to 37°C. 10 µl, 20 µl and 40 µl of the cell suspension was spread on three separate plates and allowed to grow overnight at 37°C. Isolated colonies were picked and a colony polymerase chain reaction (PCR, section 2.3.5) was performed to confirm presence of the cloned product. Positive colonies were cultured overnight and used to make glycerol stocks by mixing cell culture with 100% glycerol in a 1:1 ratio. This mixture was then snap frozen in liquid nitrogen and stored at -80°C. Plasmid DNA was extracted from positive colonies (section 2.3.10) and used for transformation into *A. tumefaciens* described in section 2.1.4 below.

2.1.4 Transformation of *A. tumefaciens*

For all cloning a chemically competent strain of *A. tumefaciens* called GV3101 was used. To a tube containing 100 µL competent GV3101 cells, 1-5 µl of 500 ng - 1000 ng plasmid DNA was added. The mixture was left on ice for 5 minutes, followed by 5 minutes in liquid nitrogen. Cells were heat shocked at 37°C for 5 minutes. Cells were then transferred to 2 mL tubes containing 1 mL liquid YEB medium and placed in an incubator shaking at 250 rpm for 2-4 hours at 28°C. 250 µl and 500 µl of the cell suspension was spread on two YEB selection plates and allowed to grow at 28°C for 2 days. Isolated colonies were picked and the presence of cloned product was confirmed using colony PCR

(section 2.3.5). Positive colonies were grown in liquid culture overnight and infiltrated into *N. benthamiana* to check for expression of the desired gene *in planta* (section 2.2.5). Cultures of colonies that expressed successfully *in planta* were used for making glycerol stocks and stored at -80°C (section 2.1.3).

2.2.1 Seed stock

Previous laboratory seed stocks of WT *A. thaliana* (ecotype: Columbia-0) and WT *N. benthamiana* were provided by Dr. Katja Graumann (Oxford Brookes University, UK) and Dr. Jennifer Schoberer (University of Natural Resources and Life Sciences, Vienna), respectively. All *A. thaliana* transfer (T)-DNA insertion lines were ordered from the European *Arabidopsis* Stock Centre (Nottingham, UK) or Arabidopsis Biological Resource Centre (ABRC, Ohio, USA), with the exception of the GABI-kat lines which were ordered from Bielefeld University (Germany). All T-DNA lines were of the ecotype Col-0 and are listed in table 2.2. Seeds were stored in sterile 1.5mL tubes in a dry place at room temperature.

Table 2.2: List of *A. thaliana* T-DNA mutant lines and their antibiotic resistance

Gene	Name	NASC number	Insertion site	Antibiotic resistance*
AtNEAP1	SAIL_846_B07	CS837770	Intron	basta
AtNEAP2	SALK_012087	N512087	Intron	kanamycin
AtNEAP2	WiscDsLoxHs194_12D	N918612	5'UTR	kanamycin
AtNEAP2	GABI_589B02	NA	5'UTR	sulphadiazine
AtNEAP2	GABI_178C02	NA	Intron	sulphadiazine
AtNEAP3	WiscDsLoxHs086_02C	N908171	Exon	kanamycin
AtNEAP4	SAIL_1239_G02	N861633	Intron	basta
AtbZIP18	SAIL_592_A12	N825194	Intron	basta
AtbZIP18	WiscDsLoxHs073_05E	CS906949	Exon	kanamycin

* Antibiotics concentration see table 2.1

2.2.2 Seed germination and plant growth

A. thaliana seeds were surface sterilised using a bleach solution containing 10% (v/v) 1N Sodium Hypochlorite (VWR, Leicestershire, UK) and 0.02% Tween 20 prior to sowing. Seeds were sterilised by shaking them in the bleach solution for 15 min and rinsing out the bleach thoroughly with three washes using sterile water.

Sterilised seeds were sown on ½ Murashige and Skoog (MS, Sigma) medium, pH 5.7 with 0.6% agar on 15 cm diameter petri plates and stratified in the dark for more than 48 hours at 4^0C. Stratification allows breaking seed dormancy by using cold and moist environment to simulate winter conditions. Transgenic *A. thaliana* seeds were sown on ½ MS agar supplemented with appropriate antibiotics (table 2.1). Seeds were then allowed to germinate and grow in long day conditions of 16 hours light at 21^0C and 8 hours in dark at 18^0C. 10-12 days old seedlings were transplanted on Levington F2S compost mixed with perlite for aeration and pre-treated with 0.2 g/L Intercept 70WG (Everris, Ipswich, UK) in 5 x 5 cm pots. To minimise transplantation shock, the seedlings were planted on thoroughly wet soil, covered with a lid to mimic humidity conditions on the MS agar plates and continued to grow in long day conditions. The flowers and siliques were kept contained in well aerated plastic cones (Lehle Seeds, Round Rock, USA) and seeds were harvested when all siliques were thoroughly dried.

N. benthamiana plants were grown on the same media, soil and long day conditions described above for *A. thaliana*. *N. benthamiana* seeds were germinated without surface sterilisation and transferred to soil in 9 x 9 cm pots after a week and used for infiltration after 4 to 5 weeks growth in the pots.

2.2.3 Crossing T-DNA lines

Under controlled greenhouse conditions with no wind and insect pollinators, *A. thaliana* is a self-pollinating species. In this study, several single mutant T-DNA lines were crossed to produce double and triple mutants to deal with redundancy of gene function. *A. thaliana* plants to be crossed were grown as

described in section 2.2.2. The mother plant was grown to a stage where it had a single floral stalk and few young flower buds. To aid visualisation of tiny floral parts an Optivisor optical glass binocular magnifier (Donegan Optical Company, Inc., Lenexa, USA) was used. All open flowers, buds with white tips, immature budding meristems and mature siliques were removed with a pair of forceps so that three to four buds remained for emasculation. The remaining flower buds were emasculated by first splitting the petals and sepals and then picking them out carefully along with all anthers. The mother plant was then pollinated using a mature flower from the father plant, by tapping the anthers on the style with the pollen visibly covering the stigma. This was repeated for all floral buds, and every floral bud was re-pollinated after 24 hours with other flowers from the same father plant. Crossed buds were marked by tying coloured threads around them for identification. Once mature, a small (approximately 7 cm^2) glazed bag was tied around individual siliques and they were allowed to dry inside the bag before collection. Hybrid seeds, expected to be heterozygous for both mutations from their homozygous parents were allowed to self, and their progeny was genotyped for identification of the homozygous double mutant line. Further triple and quadruple mutant lines can also be generated by crossing a double homozygous mutant line with a single or double homozygous mutant line respectively.

2.2.4 Primary root growth assay

A primary root growth assay was designed to study the effects of constituent mutations of *A. thaliana* T-DNA lines on root growth. All *neap* mutant lines to be studied were germinated alongside WT Col-0 seeds on square shaped ½ MS agar plates. Plates were placed perpendicular in standard long day conditions to allow gravitropic growth of roots. It was important that WT and mutant seeds were of similar age and treated identically before germination as well as sown on the same plate in order to keep all conditions consistent during and post germination. Plates were scanned every 24 hours for 1 to 8 days. Germination rate was calculated as the percentage of seeds germinated. The length of the primary root was measured using Image J analysis software. Average root length of 30 seedlings was calculated for both WT and T-DNA lines for 1 to 8

days and was compared by unpaired t test. A p value of 0.05 or less was considered significant. The primary root length assay was repeated 3 times for each mutant line alongside WT.

2.2.5 Transient transformation

Leaves of *N. benthamiana* plants were infiltrated with transgenic *A. tumefaciens* containing a binary plasmid for transient transformation using a protocol adapted from Sparkes et al. (2006). One mL of *A. tumefaciens* grown overnight to stationary phase were spun down for 3 minutes at 8000 rpm and the pellet was re-suspended in 1 mL infiltration buffer containing 5% D-glucose, 50 mM MES hydrate, 2 mM Sodium orthophosphate and 0.1 M acetosyringone in distilled water. *A. tumefaciens* cells were washed by centrifugation for 3 minutes at 8000 rpm and re-suspended in 1 mL infiltration buffer. The optical density (OD) of this cell suspension was measured using a nanodrop spectophotometer (Thermoscientific, Basingstoke, UK) and the absorption value at 600 nm was multiplied by a constant factor of 10 for further calculations. Depending on different constructs, *A. tumefaciens* were diluted using infiltration buffer to OD's ranging from 0.03 to 0.1 to be used for transformation. All NEAP-FP fusions were infiltrated at an OD of 0.1, SUN-FP fusions were infiltrated at an OD of 0.03 alongside p19 at an OD of 0.05. A list of constructs is provided in section 2.3.8.

Five to six week old *N. benthamiana* plants were used for transformation. Two plants were transferred from the greenhouse and kept overnight in long day conditions. On the day of transformation, plants were kept under a sodium light source for 1-2 hours to allow opening of the stomata in response to light. Leaf sections were infiltrated on each of the two plants by gently injecting diluted agro-bacterial suspension via fine bores made on the lower side of the leaf with a needle. Infiltration of leaf margins or apex was avoided, and if more than one construct was infiltrated care was taken to make sure the constructs were well separated by the midrib. Infiltrated plants were watered and allowed to grow in long day conditions for 2-3 days. One leaf section per plant was infiltrated in a total of two plants for confocal microscopy (section 2.5.1). Three to five leaves

on two or more plants were infiltrated per construct for protein extraction (section 2.4.1). Expression was checked using confocal microscopy 2-3 days after infiltration (section 2.5.1).

2.3.1 List of Primers

All primers were ordered from Invitrogen, Life Technologies Ltd (Paisley, UK). All primers for cloning were designed using the coding DNA sequence (CDS) beginning with the start codon and ending before the STOP codon. The CDS were obtained from the Arabidopsis information resource (TAIR; www.arabidopsis.org). Primers were designed to have a melting temperature (T_m) of about 45°C using the formula; T_m = 3(GC) + 2(AT); so that their annealing temperatures were between 50 to 55°C. The same were also used for semi-quantitative reverse transcriptase – polymerase chain reaction (qRT-PCR). Genomic DNA (gDNA) sequences were used to design primers for genotyping of *A. thaliana* T-DNA lines using a program available on http://signal.salk.edu/tdnaprimers.2.html. All CDS primers that were also used for sequencing are listed in table 2.3 and genotyping primers are listed in table 2.4.

Table 2.3: CDS template primers for AtNEAP and AtbZIP18 including their Tm and sequences

Primer name	Forward/ Reverse	Primer description	Tm (˚C)	Sequence
FNEAP1 (FTL5)	F	binds first 24 bp of AtNEAP1	63	ATGTCTTATTCTGAAAAAACGACG
RNEAP1 (RTL5)	R	binds last 24 bp of AtNEAP1 (minus stop)	56	TCTCTTGGAGACTACCACTAACAT
RT_FNEAP1	F	binds bp 150-177 spanning the first intron of AtNEAP1	54	GAGACCATTACTAGAAAAGAAGCAGAG
RT_RNEAP1	R	binds bp 834-857 spanning the last intron of AtNEAP1	54	CAACAACAATAAAACCTCTGCAGC
FNEAP2	F	binds first 25 bp of AtNEAP2	63	ATGTCGGATTCCGTCAAAACGACGG
RNEAP2	R	binds last 25 bp of AtNEAP2 (minus STOP)	56	TCTTTTGGAGATAATAACTAATATC
FNEAP3	F	binds first 20 bp of AtNEAP3	48	ATGCCAACTTCTGTTAGTCT
RNEAP3	R	binds last 19 bp of AtNEAP3 (minus STOP)	47	ACGCCTAGAAAACGCAACT
FN3dCC1a	F	binds bp 280 to 299 of NEAP3, CC1 ends at 279	47	TTTGTGAAGGAATTGGCTG
FN3dCC1b	F	same as FN3dCC1a but adds beginning of NEAP3 as overhang	47	ATGCCAACTTCTGTTAGTCTAAGAGAGGATGATCCT-TTTGTGAAGGAATTGGCTG
RN3dCC2a	R	binds bp 351 to 369 of NEAP3, CC2 starts at 370	49	ATGTGCTGATTCAGCTGAC
RN3dCC2b	R	same as RN3dCC2a, but adds region after CC2 as overhang	49	GGTCTTGACCACTGATAC-ATGTGCTGATTCAGCTGAC
FN3dCC2a	F	binds bp 556 to 574 of NEAP3, CC2 ends at 555	48	GTATCAGTGGTCAAGACC
FN3dCC2b	F	same as FN3dCC2a, but adds region before CC2 as overhang	48	GTCAGCTGAATCAGCACAT-GTATCAGTGGTCAAGACC
RN3dNLSa	R	binds bp 701 to 718, NLS starts at 719	49	AAACCTCCAGTGAGCCG
RN3dNLSb	R	same as RN3dNLSa, but adds region after NLS as overhang	49	CTTGTATTGCCACATCGTT-AAACCTCCAGTGAGCCG
FN3dNLSa	F	binds bp 856 to 875 of NEAP3, NLS ends at 855	47	AACGATGTGGCAATACAAG

Table 2.3 continued.

Primer name	Forward/ Reverse	Primer description	Tm (˚C)	Sequence
FN3dNLSb	F	same as FN3dNLSa, but adds region before NLS as overhang	47	CGGCTCACTGGAGGTTT-AACGATGTGGCAATACAAG
RN3dTMa	R	binds bp 913 to 933 of NEAP3, TM domain starts at 934	50	TTGGTTGCTAGAATGATCAGC
RN3dTMb	R	same as RN3dTMa, but adds last 12 bp after TM as overhang	50	ACGCCTAGAAAA-TTGGTTGCTAGAATGATCAGC
GWRN3dTM	R	GW primer binds end of delTM sequence cloned using RN3dTMa &b, adds attB2 sequence	50	GGGGACCACTTTGTACAAGAAAGCTGGGTC-ACGCCTAGAAAATTGGTTGC
FNEAP4	F	binds bp 1 - 18 of AtNEAP4	57	ATGTCGGCTCATTGGACG
RNEAP4	R	binds bp 316 - 336 of AtNEAP4	56	ATGATCAAGACTTGAACCACG
RNEAP4a	R	binds bp 308 - 329 of AtNEAP4	58	AGACTTGAACCACGTAATCCAC
attL1_FNEAP4	F	gateway primer, binds bp1 to 20 of AtNEAP4 with attB1 sequence	60	GGGGACAAGTTTGTACAAAAAAGCAGGCTTCCCGCCA-ATGTCGGCTCATTGGACGTT
RNEAP4_attL2	R	gateway primer, binds last 27 of AtNEAP4 with attB2 sequence	60	GGGGACCACTTTGTACAAGAAAGCTGGGTC-ATGATCAAGACTTGAACCACGTAATCC
FbZIP18	F	binds bp 1 to 21 of bZIP18	60	ATGGAGGATCCTTCTAACCCACA
RbZIP18	R	binds last 23 bp of bZIP18 (minus STOP)	57	AGTGCTGCTGCTTTCACTGAC
attL1_FbZIP	F	gateway primer, binds bp1 to 23 of AtbZIP18 with attB1 sequence	61	GGGGACAAGTTTGTACAAAAAAGCAGGCTTCCCGCCA-ATGGAGGATCCTTCTAACCCACA
RbZIP_attL2	R	gateway primer, binds last 20 bp of AtbZIP18 with attB2 sequence	61	GGGGACCACTTTGTACAAGAAAGCTGGGTC-CATAGTGCTGCTGCTTTCAC

Table 2.4: gDNA template primers for genotyping of T-DNA lines including their Tm and sequences

Primer name	Forward/ Reverse	Primer description	Tm (˚C)	Sequence
LPNEAP1	F	NEAP1_SAIL846_B07	49	CTCTGCAGCTTTCTTGTCTGG
RPNEAP1	R	NEAP1_SAIL846_B07	47	AGCTTGAAGCTTCTGCATCTG
LB3_SAIL	F	SAIL left border	55	TAGCATCTGAATTTCATAACCAATCTCGATACAC
LPNEAP2	F	NEAP2_SALK_012087	43	TTTGATTCGATGCTTATGCAG
RPNEAP2	R	NEAP2_SALK_012087	47	AGAAGCAGCACTTGTTTCTGC
LBb1.3_SALK	F	SALK left border	42	ATTTTGCCGATTTCGGAAC
Wisc_LPNEAP2	F	WiscDsLoxHs194_12D	47	TACCATATCAGAGCGGGATTG
Wisc_RPNEAP2	R	WiscDsLoxHs194_12D	45	TTGTTGCTCGAACTGTTGTTG
WiscHS_LB	F	WiscDsLoxHs left border	55	TGATCCATGTAGATTTCCCGGACATGAAG
178C02_LPN2a	F	NEAP2_GABI178C02: insertion:chr5 9409102	47	TGCACCTGAGATTCAAGTTCC
178C02_RPN2a	R	NEAP2_GABI178C02: insertion:chr5 9409102	48	TGCTTTGGTAGGGTCAGAAATC
178C02_LPN2b	F	NEAP2_GABI178C02: insertion:chr5 9409081	43	CGCTTTTGAAAGATTTGGATG
178C02_RPN2b	R	NEAP2_GABI178C02: insertion:chr5 9409081	49	GCTTCAGTTATCTCACGCTCG
589B02_LPN2a	F	NEAP2_GABI_589B02: insertion:chr5 9409811	45	AAAGGGCCATTGATTACCAAG
589B02_RPN2a	R	NEAP2_GABI_589B02: insertion:chr5 9409811	45	AGAAATTCGGAAGGGAAAGAC
589B02_LPN2b	F	NEAP2_GABI_589B02: insertion:chr5 9409738	47	AGCGAGGTTTTAGACTTTCCG
589B02_RPN2b	R	NEAP2_GABI_589B02: insertion:chr5 9409738	47	CCTTTTCAGCAGCAGAAGTTG
GABI_8474	F	GABI right border	50	ATAATAACGCTGCGGACATCTACATTTT
LPNEAP3	F	NEAP3_WiscDsLoxHs086_02C	50	TTCCTACCAAACCCAGAAACC
RPNEAP3	R	NEAP3_WiscDsLoxHs086_02C	50	TCAGCCAATTCCTTCACAAAC
LPNEAP4	F	NEAP4_SAIL_1239_G02	50	TTCACTCCAATGAAATCGAGC
RPNEAP4	R	NEAP4_SAIL_1239_G02	50	TTGTTCTTCTGGATCAGGTGG
LPbZIP_SAIL	F	bZIP18_SAIL_592_A12	47	CGCAACTTAGCTTGTTGTTCC
RPbZIP_SAIL	R	bZIP18_SAIL_592_A12	51	GAGACCTCGACACAGGCATAG
LPbZIP_WISC	F	bZIP18_WiscDsLoxHs073_05E	47	CTCTCGGATGATTCTTTGGTG
RPbZIP_WISC	R	bZIP18_WiscDsLoxHs073_05E	45	AAAATGAATCCGACTGTCACG

2.3.2 Genomic DNA extraction

gDNA was extracted from *A. thaliana* rosette leaves for genotyping. A 1.5 mL Eppendorf tube was closed over two rosette leaves to obtain two leaf discs. In the same tube a 3 mm tungsten carbide bead (QIAGEN, Manchester, UK) was added along with 400 µL gDNA extraction buffer (Table 2.5).

Table 2.5: Constituents of the gDNA extraction buffer

gDNA Extraction Buffer		Stock
200mM Tris HCl pH 7.5	2 mL	1 M
250mM NaCl	5 mL	0.5 M
25mM EDTA	0.5 mL	0.5 M
0.5% SDS	0.5 mL	10%
Sterile DW	Make up to 10 mL	

This tube containing the leaf discs, bead and buffer were homogenised for 1 min at 25 Hz in the QIAGEN Tissue LyserII (QIAGEN, Manchester, UK). Then the tubes were turned upside down in the QIAGEN Tissue LyserII and homogenised again for another minute at 25 Hz. Up to 24 samples could be processed in the QIAGEN Tissue LyserII at once. Samples were then centrifuged at 13000 rpm for 5 min at room temperature. 300 µL of supernatant was removed without disturbing the pellet and added to 300 µL of 100% isopropanol in new tubes. Tubes were left for about 10 minutes to overnight at room temperature for precipitation. Tubes were then centrifuged at 13000 rpm for 15 min at room temperature. The supernatant was removed and the pellets were washed by re-suspending in 400 µL of 70% ethanol. Tubes were centrifuged at 13000 rpm for 10 minutes at room temperature. The supernatant was discarded and the pellets were allowed to dry on a heat block at 50°C for 15 min. As alcohol inhibits PCR, complete removal and evaporation of the ethanol was important as the gDNA was to be used in a PCR reaction. Dry pellets were then dissolved in 100 µL nuclease-free water. 5 µL of this gDNA was used in a 25 µL PCR reaction (table 2.6). gDNA was stored for up to 4 weeks at 4°C and at -20°C for long term storage.

2.3.3 RNA extraction

Total RNA was extracted from 15-20 day old pooled WT A. thaliana seedlings using the RNeasy plant mini kit (QIAGEN, Manchester, UK). A maximum of 100 mg fresh leaf material was placed in RNase-free 2 mL tubes containing 1 stainless steel bead (3–7 mm mean diameter) along with 450 µl of Buffer RLC. The TissueLyser adapter sets were precooled by storing overnight at -80°C. The tissue was then homogenised for 1 min at 30 Hz. The adapter set was then disassembled and the rack of tubes was rotated. The homogenisation step was repeated for another minute at 30 Hz.

The homogenised plant tissue was added to a QIAshredder spin column (lilac) placed in a 2 ml collection tube, and centrifuged for 2 minutes at 13000 rpm. 400 µl of the supernatant of the flow-through was carefully transferred to a new tube without disturbing the cell-debris pellet in the collection tube. 200 µl of 100% ethanol was added to this supernatant and mixed immediately by pipetting. The sample was then transferred to an RNeasy spin column (pink) placed in a 2 mL collection tube and centrifuged for 15 s at 13000 rpm. The flow-through was discarded and the column was washed using 350 µl Buffer RW1 by centrifugation at 13000 rpm for 15 seconds.

In order to remove DNA contamination, a DNase digestion step was carried out in the column using the RNase-Free DNase Set (QIAGEN). 10 µl of DNase I solution diluted in 70 µl of Buffer RDD was added directly on to the column membrane and incubated at room temperature for 15 min. The column was then washed using 350 µl Buffer RW1 followed by 500 µl Buffer RPE at 13000 rpm for 15 seconds. A final wash step was performed using Buffer RPE to the column and centrifuging for 2 min at 13000 rpm. To ensure that no ethanol was carried over, the column was placed in a new 2 mL collection tube and centrifuged at full speed for 1 min. The column was then placed in a new 1.5 mL collection tube and RNA was eluted twice using 30 µl nuclease-free water for 1 min at 13000 rpm. RNA was stored as 10 µl aliquots in RNase free boxes at -80°C.

RNA yield and quality was assessed using the NanoDrop™ 1000 Spectrophotometer. RNA was quantified automatically using the formula that one O.D. at 260 nm was 40 ng/µl of RNA. RNA quality was measured as the ratio of absorbance at 260 nm/ 280 nm. A ratio of approximately 2.0 is considered as 'pure' for RNA. 500 ng (1-6 µl) of RNA was used for cDNA synthesis.

2.3.4 cDNA synthesis

cDNA was synthesised using the ProtoScript® M-MuLV First Strand cDNA Synthesis Kit (NEB). 500 ng (1-6 µl) of total RNA was mixed with 2 µl random primer mix (hexamers and d(T)23VN) in a sterile RNase-free 0.2 mL microfuge tubes. The same was repeated for a non-enzyme control that was treated exactly the same apart from non-addition of reverse transcriptase enzyme. The reaction volume was made up to 8 µl with nuclease-free water. RNA was denatured for 5 minutes at 70°C and transferred on ice immediately. 10 µl of M-MuLV reaction mix was added to both tubes. 2 µl of M-MuLV enzyme mix was added to the cDNA synthesis reaction but was replaced with nuclease-free water in the non-enzyme control. Tubes were incubated at 25°C for 5 min followed by 42°C for one hour to allow cDNA synthesis. The enzyme was then inactivated at 80°C for 5 minutes. cDNA reaction was diluted to 50 µl with 30 µl nuclease-free water for PCR. 1 to 2.5 µl of cDNA was used in the PCR reaction (tables 2.6 and 2.8). The cDNA product was stored at –20°C.

2.3.5 PCR

All PCRs, except those involving cloning were carried out using Crimson Taq Polymerase (NEB). Crimson Taq Polymerase reaction assembly is summarised in table 2.6, followed by cycling conditions in table 2.7. Gene cloning was carried out using the Q5® High-Fidelity DNA Polymerase (NEB). Q5® High-Fidelity DNA Polymerase reaction mix is summarised in table 2.8, followed by cycling conditions in table 2.9. A non-template control reaction was included at all times and a master mix containing no template DNA was prepared. PCRs were performed in a T100™ Thermal Cycler (Bio Rad, Hemel Hempstead, UK). PCR products were detected on agarose gels (section 2.3.6).

Table 2.6: PCR reaction assembly using Crimson Taq Polymerase.

Component	25 µl reaction	Final Concentration
Template DNA	variable *	
5X Reaction Buffer	5 µl	1X
10 mM dNTPs (NEB)	0.5 µl	200 µM
10 µM Forward Primer	0.5 µl	0.2 µM
10 µM Reverse Primer	0.5 µl	0.2 µM
Crimson *Taq* DNA Polymerase	0.125 µl	1.25 units/50 µl PCR
Nuclease-free water	to 25 µl	

* template DNA: 2 µl of diluted cDNA/plasmid (<1 ng) for qRT-PCR, 5 µl gDNA (<1 µg) for genotyping. For colony PCR, the microbial colony was picked in 20 µl NFW, and microwaved at 800W for 1 minute. 5 µl of boiled colony was used as template.

Table 2.7: Thermocycling conditions for Crimson Taq PCR

Step	Temperature	Time
Initial Denaturation	95°C	30 seconds
30 Cycles	95°C	30 seconds
	50-55°C	30 seconds
	68°C	1 minute/kb
Final Extension	68°C	5 minutes
Hold	4°C	

Table 2.8 PCR reaction assembly using Q5® High-Fidelity DNA Polymerase

Component	25 µl Reaction	Final Concentration
5X Q5 Reaction Buffer	5 µl	1X
10 mM dNTPs (NEB)	0.5 µl	200 µM
10 µM Forward Primer	1.25 µl	0.5 µM
10 µM Reverse Primer	1.25 µl	0.5 µM
cDNA	2 µl	< 1 ng
Q5 High-Fidelity DNA Polymerase	0.25 µl	0.02 U/µl
Nuclease-free water	14.75 µl	

Table 2.9: Thermocycling conditions for Q5® High-Fidelity PCR

Step	Temperature	Time
Initial Denaturation	98°C	30 seconds
30 Cycles	98°C	10 seconds
	*60–72°C	30 seconds
	72°C	30 seconds/kb
Final Extension	72°C	2 minutes
Hold	4°C	

*NEB Tm Calculator was used for deciding annealing temperature.

2.3.6 Agarose gel electrophoresis

PCR products, gDNA and linearised plasmids were separated on 1.5 – 2 % agarose gels prepared in 1x Tris Acetate EDTA buffer (TAE: 40 mM Tris, 20 mM acetic acid and 1 mM EDTA). The agarose solution was heated in a microwave until the agarose polymerised and was allowed to cool to 50°C, before addition of 0.625 µg/ml of ethidium bromide (Thermoscientific) and pouring into a gel cast. In case of non-crimson PCR products, 5 – 10 µL of product was diluted in 6x gel loading dye (NEB), loaded into the agarose gel wells submerged in 1x TAE buffer. Alongside DNA samples, 6 µL of Quick load® 100 bp DNA ladder (NEB) was also loaded. The gel was run at 90 V until the dye front reached the end of the gel. DNA bands were imaged using a UV transilluminator (Ultra-Violet Products Ltd., Cambridge, UK) and Uvisave gel documentation camera (UVItec Ltd., Cambridge, UK).

2.3.7 PCR clean up

PCR products for cloning were purified using the Wizard® SV Gel and PCR Clean-Up System (Promega, Southampton, UK). The DNA band, separated by agarose gel electrophoresis (section 2.3.6) was sliced from the gel and dissolved by adding 10 µl membrane binding solution per 10 mg of gel and incubated at 50–65°C. The dissolved gel solution or the PCR reaction was added to a purification mini-column inserted into a collection tube and incubated at room temperature for 1 min to bind DNA. The column was centrifuged at 13000 rpm for 1 min and the flow through was discarded. The column was then washed by addition of wash solution and centrifugation at 13000 rpm for 1 min. The wash step was then repeated with 500 µl wash solution. Any contamination with ethanol from the wash solution was eliminated by centrifuging the empty column assembly for 1 min with the micro-centrifuge lid open. Finally DNA was eluted in a sterile tube by adding 50 µl of nuclease-free water and incubation at room temperature for 1 min, followed by centrifugation at 13000 rpm for 1 min. Purified DNA was used in further cloning steps and was stored at 4°C for a period or –20°C for long term storage.

2.3.8 List of cDNA clones

All available cDNA clones in gateway entry vectors and binary destination vectors have been listed in tables 2.10 and 2.11, respectively. All cDNA clones in gateway entry vectors and binary destination vectors constructed during this study have been listed in tables 2.12 and 2.13 respectively.

Table 2.10: Description of clones available in gateway entry vectors

Gateway entry vector with CDS	Bacterial resistance*	Origin
pDONOR207 NEAP1	gentamycin	Lu 2011
pENTRY-dTOPO NEAP2	kanamycin	Graumann, unpublished
pDONOR207 NEAP3	gentamycin	Graumann, unpublished
pDONOR207 SUN2ΔSUN (contains STOP)	gentamycin	Graumann et al. 2010a
pDONOR207 SUN2ΔCC (contains STOP)	gentamycin	Graumann et al. 2010a
pDONOR207 SUN2ΔN (contains STOP)	gentamycin	Graumann et al. 2010a
pENTRY223.1 bZIP18 (contains STOP)	spectinomycin	ABRC stock

* Antibiotics concentration see table 2.1

Table 2.11: List of clones available in gateway destination vectors

Construct	Destination Vector	Bacterial resistance*	Origin
35S-NEAP1-YFP	pCambia1300-casetteB	kanamycin	Lu 2011
35S-NEAP1-CFP	pK7CWG2	spectinomycin	Lu 2011
35S-YFP-NEAP1	pCambia1300-casetteA	kanamycin	Lu 2011
35S-CFP-NEAP1	pK7WGC2	spectinomycin	Lu 2011
35S-SUN1-YFP	pCambia1300-casetteB	kanamycin	Graumann et al. 2010a
35S-SUN2-YFP	pCambia1300-casetteB	kanamycin	Graumann et al. 2010a
35S-CFP-SUN2_264	pB7WGC2	spectinomycin	Graumann et al. 2010a
35S-LINC1-YFP-HA	pEarleyGate101	kanamycin	Dittmer et al. 2007
35S-p19	pBin19	kanamycin	NA

* Antibiotics concentration see table 2.1

Table 2.12: List of entry vectors constructed during this study in the gentamycin bacterial resistant pDONOR-207 gateway entry vector

Plasmid construct	Origin
pDONOR-207 NEAP3ΔCC	pDONOR207-NEAP3
pDONOR-207 NEAP3ΔNLS	pDONOR207-NEAP3
pDONOR-207NEAP3ΔTM	pDONOR207-NEAP3
pDONOR-207 SUN2ΔSUN (minus STOP)	pDONOR207 SUN2ΔSUN (contains STOP)
pDONOR-207 SUN2ΔCC (minus STOP)	pDONOR207 SUN2ΔCC (contains STOP)
pDONOR-207 SUN2ΔN (minus STOP)	pDONOR207 SUN2ΔN (contains STOP)
pDONOR-207 bZIP18 (contains STOP)	pENTRY223.1 bZIP18 (contains STOP)

Table 2.13: List of clones constructed in the binary destination vectors

Construct	Gateway destination Vector	Bacterial resistance*
35S-YFP-NEAP2	pB7WGY2	spectinomycin
35S-NEAP2-CFP	pK7CWG2	spectinomycin
35S-CFP-NEAP2	pK7WGC2	spectinomycin
35S-YFP-NEAP3	pB7WGY2	spectinomycin
35S-NEAP3-CFP	pK7CWG2	spectinomycin
35S-CFP-NEAP3	pK7WGC2	spectinomycin
35S-NEAP3ΔCC1-CFP	pK7CWG2	spectinomycin
35S-NEAP3ΔCC2-CFP	pK7CWG2	spectinomycin
35S-NEAP3ΔNLS-CFP	pK7CWG2	spectinomycin
35S-NEAP3ΔTM-CFP	pK7CWG2	spectinomycin
35S-YFP-NEAP3ΔCC1	pCambia1300-casetteA	kanamycin
35S-YFP-NEAP3ΔCC2	pCambia1300-casetteA	kanamycin
35S-YFP-NEAP3ΔNLS	pCambia1300-casetteA	kanamycin
35S-YFP-NEAP3ΔTM	pCambia1300-casetteA	kanamycin
35S-SUN2ΔSUN-YFP	pCambia1300-casetteB	kanamycin
35S-SUN2ΔCC-YFP	pCambia1300-casetteB	kanamycin
35S-SUN2ΔN-YFP	pCambia1300-casetteB	kanamycin
35S-YFP-bZIP18	pCambia1300-casetteA	Kanamycin

* Antibiotics concentration see table 2.1

2.3.9 Gateway cloning

The Gateway® cloning technology (Invitrogen, Life Technologies Ltd., Paisley, UK) used in this study involves a two-step cloning protocol based on the site-specific recombination of bacteriophage lambda (Landy, 1989). The first step, the BP reaction involves cloning the cDNA of interest into Gateway entry vector pDONOR207. The cDNA of interest is flanked with attB sequences (primers see table 2.3) on both sides, which allows recombination with the entry vector. AttB flanking sequences were added to cDNA using Q5® High-Fidelity PCR (section 2.3.5, tables 2.8 and 2.9). The PCR product was purified (section 2.3.7) and used in a BP reaction (table 2.14).

Table 2.14: BP reaction assembly

Components	Volume
attB-PCR product (100 ng)	1-7 µl
Donor vector (150 ng/µl)	1 µl
Nuclease-free water	up to 8 µl
BP Clonase™ II enzyme mix	2 µl
Incubate reactions at 25°C overnight	
Proteinase K	1 µl
Incubate samples at 37°C for 10 minutes	

1 µL of BP reaction product was used to transform 25 µL of NEB 5α (section 2.1.3), and transformed colonies containing the cDNA were selected on gentamycin. Untransformed bacteria and ones with empty pDONOR207 (due to the lethal CcdB gene) cannot grow on gentamycin. Colonies were picked for colony PCR (section 2.3.5) and following confirmation of desired clone, plasmid DNA was extracted (section 2.3.10). Plasmid DNA at this stage was sent for Sanger sequencing to Source Bioscience (Oxford, UK). Sequencing results were aligned with the CDS using Clustal Omega (http://www.ebi.ac.uk/Tools/msa/clustalo/) or in case of lack of alignment searched for identification against the *A. thaliana* databases in TAIR (https://www.arabidopsis.org/Blast/). The sequenced pDONOR207 vector containing the cDNA of interest was used in the second step of Gateway cloning called the LR reaction (table 2.15). The LR reaction allows recombination of the cDNA of interest into several destination vectors (table 2.13) that allows fusion of an FP tag at the C- or N- terminus.

Table 2.15: LR reaction assembly

Components	Volume
Entry clone (25 - 75 ng)	variable
Destination vector (75 ng/µL)	1 µl
Topoisomerase	0.5 µl
Nuclease-free water	up to 4 µl
LR Clonase™ II enzyme mix	1 µl
Incubate reactions at 25°C overnight	
Proteinase K	1 µl
Incubate samples at 37°C for 10 minutes	

1 µL of LR reaction was used to transform 25 µL of NEB 5α (section 2.1.3), and transformed colonies were selected on the relevant antibiotics (table 2.13). Similar to BP transformations, colony PCR was followed by plasmid extraction. Plasmid DNA was then used for transformation of *A. tumefaciens* (section 2.1.4) to be infiltrated into *N. benthamiana* (section 2.2.5).

2.3.10 Plasmid DNA extraction

Plasmid DNA was extracted using the Wizard® Plus SV Miniprep DNA Purification System (Promega) at room temperature. 10ml of overnight grown bacterial culture (section 2.1.2) were centrifuged at 5000 rpm for 5 min. Pellets were re-suspended in 250 µl of re-suspension solution. 250 µl of lysis solution was then added and mixed by inverting 4 times followed by addition of 10 µl of alkaline protease solution. After incubation for 5 min, 350 µl of neutralization solution was added and mixed by inversion. The cell lysate was then cleared by centrifugation at 13000 rpm for 10 min. The cleared lysate was then decanted into a miniprep spin column inserted into a collection tube and was centrifuged at 13000 rpm for 1 min. The flow through was discarded and the column was washed with wash solution, followed by centrifugation at 13000 rpm for 1 min. The wash step was then repeated with 250 µl of wash solution. Plasmid DNA was eluted by addition of 100 µl of nuclease-free water directly to the spin column inserted into a sterile tube and centrifugation at 13000 rpm for 1 min. Plasmid DNA was used in further cloning steps and transformations and was stored at –20°C.

2.4.1 Protein extraction

Total protein was extracted from infiltrated (section 2.2.5) and non-infiltrated *N. benthamiana* leaves. Prior to extraction, expression of proteins was checked two days post infiltration using confocal microscopy (section 2.5.1). Infiltrated areas of the *N. benthamiana* leaves were cut out to remove the non-infiltrated leaf margins, midrib and lateral veins. The cut out leaf material was immediately frozen in liquid nitrogen and ground in a mortar with a pestle, without allowing it to thaw. Ground material was collected and weighed in liquid nitrogen cooled

15 mL tubes. 1 mL of protein extraction buffer (table 2.16) was used per gram of frozen ground tissue.

Table 2.16: Constituents of protein extraction buffer

Components	To make 10mL	Stock used
100 mM Tris (pH6.8)	666 µL	1.5 M
4.5 M Urea	2.7 g	
1 M Thiourea	0.76 g	
2% CHAPS	0.2 g	
0.5% Triton X-100	0.05 g	
10mM DTT	100 µL	1 M
1% Sigma Protease Inhibitor Cocktail	100 µL	
Benzonase	5.2 µL	
PMSF	50 µL	0.2 M

Frozen tissue was kept in liquid nitrogen until all samples were ready to be vortexed and moved to a rotating shaker at 4°C for 1 h. Protein mixtures were centrifuged at 13000 rpm for 10 min at 4°C in 2 mL tubes. Supernatant was removed into a new microcentrifuge tube and the centrifugation was repeated. The final supernatant was then used for precipitation of proteins; any un-precipitated protein was stored at -80°C.

For precipitation of proteins ice cold acetone, protein solution and TCA were mixed in a 8:1:1 ratio, immediately mixing by inversion after each addition. Proteins were precipitated at -20°C overnight. After the precipitation, tubes were removed and spun down at 4°C for 15 min at 13000 rpm. The supernatant was discarded and pellets were washed with 1mL ice cold acetone and centrifuged at 13000 rpm for 10 min. This wash step was repeated with 500 µL ice cold acetone. Finally protein pellets were dried at room temperature for 45 minutes. For every 150 µL of protein suspension precipitated, the resultant pellet was re-suspended in 100 µL of 1xSDS gel loading buffer containing DTT (table 2.17).

Table 2.17: Constituents for 1x SDS gel loading buffer

Components	To make 20 mL	Stock used
62.5 mM Tris HCl, pH6.8	1.25 mL	1 M
25% glycerol (w/v)	5 g	
2% SDS	4 mL	10%
0.05% bromophenol blue	0.01 g	
8 M urea (optional)	9.6 g	
350 mM DTT (add just before use)	*	1 M

* 100 µL 1M DTT to 180 µL buffer prepared above

Protein solutions in 1x gel loading buffer containing urea were heated at 37°C for 30 min. Protein solutions diluted in 1x gel loading buffer without urea were heated at 97°C for 15 min before loading into the wells. 30 µL of each protein sample was loaded on a gel. Protein samples were stored as 35 µL aliquots at -20°C.

2.4.2 Sodium Dodecyl Sulphate Polyacrylamide gel

An 8% resolving and 5% stacking sodium dodecyl sulphate (SDS) acrylamide gel of 0.75 mm thickness was prepared using the Bio-Rad Mini Protean system 3 (Sambrook 2012). Gels were either used fresh or stored for up to 1 week in a sealed box wrapped in paper towels kept moist in 1x Tris-glycine running buffer (25mM Tris, 250 mM glycine, 1% w/v SDS in distilled water) at 4°C.

The gel plates were assembled on to the Bio-Rad mini protean 3 gel holder, which was placed in the gel running tank. Running buffer was poured in the upper chamber covering the gels. After checking the upper chamber for leaks, the lower chamber was filled up to half with running buffer. Wells were rinsed gently inside out with the running buffer using thin gel loading tips.

30µL of each protein sample was loaded on a gel with 10 wells (15 µL for 15 well gel). Empty lanes were loaded with 30 µL 1x SDS loading buffer. 12 µL NEB colour plus pre-stained ladder (broad range 7-175 kDa) was diluted with 18 µL 2x SDS loading buffer. A total of 30 µL was loaded on a well on the extreme left or right hand side, with an empty well between the ladder and the protein samples.

Samples were electrophoresed through the stacking gel at 100 V and at 150 V through the resolving gel. The SDS-PAGE lasted approximately 1 hour or until the dye front had ran out of the bottom of the gel.

2.4.3 Immunoblot

An Immobilon-P PVDF membrane (Millipore, Livingston, UK) was pre-cut to gel size and activated in 100% methanol for 1 min followed by 2 min in distilled water, and equilibration in transfer buffer until the gel was ready. Two Sponges and two filter papers per blot were soaked in transfer buffer (14.4 g glycine, 3 g Tris, 200 mL 100% methanol in 800 mL distilled water) in preparation for assembling the Mini Trans-Blot® blotting cassette.

After SDS-PAGE, gel plates were removed from the plate holder. The gel was carefully removed by using a spatula to separate the two glass plates. After cutting off the stacking gel, the main gel was carefully placed on the black side of the blotting cassette, over a layer of wet sponge and filter paper. The sandwich was completed by placing the activated PVDF membrane on the gel, followed by wet filter paper and sponge. The blotting assembly was completed by insertion of an ice pack and was completely submerged in transfer buffer.

Proteins were transferred from the gel to the membrane in the Mini Trans-Blot® Electrophoretic Transfer Cell at 100 V for an hour with the black side of the blotting cassette facing the black anode side (-ve electrode) of the blotting apparatus. The transfer of proteins from gel to the PVDF membrane was confirmed by staining the blot with Ponceau stain (Sigma, Dorcet, UK).

At the end of the transfer and Ponceau stain, the blotted membrane was rinsed in PBS (Sigma) for 5 minutes and blocked in 5% milk PBST (0.5% v/v Tween 20 in PBS) for 1 h at room temperature. It was then incubated overnight with Abcam (Cambridge, UK) rabbit GFP antibody diluted 1 in 3000 in 5% milk PBST at 4°C. Before removing the primary antibody, the blot was further incubated at room temperature for 10 min. The GFP antibody solution was stored at -20°C and re-used three times. The membrane was then washed quickly three times with PBST and then three times for 10 min in PBST. A goat anti-rabbit Cy5 conjugated secondary antibody from Jackson Immunoresearch (Newmarket, UK) diluted 1:400 in PBST was then applied and incubated for 1 h in the dark. Lastly, the membrane was washed quickly three times in PBST and then three times for 10 min in PBST and kept in PBS in the dark until imaging. The blot

was imaged using a Bio-Rad ChemiDoc™ Imaging System using the Cy5 red Epi illumination excitation source and the 695/55 nm filter. Images were saved and analysed using Bio-Rad's Image lab software.

2.5.1 Confocal microscopy

A Zeiss (Welwyn Garden City, UK) LSM 510 META and an inverted LSM 510 confocal laser scanning microscopes fitted with 43x, 63x and 100x oil immersion objectives were used for imaging. Leaf sections infiltrated 2 days ago were prepared by cutting a 0.5 cm^2 section and mounting in a drop of water on a microscope slide with its lower epidermis facing the coverslip. A drop of oil was added to the coverslip as the lenses used were oil-dipping. Whole *A. thaliana* seedlings were pulled out of agar using a pair of forceps and mounted in water under a coverslip. If *A. thaliana* leaves were imaged their lower epidermis was placed facing the coverslip. To stop nuclear movement before FRAP and FRET experiments, actin filaments were depolymerised by treating leaf sections with 25 µM Latrunculin B (Calbiochem, Nottingham, UK; prepared in DMSO diluted in sterile water) for 20 minutes. Nuclei of seedlings and leaf sections were stained in 1:1 ethidium bromide: phosphate buffered saline (PBS) for 20 minutes before imaging. Imaging settings including laser, beam splitters and channel filters have been listed in table 2.18.

Table 2.18: Settings for confocal imaging of fluorophores

Fluorophore	Excitation laser	Emmision filter	Beam splitter	Microscope
CFP	458 nm	BP 470 -500	HFT 458/514	LSM 510 META
YFP	514 nm	BP 530 - 600	HFT 458/514, NFT 515	LSM 510 META
CFP + YFP	458 nm and 514 nm	BP 470 - 500, BP 530 - 600	HFT 458/514, NFT 515	LSM 510 META
mRFP	543 nm	BP 560 - 615	HFT 488/543	LSM 510 META
Ethidium bromide	514 nm	BP 585 - 615	NFT 635 Vis, NFT 515	Inverted LSM 510
CFP + Ethidium bromide	458 nm and 514 nm	BP 585 - 615, BP 475 -525	HFT 458/514, NFT 545	Inverted LSM 510

2.5.2 FRAP

FRAP is a live cell imaging technique that helps to quantify the mobility of a protein *in planta*. All FRAP experiments were carried out on YFP tagged proteins using the YFP imaging settings described in section 2.5.1 (Graumann et al. 2007). Latrunculin B treated leaf sections were imaged using the 60x objective, at a zoom factor x3 with no averaging at 258 pixel size. To minimise background photo-bleaching, the excitation 514 laser was always used between 1 to 5 %. A circular region of interest (ROI), 8 µm in diameter was drawn over a focussed region of NE that was bleached with the 20 – 30 iterations of the 514 laser at 100%. A total of 100 images were taken at the scan speed of 1 scan per second, 10 before the bleach and 90 post-bleach for a total of 30 constant sized ROI per sample. This allowed monitoring of the ROI for approximately 90 seconds after bleach, at which time point fluorescence recovery was seen to plateau. ROI data was collected and analysed using Microsoft Excel 9 (Redmond, USA) and Graphpad Prism (La Jolla, USA). Data was normalised with the pre-bleach average taken as a 100% and the first post-bleach scan taken as 0% using the formula;

$$I = 100 * [(I_t – I_o) / (I_{100} – I_0)]$$

Where, I = normalised fluorescence intensity, I_t = fluorescence intensity at a given time t, I_0 = fluorescence intensity immediately after bleach and I_{100} = average fluorescence intensity pre-bleach

The data was fit to an exponential one-phase association curve with the equation;

$$I = I_0 + (I_{max} – I_0) * (1 - \exp^{-K*t})$$

Where, I_0 = fluorescence intensity immediately after bleach, I_{max} = maximum fluorescence recovery and K = rate constant

The half time ($T_{1/2}$) of recovery defined as the time taken to attain half of the maximum fluorescence recovery post-bleach was computed as log(2)/K. Mobile protein fraction defined as maximum fluorescence recovery post-bleach was equal to I_{max}. Unpaired t test was done including 30 nuclei to compare the

mobile fractions and $T_{1/2}$ of two proteins, a p value of 0.05 or less was considered significant.

2.5.3 apFRET

The combination of CFP and YFP was used for apFRET. As CFP emission overlaps with the YFP excitation spectrum, the CFP has the potential to transfer its emission energy for excitation of the YFP. This transfer only takes place if YFP and CFP are in close proximity due to binding interactions of their fusion protein partners. This relationship is exploited by apFRET, in which while the YFP is bleached, a rise in CFP indicates interaction (Karpova and McNally 2006). All FRET experiments were performed by adapting the methods described by Graumann et al. (2010) using the LSM 510 META. To minimise background photo-bleaching, the CFP excitation 458 nm laser was used at <20% intensity, whereas the strong 514 nm YFP excitation laser was used at <5% intensity and the pin holes were maintained at < 200 µm to avoid cross-channel bleed. A circular region of interest (ROI), 8 µm in diameter of was drawn over a focussed region of NE that was bleached with the 20 – 30 iterations of the 514 laser at 100%. A total of 20 images were taken at the scan speed of 1 scan per second, 10 before the bleach and a 10 post-bleach for a total of 30 constant sized ROI. The data was normalised as a percentage of average pre-bleach fluorescence intensity using the formula;

$$I = 100 * [(I_{pre} – I_t) / I_{pre}]$$

Where, I_{pre} = Average intensity of CFP fluorescence pre-bleach and I_t = CFP fluorescence at a given time t

FRET efficiency (E_F) defined as the percentage energy transfer between the two fluorophores was also calculated from the above formula at a time point immediately after bleach. E_F was expressed as its mean $\pm$ standard error of mean (SEM) and was compared to a non-bleached control calculated at the time point immediately before bleach. Paired t test was performed including 30 nuclei to compare E_F pre- and post- bleach, a p value of 0.05 or less was considered significant.

2.5.5 Nuclear size and circularity

Assays were developed to study size and roundedness of nuclei similar to those described in Graumann et al. (2014) using 10-12 day old seedlings grown in standard long day conditions (described in Chapter 2 section 2.2.2) were used for all assays. Seedlings were stained using ethidium bromide as described in section 2.5.1. 30 nuclei from different tissues such as the root cortex, root hairs, cotyledons, leaf trichomes and leaf guard cells were studied in age-matched WT and AtNEAP mutant lines in triplicate assays. Nuclei were imaged at the plane of maximum width and length using confocal microscopy (Table 2.18). A 40x oil immersion objective and digital zoom factor of two were used to capture images using the LSM software. Images were analysed by converting into Tiff files and measuring nuclear length and width using the ImageJ software (Schneider et al. 2012). Average nuclear length and width of more than 30 AtNEAP mutant cells was compared to that of WT using unpaired t test. For the nuclear shape assay, the nuclear circularity index (CI) was calculated as a measure of nuclear roundedness. The CI of a nucleus was defined as the ratio of nuclear width to length (Zhou et al. 2012). A CI value of one indicated a perfectly round nucleus whereas a value close to zero denoted a highly elongated nucleus. All assays were performed by Marlene Salvi and Gareth Hyam using T-DNA lines characterised in this study.

2.5.6 Nuclear positioning in guard cells

10 -12 day old seedlings were stained with ethidium bromide as described in section 2.5.1. Leaf lower epidermal cells were imaged as described in table 2.18. A 40x oil immersion lens and digital zoom factor of 2 were employed. Images were captured with the LSM software and converted into Tiff files. Image J was used for analysis. The longitudinal plane (shown in Chapter 5 figure 5.11c as white dotted line) of the stomatal aperture was defined as the straight line joining the furthest ends of the pore. Positioning of a guard cell nucleus was measured by the angle formed by the longitudinal plane of aperture with a line passing through the centre of the longitudinal plane and the centre of the nucleus. The angle is shown by blue and red arrows in the

confocal micrographs in Chapter 5 figure 5.11c. This data was collected by Dr. Katja Graumann using the *neap1/neap3* double mutant T-DNA line generated in this study (Chapter 5 section 5.3.1).

2.6 MYTH

A MYTH system (Dualsystems Biotech, Switzerland) was employed to test protein-protein interactions. This assay can be used to study interactions between two membrane proteins or to identify novel interactors of a selected membrane protein. Briefly, it works on the re-constitution of the N-terminal (Nub) and C-terminal (Cub) halves of an ubiquitin molecule split between the putative interacting membrane proteins of choice. Interaction between the two proteins leads to the re-assembly of the split ubiquitin which sends a signal for proteolysis and cleaves the tagged transcription factor activating a cascade of events leading to the activation of the reporter system (Snider et al. 2010a, Snider et al. 2010b). All MYTH assays were carried out in the laboratory of Professor Christophe Tatout (Université Blaise Pascal, Clermont-Ferrand, France) using vectors constructed by Dr. Emmanuel Vanrobays (Université Blaise Pascal, Clermont-Ferrand, France) and were performed as described in (Graumann et al. 2014).

2.6.1 Yeast strain, media and growth

In this study, a *Saccharomyces cerevisiae* yeast strain NMY51 *MATa, his3Δ200, trp1-901, leu2-3,112, ade2, LYS2::(lexAop)$_4$-HIS3, ura3::(lexAop)$_8$-lacZ, ade2::(lexAop)$_8$-ADE2, GAL4* was used. Yeast were grown at 30°C in standard yeast nitrogen base (YNB: DIFCO, Bordeaux, France) media supplemented with 2% glucose, and amino acids and bases as required (Table 2.19).

Table 2.19: Concentrations of amino acids and bases used in yeast media

Final concentration (mg/ml)	
Adenine	20
Arginine	20
Histidine	20
Leucine	60
Lysine	30
Methionine	20
Phenylalanine	50
Threonine	200
Tryptophan	20
Tyrosine	30
Uracil	20

2.6.2 Prey and Bait Plasmids

Prey constructs were cloned in the pPR3N (*2μ, TRP1, Amp*^{R}) vector and bait constructs were cloned in the pBT3N (*CEN, LEU2, Kan*^{R}) vector. AtNEAP cDNA were fused to chimeric primers having 35 base pairs complementary to the linearised bait or prey plasmid on the 5′ ends, and 18 base pairs complementary to the N-terminus of AtNEAP cDNA on the 3′ end. AtNEAP cDNA were cloned in plasmids by 'gap-repair' homologous recombination in yeast (Oldenburg *et al.*, 1997). After digestion by SfI1, prey or bait plasmids and cDNA were co-transformed into yeast in the 1:3::vector:insert ratio and successfully transformed clones were selected on test medium. Clones were then subjected to colony PCR, followed by extraction of the plasmid DNA and sequencing. AtNEAP containing bait vectors were verified for self-activation and only AtNEAP1 and AtNEAP2 baits that did not self-activate were used.

2.6.3 MYTH assay

Bait and prey vectors were allowed to co-tranform in yeast. Presence of interaction was analysed by yeast growth on test medium (TM: YNB without Leu, Trp, Ade and His) at 30°C for more than 48 hours. The controls were grown on permissive medium (PM: YNB without Leu and Trp) in identical conditions as test medium. Clones were verified by colony PCR.

The *A. thaliana* cDNA library containing 3.6 million fragments (DUALSYSTEM Biotech) cloned into the prey vector pDSL-Nx (*2μ, TRP1, Amp*^{R}) was screened for novel interactors using the AtNEAP1 bait. The library consisted of cDNA from 6 day old etiolated seedlings as well as seedlings exposed to blue and far red light. A positive control prey included the yeast ER resident protein Ost1 fused to the Nub portion of yeast ubiquitin in the pOst1–NubI (*2μ, TRP1, Amp*^{R}) vector. Transformants from the screen were allowed to grow on highly restrictive medium (YNB without Leu, Trp, His, Ade) and as a backup on low stringency restrictive medium (YNB without Leu, Trp, His). Plasmid DNA was extracted from yeast colonies that grew on highly restrictive medium and sent for sequencing.

2.7 Bioinformatics

Several Bioinformatics databases were used in this study and have been described in table 2.20.

Table 2.20: List of websites for Bioinformatics databases

Website	Name and Description	References
https://www.arabidopsis.org/	The *Arabidopsis* Information Resource (TAIR): database of complete genome sequences, gene structure, gene expression, DNA and seed stocks data for *A. thaliana*	(Lamesch et al. 2012)
http://abrc.osu.edu/	The *Arabidopsis* Biological Research Centre (ABRC): resource for seed stocks, clones, cell lines, cloning vectors and host strains	
http://jsp.weigelworld.org/expviz/expviz.jsp	AtGenExpress Visualization Tool: tissue specific gene expression data for *A.thaliana* in development and hormone, light and pathogen induced stress conditions	(Schmid et al. 2005)
http://bar.utoronto.ca/efp/cgi-bin/efpWeb.cgi	*Arabidopsis* eFP Browser: electronic fluorescent pictograph of gene expression in *A. thaliana* obtained from multiple microarray and high throughput studies.	(Winter et al. 2007, Hruz et al. 2008)
https://genevestigator.com/gv/plant.jsp	GENEVESTIGATOR: search engine for gene expression in *A. thaliana* tissues curated from microarray and RNAseq experiments	(Toufighi et al. 2005)
http://bioinformatics.psb.ugent.be/plaza/versions/plaza_v2_5/	PLAZA: platform for evolutionary analyses using several plant genome sequencing databases	(Proost et al. 2009, Van Bel et al. 2012)
http://suba.plantenergy.uwa.edu.au/flatfile.php?id=	The SubCellular Proteomic Database: localisation data for various cellular compartments of *A. thaliana* as well as bioinformatic predictions and protein-protein interactions	(Hooper et al. 2014)
http://signal.salk.edu/cgi-bin/tdnaexpress	T-DNA Express: *A.thaliana* Gene Mapping Tool	(Alonso et al. 2003, Yamada et al. 2003)
http://signal.salk.edu/tdnaprimers.2.html	Primer design software for *A. thaliana* T-DNA lines	(Alonso et al. 2003)

Table 2.20 continued…

Website	Name and Description	References
http://smart.embl.de/smart/set_mode.cgi?GENOMIC=1	SMART: prediction of coiled-coils	
http://www.ch.embnet.org/software/COILS_form.html	COILS: prediction of coiled-coils	(Lupas et al. 1991)
http://paircoil2.csail.mit.edu/paircoil2.html	PairCoil2: prediction of coiled-coils	(McDonnell et al. 2006)
http://toolkit.tuebingen.mpg.de/marcoil	Marcoil: prediction of coiled-coils	(Delorenzi and Speed 2002)
http://nls-mapper.iab.keio.ac.jp/cgi-bin/NLS_Mapper_form.cgi	cNLS mapper: prediction of NLS	(Kosugi et al. 2009)
http://www.moseslab.csb.utoronto.ca/NLStradamus/	NLSstradumus: prediction of NLS	(Nguyen Ba et al. 2009)
http://aramemnon.uni-koeln.de/	ARAMEMNON: transmembrane prediction	(Schwacke et al. 2003)
http://www.sbc.su.se/~miklos/DAS/	DAS: transmembrane prediction	(Cserzo et al. 1997)
http://www.ebi.ac.uk/Tools/msa/clustalo/	Clustal Omega: multiple sequence alignment program	(Sievers and Higgins 2014)

Chapter 3

A novel family of structural coiled-coil proteins in plants

Chapter 3

A novel family of structural coiled-coil proteins in plants

3.1 Introduction

This chapter introduces the NEAP family in plants and describes the structural characteristics of its members in *A. thaliana*. As described in section 1.4 of Chapter 1, the first protein of this family, AtNEAP1 was discovered in a bioinformatics screen for KASH-like proteins. AtNEAP1, encoded by At3g05830, was identified due to the presence of its CC domains, NLS and hydrophobic TM region (Graumann unpublished). AtNEAP1 fused to yellow FP (YFP) co-localised at the NE with a cyan FP (CFP) fusion of SUN domain protein, AtSUN1 (Lu 2011). In *A. thaliana*, two sequence homologues of NEAP1 have been identified using a Basic Local Alignment Search Tool (BLAST) and have been described in section 3.3.1 (Graumann unpublished). In the present study, a fourth gene has been identified as part of the family (described in section 3.3.1).

AtNEAP1 is annotated in TAIR as an alpha helical IF-like protein. One of the NEAP1 cDNA transcripts has been submitted to the EMBL/GenBank/DDBJ database as a sequence identified in an IF antibody screen of a floral expression *A. thaliana* library (Colter and Saunders 1996). Hence the NEAP proteins are hypothesised to be components of the plant lamina, rather than being KASH-like proteins. This chapter provides a detailed characterisation of the NEAP family in terms of their protein structure, evolutionary relationships, tissue specific expression and subcellular localisation.

3.2 Aims

The work presented in this chapter aims to characterise the AtNEAP protein family by;

a) Determining protein structure and domain function by biochemical studies, sequence analysis and study of deletion and truncation mutants

b) Exploring expression patterns in *A. thaliana* tissues at different stages of growth and development and their subcellular location using fluorescent protein fusions in transient (*N. benthamiana*) and stable (*N. tabacum* bright yellow 2 [BY2] cell line) expression systems

c) Determining their phylogeny by comparison with plant and non-plant species

d) Understanding the nature of their mobility in the plant cell using confocal microscopy

3.3 Results

3.3.1 AtNEAP protein structure: prediction of functional domains

As described in section 3.1, At3g05830 was first discovered in a bioinformatics screen and has been named AtNEAP1. AtNEAP1 encodes a protein predicted to have a relative molecular mass of 41.049 kDa with an isoelectric point of 8.7849 (table 3.1). BLAST homology search using the aa sequence of AtNEAP1 has led to the identification of its *A. thaliana* homologues At5g26770 and At1g09470. At5g26770, named AtNEAP2 is 72% similar ($p = 3.4e^{-106}$) to the aa sequence of AtNEAP1. AtNEAP2 is predicted to have a relative molecular mass of 38.675 kDa and an isoelectric point of 8.8679 (table 3.1). At1g09470, named AtNEAP3 is 50% similar ($p = 1.8e^{-70}$) to AtNEAP1, has a predicted relative molecular mass of 39.001 kDa and an isoelectric point of 9.1528 kDa (table 3.1). In addition to the three previously identified NEAP proteins, this study revealed a fourth *A. thaliana* gene as part of this newly discovered family. At1G09483, putatively named AtNEAP4, is 86% similar to AtNEAP3 ($p = 8.6e^{-30}$), 60% and 56% similar to AtNEAP2 ($p = 9.3e^{-26}$) and AtNEAP1 ($p = 4.3e^{-22}$) respectively. AtNEAP4 encodes a smaller protein only about one third the size of NEAP1, 2 and 3. AtNEAP4 is predicted to have a relative molecular mass of 13.106 kDa and an isoelectric point of 9.6571 (table 3.1). The alignment of AtNEAP sequences using CLUSTAL Omega (Sievers et al. 2011) shows regions of high similarity (figure 3.1). The alignment shows that AtNEAP1, 2, 3 and 4 contain highly conserved stretches of aa and highlights the absence of approximately 230 aa in AtNEAP4 compared to AtNEAP1, 2 and 3 (figure 3.1).

Several algorithms were employed to predict structural and functional domains of AtNEAP proteins. The CC regions were predicted using SMART, COILS, PairCoil2 and Marcoil (Lupas et al. 1991, Delorenzi and Speed 2002, McDonnell et al. 2006, Letunic et al. 2012). AtNEAP1, AtNEAP2 and AtNEAP3 are consistently predicted by the different algorithms to contain extensive CC domains (figure 3.1 and table 3.2). The large CC region of AtNEAP1 extends from 54-184 aa; followed by a smaller CC stretch from 221-266 aa (table 3.2). Similarly AtNEAP2 has a large CC region from 54-185 aa as well as the smaller

CC region from 220-298 aa. The large CC domain seen in AtNEAP1 and 2 is split into two CC regions in AtNEAP3 stretching from 13-93 aa and 124-185 aa separated by a linker. A smaller CC region similar to AtNEAP1 and 2 extends from 221-306 aa in AtNEAP3. The sequence of the long CC regions is lost in AtNEAP4, however the smaller CC domain is present from 44-74 aa (figures 3.1 and 3.2).

Table 3.1: Molecular characteristics of AtNEAP1, AtNEAP2, AtNEAP3 and AtNEAP4, obtained from TAIR.

Locus	**Coding sequence length (nucleotides)**	**Peptide length (amino acids)**	**Predicted MW (Daltons, Da)**	**Isoelectric point (pI)**	**Name used in thesis**	**P-value (compared to At3g05830)**
At3g05830	1050	349	41048.9	8.7849	AtNEAP1	-
At5g26770	1008	335	38675.1	8.8679	AtNEAP2	$3.4x10^{-6}$
At1g09470	1011	336	39001	9.1528	AtNEAP3	$1.8x10^{-7}$
At1g09483	339	112	13106.9	9.6571	AtNEAP4	$3.1x10^{-18}$

The presence of an NLS was predicted using the cNLS mapper and NLSstradumus (Kosugi et al. 2009, Nguyen Ba et al. 2009). While the cNLS mapper uses known classical NLS sequences specific to the importin α pathway from plants, NLSstradumus uses classical NLS sequences known in yeast. There are several possibilities of NLS highly conserved among all four AtNEAP proteins (figure 3.1). These include two possible monopartite NLS sequences KKK or KKKVLK and two bipartite NLS combinations of KTK-X_9-RR or KTK-X_{16}-KKK (table 3.2).

Hydrophobic regions with potential to be TM domains were obtained from a consensus prediction compiling 17 different algorithms via the ARAMEMNON database of plant membrane proteins with *A. thaliana* as the reference model (Schwacke et al. 2003). AtNEAP1, 2 and 3 are predicted to have a stretch of conserved hydrophobic aa at the C- terminus (table 3.2). The hydrophobicity prediction for AtNEAP4 from ARAMEMNON was inconclusive; consequently Dense Alignment Surface (DAS) TM prediction server was used (Cserzo et al. 1997). The predicted hydrophobic region in AtNEAP4 is smaller yet shares the VVXMS motif as a highly conserved feature with the other three AtNEAP proteins (figure 3.1). Interestingly, the hydrophobic region in NEAP4 is followed

by a 15 aa long non-hydrophobic tail which is not conserved in the other three NEAP proteins (figure 3.1).

3.3.2 NEAP-like proteins in other species

A. thaliana NEAP proteins were found to have no sequence orthologues in metazoans and fungi (data not shown). However they show high sequence similarity within the plant kingdom. PLAZAv3.0 (http://bioinformatics.psb.ugent.be/plaza/), a platform for plant comparative genomics, integrates various genome sequencing initiatives within the green plant lineage including higher plants and photosynthetic microbes (Van Bel et al. 2012). BLAST analysis across the various plant genomes in PLAZAv3.0 predicted that NEAP proteins form part of a family containing a total of 54 NEAP-like proteins in 27 plant species including several monocot and dicot species (figure 3.3). The NEAP protein family is annotated to have gene ontology characteristics representing molecular function as structural molecules, components of the actin cytoskeleton, and involvement in biological process such as cell or biological adhesion.

PLAZA also allows analysis of phylogenetic relationships between sequenced genomes of 31 species in the plant lineage viridiplantae as well as 16 species of eukaryotic photosynthetic microbes. No sequences similar to *A.thaliana* NEAP proteins were found in the 16 algal genomes analysed as well as none beyond the Magnoliophyta clade within higher plants. One NEAP-like protein is found in *Amborella trichopoda* (Baill), a species at the base of the angiosperm clade but not in the bryophyte moss, *Physcomitrella patens* (Hedw.) (figure 3.3).

Construction of a phylogenetic tree using NEAP orthologues in PLAZA shows that *A. thaliana* NEAP proteins cluster on a branch exclusive to the brassicaceae family (figure 3.4). Similarly, the two monocot species included in the analysis are grouped together on a sub-branch (figure 3.4). The overall theme of distribution of NEAP-like proteins follows a phylogenetic order with closely related species clustering on related branches in most instances (figure 3.4). However, species within the order fabidae are distributed on two separate branches (figure 3.4). Multiple sequence alignment of NEAP-like proteins used for construction of the phylogenetic tree shows a high degree of conservation and similarity maintained in various plant species (figure 3.5).

3.3.3 Expression levels of AtNEAP mRNA in plant tissues

To explore expression profiles of AtNEAP proteins *in planta*, GeneVestigator (https://www.genevestigator.com/gv/) and the BAR Arabidopsis eFP browser (http://bar.utoronto.ca/welcome.htm) were queried (Toufighi et al. 2005, Hruz et al. 2008). mRNA expression data from GeneVestigator microarrays shows that AtNEAP1 (red) and AtNEAP2 (blue) are expressed at medium levels in whole seedlings, inflorescence, shoot and leaf tissues (figure 3.6a). AtNEAP3 is generally expressed at low levels, but at medium levels in inflorescence tissues. AtNEAP4 is expressed at low levels in all tissue types on the array (figure 3.6a). A different array from GeneVestigator confirmed medium expression of AtNEAP1 and 2 described above (figure 3.6b). The array also showed high levels of expression of AtNEAP1 in seed, embryos, endosperm and guard cell protoplasts (figure 3.6b). Higher expression of AtNEAP1 in developing embryos up to walking stick stage, endosperm and guard cells was confirmed by a different array available on the BAR Arabidopsis eFP browser, which also showed high expression in developing flowers, the shoot apex transitioning to floral buds and senescent leaves (figure 3.7). Similarly AtNEAP2 was expressed at high levels in developing embryos up to the curled cotyledon stage, guard cells and cauline and senescent leaves (figure 3.8). The general expression level of AtNEAP1 mRNA (figure 3.7) is relatively high compared to that of AtNEAP2 (figure 3.8).

3.3.4 Sub-cellular localisation of AtNEAP 1, 2 and 3

To study the sub-cellular localisation of AtNEAP proteins, their CDS were fused to CFP or YFP as described in Chapter 2; section 2.3.9 under the Cauliflower Mosaic Virus (CMV), 35S promoter. The constructs were agro-infiltrated into *N. benthamiana* leaf epidermal cells together with a construct expressing the p19 protein (suppressor of RNA silencing). Expression was observed in leaves three days post infiltration by confocal microscopy. The detailed method is described in Chapter 2 section 2.5.1. Figure 3.9 shows results of one experiment, which was representative of two replicates each on five or more occasions. The fluorescence observed was at the nuclear periphery for both N-terminal and C-terminal fusions (figures 3.9 and 3.10). In case of N-terminal fusions, leaves had

been co-infiltrated with Histone H2B-CFP, which marks the location of chromatin (Martin et al. 2009). In each case (AtNEAP1, 2 and 3: figure 3.9.a, b and c respectively) the NEAP-YFP fluorescence was closely associated with the outer surface of the histone fluorescence forming an almost continuous ring of variable thickness with no chromatin-associated fluorescence observed, (figure 3.9). NEAP protein fluorescence also accumulated in the perinuclear cytoplasm and was found to cause NE deformations in figure 3.9b and c.

Similar results were obtained using the C-terminal constructs (figure 3.10). Though in this case, AtNEAP1 fluorescence was observed in the peripheral cytoplasm as well as at the nuclear periphery (figure 3.10.a), possibly as a result of over-expression on the 35S promoter. In this case chromatin was stained using ethidium bromide. Once again, NEAP fluorescence was closely associated with the periphery of the chromatin fluorescence and formed an almost continuous ring, not penetrating into the area of chromatin.

In addition to the above, a stably expressing *N. tabacum* BY2 cell line was available (Lu 2011). AtNEAP1-YFP was expressed under a 35S promoter. Figure 3.10.d shows nuclear periphery staining like that of transiently expressing cells. Unfortunately, this line was lost before further experiments were carried out and has not been re-created. Importantly, fluorescence was concentrated at the nuclear periphery and was not observed in other cellular locations, suggesting the cytoplasmic location of AtNEAP1-CFP seen in transient expression (figure 3.10.a) may be an over-expression artefact. Localisation data could not be obtained for AtNEAP4, as AtNEAP4 mRNA could not be isolated and amplified from *A. thaliana* tissues.

3.3.5 Deletion of AtNEAP3 protein domains

The functions and activity of the protein domains predicted in section 3.3.1 and listed in table 3.2 were studied by deleting selected conserved domains from AtNEAP3. The constructs were prepared (primers described in Chapter 2; table 2.3) by deleting the CC1 (aa: 13-93), CC2 (aa: 124-185), NLS (aa: 239-264) and TM (aa: 314-333) domains from AtNEAP3 and fused to YFP on its N-terminus under the CaMV 35S promoter. The construct was agro-infiltrated into *N. benthamiana* leaf epidermal cells together with a construct expressing the p19

protein. Expression was observed in leaves three days post infiltration by confocal microscopy. Figure 3.11 shows result of one experiment, which was representative of two replicates each on five or more occasions. The fluorescence observed at the nuclear periphery for N-terminal YFP fusion of AtNEAP3 was affected by deletion of the different domains. Deletion of the N-terminal CC1 domain of AtNEAP3 made the mutant YFP-AtNEAP3ΔCC1 protein dissociate into the nucleoplasm and some diffuse fluorescence was also observed in the cytoplasm (figure 3.11a). Expression of YFP-AtNEAP3ΔCC2 domain deletion did not differ from the full length construct and also resulted in fluorescent signal at the nuclear periphery (figure 3.11b). Deletion of the peptide predicted to hold the NLS, made the mutant YFP-AtNEAP3ΔNLS protein largely cytoplasmic and nucleoplasmic to some extent (figure 3.11c). Deleting the predicted TM domain of AtNEAP3 affected nuclear periphery localisation of the truncated protein; YFP-AtNEAP3ΔTM was seen predominantly in the nucleoplasm excluding the nucleolus (figure 3.11d).

3.3.6 Immunoblot analysis of AtNEAP proteins

YFP-AtNEAP1, YFP-AtNEAP2 and YFP-AtNEAP3 proteins expressed transiently in *N. benthamiana* leaves under the 35S promoter were extracted using a high urea based buffer (described in Chapter 2, section 2.4.1). Non-infiltrated *N. benthamiana* leaves were used for extraction of proteins as a negative control. Protein extracts were concentrated by precipitation using TCA-acetone and re-suspended in a reducing buffer containing DTT, SDS and 4.5M urea (described in Chapter 2, table 2.17). Proteins were separated using SDS-PAGE and analysed on a Western blot using anti-GFP antibody (For method see Chapter 2.4.2). YFP-AtNEAP proteins could not be solubilised in the absence of urea (data not shown). Also, YFP-AtNEAP expression levels *in planta* were found to be too low for detection despite the 35S promoter (data not shown). Hence the extracts were concentrated ten-fold post precipitation, which allowed visualisation of specific bands in the infiltrated samples. On an eight percent acrylamide gel, one YFP-AtNEAP specific band is observed for each construct which is the largest band in their respective lanes. Several lower bands are seen in all the lanes including the non-infiltrated control lane, which could be a result of non-specific binding of anti-GFP antibody to endogenous

proteins.YFP-AtNEAP1 runs just above the 60 kDa protein marker. Similarly YFP-AtNEAP2 band is seen at approximately 60 kDa. The YFP-AtNEAP3 band runs at a relative molecular mass of approximately 65 kDa (figure 3.12). Subtracting the molecular mass of YFP (27 kDa) from each of the three proteins, leaves AtNEAP1 and AtNEAP2 at approximately 34 kDa and 33 kDa and AtNEAP3 at approximately 38 kDa, which are smaller than their predicted masses of 41, 38 and 39 kDa each respectively (table 3.1).

3.3.7 Analysis of AtNEAP mobility at the NE

As shown in figures 3.9 and 3.10; fluorescent protein fusions of AtNEAP1, AtNEAP2 and AtNEAP3 localise to the nuclear periphery *in planta*. The mobility of N-terminally tagged YFP constructs of AtNEAP1, AtNEAP2 and AtNEAP3 proteins was tested using a confocal microscopy technique FRAP, described in Chapter 2, section 2.5.2). Briefly, the YFP-AtNEAP fusion protein was expressed transiently in *N. benthamiana* leaves, which were subjected to treatment with 25 µM Latrunculin B for 30 minutes, prior to the bleach. YFP fluorescence in a small area of the NE was bleached using a full strength 514nm laser in a total of 30 nuclei collected from duplicate infiltrations in three experiments. Fluorescence recovery was recorded for up to 90 seconds. Mobile protein fraction defined as maximum fluorescence recovery post-bleach was calculated as 20.6 $\pm$ 1.8%, 17.7 $\pm$ 1.5% and 46.9 $\pm$ 5.3% respectively for N-terminal YFP fusions of AtNEAP1, 2 and 3 (figure 3.13). The half time ($T_{1/2}$) of recovery defined as the time taken to attain half of the maximum fluorescence recovery post-bleach was calculated as 3.6 $\pm$ 0.17 seconds, 2.3 $\pm$ 2.4 seconds and 9.5 $\pm$ 3.5 seconds for YFP-AtNEAP1, YFP-AtNEAP2 and YFP-AtNEAP3 respectively. The mobile fraction as well as the $T_{1/2}$ of recovery of YFP-AtNEAP3 was significantly greater than that of YFP-AtNEAP1 ($p<0.0001$) and YFP-AtNEAP2 ($p<0.0001$). A C-terminal YFP fusion of AtNEAP1 had 25.9 $\pm$ 2.5% in the mobile fraction and a $T_{1/2}$ of 6 $\pm$ 1.9 seconds (figure 3.14). The p value ($p<0.05$) of an unpaired t-test suggested that the mobile fraction of YFP-AtNEAP1 was significantly smaller compared to the mobile fraction of AtNEAP1-YFP, and the $T_{1/2}$ of recovery was also significantly ($p<0.005$) lower in YFP-AtNEAP1.

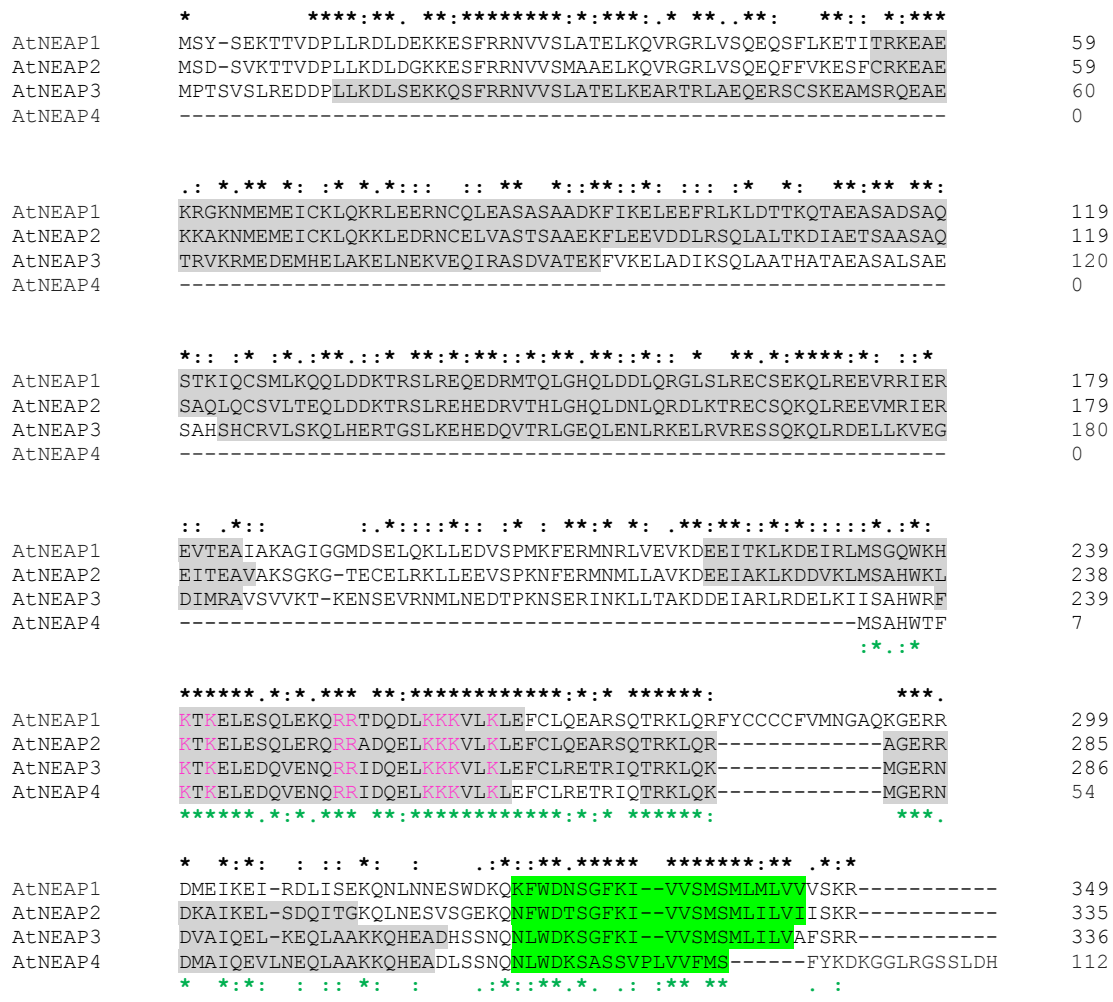

Figure 3.1: CLUSTAL Omega (1.2.1) multiple sequence alignment of AtNEAP1, 2, 3 and 4 and prediction of functional domains in the protein structure of AtNEAP1, 2, 3 and 4. Asterisk (*) denotes consensus sequences between AtNEAP1, 2 and 3. Green asterisk (*) denotes sequences conserved between AtNEAP1, 2, 3 and 4. Coiled-coil (CC) domains are highlighted in grey, NLS is coloured pink and TM domains are highlighted in green. Coiled-coil regions were predicted using SMART, COILS, PairCoil2 and Marcoil (Lupas et al. 1991, Delorenzi and Speed 2002, McDonnell et al. 2006, Letunic et al. 2012). The NLS was predicted using the cNLS mapper and NLSstradumus (Kosugi et al. 2009, Nguyen Ba et al. 2009). TM domains were predicted using ARAMEMNON and DAS (Cserzo et al. 1997; Schwacke et al. 2003).

Table 3.2: Predicted amino acid sequences of coiled-coil, NLS and transmembrane domains in AtNEAP proteins.

Amino acid stretch	AtNEAP1	AtNEAP2	AtNEAP3	AtNEAP4
Coiled-coil domains	1. 54-184 -------- 2. 221-266	1. 54-185 -------- 2. 220-298	1. 13-93 2. 124-185 3. 221-306	-------- -------- 1. 44-74
NLS	239-264	238-263	239-264	8-33
Trans-membrane domain	324-345	311-331	314-333	81-97

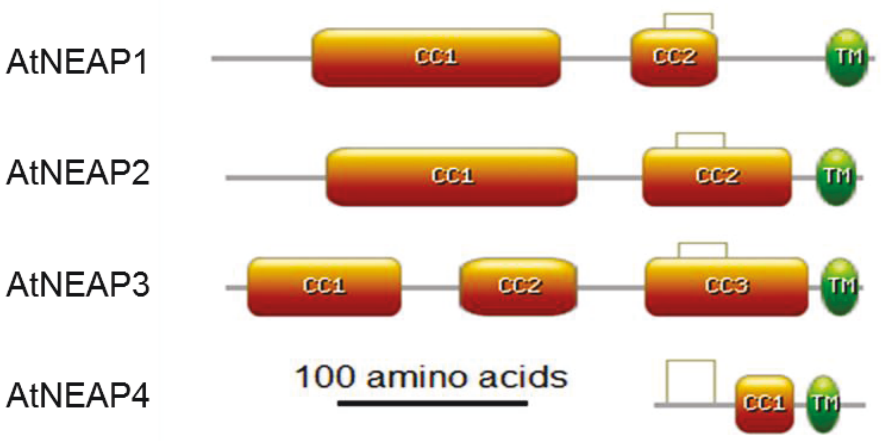

Figure 3.2: Schematic representation of AtNEAP1, 2, 3 and 4 including coiled-coil (CC) domains shown in orange rectangles, NLS shown by grey boxes and TM domains in green circles. Cartoons were created using a program on http://prosite.expasy.org/mydomains/

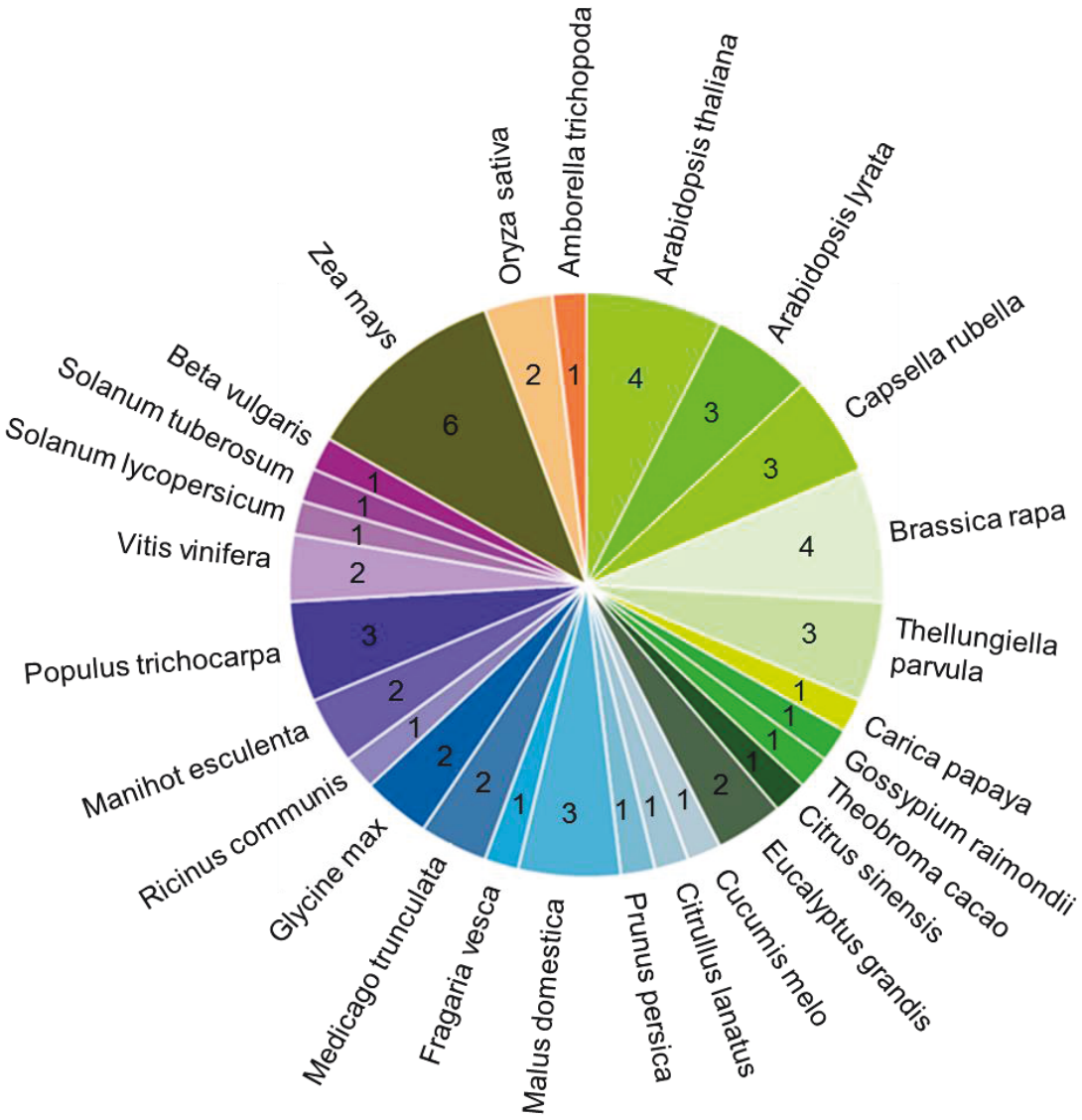

Figure 3.3: Pie chart showing 54 predicted genes that have sequence similarity to the *A.thaliana* NEAP proteins in 27 species within the Magnoliophyta clade. All species in the chart have been ordered on the basis of their phylogenetic tree. The data was obtained from PLAZA v3.0 (Proost et al. 2009, Van Bel et al. 2012).

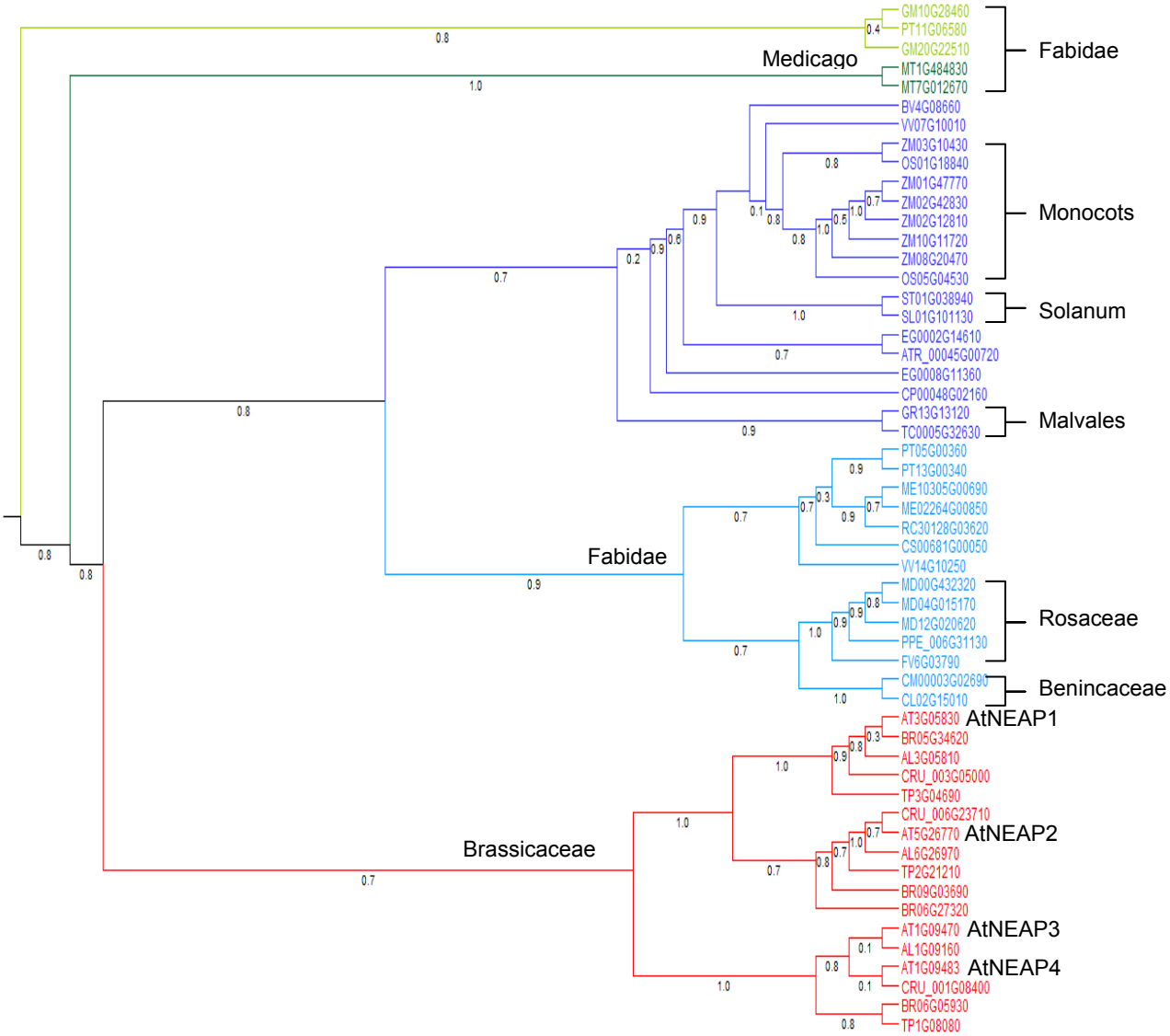

Figure 3.4: Analysis of phylogenetic distribution of NEAP-like proteins in 27 species within the Magnoliophyta clade in higher plants shows closely related species clustering on related branches. *A. thaliana* NEAP proteins cluster on a branch exclusive to the brassicaceae family. NEAP-like proteins in the order fabidae are however seen segregated on different branches. The data was obtained from PLAZA v3.0 (Proost et al. 2009, Van Bel et al. 2012).

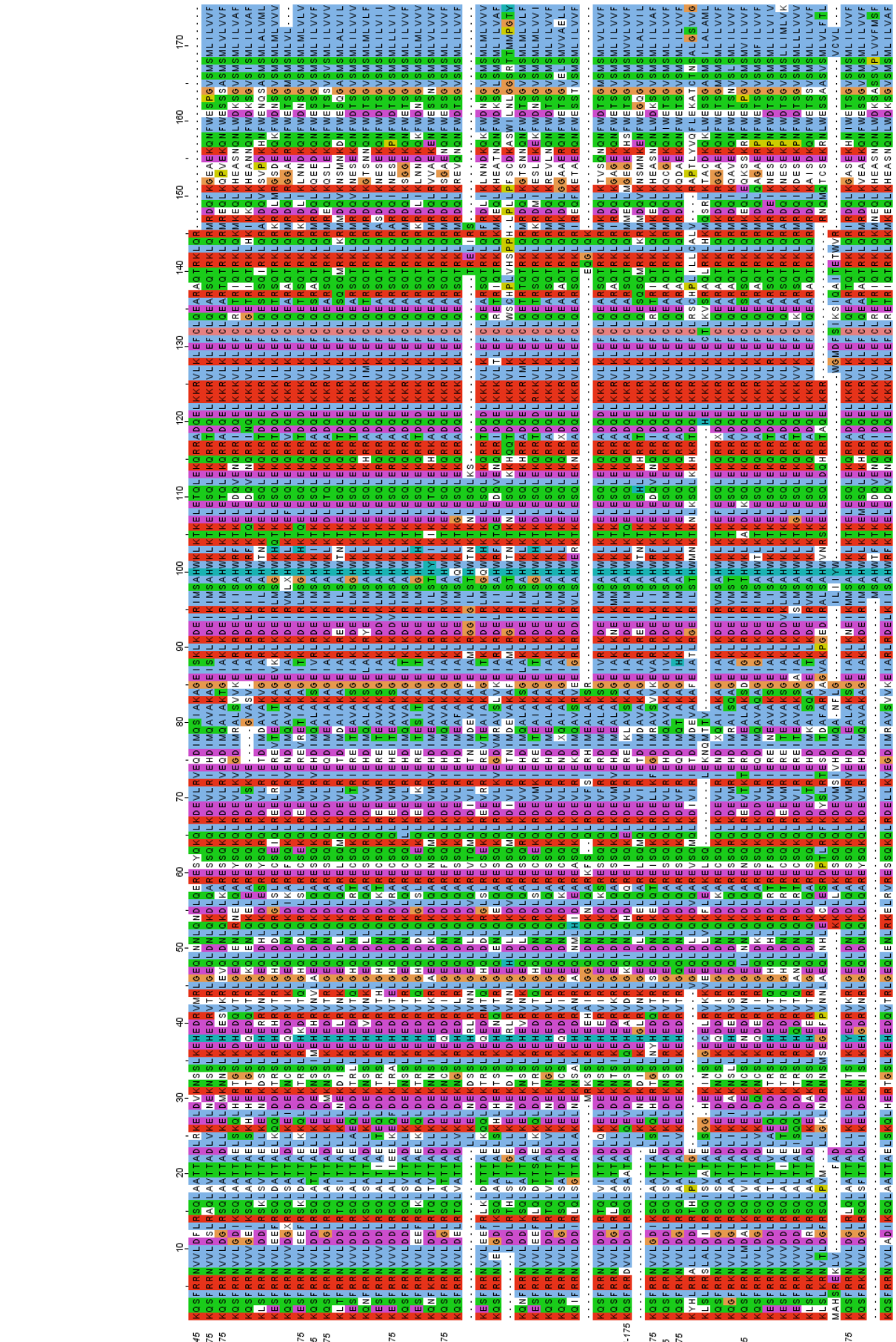

Figure 3.5: Alignment of NEAP-like protein sequences using Jalview in several plant species after removal of non-conserved gaps showing a high degree of conservation denoted by the same colour. The consensus sequence is depicted in black.

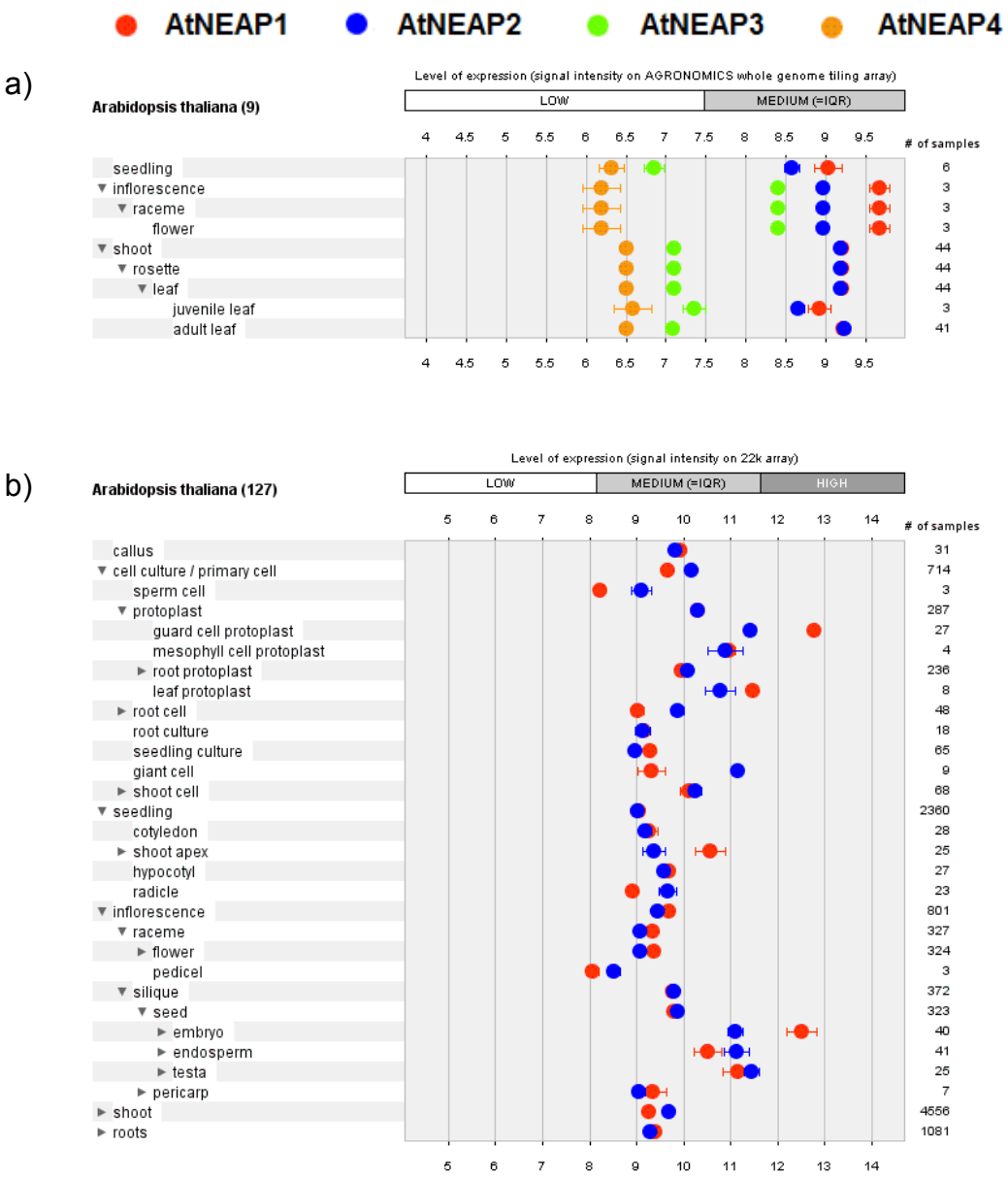

Figure 3.6: Expression profile of AtNEAP1, 2, 3 and 4 mRNA obtained from GeneVestigator (Toufighi et al. 2005). a) Microarray data shows AtNEAP1 (red) and AtNEAP2 (blue) expressed at medium levels in all tissues. AtNEAP3 (green) is expressed at low levels, except at medium levels in inflorescence tissues. AtNEAP4 (orange) is expressed at low levels in all tissue types on the array. b) A different array confirms medium expression of AtNEAP1 (red) and AtNEAP2 (blue), while showing up-regulation in embryo and guard cell protoplasts.

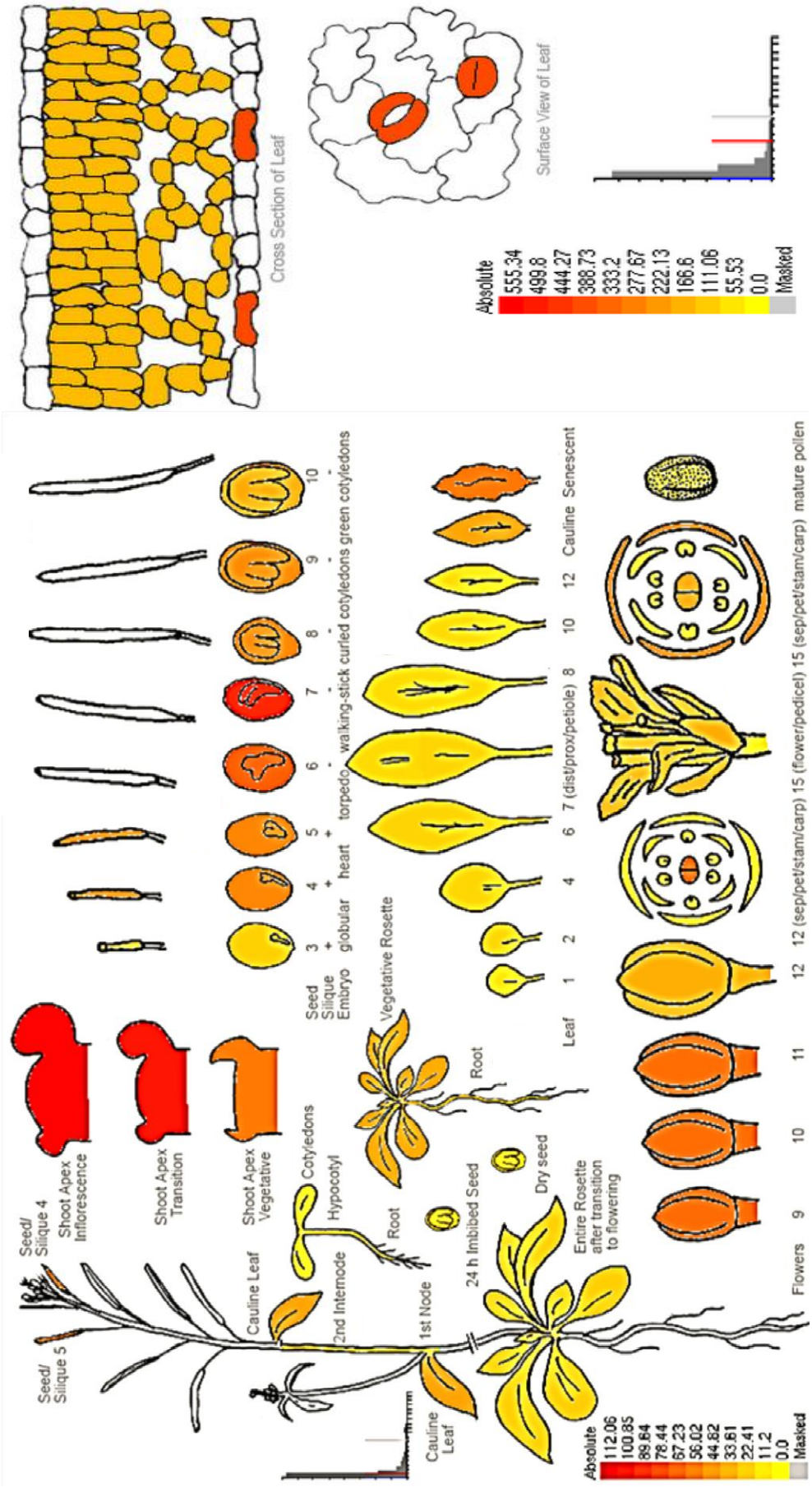

Figure 3.7: Expression levels of AtNEAP1 mRNA in different tissues acquired from BAR Arabidopsis eFP browser (Winter et al. 2007, Hruz et al. 2008). AtNEAP1 expression is up-regulated in the shoot apex, inflorescence, embryos, senescent leaves and guard cells.

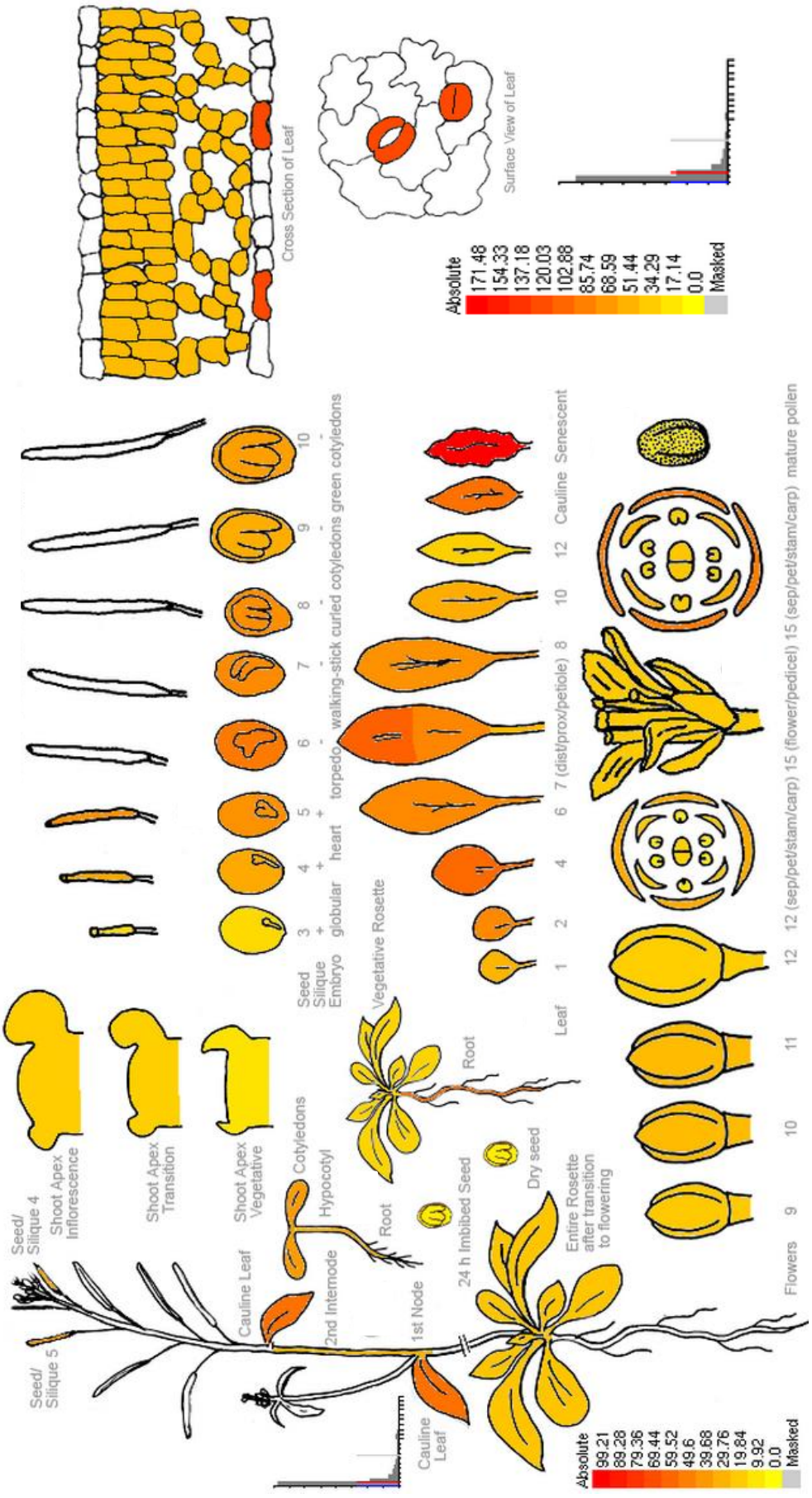

Figure 3.8: Expression levels of AtNEAP2 mRNA in different tissues acquired from BAR Arabidopsis eFP browser (Winter et al. 2007, Hruz et al. 2008). AtNEAP2 expression is up-regulated in senescent leaves and guard cells.

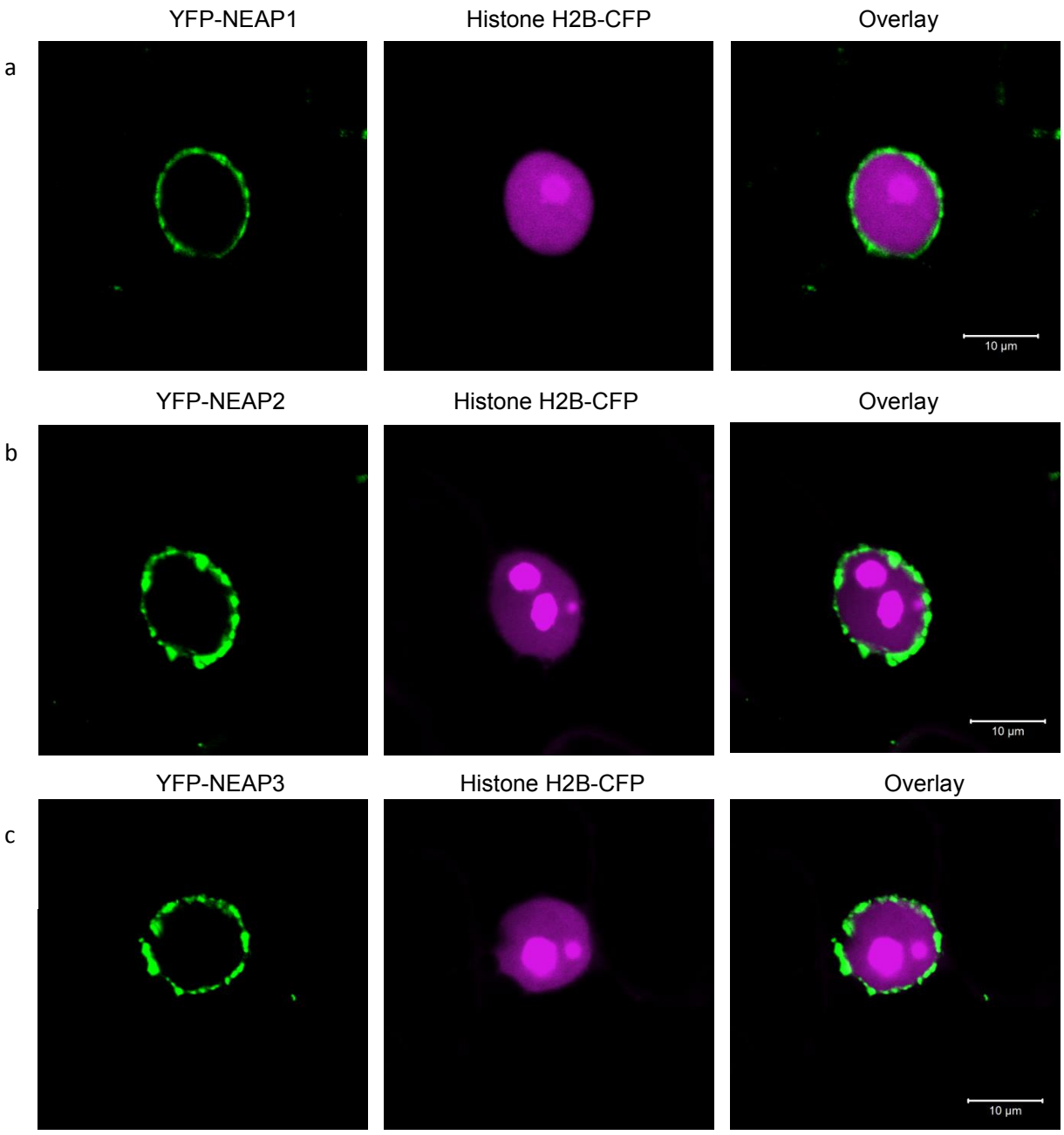

Figure 3.9: Confocal micrographs showing N-terminus YFP fusions of AtNEAP proteins (green) and C-terminus fusion of Histone H2B-CFP (magenta); expressed transiently under the 35S promoter in *N. benthamiana* leaf epidermal cells in presence of the suppressor of RNA silencing protein p19. YFP-AtNEAP1 (a), YFP-AtNEAP2 (b) and YFP-AtNEAP3 (c) localise at the nuclear periphery around chromatin labelled by Histone H2B-CFP. Scale bar = 10µm.

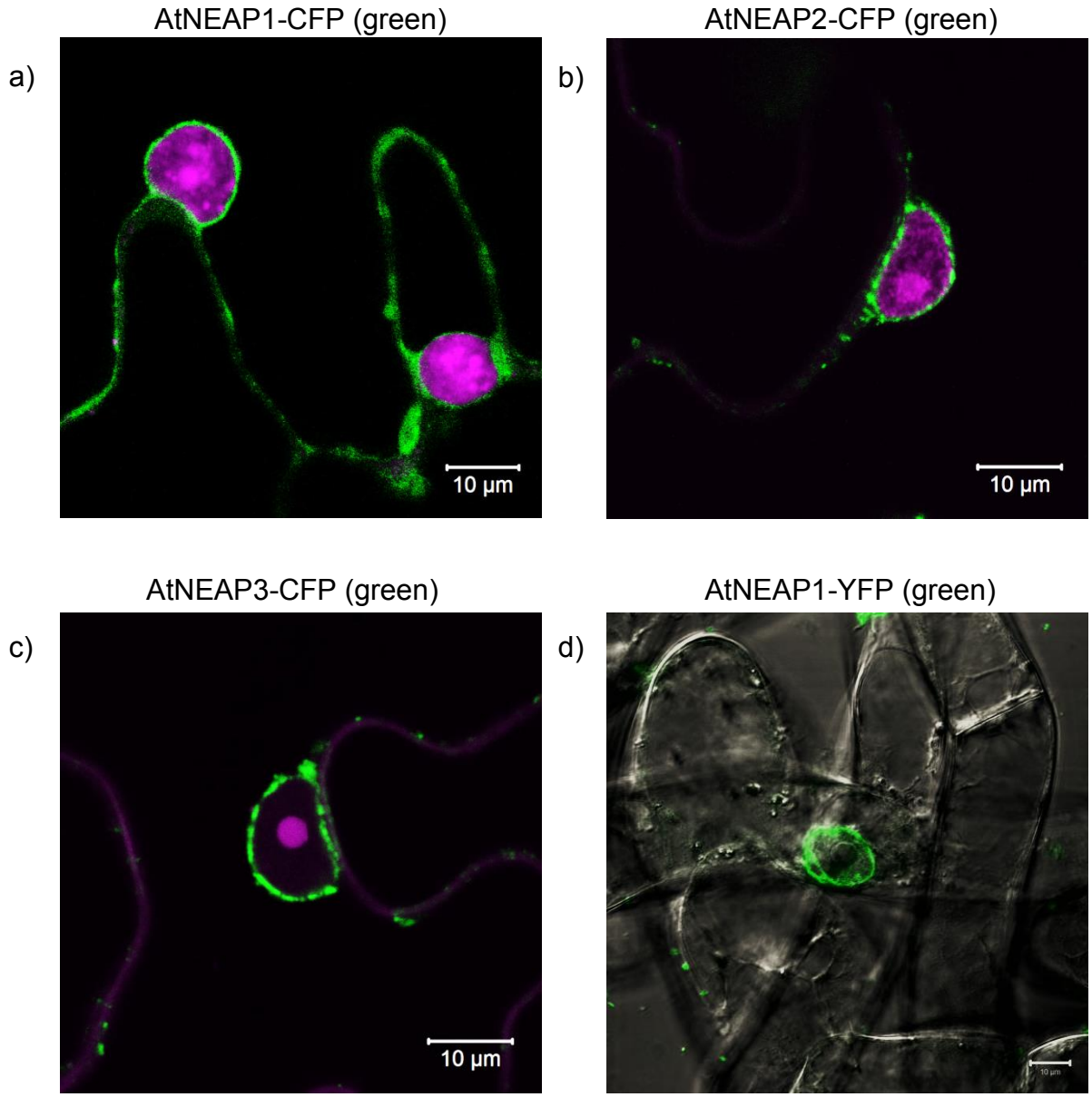

Figure 3.10: Confocal micrographs showing ethidium bromide (magenta) stained chromatin enveloped by C-terminus fusions of AtNEAP1-CFP (a), AtNEAP2-CFP (b) and AtNEAP3-CFP (c) in green, expressed transiently under the 35S promoter in *N. benthamiana* leaf epidermal cells in presence of the suppressor of RNA silencing protein p19. AtNEAP1-YFP (green) localises to the nuclear envelope, stably expressed under the 35S promoter in a tobacco BY2 cell (d). Scale bar = 10µm.

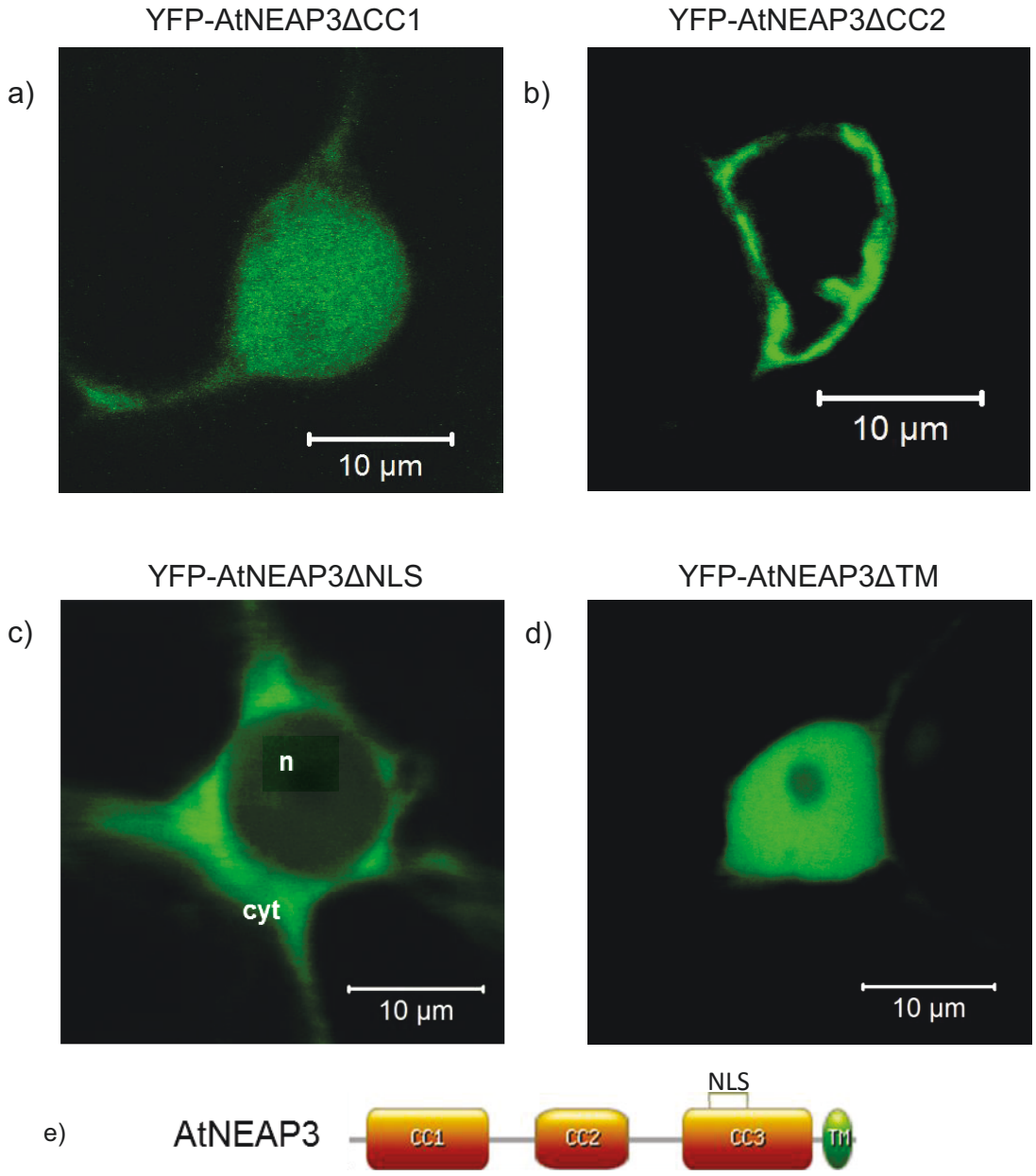

Figure 3.11: Confocal micrographs showing transient expression of AtNEAP3 domain deletion mutants under the 35S promoter in *N. benthamiana* leaf epidermal cells in presence of the suppressor of RNA silencing protein p19. a) Amino terminal fusion YFP-AtNEAP3ΔCC1 (green) localises to the nucleoplasm. b) YFP-AtNEAP3ΔCC2 (green) localises to the nuclear periphery. c) YFP-AtNEAP3ΔNLS (green) is predominantly cytoplasmic (depicted by cyt) and to some extent nucleoplasmic (denoted by n). d) YFP-AtNEAP3ΔTM (green) localises to the nucleoplasm. Scale bar = 10µm. e) Cartoon showing the coiled-coil domains, NLS and TM domain of AtNEAP3 deleted in the constructs above.

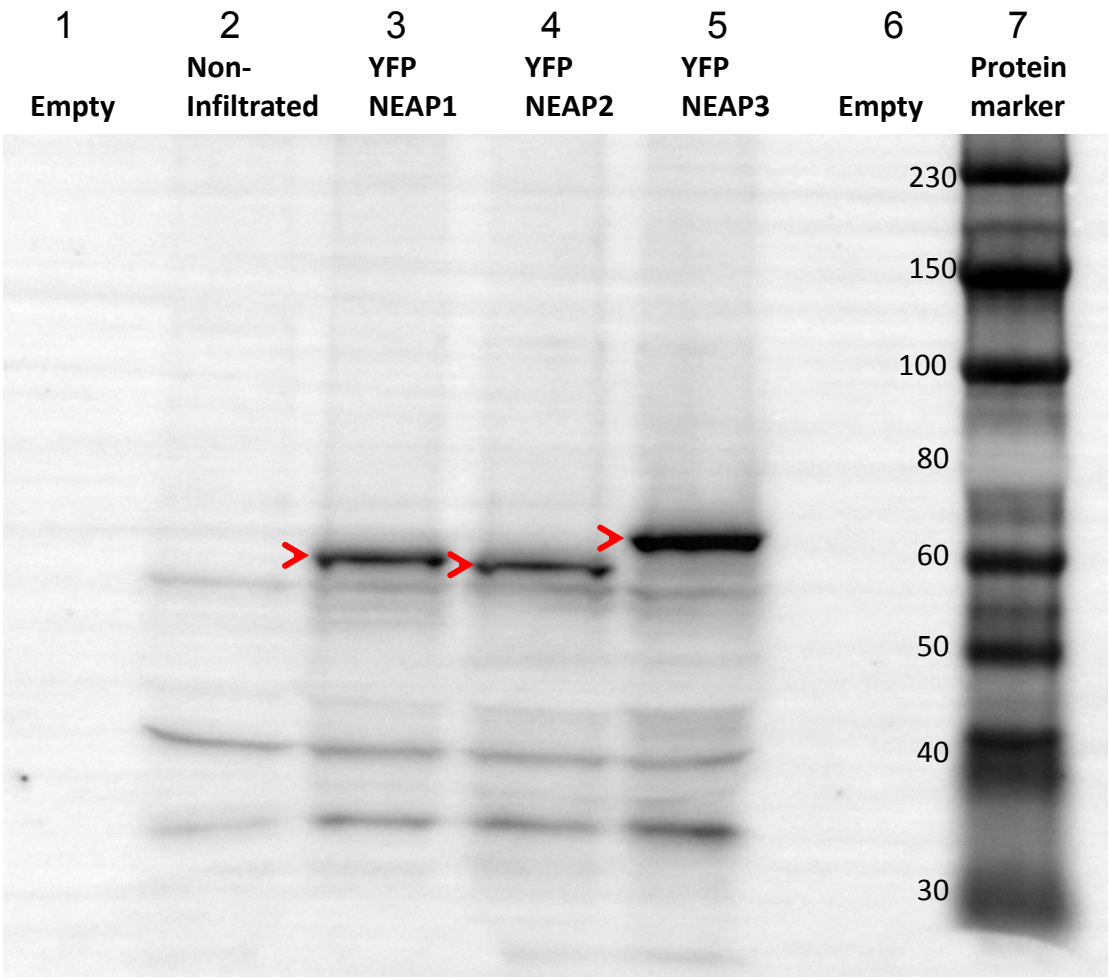

Figure 3.12: Protein extract from *N. benthamiana* leaves transiently expressing YFP-AtNEAP1, YFP-AtNEAP2 and YFP-AtNEAP3 proteins in the presence of p19, the suppressor of RNA silencing. The proteins are resolved on an 8% SDS-PAGE and detected on a Western Blot using YFP antibody (described in Chapter 2, section 2.4). YFP-AtNEAP1 runs marginally above the 60kDa marker, YFP-AtNEAP2 runs at approximately 60kDa and YFP-AtNEAP3 runs at approximately 65kDa, shown by red arrows. Protein molecular masses marked in red include the molecular weight of the YFP (~27kDa) tag in addition to their respective NEAP proteins. Thus, the net molecular masses of AtNEAP1, AtNEAP2 and AtNEAP3 were approximately 34, 33 and 38 kDa respectively.

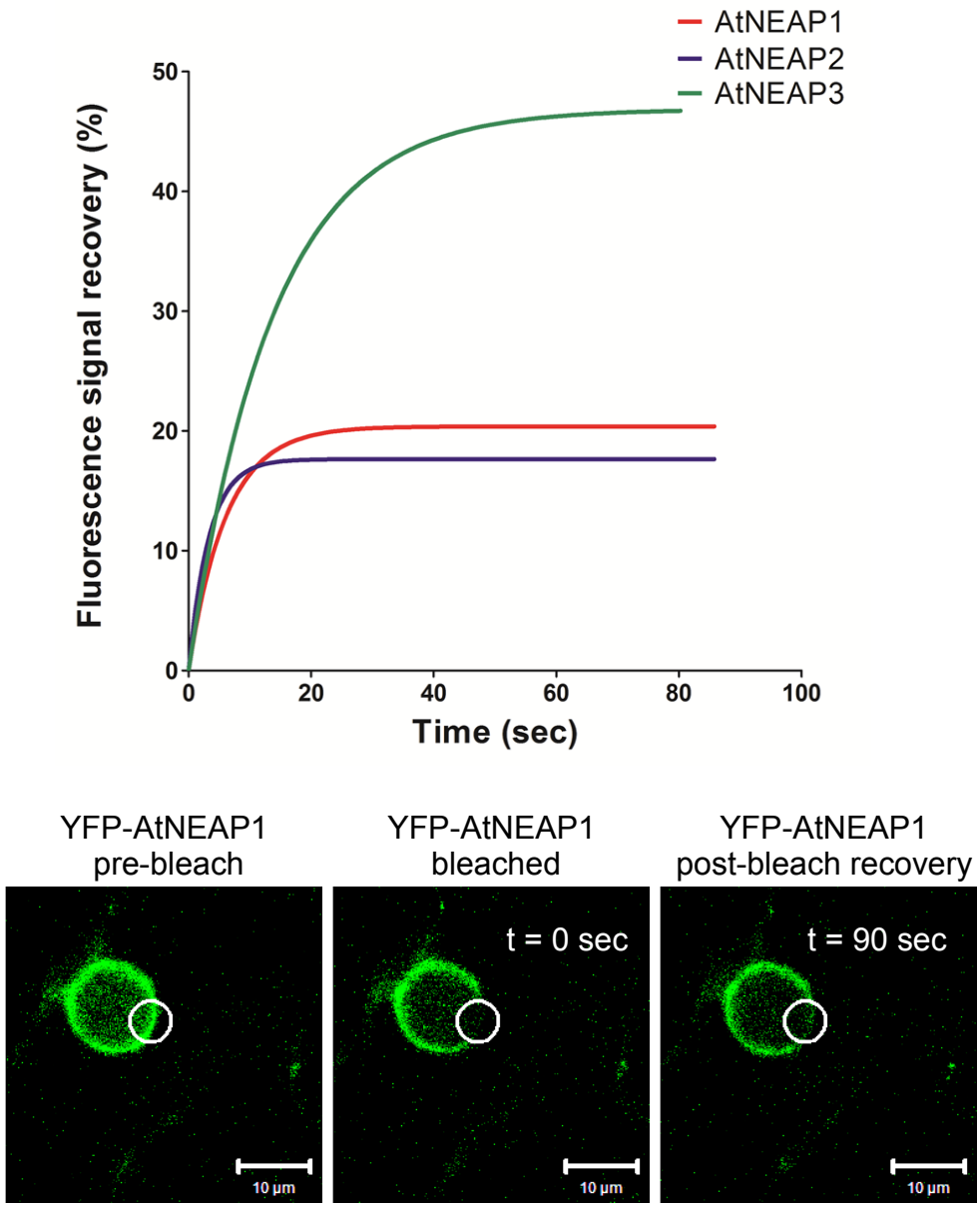

Figure 3.13: Fluorescence recovery curves of YFP-AtNEAP1 (red), YFP-AtNEAP2 (blue) and YFP-AtNEAP3 (green) obtained after photo-bleaching of proteins *in planta*. Time zero on graph denotes time of bleach. Maximum recovery and half time values are expressed as Mean ± standard error of mean (SEM). Result of an unpaired t-test showed that the maximum fluorescence recovery of YFP-AtNEAP3 was significantly ($p<0.0001$) higher than YFP-AtNEAP1 and YFP-AtNEAP2.

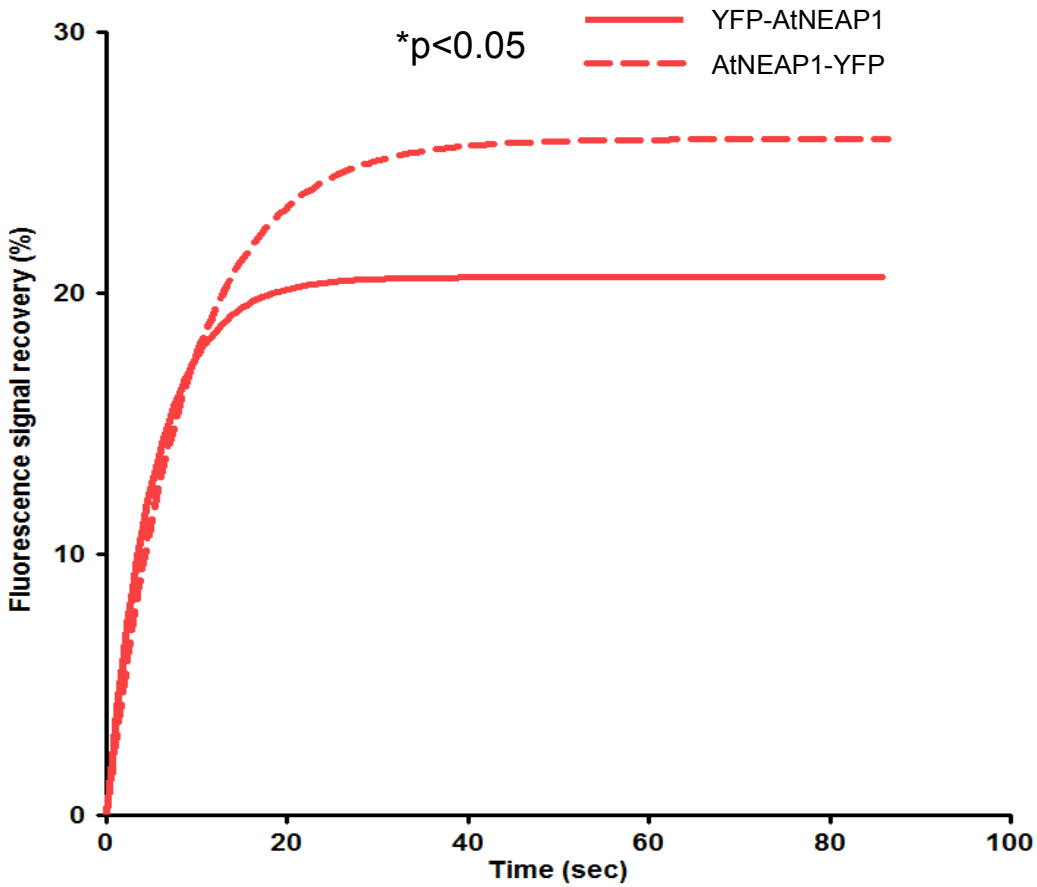

Figure 3.14: Fluorescence recovery curves of YFP-AtNEAP1 (solid red) compared to AtNEAP1-YFP (dotted red) *in planta*. Time zero on graph denotes time of bleach. Maximum recovery and half time values are expressed as Mean ± SEM. Result of an unpaired t-test showed that the two curves were significantly different (p = 0.02).

Chapter 4

NEAP-protein interactions at the nuclear envelope

Chapter 4
NEAP-protein interactions at the nuclear envelope

4.1 Introduction

As described in Chapter 3, the NEAPs are a novel family of plant-specific proteins. Their extensive CC domains, NLS and hydrophobic C-termini are reminiscent of IF-like organisation (Dechat et al. 2010). Their resistance to biochemical extraction in the presence of high ionic salt and Triton X-100 is not dissimilar to that seen in other nuclear matrix proteins (Foisner and Gerace 1993, Masuda et al. 1997). In addition, their INM localisation dependant on the active NLS and TM domains and their ability to form immobilised assemblies, suggest the hypothesis that NEAPs are nuclear IF-like proteins and could function as membrane intrinsic components of the lamina in plants.

As stated in Chapter 1, plant genomes lack sequence homologues to the metazoan lamins. In the absence of lamins, an alternative family of NMCP proteins has been described as the first lamin analogues in plants (Ciska and Moreno Diaz de la Espina 2014). The similarities between the NEAP and NMCP protein families has been discussed in Chapter 3, section 3.4 with respect to their protein structure, tissue specific expression, subcellular localisation, biochemical nature and membrane affinities.

It is known from metazoan systems that the different types of lamin proteins form complex cross interaction networks at the nuclear periphery interacting with INM integral proteins, filamentous lamina components as well as chromatin binding proteins (Dechat et al. 2010). This chapter explores the interactions of NEAP proteins at the NE with known and putative plant lamina components as well as the INM integral SUN domain family known to interact with metazoan lamins.

4.2 Aims

The main aim of the work presented in this chapter was to dissect the protein-protein interaction network of AtNEAP proteins by;

a. Studying the effect of co-expression of AtNEAP proteins with each other, with AtNMCP1, and with AtSUN domain proteins on sub-cellular localisation using different N- and C- terminal combinations of FP tags and confocal microscopy

b. Using apFRET to detect the presence of interactions between AtNEAP proteins, AtNMCP1 and AtSUN domain proteins co-localised at the NE;

c. Confirming AtNEAP protein interactions detected in aim b with MYTH assays

d. Identification of novel proteins that interact with AtNEAP1 by screening an *A. thaliana* cDNA library using the MYTH system

4.3 Results

4.3.1 Co-localisation and interactions of AtNEAP proteins with each other

Different combinations of N- and C-terminal fusions of AtNEAP proteins to YFP and CFP were co-expressed in order to study their effect on localisation indicating possible interaction. The constructs were infiltrated in *N. benthamiana* leaves in the presence of an inhibitor of RNA silencing protein, p19, and allowed to express transiently under the CMV 35S promoter. Leaf epidermal cells were observed using the confocal microscope 2 days post infiltration. The detailed protocol is described in Chapter 2 (sections 2.2.5 and 2.5.1). All confocal micrographs shown in this chapter are from an experiment representative of the data collected in duplicates on 5 or more occasions.

When an N-terminal YFP fusion of AtNEAP1 was expressed with a C-terminal CFP of AtNEAP1 both the YFP and the CFP fluorescence was seen concentrated at the nuclear periphery as a ring of variable thickness, with a small amount of fluorescence visible in the cytoplasm (figure 4.1a). Similarly YFP-AtNEAP2 co-localised with AtNEAP2-CFP (figure 4.1b) and YFP-AtNEAP3 was co-localised with AtNEAP3-CFP (figure 4.1c) at the nuclear periphery and the cellular periphery (cytoplasm). In some cases the AtNEAP fluorescence was found to aggregate in punctate structures at the nuclear periphery as seen in figure 4.1c.

Figure 4.2 shows the expression of N-terminally fused YFP-AtNEAP with other C-terminally fused AtNEAP-CFP proteins. When YFP-AtNEAP1 was expressed with C-terminal CFP fusion of AtNEAP2 (figure 4.2a) and AtNEAP3 (figure 4.2c), both proteins were co-localised at the nuclear periphery and in the cytoplasm. This result was also seen with YFP-AtNEAP2 co-expressed with AtNEAP3-CFP (figure 4.2b).

Interestingly when C-terminal CFP and YFP fusions of AtNEAP proteins were co-expressed, they were seen to dislocate from the nuclear periphery and disperse into the nucleoplasm. When a C-terminal YFP fusion of AtNEAP1 was

co-expressed with C-terminal CFP fusion of itself (figure 4.3a), AtNEAP2 (figure 4.3b) and AtNEAP3 (figure 4.3c); both the proteins lost the nuclear peripheral association and localised evenly to the nucleoplasm except the nucleolus. In all cases a small amount of AtNEAP fluorescence was also seen localised to the cytoplasm as seen at the cell periphery in figure 4.3. C-terminal YFP fusions of AtNEAP2 and AtNEAP3 were not constructed and were excluded from this study.

Furthermore when the YFP and CFP were fused to the N-termini of any two AtNEAP proteins, although they maintained their association with the NE, they lost the smooth ring-like appearance and appeared like irregular shaped beads on a string along the nuclear envelope (figures 4.4 and 4.5). Combinations of YFP-AtNEAP1 and CFP-AtNEAP1 (figure 4.4a), YFP-AtNEAP2 and CFP-AtNEAP2 (figure 4.4b) and YFP-AtNEAP3 and CFP-AtNEAP3 (figure 4.4c) showed co-localisation of both proteins into puncta at the nuclear periphery, along with some co-localised puncta in the cytoplasm. A similar co-localisation of proteins was also seen with co-expression of YFP-AtNEAP1 and CFP-AtNEAP2 (figure 4.5a), YFP-AtNEAP2 and CFP-AtNEAP3 (figure 4.5b) and YFP-AtNEAP3 and CFP-AtNEAP1 (figure 4.5c).

The interactions between AtNEAP proteins were tested using apFRET. This confocal microscopy technique relies on the principle that the CFP emission spectrum overlaps with the YFP excitation spectrum, and that the CFP has the potential to transfer its emission energy for excitation of the YFP (Karpova and McNally 2006, Sparkes et al. 2011). This transfer only takes place if YFP and CFP are in close proximity due to binding interactions of their fusion protein partners. The method is described in Chapter 2; section 2.5.3. Briefly, it involved transient co-expression of N-terminal CFP and YFP fusions of two AtNEAP proteins in *N. benthamiana* leaves, which were treated with 25μM Latrunculin B for 30 minutes, prior to the bleach. In a small region of the NE, the CFP fluorescence intensity was measured before and after YFP was bleached. Each data set comprised 30 nuclei collected from duplicate infiltrations in three separate experiments. A rise in CFP fluorescence post YFP bleach indicated interaction. FRET efficiency (E_F) defined as the percentage CFP fluorescence

intensity increase after YFP bleach was expressed as the mean ± SEM and was compared to the CFP E_F of a non-bleached control (figure 4.6).

The graph in figure 4.6 shows that there was no significant increase in CFP-AtNEAP1 fluorescence post YFP-AtNEAP1 bleach compared to the non-bleach control ($p=0.185$), indicating that AtNEAP1 does not interact with itself in this system. However, AtNEAP2 and AtNEAP3 showed interaction with themselves as shown by the significant ($p<0.001$) increase in CFP-AtNEAP2 (E_F 21.3 ± 1.7%) and CFP-AtNEAP3 (E_F 18.4 ± 1.9%) after the co-expressed YFP-AtNEAP2 and YFP-AtNEAP3 were bleached, respectively; compared to the non-bleached control (figure 4.6). Furthermore, bleaching YFP-AtNEAP3 also led to a significant ($p<0.001$) increase in co-expressed CFP-AtNEAP1 and CFP-AtNEAP2 fluorescence with calculated E_F of 16.6 ± 1.5% and 18.6 ± 1.4%, respectively. Also, bleaching YFP-AtNEAP1 led to a significant ($p<0.001$) increase in co-expressed CFP-AtNEAP2 (E_F 10.21± 1.1%). Thus AtNEAP1, AtNEAP2 and AtNEAP3 interacted with each other within this system.

Further, the AtNEAP3 domain deletion mutants described in Chapter 3, section 3.3.5 namely, YFP-AtNEAP3ΔCC1, YFP-AtNEAP3ΔCC2, YFP-AtNEAP3ΔNLS and YFP-AtNEAP3ΔTM were co-expressed with full length CFP-AtNEAP3 to study the effect on their localisation (figure 4.7). YFP-AtNEAP3ΔCC1, which was nucleoplasmic when expressed on its own (Chapter 3, figure 3.11a), was found to co-localise with CFP-AtNEAP3 in the nucleoplasm, cytoplasm and at the nuclear periphery, where fluorescence was strongest (figure 4.7a). Also, YFP-AtNEAP3ΔCC2 which localised at the nuclear periphery when expressed on its own (Chapter 3, figure 3.11b) was found to co-localise with CFP-AtNEAP3 at the nuclear periphery (figure 4.7b). Further YFP-AtNEAP3ΔNLS which was localised to the nucleoplasm and cytoplasm when expressed singly (Chapter 3, figure 3.11c) was found to co-localise with CFP-AtNEAP3 in the nucleoplasm, cytoplasm and at the nuclear periphery, where fluorescence was strongest (figure 4.7c). Finally, figure 4.7d shows CFP-AtNEAP3 localised at the nuclear periphery and co-localised with YFP-AtNEAP3ΔTM in the nucleoplasm and cytoplasm. Thus localisation of YFP-AtNEAP3ΔTM (Chapter 3. figure 3.11d) does not change when expressed in combination with CFP-AtNEAP3 (figure 4.7d). YFP-AtNEAP3ΔCC1, YFP-AtNEAP3ΔCC2 and YFP-

AtNEAP3ΔNLS, all co-localised with CFP-AtNEAP3 at the NE and will be tested for interaction using apFRET and the MYTH assays (Chapter 6 section 6.3.2).

4.3.2 Co-localisation of AtNEAP proteins with *A. thaliana* NMCP1

A 35S promoter driven genomic DNA construct of the *A. thaliana* homologue of carrot NMCP1 (also called LINC1, CRWN1 or KAKU2) fused to C-terminal YFP was previously supplied to the laboratory by Eric Richards (Boyce Thompson Institute for Plant Research, New York, Dittmer et al. 2007, Sakamoto and Takagi 2013, Goto et al. 2014). AtNMCP1 when infiltrated in *N. benthamiana* leaves in the presence of p19 localised to the nucleoplasm and cytoplasm after three days and to the nucleoplasmic periphery after five days (figure 4.8d). However when co-expressed with any AtNEAP protein fused to N- or C-terminal CFP, AtNMCP1-YFP failed to localise to the nuclear periphery and remained nucleoplasmic until 5-6 days after infiltration (figures 4.8 and 4.9). When co-expressed with AtNMCP1-YFP, the N-terminal CFP fusions of AtNEAP1 (figure 4.8a), AtNEAP2 (figure 4.8b) and AtNEAP3 (figure 4.8c) were found to be co-localised in the nucleoplasm with AtNMCP1-YFP as well as in the cytoplasm. Interestingly, C-terminal CFP fusions of AtNEAP1 (figure 4.9a), AtNEAP2 (figure 4.9b) and AtNEAP3 (figure 4.9c) were localised to the nuclear periphery, cytoplasm and to some extent to the nucleoplasm when co-expressed with AtNMCP1-YFP. In the absence of co-localisation of AtNEAP proteins with AtNMCP1 at the nuclear periphery, apFRET could not be used to test their interaction. Their interaction will be tested using MYTH (Chapter 6 section 6.3.2).

4.3.3 Co-localisation and interactions of AtNEAP proteins with the SUN domain family

To study the effect of co-expression, different combinations of N- and C-terminal YFP fusions of AtSUN1 and AtSUN2 were co-infiltrated with N- and C-terminal CFP fusions of AtNEAP1, AtNEAP2 and AtNEAP3 in *N. benthamiana* leaves in the presence of p19 (infiltration method in Chapter 2 section 2.2.5).

When an N- terminal YFP fusion of AtSUN1 (figure 4.10) or AtSUN2 (figure 4.11) was co-expressed with an N-terminal YFP fusion of AtNEAP1, AtNEAP2 or AtNEAP3; the YFP-AtSUN protein co-localised with the CFP-AtNEAP protein at the nuclear periphery. However, when AtNEAP1-CFP, AtNEAP2-CFP and AtNEAP3-CFP were co-expressed with YFP-AtSUN1 (figure 4.12) or YFP-AtSUN2 (figure 4.13), the AtNEAP-CFP proteins were found to localise to the nucleoplasm and failed to co-localise with the co-expressed YFP-AtSUN protein at the nuclear periphery.

Interestingly, when the above C-terminal CFP fusions of AtNEAP1, AtNEAP2 or AtNEAP3 were co-expressed with a C-terminal YFP fusion of AtSUN1 (figure 4.14) or AtSUN2 (figure 4.15), the AtNEAP-CFP co-localised with the AtSUN-YFP at the nuclear periphery. However, unlike the N-terminal YFP-AtSUN and C-terminal AtNEAP-CFP co-expression (figures 4.12 and 13), when AtSUN1-YFP (figure 4.16) or AtSUN2-YFP (figure 4.17) was co-expressed with N-terminal CFP fusions of AtNEAP1, AtNEAP2 or AtNEAP3, they co-localised at the nuclear periphery. In summary AtNEAP proteins co-localise with AtSUN1 and AtSUN2 at the NE, apart from when N-terminal constructs of AtSUN proteins were co-expressed with C-terminal constructs of AtNEAP proteins, which resulted in the AtNEAP proteins being localised to the nucleoplasm.

Using apFRET, C-terminal YFP fusions of AtSUN1 and AtSUN2 were seen to interact with C-terminal CFP fusions of AtNEAP1, AtNEAP2 and AtNEAP3. Bleaching AtSUN1-YFP led to a significant ($p<0.005$) increase in co-expressed AtNEAP1-CFP, AtNEAP2-CFP and AtNEAP3-CFP fluorescence with averages E_F of 6.9 $\pm$ 0.7%, 7.8 $\pm$ 0.7%, and 3.9 $\pm$ 0.4%, respectively (figure 4.18). Similarly, bleaching AtSUN2-YFP led to a significant ($p<0.0001$) increase in co-expressed AtNEAP1-CFP, AtNEAP2-CFP and AtNEAP3-CFP fluorescence with average FRET efficiencies of 18.4 $\pm$ 1.4%, 14.43 $\pm$ 0.9%, and 26.9 $\pm$ 1.9%, respectively (figure 4.18).

To further understand the nature of NEAP-SUN interactions, several domain deletion mutants of AtSUN2 were examined. C-terminal YFP fusions of AtSUN2 mutants containing a deletion of their N-terminus (AtSUN2ΔN-YFP), CC (AtSUN2ΔCC-YFP) and SUN domain (AtSUN2ΔSUN-YFP; Graumann et al.

2010) were co-expressed with AtNEAP1-CFP, AtNEAP2-CFP and AtNEAP3-CFP. Both AtSUN2ΔCC-YFP and AtSUN2ΔSUN-YFP co-localised with C-terminal CFP fusions of AtNEAP proteins at the nuclear periphery (figure 4.19 and 4.20). Figure 4.19 shows AtSUN2ΔCC-YFP co-localised with AtNEAP1-CFP, AtNEAP2-CFP and AtNEAP3-CFP at the nuclear periphery. Figure 4.20 shows AtSUN2ΔSUN-YFP co-localised with AtNEAP1-CFP, AtNEAP2-CFP and AtNEAP3-CFP at the nuclear periphery.

When tested using apFRET, AtSUN2ΔCC-YFP interacted with AtNEAP1-CFP, AtNEAP2-CFP and AtNEAP3-CFP with an E_F of 9.1 $\pm$ 0.7%, 13.2 $\pm$ 1.3 % and 11.1 $\pm$ 1.0%, respectively (figure 4.21). AtSUN2ΔSUN-YFP also interacted with AtNEAP1-CFP, AtNEAP2-CFP and AtNEAP3-CFP with an E_F of 18.7 $\pm$ 1.3 %, 18.5 $\pm$ 1.2 % and 15.7 $\pm$ 2.5%, respectively (figure 4.21).

The nucleoplasmic localisation of AtSUN2ΔN-YFP (figure 4.22d) was marginally altered in the presence of C-terminal CFP fusions of AtNEAP proteins (figure 4.22a, b and c). In every cell observed, along with its nucleoplasmic localisation, AtSUN2ΔN-YFP labelled the nuclear periphery when co-expressed with AtNEAP1-CFP (figure 4.22a), AtNEAP2-CFP (figure 4.22b) and AtNEAP3-CFP (figure 4.22c). Further apFRET and MYTH assays will be performed to test if AtSUN2ΔN-YFP interacts with AtNEAP-CFP (Chapter 6 section 6.3.2). An N-terminal CFP truncation mutant containing the first 264 N-terminal amino acids of AtSUN2 (CFP-AtSUN2_264; Graumann et al., 2010) was also co-expressed with YFP-AtNEAP proteins. Co-expression with YFP-AtNEAP1 (figure 5.23a), YFP-AtNEAP2 (figure 5.23b) and YFP-AtNEAP3 (figure 5.23c) did not change the nucleoplasmic localisation of CFP-AtSUN2_264 and NE localisation of YFP-AtNEAP3. With the lack of co-localisation at the NE, apFRET could not be done for these combinations. As part of future work, MYTH assays will be carried out to test the interaction *ex vivo* (Chapter 6 section 6.3.2). Also AtSUN1 and AtSUN2 will be co-expressed with the AtNEAP3 deletion constructs described in Chapter 3, section 3.3.5 namely, YFP-AtNEAP3ΔCC1, YFP-AtNEAP3ΔCC2, YFP-AtNEAP3ΔNLS and YFP-AtNEAP3ΔTM to see if co-expression affects localisation (Chapter 6 section 6.3.2). Their interaction will also be tested using apFRET and MYTH (Chapter 6 section 6.3.2).

4.3.4 Confirmation of interactions using MYTH

The MYTH system was employed to confirm the NEAP-SUN interactions and NEAP-NEAP interactions identified by apFRET. This assay can be used to study interactions between two membrane proteins or to identify novel interactors of a selected membrane protein (described in Chapter 2 section 2.6). Briefly, it works via re-constitution of the N-terminal (Nub) and C-terminal (Cub) halves of an ubiquitin molecule split between the putative interacting membrane proteins of choice (Snider et al. 2010). Interaction between the two proteins leads to the re-assembly of the split ubiquitin, which sends a signal for proteolysis and cleaves the tagged transcription factor (TF) activating a cascade of events leading to the activation of the reporter system (Snider et al. 2010). The presence of interaction is reported by the growth of transformed yeast colonies on restrictive medium. Colony growth on permissive medium was indicative of successful transformation. Transformation with empty prey vector was used as negative control, whereas an ER protein fused to the N-terminus of a split ubiquitin molecule was used as positive control in all experiments. All MYTH assays were performed in the laboratory of Professor Christophe Tatout (Université Blaise Pascal, Clermont-Ferrand, France) using vectors constructed by Dr. Emmanuel Vanrobays (Université Blaise Pascal, Clermont-Ferrand, France).

In an attempt to confirm some of the NEAP interactions observed *in planta* (sections 4.3.1 and 4.3.2), two bait vectors containing AtNEAP1 and AtNEAP2 were used. The AtNEAP3 bait vector constructed was found to activate the detection mechanism even in the absence of prey and was discarded as leaky. When yeast containing the AtNEAP1 bait were transformed with AtNEAP1, AtNEAP2 and AtNEAP3 prey vectors, all transformations successfully yielded colonies on restrictive medium (figure 4.24a), thus confirming the AtNEAP1-AtNEAP2 and AtNEAP1-AtNEAP3 interaction identified previously *in planta* (figure 4.6). Interestingly, the AtNEAP1-AtNEAP1 interaction identified in the MYTH assay was not detected by apFRET *in planta* (figure 4.6).

Further, yeast containing AtNEAP2 bait was transformed with AtSUN1 and AtSUN2, as well as the mid-SUN domain proteins AtSUN3, AtSUN4 and

AtSUN5 coding prey vectors to test NEAP-SUN interactions. The growth of colonies on restrictive medium confirmed the interactions of AtNEAP2 with AtSUN1 and AtSUN2, as well as identifying NEAP interactions with the mid-SUN domain proteins AtSUN3, AtSUN4 and AtSUN5 for the first time (figure 4.24b). NEAP interactions with mid-SUN proteins will be studied *in planta* using apFRET (Chapter 6 section 6.3.2).

4.3.5 Screening an *A. thaliana* cDNA library for novel protein interaction partners of AtNEAP1 using the MYTH assay

The above MYTH assay was also employed to screen the *A.thaliana* cDNA library for novel AtNEAP1 interaction partners (method described in Chapter 2 section 2.6). Briefly, 3.6 million cDNA fragments were screened for interactors of AtNEAP1 bait, 36 colonies grew on highly restrictive medium and 120 clones grew on low stringency restrictive medium. Isolated cDNA fragments were re-transformed into yeast containing the AtNEAP1 bait and allowed to grow on restrictive medium. Twenty five colonies were transformed and grew for a second time on restrictive medium, and were sent for sequencing. Nine of the 25 colonies sequenced returned a single gene that also grew on the highest restrictive medium used, At2g40620 (Table 4.1). At2g40620 is a basic-leucine zipper (bZIP) TF and annotated in TAIR as bZIP18 (Jakoby et al. 2002). Additionally, At3G16240 annotated delta tonoplast instrisic protein (TIP) localised to the vacuole and ER, was sequenced from three colonies that also grew on highly restrictive medium. Seven hits were proteins that were known to be localised to the chloroplast (Table 4.1). Two of those proteins, At2G10940 and At2G34430 have previously been identified in the crude nuclear lamina fraction by mass spectrometry (Sakamoto and Takagi 2013) and two others, At3G21200 and At4g20260 were predicted within the SubCellular Proteomic Database (SUBA3) to be localised to the nucleus (Tanz et al. 2013). Another interesting candidate was At5G12250, a beta 6 tubulin subunit which is a component of the microtubule cytoskeleton (table 4.1).

4.3.6 A novel AtNEAP1 interacting protein

As stated previously in section 4.3.5 the most interesting candidate from the MYTH cDNA library screen was AtbZIP18. In order to confirm its nuclear localisation as well as test its interaction with AtNEAP1 *in planta* the CDS of AtbZIP18 was fused to YFP on its N-terminus under the CMV 35S promoter and expressed transiently in *N. benthamiana* with p19 (method described in Chapter 2 sections 2.2.5 and 2.3.9). YFP-AtbZIP18 was localised to the nucleoplasm (figure 4.25a) and cytoplasm (figure 4.25b) in leaf epidermal cells. When co-expressed with YFP-AtbZIP18, an N-terminal CFP fusion of AtNEAP1 failed to accumulate at the nuclear periphery and was found to co-localise with the YFP-bZIP18 in the nucleoplasm and to some extent in cytoplasmic strands and the cell periphery (figure 4.25c). Co-expression of YFP-AtbZIP18 with AtNEAP1-CFP also yielded the same result leading to co-localisation of the two proteins in the nucleoplasm and cytoplasm (figure 4.25d). The nucleoplasmic co-localisation with YFP-bZIP18 was also seen with N- and C-terminal fusions of AtNEAP2 and AtNEAP3 (data not shown). The interaction of AtbZIP18 with AtNEAP1, AtNEAP2 and AtNEAP3 will be tested using apFRET (Chapter 6 section 6.3.2). Finally, all observed protein-protein interactions of AtNEAP proteins have been summarised in table 4.2, which also highlights proposed future work.

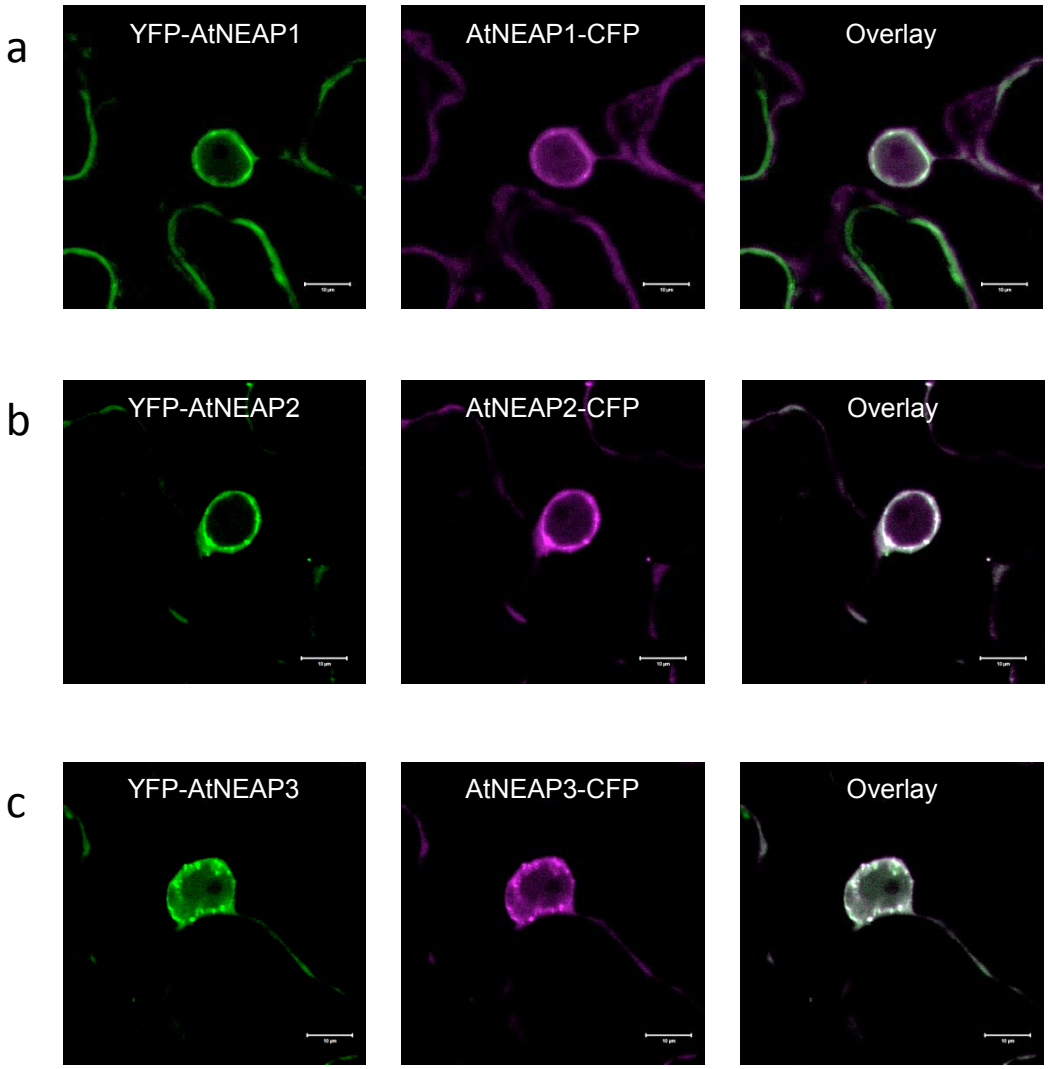

Figure 4.1: Confocal micrographs showing N-terminal YFP (green) fusions of AtNEAP proteins co-localised with C-terminal CFP (magenta) fusions of themselves at the nuclear periphery as well as localisation in the cytoplasm (seen at the cell periphery) expressed transiently under the 35S promoter in *N. benthamiana* leaf epidermal cells in presence of the suppressor of RNA silencing protein p19. Scale bar = 10µm.

a. YFP-AtNEAP1 and AtNEAP1-CFP
b. YFP-AtNEAP2 and AtNEAP2-CFP
c. YFP-AtNEAP3 and AtNEAP3-CFP

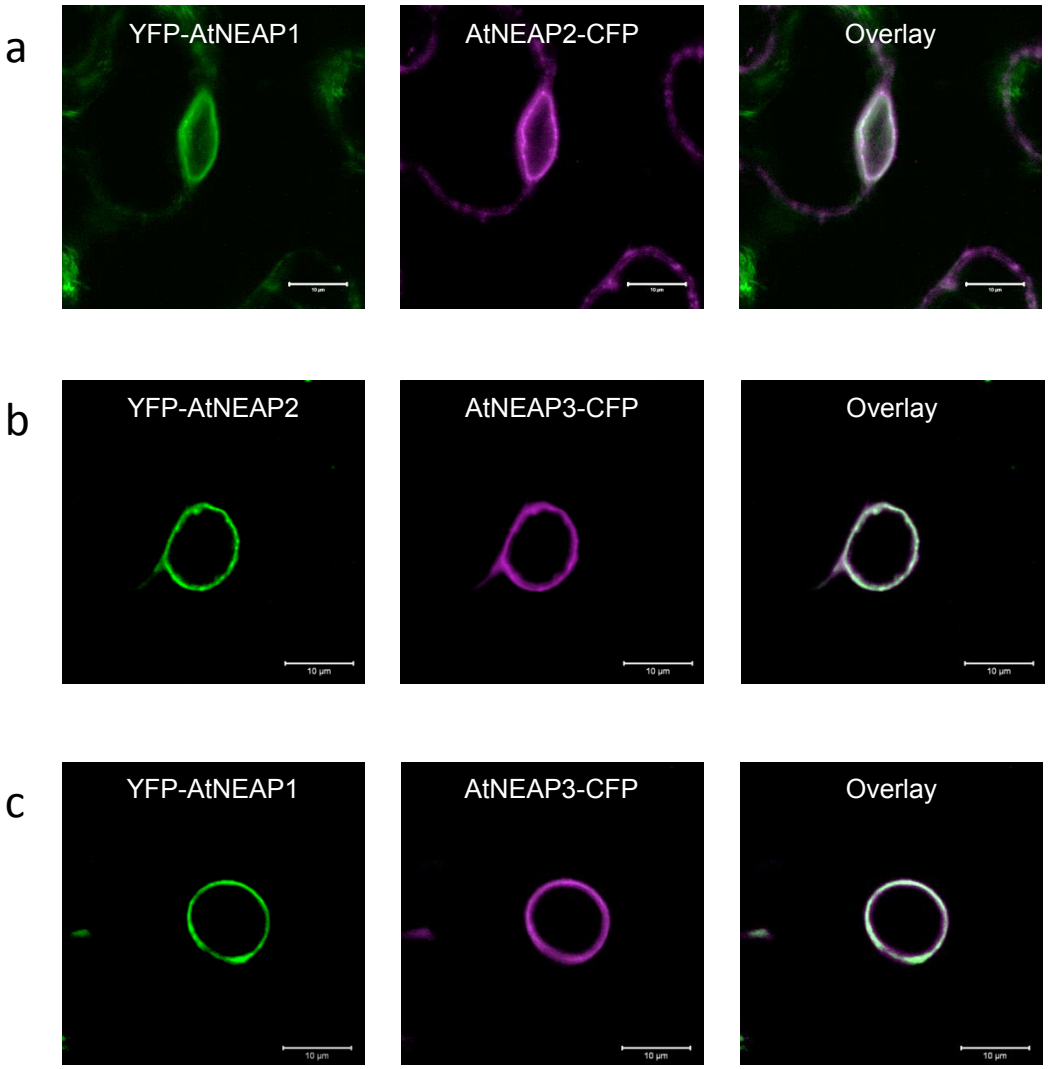

Figure 4.2: Confocal micrographs showing N-terminal YFP (green) fusions and C-terminal CFP (magenta) fusions of AtNEAP proteins co-localised at the nuclear periphery as well as localisation in the cytoplasm (seen at the cell periphery in a) expressed transiently under the 35S promoter in *N. benthamiana* leaf epidermal cells in presence of p19. Scale bar = 10µm.

a. YFP-AtNEAP1 and AtNEAP2-CFP
b. YFP-AtNEAP2 and AtNEAP3-CFP
c. YFP-AtNEAP1 and AtNEAP3-CFP

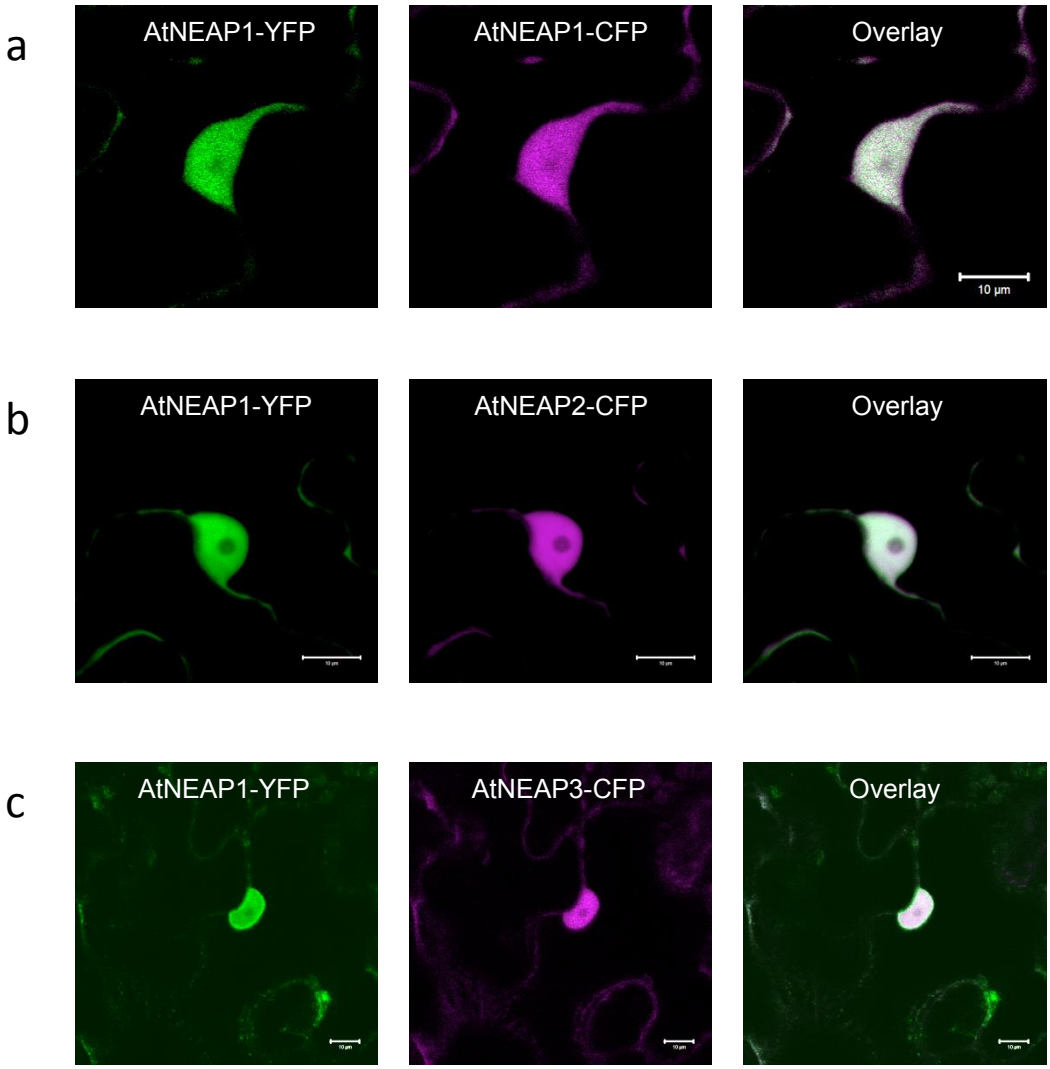

Figure 4.3: Confocal micrographs showing C-terminal YFP (green) fusions and C-terminal CFP (magenta) fusions of AtNEAP proteins co-localised in the nucleoplasm excluding the nucleolar region and in the cytoplasm (seen at the cell periphery) expressed transiently under the 35S promoter in *N. benthamiana* leaf epidermal cells in presence of p19. Scale bar = 10µm.

a. AtNEAP1-YFP and AtNEAP1-CFP
b. AtNEAP1-YFP and AtNEAP2-CFP
c. AtNEAP1-YFP and AtNEAP3-CFP

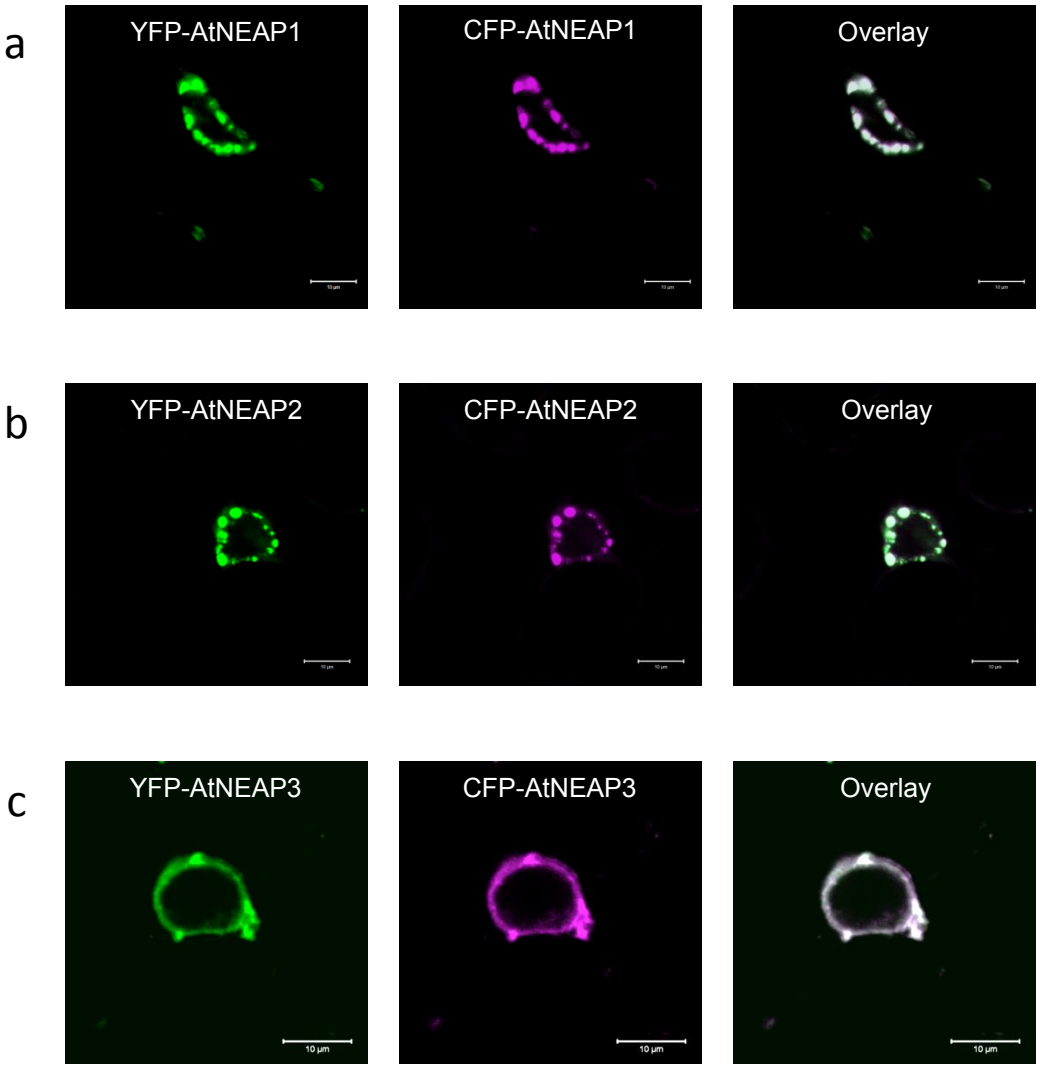

Figure 4.4: Confocal micrographs showing N-terminal YFP (green) fusions of AtNEAP proteins co-localised with N-terminal CFP (magenta) fusions of themselves at the nuclear periphery as an uneven ring interspersed with irregular punctate structures and in the cytoplasm (not seen) expressed transiently under the 35S promoter in *N. benthamiana* leaf epidermal cells in presence of p19. Scale bar = 10µm.

a. YFP-AtNEAP1 and CFP-AtNEAP1
b. YFP-AtNEAP2 and CFP-AtNEAP2
c. YFP-AtNEAP3 and CFP-AtNEAP3

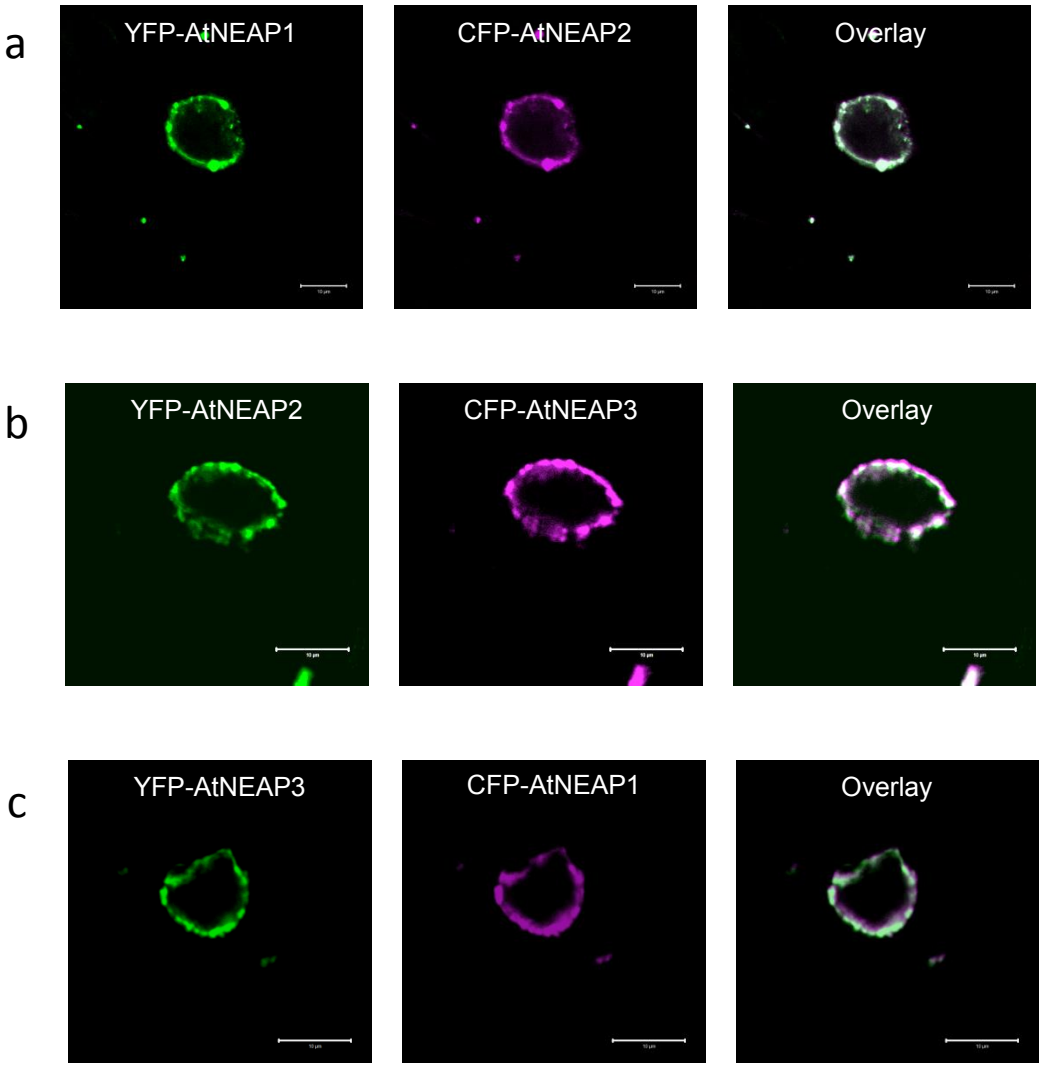

Figure 4.5: Confocal micrographs showing N-terminal YFP (green) fusions and N-terminal CFP (magenta) fusions of AtNEAP proteins co-localised at the nuclear periphery as an uneven ring interspersed with irregular punctate structures and in the cytoplasm (not seen) expressed transiently under the 35S promoter in *N. benthamiana* leaf epidermal cells in presence of p19. Scale bar = 10µm.

a. YFP-AtNEAP1 and CFP-AtNEAP2
b. YFP-AtNEAP2 and CFP-AtNEAP3
c. YFP-AtNEAP3 and CFP-AtNEAP1

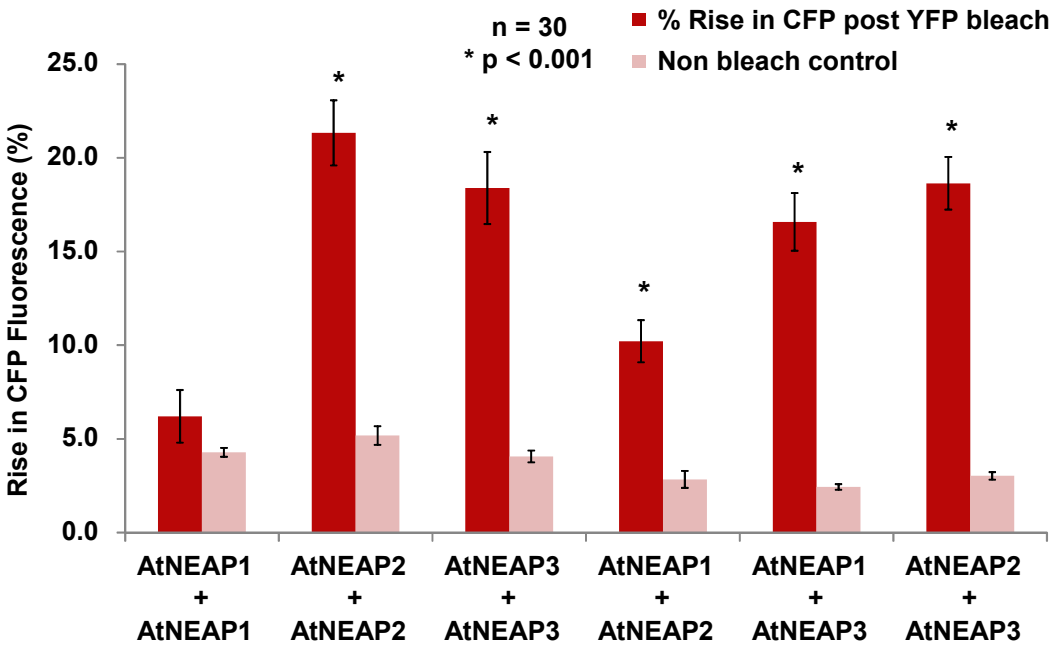

Figure 4.6: Bar graph showing change in CFP fluorescence in a region of bleached (red) versus a control non-bleached (pink) region of YFP fluorescence. A significant increase in CFP fluorescence indicates interaction with each other *in planta*. The paired bars represent the following combinations from left to right:

YFP-AtNEAP1 + CFP-AtNEAP1, YFP-AtNEAP2 + CFP-AtNEAP2, YFP-AtNEAP3 + CFP-AtNEAP3, YFP-AtNEAP1 + CFP-AtNEAP2, YFP-AtNEAP3 + CFP-AtNEAP1, and YFP-AtNEAP3 + CFP-AtNEAP2.

Values are expressed as percentage mean $\pm$ standard error of mean (SEM) and compared to a non-bleached control region (n=30). Paired t test was performed between the bleached and non bleached populations ($p<0.001$).

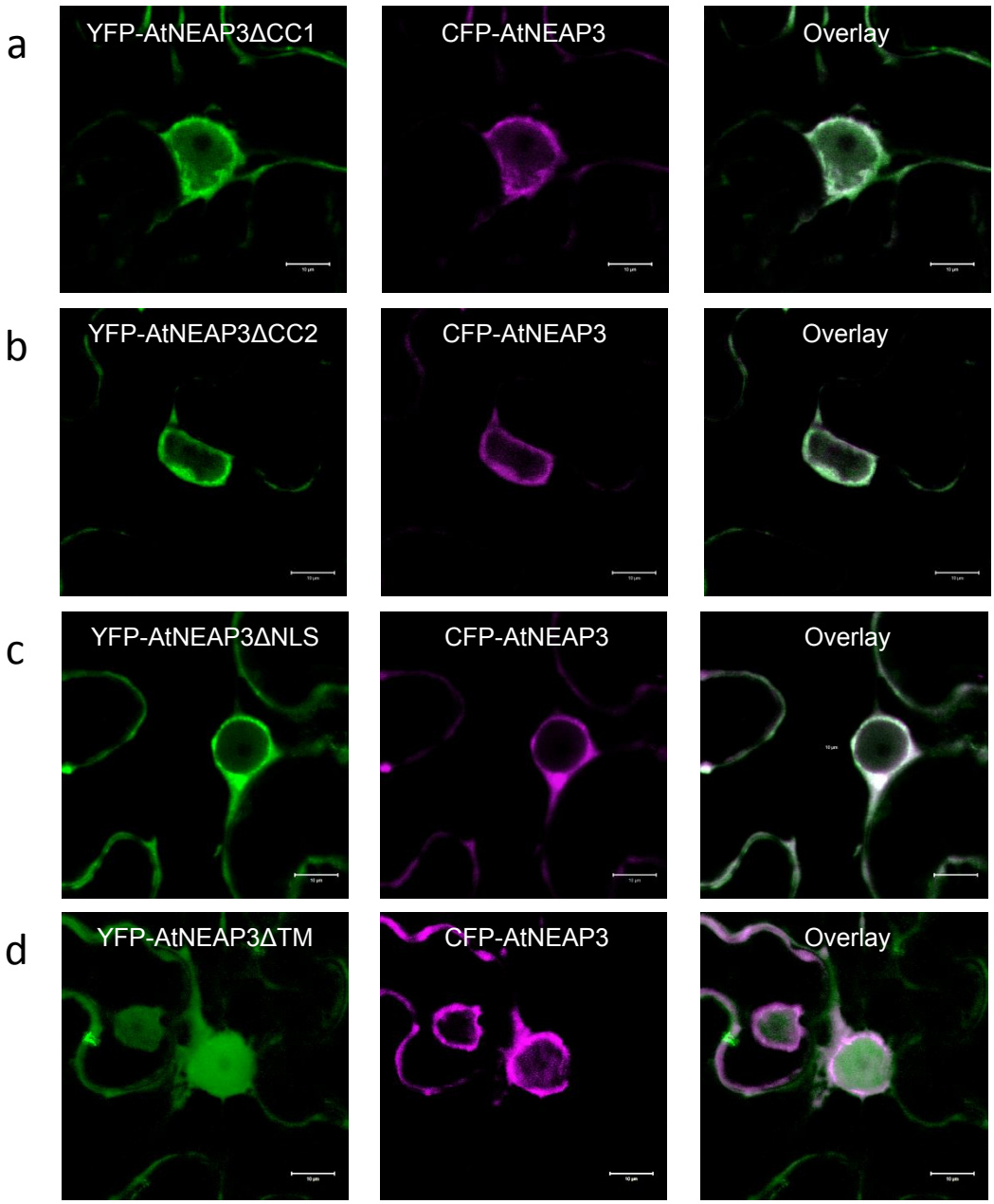

Figure 4.7: Confocal micrographs showing N-terminal CFP (magenta) fusions of AtNEAP3 at the nuclear periphery, nucleoplasm and cytoplasm when expressed with deletion constructs of AtNEAP3 fused to YFP (green) on their N-terminus. Expression was transient under the 35S promoter in *N. benthamiana* leaf epidermal cells in the presence of p19. Scale bar = 10µm.

a. YFP-AtNEAP3ΔCC1 localised at the nuclear periphery, nucleoplasm and cytoplasm
b. YFP-AtNEAP3ΔCC2 localised at the nuclear periphery, nucleoplasm and cytoplasm
c. YFP-AtNEAP3ΔNLS localised at the nuclear periphery, nucleoplasm and cytoplasm
d. YFP-AtNEAP3ΔTM localised in nucleoplasm and cytoplasm

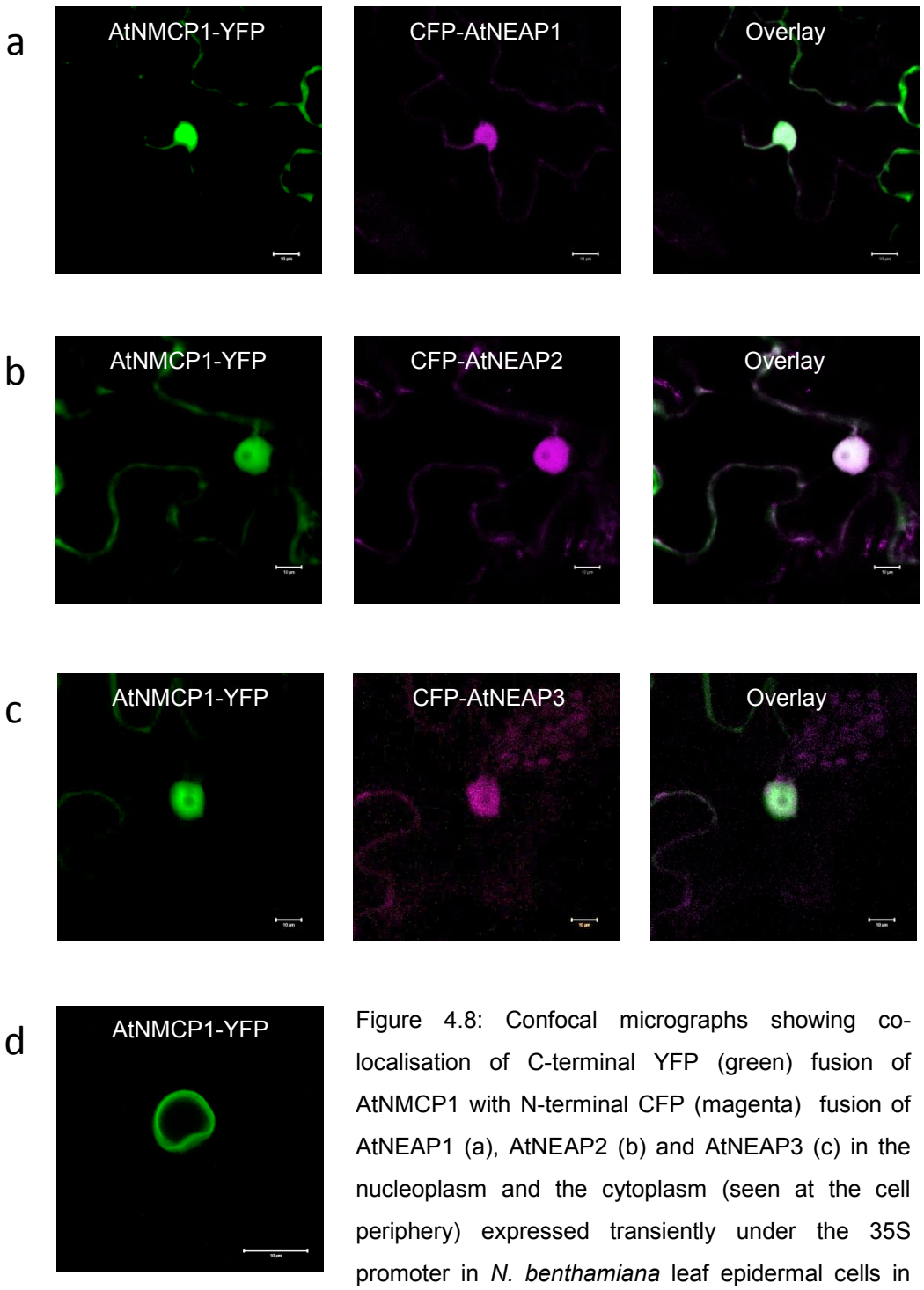

Figure 4.8: Confocal micrographs showing co-localisation of C-terminal YFP (green) fusion of AtNMCP1 with N-terminal CFP (magenta) fusion of AtNEAP1 (a), AtNEAP2 (b) and AtNEAP3 (c) in the nucleoplasm and the cytoplasm (seen at the cell periphery) expressed transiently under the 35S promoter in *N. benthamiana* leaf epidermal cells in presence of p19 after 5 days. d. shows localisation of AtNMCP1-YFP at the nuclear periphery when expressed on its own after 5 days. Scale bar = 10µm.

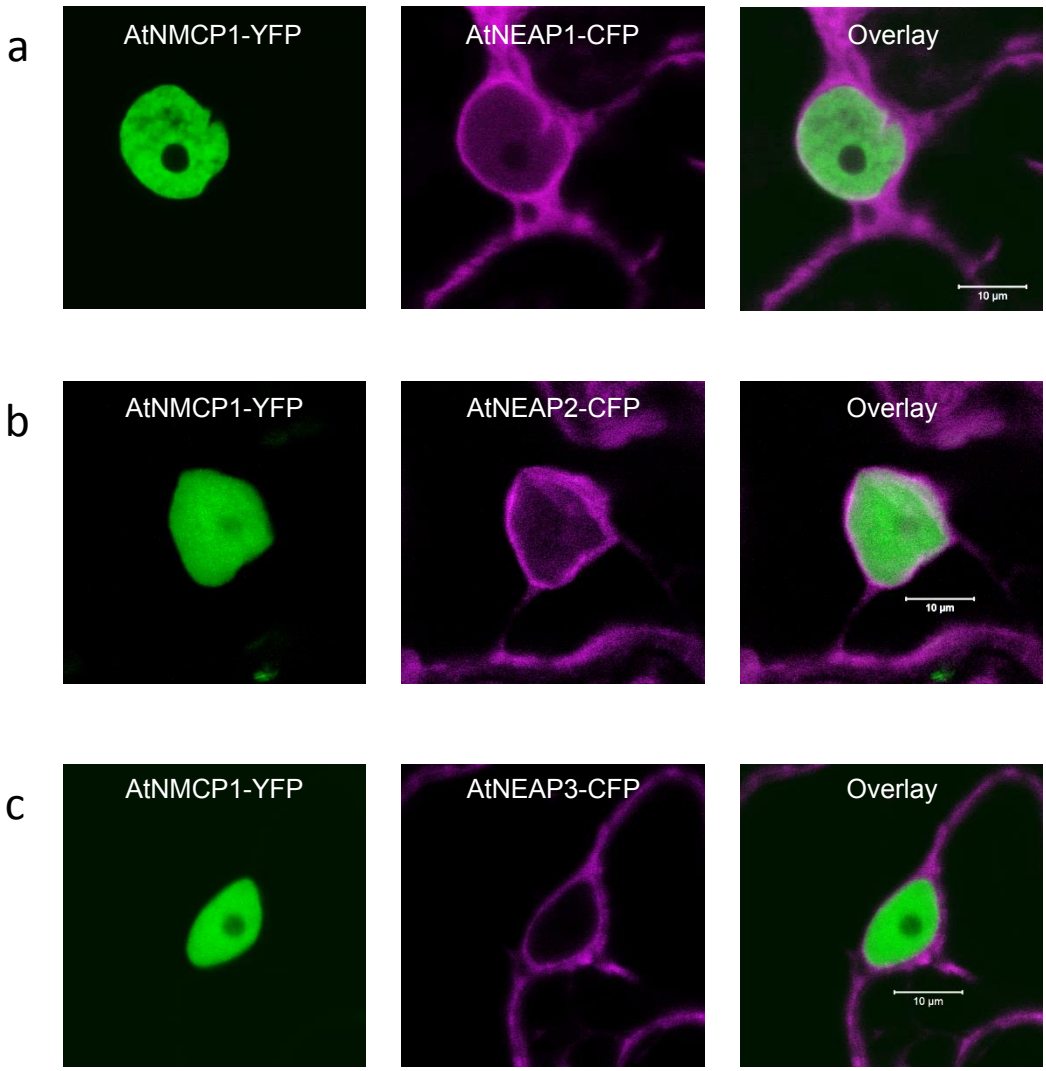

Figure 4.9: Confocal micrographs showing nucleoplasmic localisation of C-terminal YFP (green) fusion of AtNMCP1 with C-terminal CFP (magenta) fusions of AtNEAP1 (a), AtNEAP2 (b) and AtNEAP3 (c) localised to the nuclear periphery and the cytoplasm (seen at the cell periphery) expressed transiently under the 35S promoter in *N. benthamiana* leaf epidermal cells in the presence of p19 after 5 days. Scale bar = 10µm.

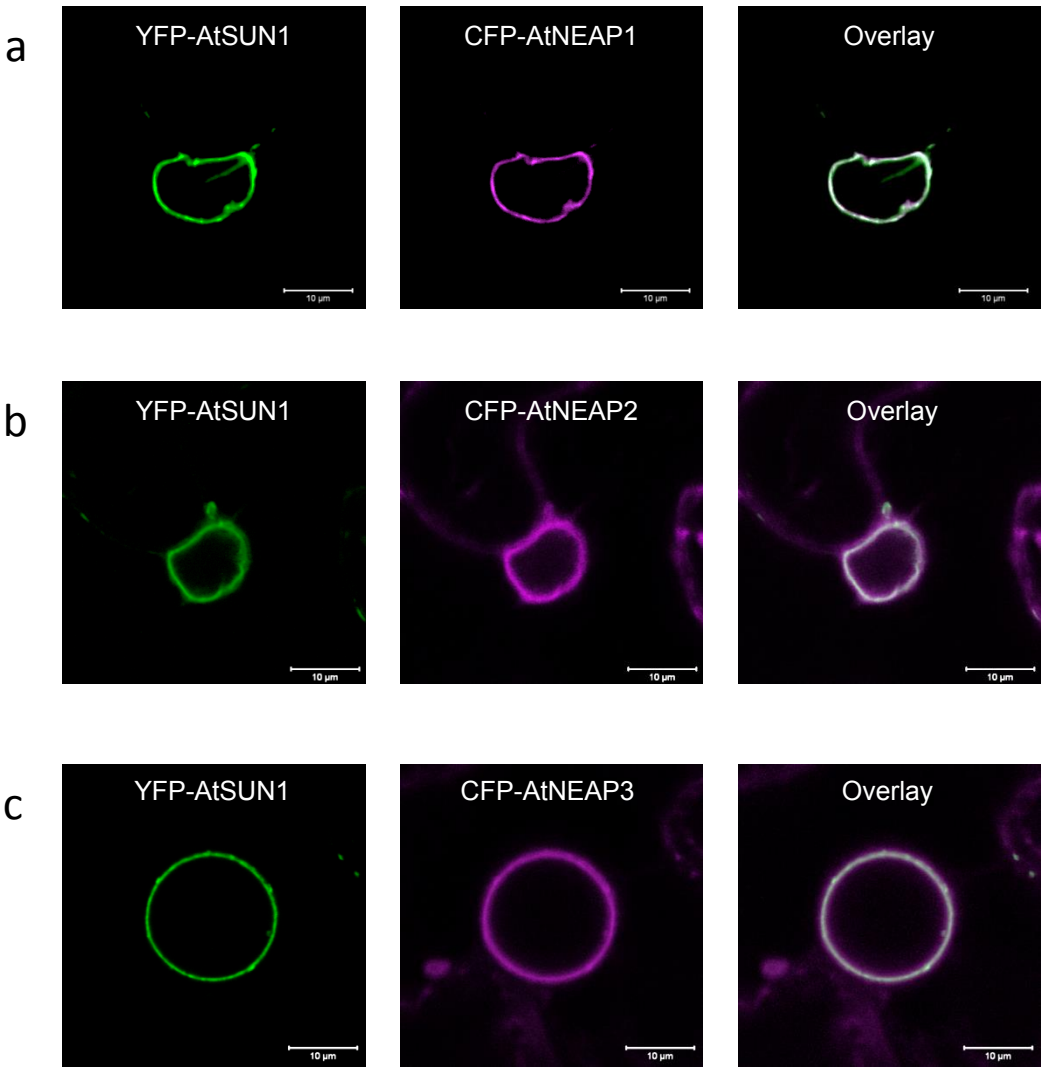

Figure 4.10: Confocal micrographs showing co-localisation of N-terminal YFP (green) fusion of AtSUN1 with N-terminal CFP (magenta) fusions of AtNEAP1 (a), AtNEAP2 (b) and AtNEAP3 (c) at the nuclear periphery expressed transiently under the 35S promoter in *N. benthamiana* leaf epidermal cells in presence of p19. Scale bar = 10µm.

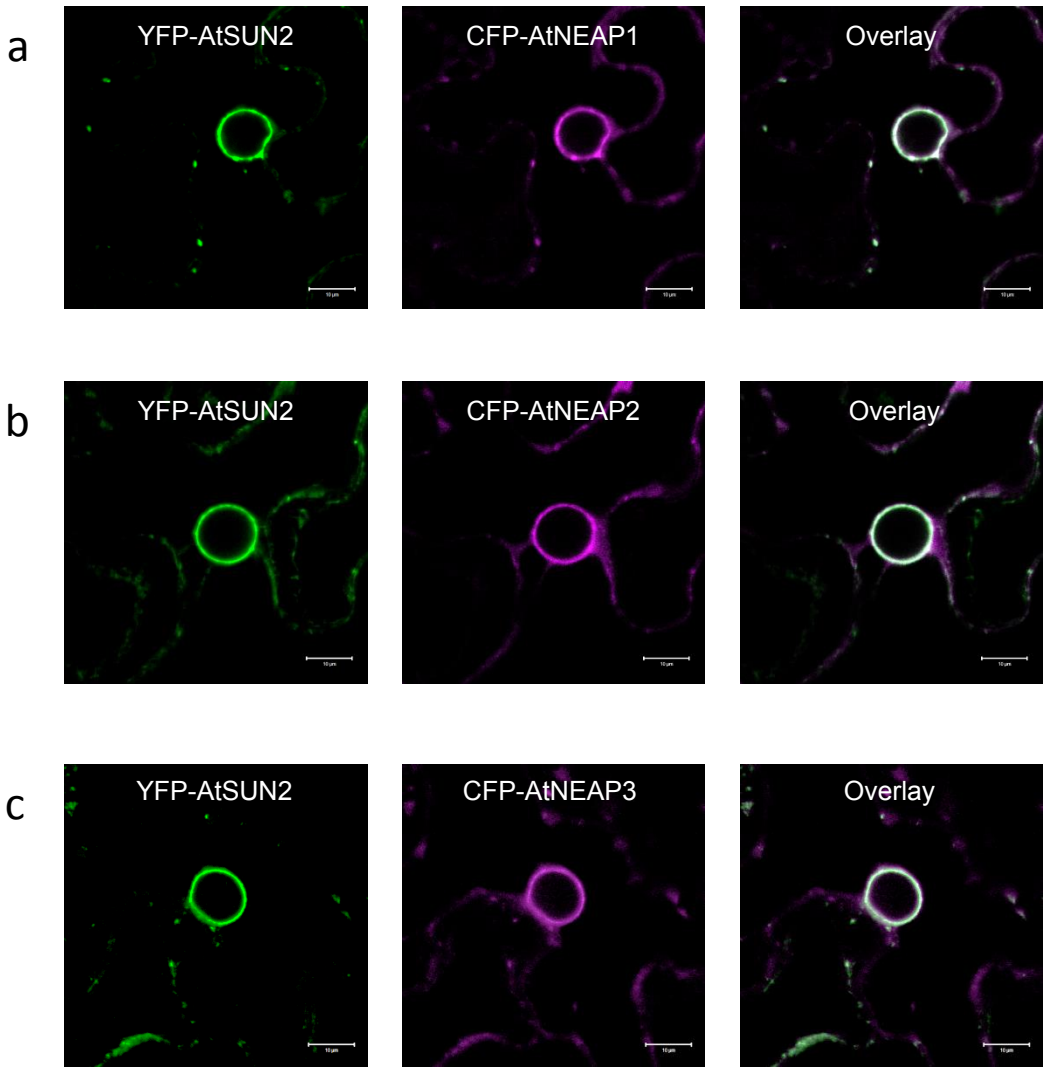

Figure 4.11: Confocal micrographs showing co-localisation of N-terminal YFP (green) fusion of AtSUN2 with N-terminal CFP (magenta) fusions of AtNEAP1 (a), AtNEAP2 (b) and AtNEAP3 (c) at the nuclear periphery and in the cytoplasm expressed transiently under the 35S promoter in *N. benthamiana* leaf epidermal cells in presence of p19. Scale bar = 10μm.

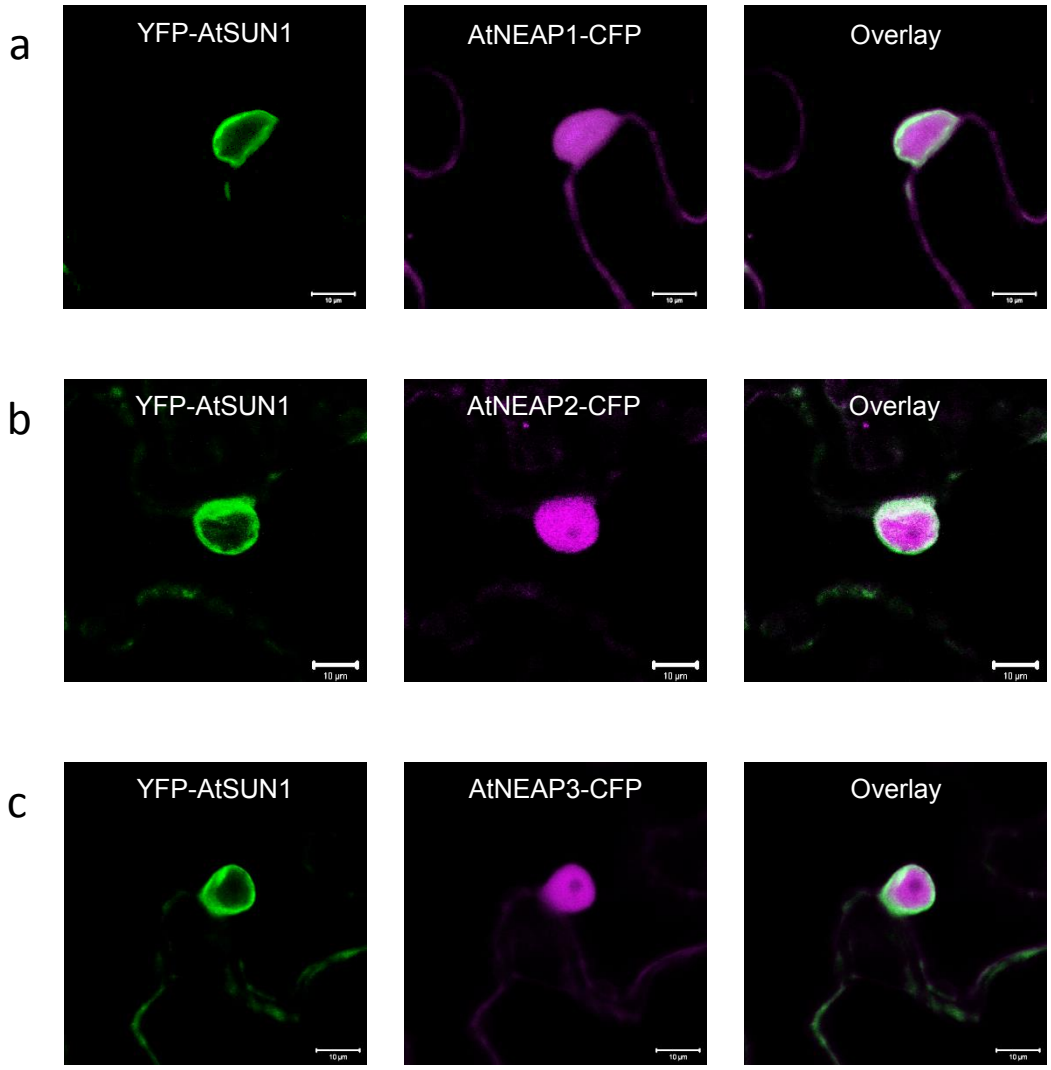

Figure 4.12: Confocal micrographs showing localisation of N-terminal YFP (green) fusion of AtSUN1 at the nuclear periphery with C-terminal CFP (magenta) fusions of AtNEAP1 (a), AtNEAP2 (b) and AtNEAP3 (c) localised to the nucleoplasm and cytoplasm expressed transiently under the 35S promoter in *N. benthamiana* leaf epidermal cells in presence of p19. Scale bar = 10µm.

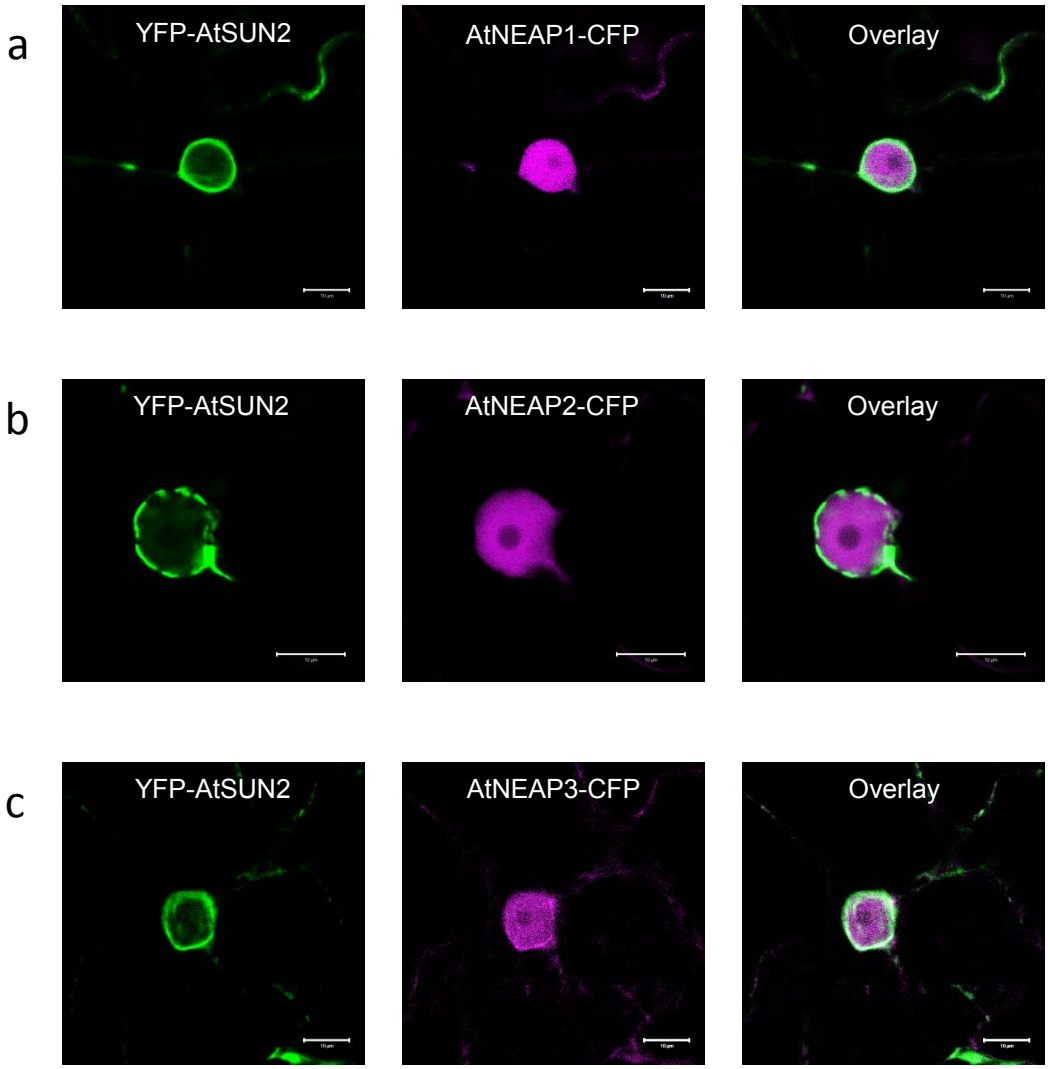

Figure 4.13: Confocal micrographs showing localisation of N-terminal YFP (green) fusion of AtSUN2 at the nuclear periphery with C-terminal CFP (magenta) fusions of AtNEAP1 (a), AtNEAP2 (b) and AtNEAP3 (c) localised to the nucleoplasm expressed transiently under the 35S promoter in *N. benthamiana* leaf epidermal cells in presence of p19. Scale bar = 10µm.

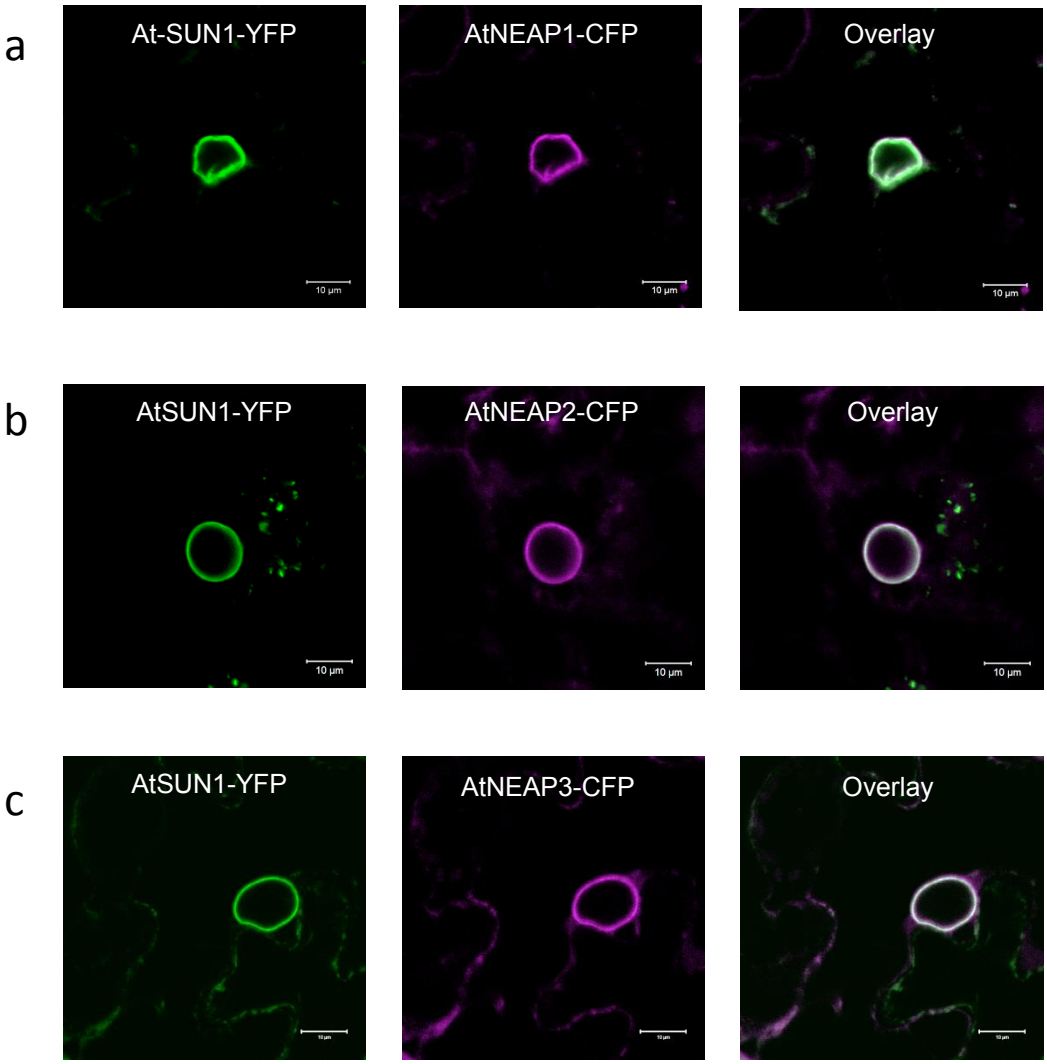

Figure 4.14: Confocal micrographs showing co-localisation of C-terminal YFP (green) fusion of AtSUN1 with C-terminal CFP (magenta) fusions of AtNEAP1 (a), AtNEAP2 (b) and AtNEAP3 (c) at the nuclear periphery and in the cytoplasm (seen at the cell periphery in a) expressed transiently under the 35S promoter in *N. benthamiana* leaf epidermal cells in presence of p19. Scale bar = 10µm.

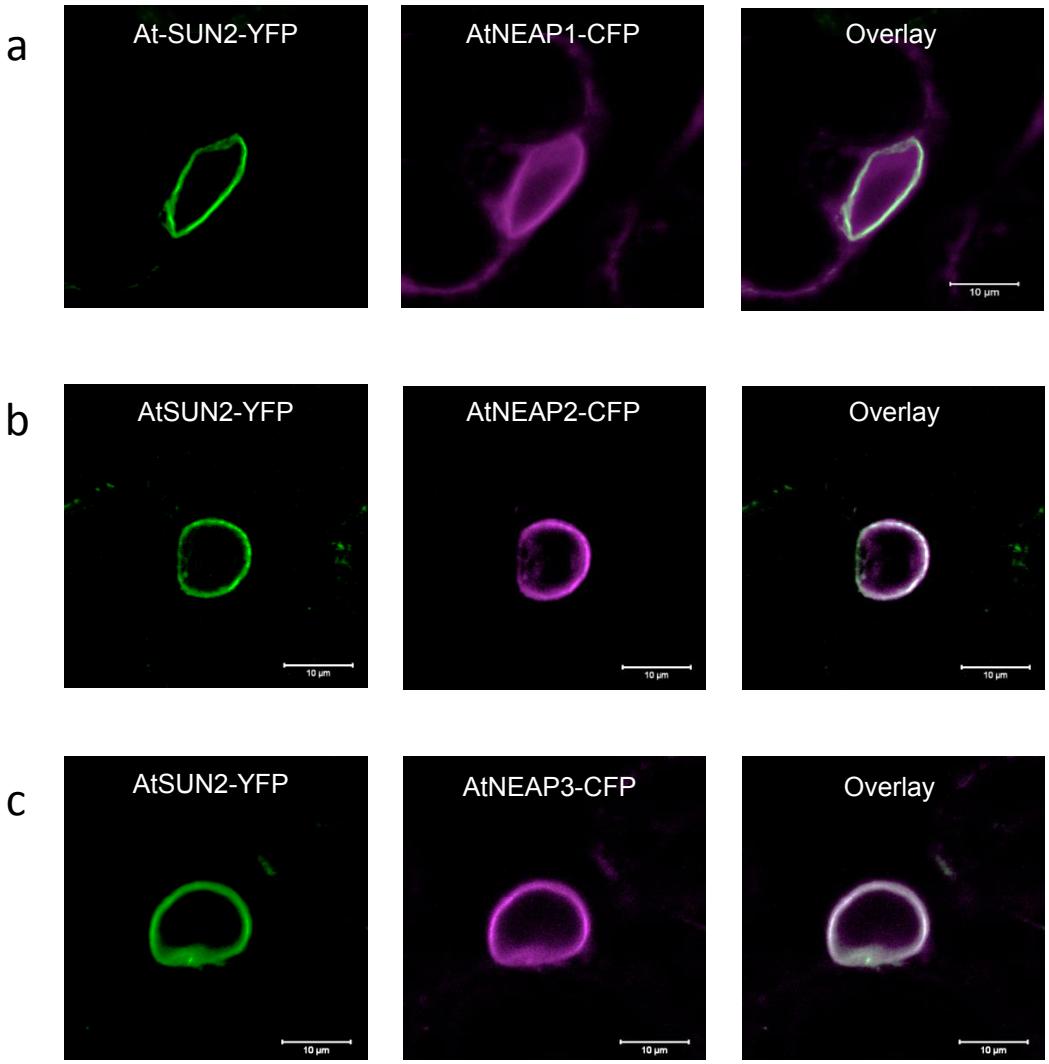

Figure 4.15: Confocal micrographs showing co-localisation of C-terminal YFP (green) fusion of AtSUN2 with C-terminal CFP (magenta) fusions of AtNEAP1 (a), AtNEAP2 (b) and AtNEAP3 (c) at the nuclear periphery expressed transiently under the 35S promoter in *N. benthamiana* leaf epidermal cells in presence of p19. Scale bar = 10µm.

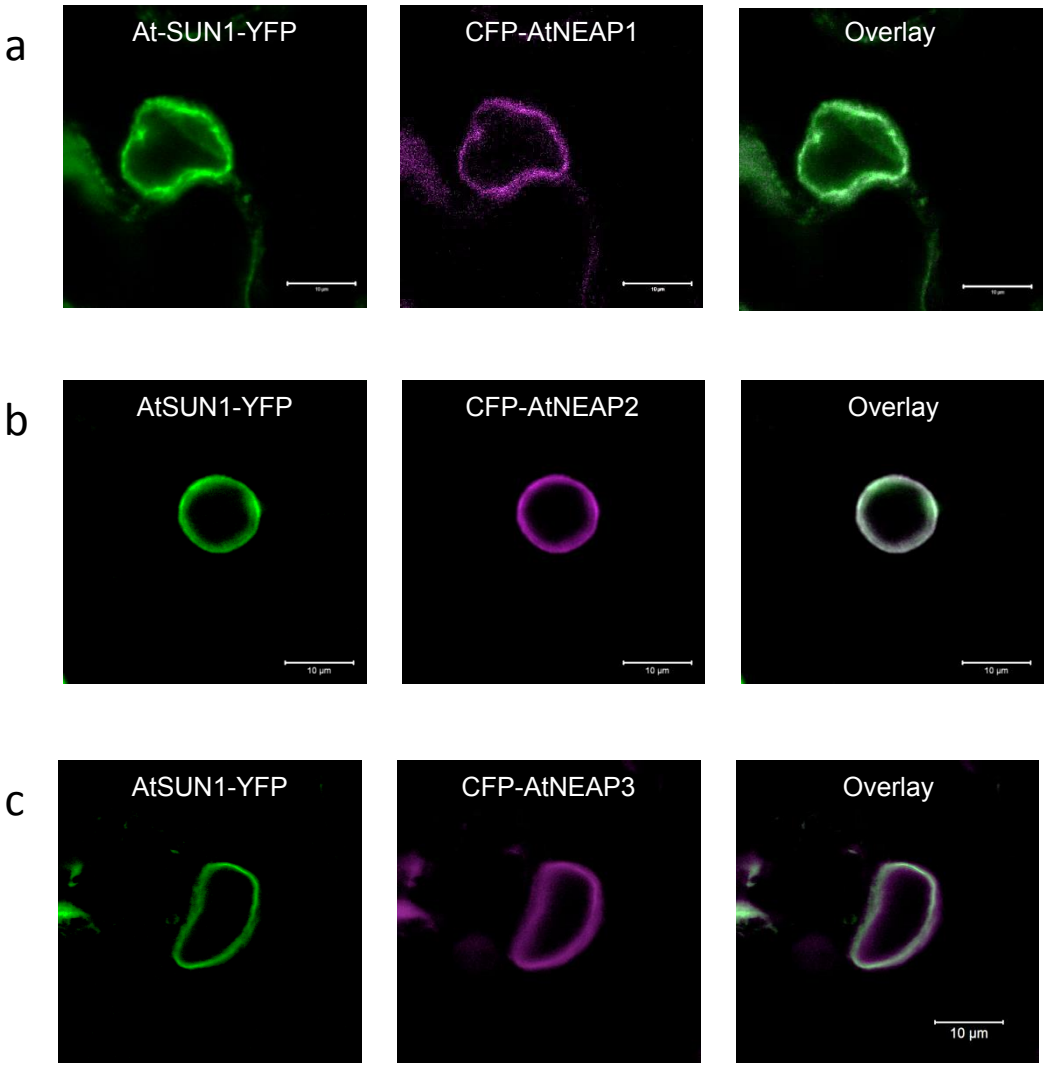

Figure 4.16: Confocal micrographs showing co-localisation of C-terminal YFP (green) fusion of AtSUN1 with N-terminal CFP (magenta) fusions of AtNEAP1 (a), AtNEAP2 (b) and AtNEAP3 (c) at the nuclear periphery and in the cytoplasm (seen at the cell periphery in a) expressed transiently under the 35S promoter in *N. benthamiana* leaf epidermal cells in presence of p19. Scale bar = 10µm.

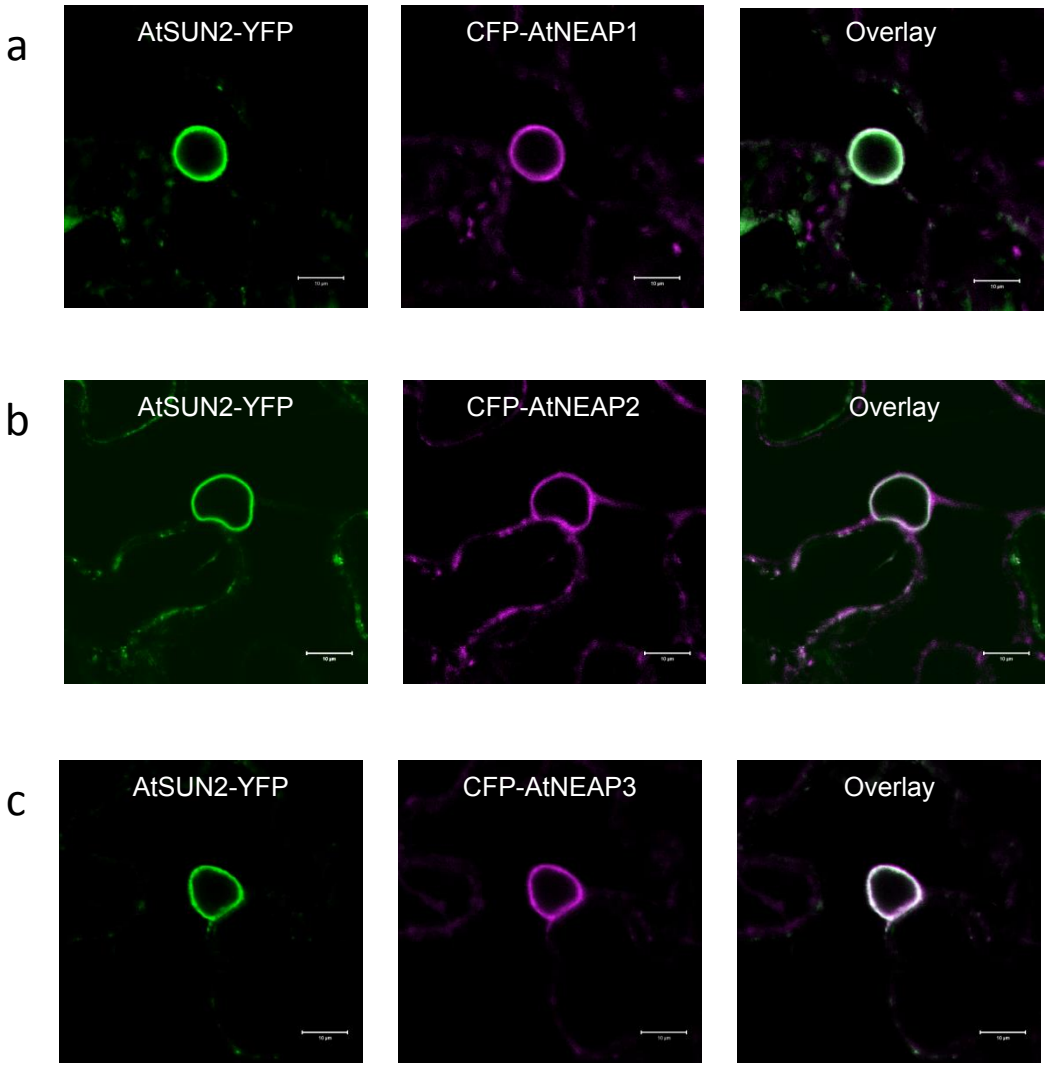

Figure 4.17: Confocal micrographs showing co-localisation of C-terminal YFP (green) fusion of AtSUN2 with N-terminal CFP (magenta) fusions of AtNEAP1 (a), AtNEAP2 (b) and AtNEAP3 (c) at the nuclear periphery and in punctate structures in the cytoplasm (seen at the cell periphery) expressed transiently under the 35S promoter in *N. benthamiana* leaf epidermal cells in presence of p19. Scale bar = 10µm.

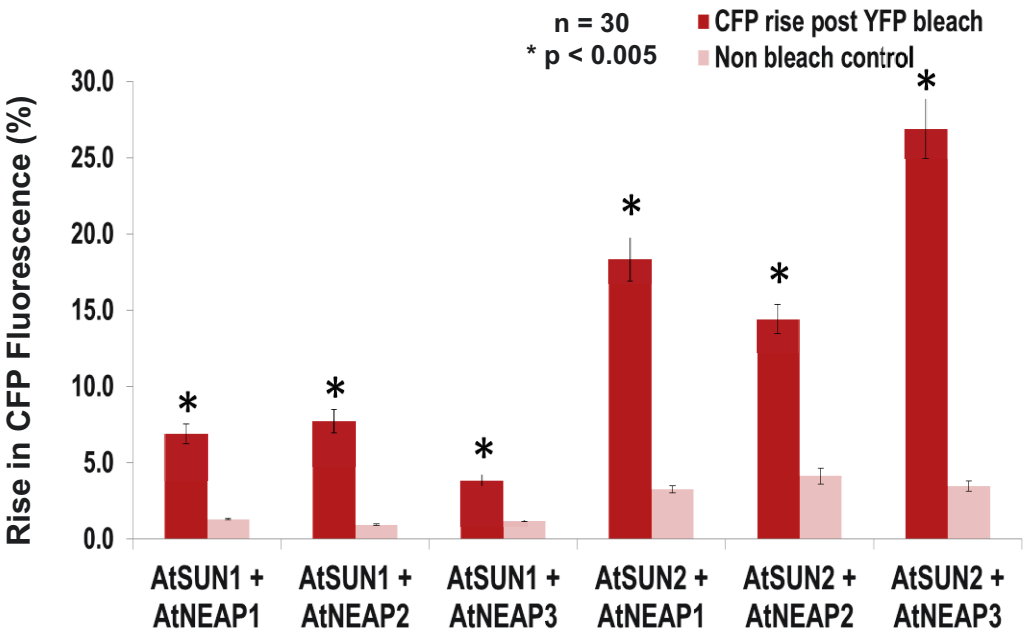

Figure 4.18: Bar graph showing change in CFP fluorescence in a region of bleached (red) versus a control non-bleached (pink) region of YFP fluorescence. A significant increase in CFP fluorescence indicates interaction with each other *in planta*. The paired bars represent the following combinations from left to right:

AtSUN1-YFP + AtNEAP1-CFP, AtSUN1-YFP + AtNEAP2-CFP, AtSUN1-YFP + AtNEAP3-CFP, AtSUN2-YFP + AtNEAP1-CFP, AtSUN2-YFP + AtNEAP2-CFP, and AtSUN2-YFP + AtNEAP3-CFP.

Values are expressed as percentage mean $\pm$ SEM where n=30. Paired t test was performed between the bleached and non bleached populations (*p<0.005).

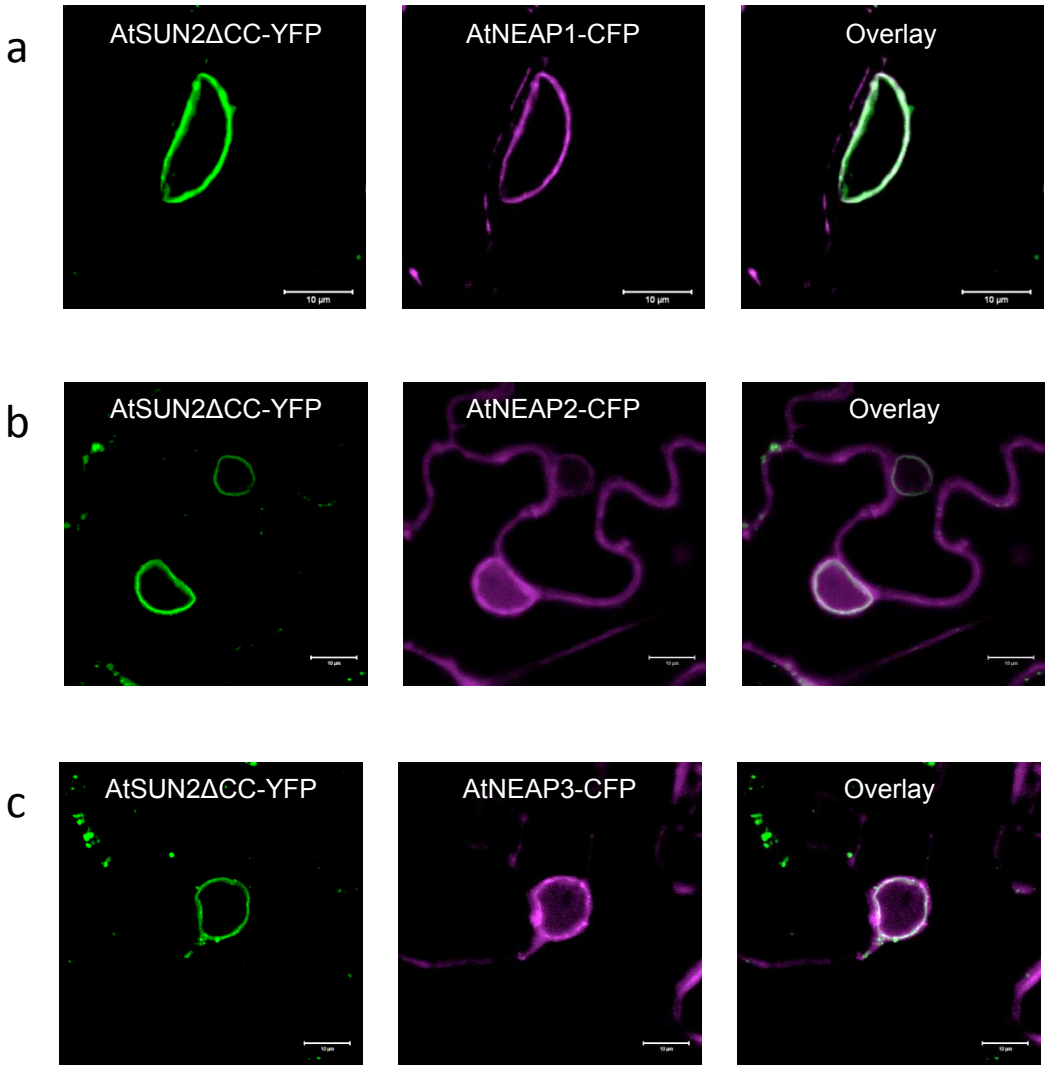

Figure 4.19: Confocal micrographs showing co-localisation of C-terminal YFP (green) fusion of AtSUN2ΔCC with C-terminal CFP (magenta) fusions of AtNEAP1 (a), AtNEAP2 (b) and AtNEAP3 (c) at the nuclear periphery expressed transiently under the 35S promoter in *N. benthamiana* leaf epidermal cells in presence of p19. Scale bar = 10μm.

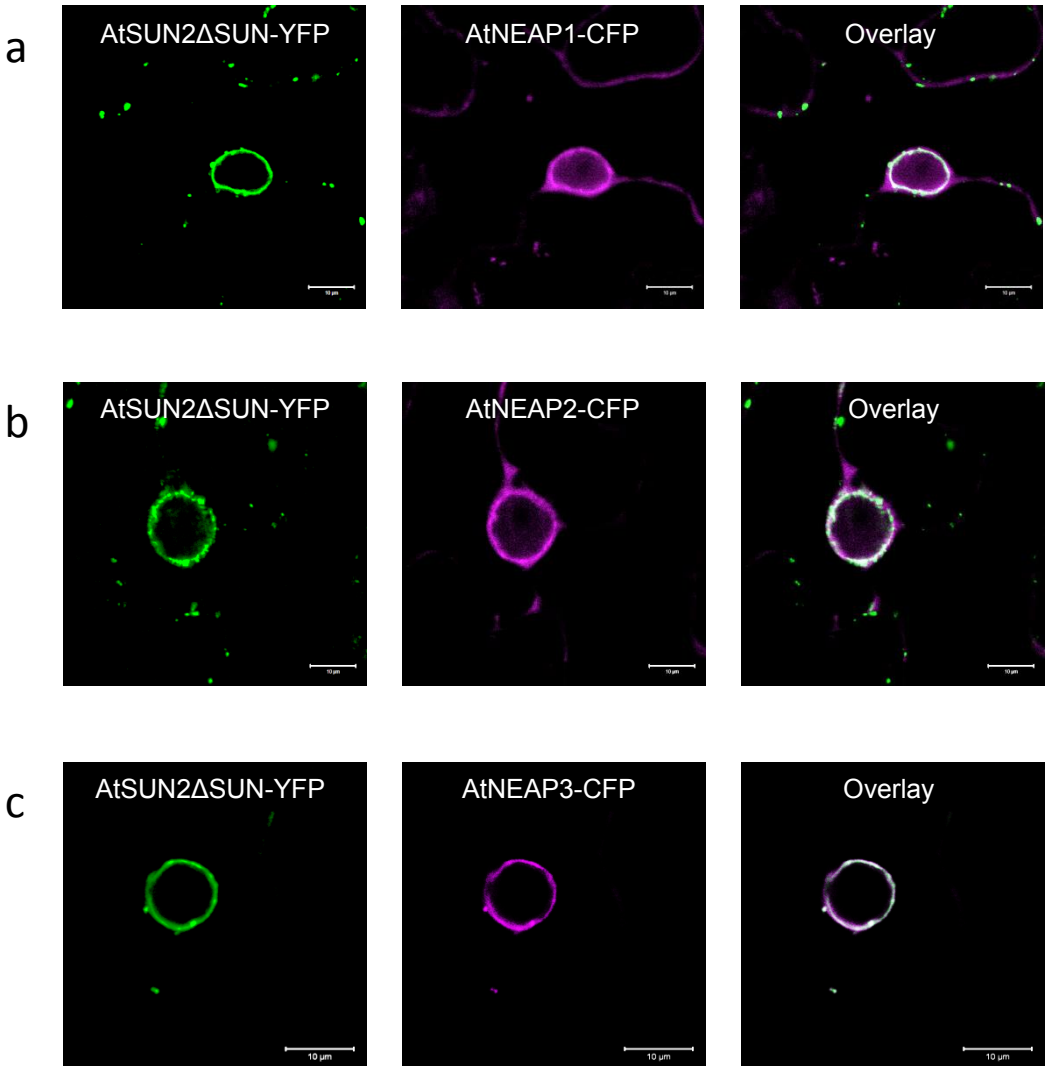

Figure 4.20: Confocal micrographs showing co-localisation of C-terminal YFP (green) fusion of AtSUN2ΔSUN with C-terminal CFP (magenta) fusions of AtNEAP1 (a), AtNEAP2 (b) and AtNEAP3 (c) at the nuclear periphery expressed transiently under the 35S promoter in *N. benthamiana* leaf epidermal cells in presence of p19. Scale bar = 10µm.

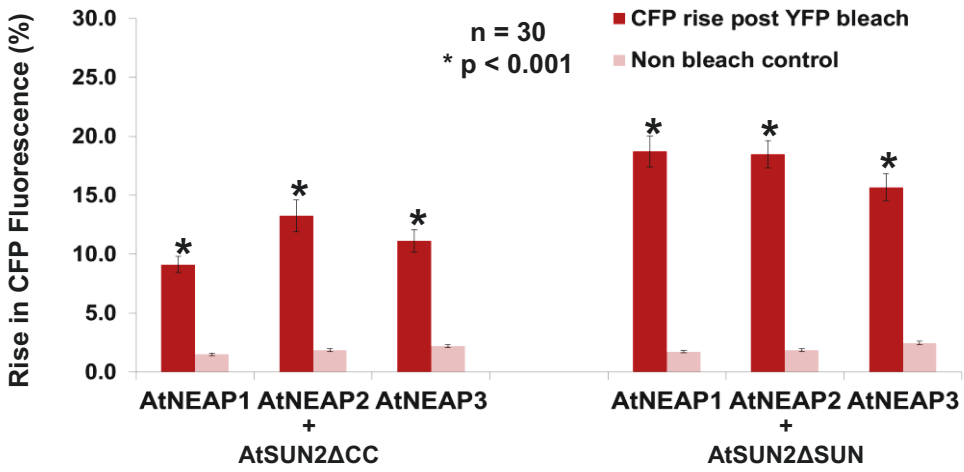

Figure 4.21: Bar graph showing change in CFP fluorescence in a region of bleached (red) versus control non-bleached (pink) region of YFP fluorescence. A significant increase in CFP fluorescence indicates interaction of the two proteins with each other *in planta*. The paired bars in the chart above represent the following combinations from left to right:

AtSUN2ΔCC-YFP + AtNEAP1-CFP,

AtSUN2ΔCC-YFP + AtNEAP2-CFP,

AtSUN2ΔCC-YFP + AtNEAP3-CFP,

AtSUN2ΔSUN-YFP + AtNEAP1-CFP,

AtSUN2ΔSUN-YFP + AtNEAP2-CFP, and

AtSUN2ΔSUN-YFP + AtNEAP3-CFP.

Values are expressed as percentage mean $\pm$ SEM (n=30). Paired t test was performed between the bleached and non bleached populations (*p<0.001).

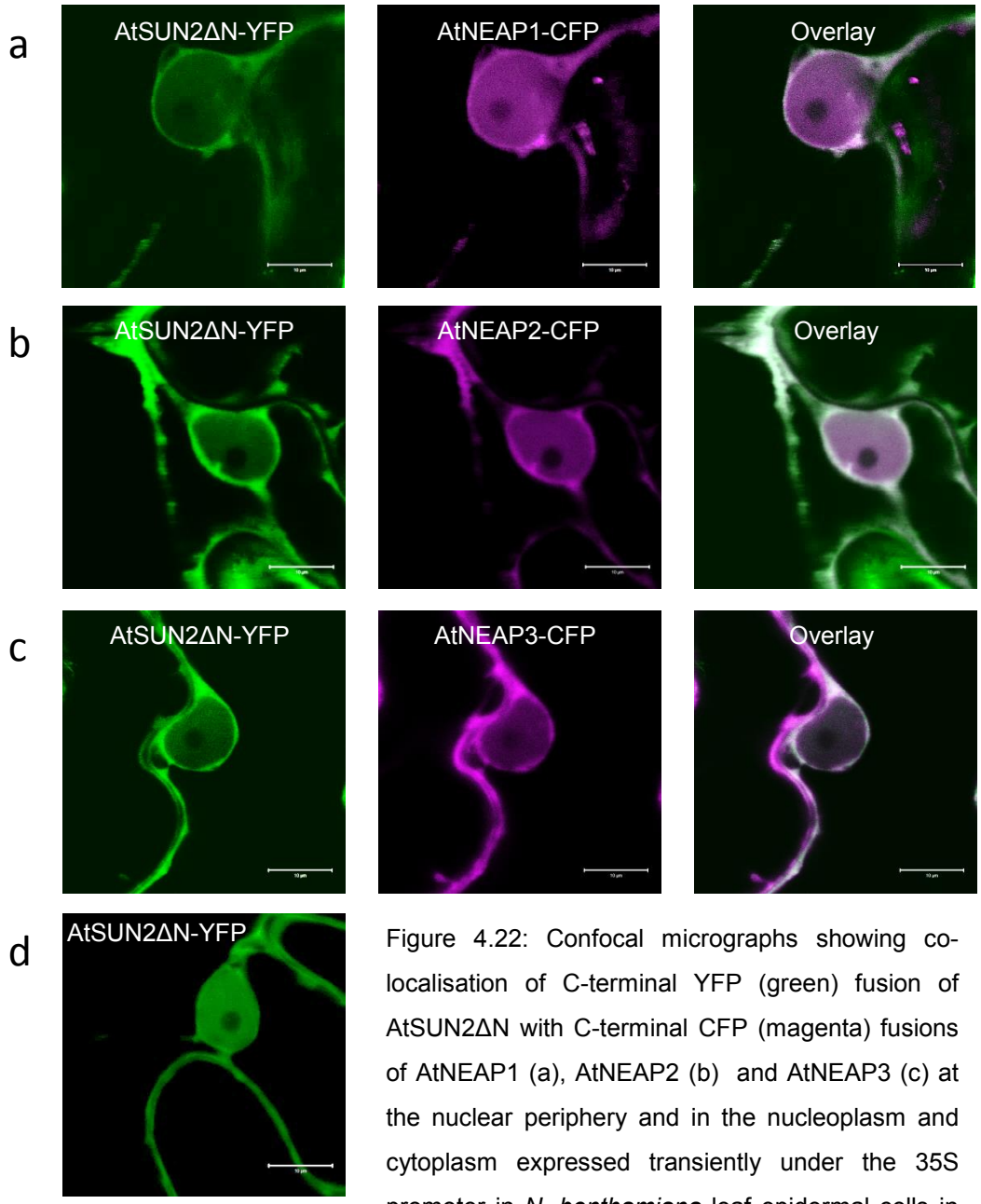

Figure 4.22: Confocal micrographs showing co-localisation of C-terminal YFP (green) fusion of AtSUN2ΔN with C-terminal CFP (magenta) fusions of AtNEAP1 (a), AtNEAP2 (b) and AtNEAP3 (c) at the nuclear periphery and in the nucleoplasm and cytoplasm expressed transiently under the 35S promoter in *N. benthamiana* leaf epidermal cells in presence of p19. d. shows localisation of AtSUN2ΔN-YFP in the nucleoplasm and cytoplasm when expressed on its own. Scale bar = 10µm.

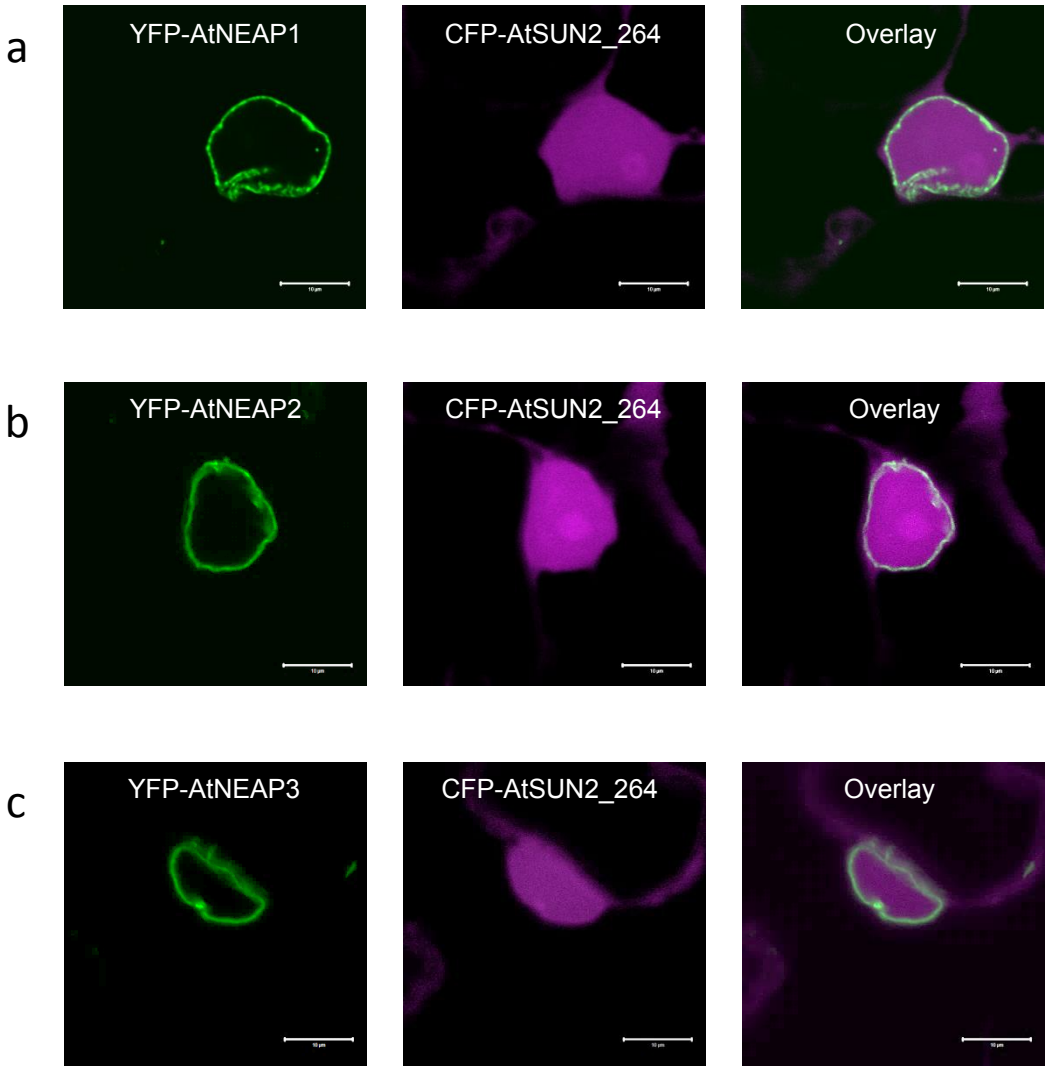

Figure 4.23: Confocal micrographs showing nucleoplasmic and cytoplasmic localisation of N-terminal CFP (magenta) fusion of AtSUN2_264 with N-terminal YFP (green) fusions of AtNEAP1 (a), AtNEAP2 (b) and AtNEAP3 (c) localised to the nuclear periphery and the cytoplasm (not seen) expressed transiently under the 35S promoter in *N. benthamiana* leaf epidermal cells in the presence of p19. Scale bar = 10μm.

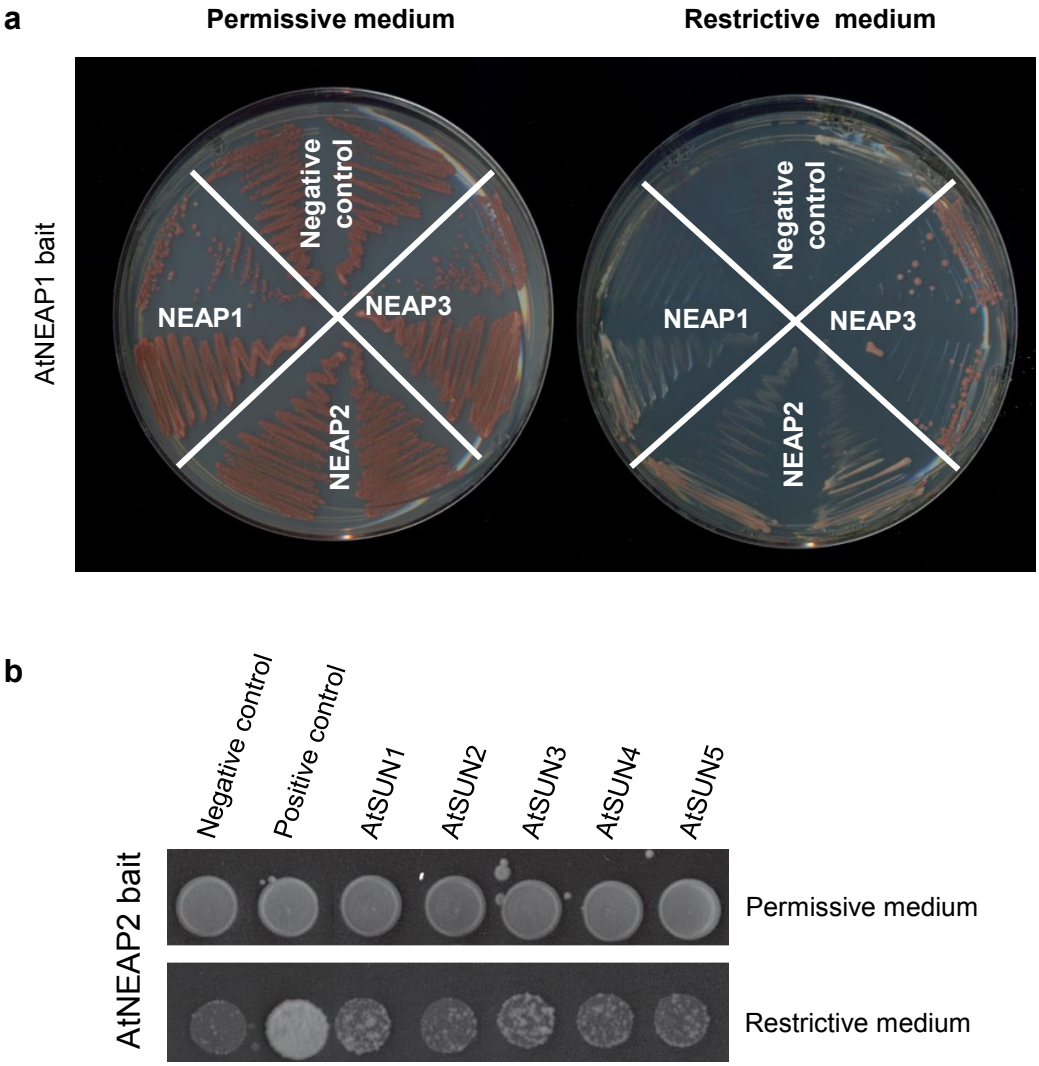

Figure 4.24: The split ubiquitin membrane yeast two hybrid (MYTH) assay showing yeast transformation colonies grown on permissive medium (indicating successful prey transformation) and on restrictive medium (indicating interaction).

a. Plates show streaked yeast colonies containing AtNEAP1 bait transformed with prey vectors containing AtNEAP1, AtNEAP2 and AtNEAP3
b. Spotted colonies of yeast containing AtNEAP2 bait transformed with AtSUN1, AtSUN2, AtSUN3, AtSUN4 and AtSUN5 prey vectors.

Transformation with empty prey vector was used as negative control. Positive control was an ER protein fused to N-terminus of a split ubiquitin molecule.

Table 4.1: Genes identified in a MYTH screen of an *A. thaliana* floral cDNA library as putative interaction partners of AtNEAP1

Gene	Name	Description	Localisation	References
At2G40620	Basic-leucine zipper (bZIP) transcription factor family protein	DNA binding transcription factor. Current screen: Identified 9 times as a hit and growth on highly restrictive medium	nucleus	Jakoby et al. 2002
At2G10940	Bifunctional inhibitor/lipid-transfer protein/seed storage 2S albumin superfamily protein	Identified in the crude nuclear lamina fraction by Mass Spectrometry	chloroplast, plasma membrane	Sakamoto and Takagi 2013
At2G34430	Chlorophyll-protein complex II subunit B1	Identified in the crude nuclear lamina fraction by Mass Spectrometry	chloroplast	Sakamoto and Takagi 2013
At3G21200	Proton gradient regulation 7	Predicted: nucleus	chloroplast	Ferro et al. 2010, Tanz et al. 2013
At4g20260	plasma-membrane associated cation-binding protein 1	Predicted: nucleus	plasma membrane, chloroplast, vacuole	Nagasaki et al. 2008, Whiteman et al. 2008, Ferro et al. 2010, Tanz et al. 2013
AtCG00720	Subunit of the cytochrome b6f complex		chloroplast thylakoid membrane	Ferro et al. 2010
At4G25100	Fe-superoxide dismutase		plasma membrane, mitochondia, chloroplast	Mitra et al. 2009, Ferro et al. 2010, Klodmann et al. 2011
At5G13450	Delta subunit of mitochondrial ATP synthase complex		mitochondria, plasma membrane	Mitra et al. 2009, Klodmann et al. 2011
At3G18370	C2 domain-containing protein	Predicted: nucleus	ER	Nikolovski et al. 2012, Tanz et al. 2013
At3G16240	Delta tonoplast intrinsic protein	Current screen: Identified 3 times as a hit and growth on highly restrictive medium	vacuole	Gattolin et al. 2005
At4G34720	vacuolar ATPase 16 kDa proteolipid		vacuole, plasma membrane	Alexandersson et al. 2004, Shimaoka et al. 2004
At1G23490	ADP-ribosylation factor 1	A member of ARF GTPase family. Current screen: Growth on highly restrictive medium	golgi, plasma membrane	Elmore et al. 2012, Parsons et al. 2012
At5G59540	2-oxoglutarate and Fe-dependent oxygenase superfamily protein	Current screen: Growth on highly restrictive medium, Predicted: nucleus	cytosol, peroxisome	Tanz et al. 2013
At4G14130	Xyloglucan endotransglycosylase-related protein		apoplast, cell wall	Tanz et al. 2013
At5G12250	Beta-6 tubulin	Tubulin subunits were isolated in a proteomic study of the arabidopsis nuclear matrix and the nucleolar proteome	microtubule cytoskeleton	Calikowski et al. 2003, Pendle et al. 2005

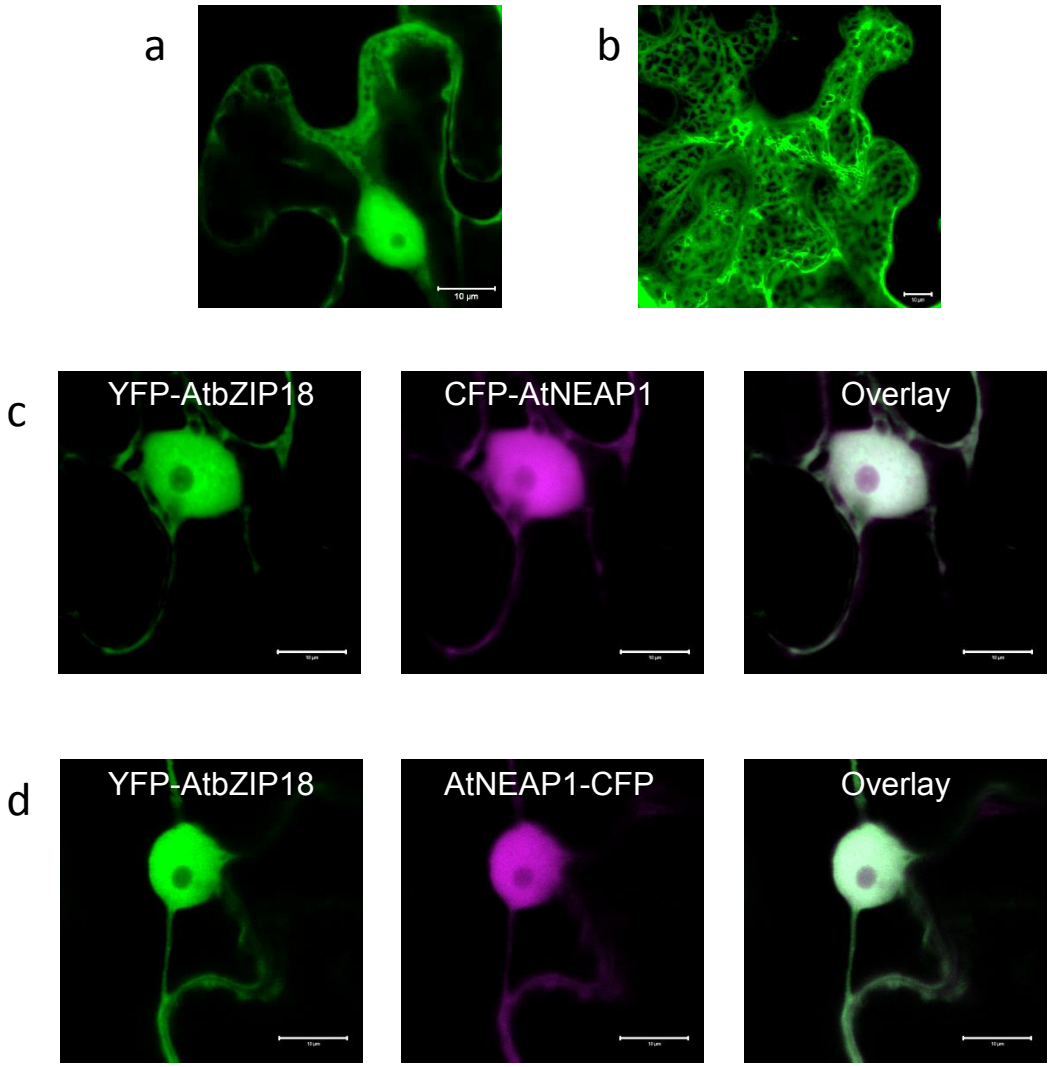

Figure 4.25: Confocal micrographs showing YFP-bZIP18 localised to the nucleoplasm (a) and cytoplasm (b) and co-localised with CFP-AtNEAP1 (c) and AtNEAP1-CFP(d) in the nucleoplasm and cytoplasm (seen at the cell periphery) expressed transiently under the 35S promoter in *N. benthamiana* leaf epidermal cells in presence of p19. Scale bar = 10µm.

Table 4.2: Summary of protein-protein interactions between AtNEAP and other nuclear proteins. Positive interactions are shown in green, negative interactions are shown in red and untested interactions are shown in black.

	AtNEAP1	AtNEAP2	AtNEAP3	AtbZIP18
AtNEAP1	apFRET, MYTH	apFRET, MYTH	apFRET, MYTH	MYTH
AtNEAP2	apFRET, MYTH	apFRET, To be done: MYTH	apFRET, To be done: MYTH	To be done: apFRET, MYTH
AtNEAP3	apFRET, MYTH	apFRET, To be done: MYTH	apFRET, To be done: MYTH	To be done: apFRET, MYTH
AtNEAP3ΔCC1	To be done: apFRET, MYTH	To be done: apFRET, MYTH	To be done: apFRET, MYTH	To be done: apFRET, MYTH
AtNEAP3ΔCC2	To be done: apFRET, MYTH	To be done: apFRET, MYTH	To be done: apFRET, MYTH	To be done: apFRET, MYTH
AtNEAP3ΔNLS	To be done: apFRET, MYTH	To be done: apFRET, MYTH	To be done: apFRET, MYTH	To be done: apFRET, MYTH
AtNEAP3ΔTM	To be done: MYTH	To be done: MYTH	To be done: MYTH	To be done: MYTH
AtNMCP1	To be done: MYTH	To be done: MYTH	To be done: MYTH	To be done: MYTH
AtSUN1	apFRET, To be done: MYTH	apFRET, MYTH	apFRET, To be done: MYTH	
AtSUN2	apFRET, To be done: MYTH	apFRET, MYTH	apFRET, To be done: MYTH	
AtSUN2ΔCC	apFRET, To be done: MYTH	apFRET, To be done: MYTH	apFRET, To be done: MYTH	
AtSUN2ΔSUN	apFRET, To be done: MYTH	apFRET, To be done: MYTH	apFRET, To be done: MYTH	
AtSUN2ΔN	To be done: MYTH	To be done: MYTH	To be done: MYTH	
AtSUN2_264	To be done: MYTH	To be done: MYTH	To be done: MYTH	
AtSUN3	To be done: apFRET, MYTH	MYTH, To be done: apFRET	To be done: apFRET, MYTH	
AtSUN4	To be done: apFRET, MYTH	MYTH, To be done: apFRET	To be done: apFRET, MYTH	
AtSUN5	To be done: apFRET, MYTH	MYTH, To be done: apFRET	To be done: apFRET, MYTH	

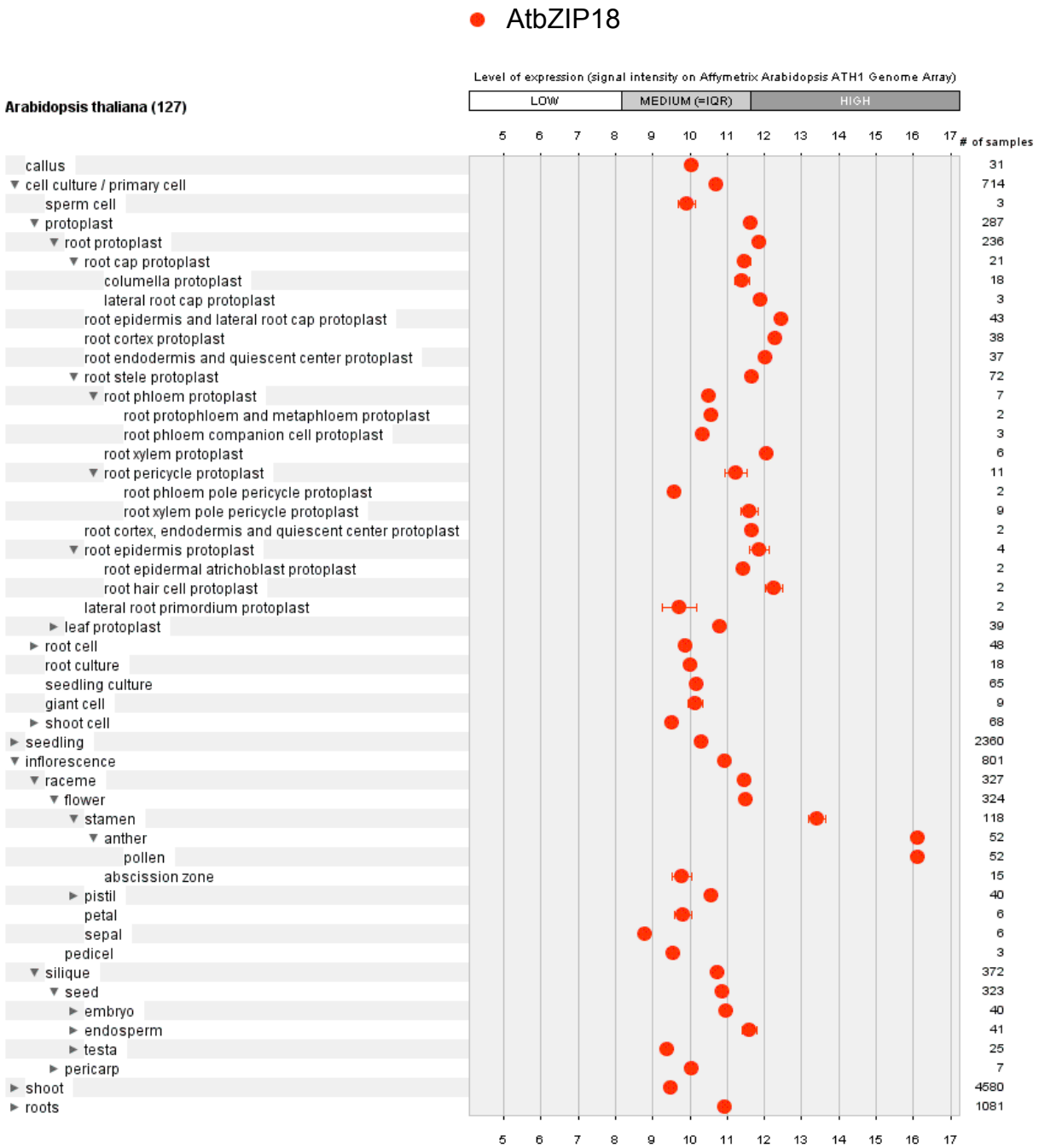

Figure 4.26: Expression profile of AtbZIP18 mRNA obtained from GeneVestigator shows AtbZIP18 (red) expressed at medium to high levels in all tissues (Toufighi et al. 2005). Highest expression was seen in pollen and anther. Medium to high levels were observed in stamen, peripheral endosperm, root epidermis and lateral root cap and root cortex protoplasts.

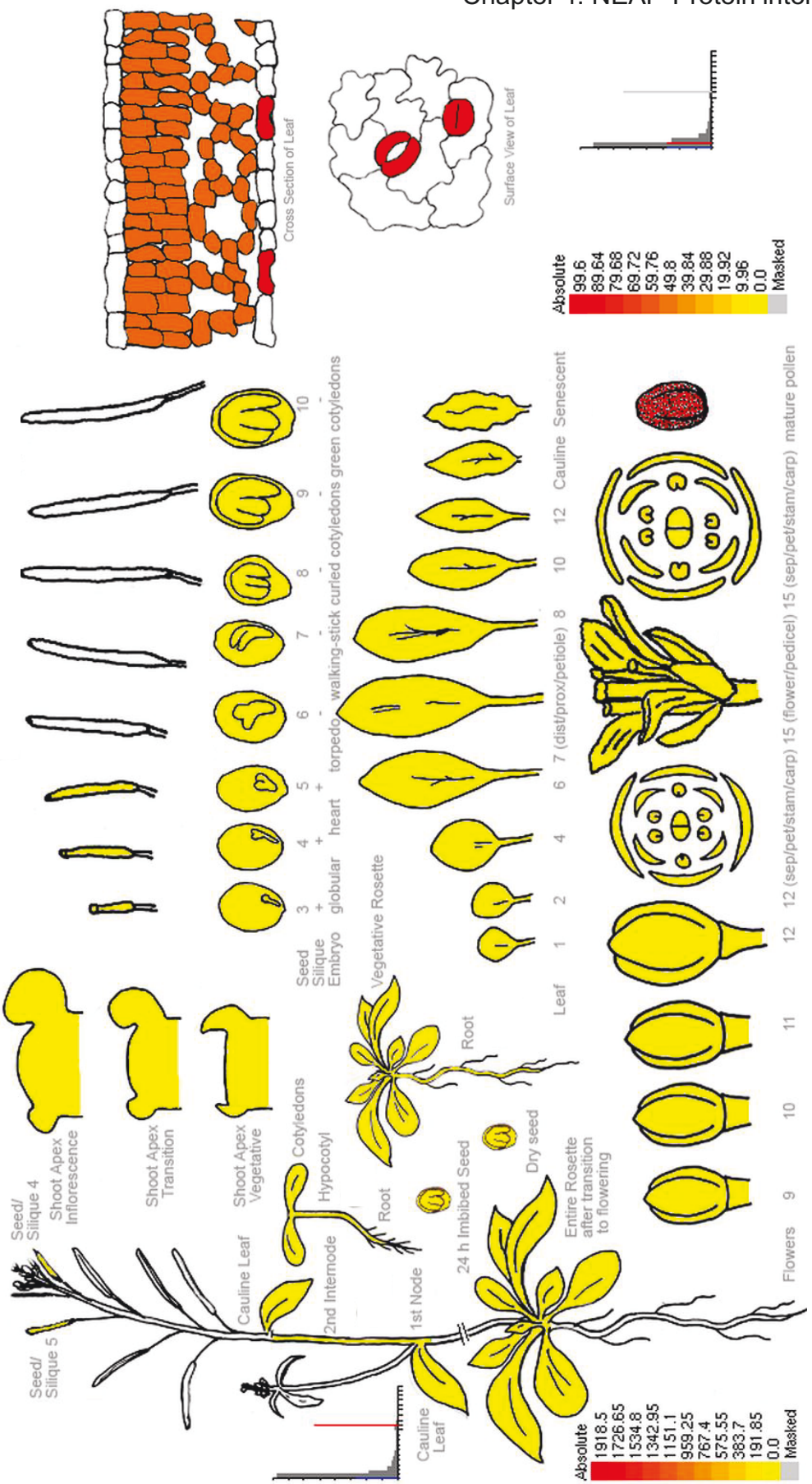

Figure 4.27: Expression levels of AtbZIP18 mRNA in different tissues acquired from BAR Arabidopsis eFP browser (Winter et al. 2007, Hruz et al. 2008). AtbZIP expression is specifically up-regulated in the pollen and guard cells.

4.4 Discussion

4.4.1 AtNEAP1, AtNEAP2 and AtNEAP3 co-localise and interact with each other *in planta*

As described in section 4.3.1, co-expression of N-terminal FP-AtNEAP with C-terminal AtNEAP-FP led to co-localisation of both proteins at the nuclear periphery within a ring of variable thickness and in some punctate structures (figures 4.1 and 4.2). This was, however, not observed when the FP molecule was fused to the C-terminus of both co-expressed AtNEAP proteins, in which case the two proteins failed to associate to the nuclear envelope and co-localised in the nucleoplasm (figure 4.3). This nucleoplasmic localisation suggests that when over-expressed, the C-terminal FP molecule creates a hindrance for the AtNEAP protein C-terminus to be inserted effectively in the membrane. The AtNEAP C-terminus is highly conserved (Chapter 3 figure 3.1) and has been shown to contain an active TM domain (Chapter 3 section 3.4.4) the function of which may be interrupted by the presence of the FP tag. Alternatively, the untagged N-terminus when overexpressed may take part in multiple interactions with other free N-termini resulting in protein aggregation in the nucleoplasm. However the former theory of C-terminal FP hindrance seems a more plausible explanation considering N-terminally tagged AtNEAP proteins were found to interact with each other *in planta* (figure 4.6). Interestingly, when two N-terminally tagged NEAP proteins were co-expressed, they showed the beads on a string phenotype described in section 4.3.1 (figures 4.4 and 4.5). Interestingly, the beads were not nucleoplasmic but remained on the NE string indicating that the C-terminus kept them anchored. The formation of beads or aggregates could be a result of multiple cross-linking and interactions made possible by either having an FP-free C-terminus or having it on the N-terminus. Interaction of two N-terminally tagged NEAP proteins in apFRET indicates that the N-termini are very closely placed (less than 10nm) for successful energy transfer between the CFP and YFP. However, whether the proximity of the N-termini is driven by active interaction of the N-terminus or if they merely sit close

together as a result of interactions at the C-terminus or other regions of the proteins is unknown. Over-expression of other NE proteins such as the SUN domain proteins can sometimes lead to similar beads on a string phenotype and that might be how the NE membrane system copes with over-expressed proteins (Graumann et al. 2010).

AtNEAP2 and AtNEAP3 were shown to interact with themselves using apFRET, whereas AtNEAP1 did not (figure 4.6). AtNEAP1 bait however showed interaction with AtNEAP1 prey in the MYTH system (figure 4.24a). Detection of interaction in apFRET is dependent on the close proximity (less than 10 nm apart) of the fluorophore tags of the two interacting proteins (Sparkes et al. 2011). The absence of FRET does not prove absence of interaction; it could suggest that the orientation of the interacting proteins did not bring the fluorophores close together. This may explain why NEAP1-NEAP1 interaction was not detected in apFRET but was observed in MYTH. The MYTH system has its own limitations. As described in section 4.3.4 detection of interaction (which usually occurs in the ER) relies on recombination of the two halves of the split ubiquitin molecule tagged on to the bait and prey proteins (Snider et al. 2010). Recombination leads to detachment of the TF, followed by its import into the nucleus to activate the reporter system (Snider et al. 2010). This presents a caveat in case of nuclear proteins, where since the bait is localised to the nucleus, there is a risk of activating the reporter system without the TF being proteolytically cleaved in the ER. This may explain why the AtNEAP3 bait showed colony growth in the absence of prey and was rendered unfit for use.

Thus AtNEAP proteins interact with themselves and with each other suggesting the formation of homomeric as well as heteromeric complexes. As described in chapter 1 section 1.2.1, lamins are also known to form homomeric and heteromeric complexes *in vitro* and are preferentially drawn into homodimers (Burke and Stewart 2013). Lamins A and B have been shown to self-polymerise *in vivo* to form separate filamentous networks capable of interaction with each other (Goldberg et al. 2008). Knowing their IF-like protein structure, it is possible that AtNEAP homomers could associate with themselves and extend into polymeric filaments. Cross-interaction of AtNEAP proteins may impart the potential homomeric filaments the ability to interact with each other, forming an

overlapping network. The plant lamina has been shown to be made of two types of filaments, 10-13 nm and 5-8 nm in thickness, however, the assembly, structure and protein composition of plant nucleoskeletal filaments has not been described so far (Li and Roux 1992, Blumenthal et al. 2004, Fiserova et al. 2009). The possibility of multiple permutations of homomers and heteromers can aid the formation of complex networks with a small number of protein molecules and may explain the two filament sizes in the plant lamina.

CFP-AtNEAP3ΔCC1 and CFP-AtNEAP3ΔNLS, which were nucleoplasmic when expressed on their own, co-localised at the nuclear periphery with YFP-AtNEAP3 (figure 4.7). The localisation of CFP-AtNEAP3ΔCC2 at the nuclear periphery and CFP-AtNEAP3ΔTM in the nucleoplasm remained unchanged when co-expressed with YFP-AtNEAP3 (figure 4.7) indicating a putative role of the CC and TM domain in mediating NEAP-NEAP interactions. The change in localisation of CFP-AtNEAP3ΔCC1 and CFP-AtNEAP3ΔNLS suggests possible interaction of the deletion constructs with YFP-AtNEAP3. As future work apFRET experiments are planned in order to ascertain AtNEAP protein domains responsible for interaction with each other (Chapter 6 section 6.3.2).

4.4.2 Co-expression with AtNEAP proteins affects localisation of AtNMCP1 at the nuclear periphery

As shown in figures 4.8 and 4.9, co-expression of AtNEAP proteins with AtNMCP1-YFP leads to dislocation of AtNMCP1 from the NE and accumulation in the nucleoplasm. Interestingly, the failure of AtNMCP1-YFP to localise to the nuclear periphery was irrespective of the terminal of FP tag of the AtNEAP proteins. In addition, co expression of AtNMCP1-YFP also makes YFP-AtNEAP1 nucleoplasmic. The nucleoplasmic phenotype of AtNMCP1 could be a result of competition with AtNEAP proteins for interaction with the SUN domain proteins. Both AtNMCP1 and AtNEAP proteins (section 4.3.3) have been shown to interact with the AtSUN proteins in the INM (Graumann 2014). The ability of AtNMCP1 and AtNEAP proteins to affect each other's localisation suggests the presence of interaction between them either directly or via common interaction partners such as the SUN domain proteins. Putative interactions between the

AtNEAP and AtNMCP1 indicates that the networks formed by AtNEAP and AtNMCP1 may cross-interact as well as compete with each other for SUN interaction.

4.4.3 AtSUN domain proteins co-localise and interact with AtNEAP1, AtNEAP2 and AtNEAP3 *in planta*

As seen in figures 4.10, 4.11, 4.14, 4.15, 4.16 and 4.17; AtSUN1 and AtSUN2 were co-localised with AtNEAP proteins, except where an N-terminal YFP tagged AtSUN protein was co-expressed with a C-terminal CFP fused AtNEAP protein (figures 4.12 and 4.13). As previously suggested in section 4.4.1, the C-terminal CFP could create a hindrance for membrane retention, however this is contradicted by the fact that a C-terminal CFP tagged AtNEAP protein always co-localised with a C-terminal YFP tagged AtSUN protein (figures 4.14 and 4.15). Furthermore, N-terminal FP tagged NEAP and SUN combinations co-localise at the nuclear periphery (figures 4.10 and 4.11). Thus in this case, the specific combination of a C-terminal FP tagged AtNEAP and an N-terminal FP tag on the AtSUN protein is responsible for mis-localisation of the AtNEAP proteins. Thus a combination of lack of anchoring of the NEAP TM domain and failure of interaction with the SUN N-terminus due to the presence of the FP tag, may explain this phenotype. However the SUN N-terminus is suggested to be non-essential for NEAP-SUN interaction later in this section.

As stated earlier, the ability to affect protein localisation is indicative of interaction, in this study confirmed using apFRET as well as MYTH (figures 4.18 and 4.24). Interaction of AtNEAP proteins with the classical SUN domain family is consistent with other known lamina components such as metazoan lamins as well as NMCPs in plants (Haque et al. 2006, Haque et al. 2010, Graumann 2014). Haque et al. (2010) showed that mammalian Lamin A interacted with the N-terminus of mammalian SUN1 and SUN2. Additionally, Graumann (2014) has shown that *Arabidopsis* NMCP1 is anchored to the NE by SUN domain proteins and that the N-terminus of SUN1 and SUN2 is essential for this interaction. In this study, an AtSUN2 N-terminal deletion mutant was found to localise to the nucleoplasm (figure 4.22d). Interestingly, co-expression of AtNEAP-CFP

affected localisation of the N-terminal deletion mutant of AtSUN2. Presence of the AtNEAP protein encouraged association of the AtSUN2 N-terminus deletion mutant to the nuclear periphery suggesting possible interaction between the two (figure 4.22). This suggests that the N-terminus was not essential for NEAP-SUN interaction but remains to be confirmed by apFRET or MYTH (Chapter 6 section 6.3.2). This was also confirmed by co-expressing a FP tagged construct containing the N-terminal 264 amino acids of AtSUN2 with AtNEAP proteins. The co-expression did not affect the NE association of AtNEAP proteins, nor did it change the nucleoplasmic localisation of the AtSUN2 N- terminus (figure 4.23).

SUN-NEAP interaction was detected in apFRET when the CFP and YFP were on the C-termini of both proteins. The knowledge that the AtSUN C-terminus is localised to the periplasmic space leads to the fact that the AtNEAP C-terminus must be in the periplasm or membrane embedded very close to the periplasm. Deletion of the C-terminal SUN domain did not disrupt NEAP-SUN interaction (figure 4.21) suggesting that the SUN domain was not required for interaction. Interestingly, NEAP proteins were first identified in a search for KASH-like proteins (Chapter 3 section 3.1). The interaction between the SUN domain and the KASH domain is highly conserved and indispensable for the definition of the two families (Crisp et al. 2006). The presence of NEAP-SUN interaction in the absence of the SUN domain confirms that AtNEAPs are not KASH domain proteins (Crisp et al. 2006).

Further, deletion of the CC domain of AtSUN2 also had no effect on NEAP-SUN interaction (figure 4.21). In summary, a specific region or domain of AtSUN2 protein could not be identified as responsible for its NEAP interaction as all previously identified and characterised domain deletion mutants interacted with AtNEAP proteins. It may also suggest that more than one domain of the SUN protein is responsible for NEAP interaction. Additionally, deletion of domains was based on domains predicted by algorithms (see Chapter 2 table 2.20) and the inconclusive results could indicate inefficient predictions and incomplete deletions. Further domain deletions of AtSUN2 protein will be made and studied to investigate the linker domains between TM and CC domain, and between CC and SUN domain (Chapter 6 section 6.3.2).

In addition to apFRET, a MYTH assay not only confirmed NEAP interaction with the classical SUN domain proteins but also identified NEAP interactions with the mid-SUN domain proteins AtSUN3, AtSUN4 and AtSUN5 (figure 4.24b). The identification of NEAP interactions with the mid-SUN domain proteins is the first of its kind with putative plant lamina components. The interactions of mid-SUN domain proteins with AtNEAP proteins will be tested using apFRET (Chapter 6 section 6.3.2). Mid-SUN proteins also interact with AtSUN1 and AtSUN2 (Graumann et al. 2014). Thus the classical SUN domain, the mid-SUN domain and the NEAP protein families may be involved in forming multiway complexes at the NE causing the NEAP proteins to be putative components of plant LINC complexes.

4.4.4 AtbZIP18 is a novel AtNEAP interacting partner having DNA binding ability

As described in section 4.3.5, AtbZIP18 was the strongest candidate from the *A. thaliana* cDNA library screen for AtNEAP1 interaction partners. It grew on highly restrictive medium and was identified 9 times separately acting as an internal replicate in the screen. Co-expression with AtbZIP18 affected the ability of AtNEAP proteins to associate with the NE as both co-localised in the nucleoplasm indicating interaction *in planta* (figure 4.25). AtbZIP18 belongs to a family of TFs containing the basic region leucine zipper (bZIP) domain. bZIP TFs are conserved across eukaryotes including metazoans, yeast as well as plants (Llorca et al. 2014). In plants bZIP TFs have been described in *G. max* (131 genes), *Z. mays* (125 genes), *S. bicolor* (92 genes), *O. sativa* (89 genes), *A. thaliana* (75 genes) and *V. vinifera* (55 genes) (Jakoby et al. 2002, Nijhawan et al. 2008, Wang et al. 2011, Wei et al. 2012, E et al. 2014, Liu et al. 2014). bZIP TFs have been shown to have functions in plant pathogen response, light and stress signalling and salicylic acid, absiscic acid and jasmonic acid hormone signalling (Hsieh et al. 2012, E et al. 2014, Llorca et al. 2014). They are also important for plant development processes such as flowering, seed development, senescence and seedling maturation (Abe et al. 2005, Nijhawan et al. 2008, Alonso et al. 2009, Smykowski et al. 2010, E et al. 2014, Llorca et al. 2014).

The bZIP domain comprises a basic region followed by a leucine zipper domain (Hurst 1994, Amoutzias et al. 2007). The basic region is a highly conserved alpha helix containing an NLS and a DNA binding N-x_7-R/K segment where x is any amino acid (Miller et al. 2003). The leucine zipper domain is comparatively diverse and contains a CC region of heptad repeats of leucine or other hydrophobic amino acids responsible for dimerisation (Schumacher et al. 2000). The alpha helical basic regions of two bZIP proteins wrap themselves around their CC dimer forming a zipper-like Y shaped structure which holds DNA (Glover and Harrison 1995). bZIP proteins are known to bind palindromic and non-palindromic DNA sequences containing an ACGT core (Foster et al. 1994). DNA binding specificity and gene activation or repression is determined by the affinity of the bZIP dimer regulated by their constituent monomers, amino acid content, phosphorylation and redox status as well as DNA flexibility (Schumacher et al. 2000, Shaikhali et al. 2012, Llorca et al. 2014).

The AtbZIP18 protein identified in this study as an interactor of AtNEAP1 has been classified as a member of group I carrying a characteristic lysine instead of arginine (N-x_7-K) in the basic region (Jakoby et al. 2002). The lysine is known to have higher affinity for non-palindromic sequences (Fukazawa et al. 2000). Some members of this group are important for vascular tissue development where they have been shown to be expressed and to regulate gene expression (Yin et al. 1997, Ringli and Keller 1998, Fukazawa et al. 2000). AtbZIP18 has not been characterised in any studies until now. Genevestigator arrays (figure 4.26) show that AtbZIP18 expression is highest in pollen and anther, and medium to high in stamen, peripheral endosperm, root epidermis and lateral root cap and root cortex protoplasts (Toufighi et al. 2005, Hruz et al. 2008). The eFP browser (figure 4.27) also showed AtbZIP18 expression to be high in pollen and stomatal guard cells (Winter et al. 2007). Wang et al. (2008) also showed AtbZIP18 to be upregulated during pollen germination and pollen tube growth and may suggest its role in gene regulation during these processes. High expression of AtbZIP18 in guard cells, similar to that seen for AtNEAP1 and AtNEAP2 (Chapter 3 section 3.3.3) suggests their role in common functions in guard cells.

In metazoans, several components of the lamina such as lamins and other lamin-binding INM proteins tether chromatin and regulate gene expression (Dechat et al. 2010). NMCP proteins have been shown to associate with chromatin at different stages of cell division playing an important role in chromatin organisation and segregation (Kimura et al. 2010, Sakamoto and Takagi 2013). However, whether the association of NMCP proteins with chromatin is direct or mediated by other chromatin binding partners is not known. Thus the AtNEAP interacting protein, AtbZIP could be the first chromatin binding partner to be identified associated to the plant NE and putatively to the lamina with the ability to regulate gene function.

Another candidate based on identification from three colonies and growth on highly restrictive medium was At3G16240, a delta tonoplast instrisic protein (δTIP). δTIP is localised to the vacuole with no known or predicted association with the nucleus (Gattolin et al. 2009, Gattolin et al. 2011). Importantly there are ten TIP proteins in *A. thaliana*, but specific identification of δTIP three times could be worth exploring further. However it could be a false positive interacting in the yeast ER, but no nuclear co-localisation in a plant cell.

Several chloroplast localised proteins were also identified in the MYTH screen. At2G10940 and At2G34430 identified in the current study have previously been isolated from crude nuclear lamina fractions by Mass Spectrometry (Sakamoto and Takagi 2013). Chloroplast related proteins have been previously found as contaminants in nuclear matrix related screens (Calikowski et al. 2003, Sakamoto and Takagi 2013). However identification in the MYTH system rules out contamination, and indicates true interaction albeit in the ER. The question to explore is whether the interaction occurs *in planta*, and if it does whether it occurs in the nucleus or the chloroplast.

Another candidate was a beta-6 tubulin subunit, which is a component of the microtubule cytoskeleton. Interestingly β-6 tubulin was previously identified from the nucleus in a nucleolar proteome analysis (Pendle et al. 2005). Additionally several tubulin subunits, but not β-6 tubulin were isolated in a proteomic study of the A. thaliana nuclear matrix (Calikowski et al. 2003). It will be interesting to

explore whether this interaction occurs *in planta* and what putative structural functions these NEAP-tubulin complexes could perform.

4.5 Conclusions

AtNEAP1, AtNEAP2 and AtNEAP3 interact with themselves, forming homomeric complexes, and with each other, forming homomeric and hetromeric complexes. The involvement of the CC domain, NLS or TM domains in this interaction have been investigated but could not clearly be identified in this study. AtNEAP1, AtNEAP2 and AtNEAP3 affect localisation of AtNMCP1 possibly by interacting either directly or indirectly with it. AtNEAP1, AtNEAP2 and AtNEAP3 interact with AtSUN1 and AtSUN2. However, none of the deleted AtSUN2 domains, namely, the CC domains, the SUN domain or the N-terminus were found to be necessary for NEAP interaction.

Finally, AtbZIP18 was identified as a novel AtNEAP1 interactor with the ability to bind and tether DNA to the NE via its NEAP interaction and regulate gene function.

Description of functions of NEAP proteins studied using a reverse genetics approach by analysing *A. thaliana* lines containing T-DNA insertions in each of the four AtNEAP genes resulting in aberrant or no mRNA transcription are presented in Chapter 5.

Chapter 5

Functions of NEAP proteins

in planta

Chapter 5

Functions of NEAP proteins *in planta*

5.1 Introduction

Previous results in chapters 3 and 4 are suggestive that AtNEAP proteins may be novel components associated with the plant lamina. Chapter 3 elucidated the IF-like characteristics of AtNEAP proteins including their extensively CC protein structure (section 3.3.1) as well as their biochemical resistance to extraction by high ionic salts and detergents (section 3.3.6). In chapter 3 section 3.3.4, the sub-cellular localisation of AtNEAP proteins was confirmed to be at the nuclear periphery. While nucleoplasmic localisation of AtNEAP-FP (Chapter 4 figure 4.3) expressed at a high concentration indicated localisation at the INM-nucleoplasmic interface; the topology of interaction of AtNEAP proteins with AtSUN proteins further suggested their INM-intrinsic nature (Chapter 4 section 4.4.3). AtNEAP proteins were shown to interact with themselves forming homomeric complexes as well as with each other forming heteromeric complexes suggesting the ability to form complex networks at the nuclear periphery (Chapter 4 figures 4.6 and 4.24a).

This chapter investigates the putative functions of AtNEAP proteins. In metazoans as well as plants, mutations in proteins associated with LINC complexes such as SUN, KASH and lamina associated genes have been associated with abnormalities in nuclear structure such as misshaped nuclei, presence of nuclear membrane blebs, defective nuclear movements and chromatin organisation (Dittmer et al. 2007, Dechat et al. 2010, Sakamoto and Takagi 2013, Jevtic et al. 2014). Functional analyses in this chapter focusses on the use of T-DNA lines to knockout (KO) of knockdown (KD) AtNEAP and AtbZIP18 genes and characterising them for changes in plant growth and nuclear morphology.

5.2 Aims

The aim of this chapter was to study NEAP protein function *in planta*. This included:

a. Characterising single NEAP mutant *A. thaliana* T-DNA lines for genomic insertion and mRNA KD or KO

b. Crossing characterised single mutant T-DNA lines to generate double, triple and quadruple mutant lines

c. Comparing the root lengths of characterised single and double mutant T-DNA lines with WT Col-0 plants

d. Comparing nuclear size and circularity of mutant T-DNA lines with WT nuclei in different tissues

e. Analysis of nuclear positioning in guard cells of a double mutant versus WT

5.3 Results

5.3.1 Characterisation of T-DNA lines

In this Chapter, a reverse genetics approach was employed to identify the function of NEAP proteins *in situ* by use of *A. thaliana* lines containing a mutation in specific genes of interest. Table 5.1 shows *A. thaliana* insertion lines known to contain T-DNA in several NEAP genes ordered from NASC or GABI (Alonso et al. 2003, Kleinboelting et al. 2012). As described in Chapter 2, section 2.2.2 seeds were germinated on ½ MS agar. Seedlings were transferred to soil after 10-12 days. Plants were grown in long day (16 hour light and 8 hour dark) cycle (Chapter 2 section 2.2.2).

Table 5.1: Characteristics of *A. thaliana* lines containing T-DNA insertions in AtNEAP1, AtNEAP2, AtNEAP3, AtNEAP4 and AtbZIP18 genes.

No.	Gene	Name	Insertion site	Genotype	mRNA level: RT-PCR	Name used in this thesis
1	AtNEAP1	SAIL_846_B07	Intron	Homozygous	knockout	*neap1*
2	AtNEAP2	SALK_012087	Intron	No T-DNA insertion		
3	AtNEAP2	WiscDsLoxHs194_12D	5'UTR	Homozygous	no knockdown	
4	AtNEAP2	GABI_589B02	5'UTR	Homozygous	unconfirmed	*neap2*
5	AtNEAP2	GABI_178C02	Intron	Heterozygous	unconfirmed	
6	AtNEAP3	WiscDsLoxHs086_02C	Exon	Homozygous	knockout	*neap3*
7	AtNEAP4	SAIL_1239_G02	Intron	Homozygous	unconfirmed	*neap4*
8	AtbZIP18	SAIL_592_A12	Intron	Heterozygous	unconfirmed	
9	AtbZIP18	WiscDsLoxHs073_05E	Exon	Homozygous	unconfirmed	*bzip18*

T-DNA lines were screened in three steps. First the seedlings were grown on selective antibiotics to screen for resistance conferred by the inserted T-DNA (Chapter 2, table 2.2). Secondly, selected seedlings were subjected to genotyping. Genotyping included extraction of gDNA followed by PCR amplification using a mix of one insert-specific and two gene-specific primers (Chapter 2 section 2.3.5 and table 2.4). The non-mutated WT gene was represented on an agarose gel as a 1kb band and the mutagenic insertion in the gene of interest was represented as a 500 base pair band. WT plants showed a single 1 kb band, plants homozygous for the T-DNA insertion showed a single 500 base pair band and plants heterozygous for the insertion showed

both bands, the 1kb and the 500 base pair. Lastly, mRNA was extracted from lines genotyped as homozygous and used in semi-quantitative RT-PCR to detect changes in levels of mRNA expression (Chapter 2 section 2.3.5). The WT mRNA band represents the CDS of the respective gene. A complete KO plant showed no band whereas a partial KD was represented by a band of reduced intensity. A band of similar intensity to the WT denoted unchanged levels of mRNA. As a control for genomic contamination an RT enzyme negative control was included. AtPP2A was used as an internal quantitative control for the RT-PCR. AtPP2A mRNA levels were expected to remain unchanged between WT and mutants (Czechowski et al. 2005).

Figure 5.1 shows characterisation of the SAIL_846_B07 line which contains a T-DNA insertion in an intronic region of AtNEAP1. Some seedlings were found to have no insert (figure 5.1a lane 8) and some were found to have the T-DNA insertion in a single allele of AtNEAP1 (figure 5.1a lanes 4, 5 and 6). Examples of two homozygous plants containing a single T-DNA insertion band (500 kb) are shown in figure 5.1a (lanes 7 and 9). RT-PCR on 8-10 day old seedlings of the genotyped SAIL_846_B07 homozygous line showed absence of AtNEAP1 mRNA compared to WT confirming it to be a complete KO (figure 5.1b). This line henceforth denoted as *neap1* was used for phenotyping experiments (figures 5.6a, 5.8 and 5.9).

Likewise, the WiscDsLoxHS194_12D line expected to contain a T-DNA insertion in the 5' untranslated region (UTR) of AtNEAP2 was genotyped (figure 5.2). As shown in figure 5.2a (lane 2) a homozygous insertion line was identified and used in semi-quantitative RT-PCR. RT-PCR however showed no reduction in AtNEAP2 mRNA levels compared to the WT (figure 5.2b), indicating that despite the presence of the insertion in both alleles, transcription of AtNEAP2 mRNA remained unaffected in the T-DNA line. Three more AtNEAP2 mutant lines were ordered and genotyped. None of the seedlings of the SALK_12087 line were found to contain the expected T-DNA insertion (figure 5.3a). Genotyping of the GABI_589B02 line expected to contain a T-DNA insertion in the 5' UTR of AtNEAP2, identified several heterozygous (for example: figure 5.3b lane 3) and homozygous (for example: figure 5.3b lane 2) plants. The genotyped homozygous line GABI_589B02 was named *neap2* and used for

phenotyping experiments (figures 5.7a, 5.8 and 5.9). Genotyping of another T-DNA line GABI_178C02 expected to contain a T-DNA insertion in the intronic region of AtNEAP2 led to the identification of heterozygous plants (figure 5.3c lanes 3, 4 and 5). Typical Mendelian inheritance predicts one in four progeny of the heterozygous lines to be homozygous. Hence the heterozygous lines were allowed to self-pollinate for collection of seeds and further genotyping for identification of a homozygous line (Chapter 6 section 6.3.3). To verify a KO or KD of AtNEAP2 in these homozygous lines, RT-PCR experiments are planned as future work (Chapter 6 section 6.3.3).

A WiscDsLoxHS086_02C line expected to contain a T-DNA insertion in one of the exons of AtNEAP3 was genotyped and a homozygous line was identified (figure 5.4a). Further, semi-quantitative RT-PCR showed absence of AtNEAP3 mRNA in the genotyped homozygous WiscDsLoxHS086_02C line compared to WT, confirming it to be a KO mutant for AtNEAP3. This line was named *neap3* and used for phenotyping experiments (figures 5.6b, 5.8 and 5.9).

A SAIL_1239_G02 line expected to contain a T-DNA insertion in an intronic region of AtNEAP4 was genotyped and homozygous lines were identified (figure 5.5a lanes 1 and 2), putatively named as *neap4* and used in phenotyping experiments (figures 5.7b and 5.10). KO or KD status will be confirmed as part of future work.

Two lines, SAIL_592_G02 and WiscDsLoxHS073_05E, expected to contain a T-DNA insertion in an intron and exon respectively of AtbZIP18 gene were genotyped. A heterozygous SAIL_592_G02 plant was identified (figure 5.5a lanes 3 and 4) and allowed to self-pollinate for seed collection. The progeny of the heterozygous mutant plant will be genotyped for the identification of one homozygous mutant expected in four offspring (Chapter 6 section 6.3.3). A homozygous WiscDsLoxHS073_05E line was identified (figure 5.5a lanes 5 and 6), putatively named *bzip18* and used in preliminary phenotyping experiments (figure 5.12). mRNA KD or KO will be confirmed in the *bzip18* lines in future experiments (Chapter 6 section 6.3.3).

Two T-DNA lines, *neap1* and *neap3,* were successfully identified to contain a homozygous insertion in their respective genes and were also confirmed to be KO mutants. Therefore, the *neap1* line was crossed with the *neap3* mutant line

and their *neap1/neap3* double heterozygous offspring were allowed to self-pollinate. Their seeds were collected and 24 seedlings were screened. Figure 5.5b shows an example of a *neap1/neap3* double homozygous mutant plant genotype having the 500 base pair insert bands in both AtNEAP1 (lane1) and AtNEAP3 (lane4) genes while showing the absence of the WT band (1kb). Along with the *neap1*, *neap3* and *neap1/neap3* mutant lines; *neap2*, *neap4* and *bzip18* lines were also genotyped as homozygous. All lines were used for phenotyping experiments.

5.3.2 Plant growth phenotypes of AtNEAP mutant lines

Under standard growth conditions (described in Chapter 2 section 2.2), all AtNEAP mutant T-DNA lines including *neap1*, *neap2*, *neap3*, *neap4* and *neap1/neap3* were phenotypically normal (data not shown). All lines were capable of successful seed germination; root, leaf and flower development and seed production. All single *neap* mutant lines were used in crossing experiments, and were found to have viable pollen capable of cross pollination and production of healthy embryos.

To study subtle changes in growth, a primary root length assay was developed. For this assay, a *neap* mutant line was germinated alongside WT Col-0 seeds on square shaped ½ MS agar plates. Plates were placed perpendicular in standard long day conditions to allow gravitropic growth of roots. Both WT and mutant seeds were of similar age and treated identically before germination as well as sown on the same plate in order to keep all conditions consistent during and post germination.

Germination rate, calculated as the percentage of seeds germinated, was found to be consistently high, between 95-100% for all mutant lines and no difference was observed in comparison to WT germination rates (data not shown). Plates were scanned every 24 hours for 8 days and length of the primary root was measured using Image J analysis software (Chapter 2 section 2.2.4). Average root length was calculated, and WT and mutant data for 30 seedlings was compared by unpaired t test. The primary root length assay was repeated 3 times for each mutant line; the results shown in figures 5.6 and 5.7 are from an

experiment representative of the three replicates. Each experiment compared 30 mutant seedlings to WT.

Figure 5.6a shows that the average primary root lengths of *neap1* KO seedlings were similar to that of WT Col-0 between 1 to 5 days. The average primary roots of *neap1* were shorter than WT on days 7 and 8, but the difference was not statistically significant ($p>0.05$). The average primary root lengths on day 8 for WT and *neap1* were 0.73 $\pm$ 0.13 cm and 0.60 $\pm$ 0.09 cm ($p = 0.22$). Similar results were observed for the *neap2* line in the primary root length assay. As seen in figure 5.7a, *neap2* primary root lengths were similar to that of WT between 1 to 5 days, and shorter on days 7 and 8. However, as in the case of *neap1* the difference was not statistically significant. The average primary root lengths on day 8 for WT and *neap2* were 0.73 $\pm$ 0.13 cm and 0.52 $\pm$ 0.08 cm ($p = 0.12$). The primary root lengths of the *neap3* KO line were not different to that of WT from 1 to 8 days (figure 5.6b). The average primary root lengths on day 8 for WT and *neap3* were 1.01 $\pm$ 0.1 cm and 0.97 $\pm$ 0.11 cm ($p = 0.313$). Interestingly, the *neap1/neap3* double KO line had significantly shorter primary roots compared to WT from 2 to 8 days (figure 5.6c). The average primary root lengths on day 8 for WT and *neap1/neap3* were 1.67 $\pm$ 0.09 cm and 1.28 $\pm$ 0.1 cm ($p = 0.002$). The *neap4* line showed the strongest phenotype of all single AtNEAP mutant lines. The average primary root lengths of *neap4* were significantly shorter than WT from 3 to 8 days (figure 5.7b). The average primary root lengths on day 8 for WT and *neap4* were 0.73 $\pm$ 0.13 cm and 0.42 $\pm$ 0.09 cm ($p = 0.04$).

In summary, the average primary root lengths of AtNEAP mutant lines are not different from that of WT, except the *neap1/neap3* and *neap4* lines which show significant ($p<0.05$) shortening of primary roots as early as day2 and day3 of root development, respectively.

5.3.3 Nuclear phenotypes of AtNEAP mutant lines

Any changes in nuclear morphology of AtNEAP mutant T-DNA lines was studied using assays for nuclear size, nuclear shape or roundedness and nuclear positioning. Ten day old seedlings grown in standard long day conditions (described in Chapter 2 section 2.2.2) were used for all assays.

Seedlings were stained in 1:1 ethidium bromide: PBS for 20 minutes and imaged using confocal microscopy (Chapter 2 section 2.5.1). Nuclei of different cell types including root cortex, root hairs, cotyledons, leaf trichomes and leaf guard cells of age-matched WT and AtNEAP mutant lines were imaged at the plane of maximum width and length. Images were analysed by measuring nuclear length and width using the ImageJ software. For the nuclear size assay, average nuclear length and width of more than 30 AtNEAP mutant cells was compared to that of WT using unpaired t test. For the nuclear shape assay, the nuclear circularity index (CI) was calculated as a measure of nuclear roundedness. The CI of a nucleus was defined as the ratio of nuclear width to length (Zhou et al., 2012). A CI value of one indicates a perfectly round nucleus whereas a value close to zero denotes a highly elongated nucleus. All assays were performed 3 times and the results presented below are from a single representative assay (methods described in Chapter 2 section 2.5.5).

Figure 5.8a shows the comparison of average nuclear length and width of root hair nuclei in *neap1*, *neap2* and *neap3* KO mutants with WT, followed by a comparison of their CIs in figure 5.8b. As seen in figure 5.8a, *neap1* mutant root hair nuclei were significantly ($p < 0.05$) longer (20.87 $\pm$ 1.05 µm) compared to WT (17.01 $\pm$ 1.43 µm; p=0.02). They were also wider (7.71 $\pm$ 0.47 µm) than WT (6.88 $\pm$ 0.60 µm); however the increase in width was not statistically significant (p=0.14). Average nuclear length of single KO *neap2* (16.56 $\pm$ 0.62 µm, p = 0.39) and *neap3* (15.19 $\pm$ 0.93 µm, p = 0.14) mutant root hair nuclei were similar compared to WT (17.01 $\pm$ 1.43 µm). Similarly, average nuclear width of single KO *neap2* (6.45 $\pm$ 0.36 µm, p = 0.27) and *neap3* (6.49 $\pm$ 0.34 µm, p = 0.29) mutant root hair nuclei were similar compared to WT (6.88 $\pm$ 0.60 µm). Also there was no significant ($p > 0.05$) difference in the CIs of single KO *neap1* (0.40 $\pm$ 0.03), *neap2* (0.40 $\pm$ 0.02) and *neap3* (0.46 + 0.03) root hair nuclei compared to WT (0.46 $\pm$ 0.04). Thus apart from an increase in nuclear length in the *neap1* single KO line, mutations in AtNEAP genes did not affect nuclear size and roundedness in root hairs.

Figure 5.8c shows that WT root cortex cells had an average nuclear length of 7.11 $\pm$ 0.26 µm and an average nuclear width of 4.45 $\pm$ 0.12 µm. Root cortex nuclei of the *neap1* mutant line were significantly larger than WT showing a

significant increase ($p < 0.00001$) in average nuclear length (14.89 ± 0.49 µm) as well as nuclear width (7.05 ± 0.29 µm). On the contrary, *neap2* root cortex nuclei were significantly smaller with a significant decrease in both average nuclear length (6.08 ± 0.25 µm, $p = 0.004$) and width (3.97 ± 0.19 µm, $p = 0.02$) compared to WT (figure 5.8c). Further, the average length of *neap3* (5.89 ± 0.19 µm) root cortex nuclei were significantly ($p = 0.0003$) shorter, with no difference in nuclear width (4.50 ± 0.12 µm, $p = 0.39$) compared to WT. Interestingly, the CI of *neap1* (0.48 ± 0.02) root cortex nuclei was significantly ($p < 0.00001$) reduced indicating highly elongated shape relative to WT (0.64 ± 0.02) root cortex nuclei. While there was no difference ($p = 0.29$) in CI of *neap2* (0.67 ± 0.03) root cortex nuclei, *neap3* (0.78 ± 0.03) showed a significant increase ($p = 0.0009$) in CI indicating increased roundedness relative to WT.

Thus in summary in root cortex cells, *neap1* mutant nuclei were larger and elongated, *neap2* mutant nuclei were smaller with no effect on circularity and *neap3* mutant nuclear lengths were shorter and highly circular. All root hair and root cortex nuclear data was collected by Marlene Salvi under my supervision using mutant lines characterised in section 5.3.1. This analysis will also be performed on the *neap4* and *neap1/neap3* double mutant lines (Chapter 6 section 6.3.3).

Figure 5.9a shows comparison of average nuclear length and width in leaf trichome cells of *neap1*, *neap2* and *neap3* mutant lines with WT. The average length and width of WT leaf trichome nuclei was 15.21 ± 0.69 µm and 10.61 ± 0.45 µm respectively. As seen in figure 5.9a there was no difference ($p > 0.05$) between the average nuclear length of *neap1* (13.32 ± 1.08 µm, $p = 0.08$) and *neap2* (13.82 ± 0.92 µm, $p = 0.11$) mutant lines compared to WT. Likewise there was no difference between the average nuclear width of *neap1* (9.19 ± 0.76 µm, $p = 0.06$) and *neap2* (9.68 ± 0.68 µm, $p = 0.13$) mutant lines compared to WT. The average nuclear length of *neap3* (13.19 ± 0.49 µm) mutant trichome nuclei was significantly ($p = 0.01$) shorter than WT, while their average width (9.94 ± 0.49 µm) was similar ($p = 0.16$) to that of WT nuclei (figure 5.9a). The CI's of *neap1* (0.71 ± 0.04, $p = 0.37$), *neap2* (0.73 ± 0.04, $p = 0.44$) and *neap3* (0.76 ± 0.02, $p = 0.24$) mutant leaf trichome nuclei were not different to that of

WT (0.72 ± 0.03; figure 5.9b). Trichome nuclei of *neap1/neap3* double mutant and the *neap4* mutant lines will also be analysed (Chapter 6 section 6.3.3).

Figure 5.9c shows that the nuclei in *neap1* (12.07 ± 0.48 µm, p = 0.01), *neap2* (14.26 ± 0.64 µm, p < 0.00001) and *neap3* (13.14 ± 0.43 µm, p = 0.0004) mutant cotyledons were significantly longer than WT (10.31 ± 0.65 µm). While the average width of *neap1* (4.97 ± 0.17 µm) cotyledon nuclei was similar (p > 0.05) to that of WT (4.57 ± 0.30 µm), nuclei of *neap2* (5.76 ± 0.21 µm, p = 0.001) and *neap3* (6.36 ± 0.20 µm, p < 0.00001) cotyledons had significantly higher widths compared to WT (figure 5.9c). However changes in nuclear size did not significantly affect the CI of cotyledon nuclei. Figure 5.9d shows that the CIs of *neap1* (0.42 ± 0.01), *neap2* (0.42 ± 0.02) and *neap3* (0.49 ± 0.01) nuclei were not significantly (p > 0.05) different from WT (0.46 ± 0.02) cotyledons. In summary, *neap2* and *neap3* cotyledons had significantly larger nuclei, while nuclear circularity was not affected in any of the three mutants. Leaf trichome and cotyledon nuclei data for *neap1*, *neap2* and *neap3* was collected by Marlene Salvi under my supervision using mutant lines characterised in section 5.3.1.

Figure 5.10a shows the comparison of average nuclear length and width in cotyledons of the *neap4* mutant line with WT. The average length and width of WT cotyledon was 10.05 ± 0.34 µm and 5.48 ± 0.14 µm respectively. The average nuclear length of *neap4* (11.39 ± 0.43 µm) cotyledons was significantly increased (p = 0.02) and their average width (4.37 ± 0.41 µm) was significantly reduced (p = 0.001) compared to WT. As a result their CI was significantly (p = 0.02) reduced (0.43 ± 0.004), indicating an increase in elongation of *neap4* nuclei relative to WT (0.49 ± 0.004) cotyledons (figure 5.10b). Nuclear shape and size data for *neap4* line was collected by Gareth Hyam using the *neap4* mutant line characterised in section 5.3.1. Cotyledons of *neap1/neap3* double mutant line remain to be analysed (Chapter 6 section 6.3.3).

Some preliminary analysis of nuclear size, shape and positioning in the *neap1/neap3* leaf guard cells was performed by Katja Graumann (figure 5.11). Guard cells of the *neap1/neap3* line had significantly (p < 0.00001) reduced average nuclear length (3.97 ± 0.04 µm) compared to WT (4.30 ± 0.06 µm, figure 5.11a). Their average nuclear width (2.99 ± 0.06 µm) was similar (p =

0.08) to that of WT (2.87 ± 0.04 µm) guard cells (figure 5.11a). As a result of reduced lengths, the CI of *neap1/neap3* (0.74 ± 0.01) guard cell nuclei was significantly higher ($p < 0.00001$) than WT (0.65 ± 0.01), indicating an increase in circularity of double mutant nuclei (figure 5.11b).

The positioning of nuclei in guard cells was studied next (Chapter 2 section 2.5.6). The confocal micrograph in figure 5.11c shows that in WT guard cells, nuclei are positioned very close to the centre of the longitudinal plane of the stomatal pore or aperture. The central position of guard cell nuclei in *A. thaliana* was consistent with that previously reported by Zhou et al. (2014). The longitudinal plane (shown in figure 5.11c as white dotted line) of the stomatal aperture was defined as the straight line joining the furthest ends of the pore. On the contrary, the *neap1/neap3* KO guard cell nuclei were positioned further away from the centre of the longitudinal plane (figure 5.11c). Positioning of a guard cell nuclei was measured by the angle formed by the longitudinal plane of aperture with a line passing through the centre of the longitudinal plane and the centre of the nucleus. The angle is shown by blue and red arrows in the confocal micrographs (figure 5.11c). The graph in figure 5.11d shows that the angle of guard cell positioning relative to the stomatal aperture was significantly ($p = 0.04$) smaller in *neap1/neap3* KO (angle = 52.39 ± 18.46 degrees) nuclei compared to WT (angle = 71.83 ± 6.21 degrees). Thus in summary, *neap1/neap3* KO guard cell nuclei are significantly smaller and circular compared to WT. They are also positioned significantly further away from the centre of the longitudinal plane of the stomatal aperture. Guard cell nuclei of other AtNEAP single mutant lines will be analysed (Chapter 6 section 6.3.3).

5.3.4 Phenotypic characterisation of *bzip18* mutant line

As first described in chapter 4 section 4.3.6, AtbZIP18 was identified as a novel interactor of AtNEAP1. The *bzip18* mutant line genotyped in section 5.3.1, was analysed using the primary root length assay and the nuclear size and shape assays used for AtNEAP mutant lines above. Figure 5.12a shows the primary root length assay for *bzip18* line versus WT. The average primary root length of *bzip18* mutant line was not different to that of WT from 1 to 8 days, indicating no effect on root growth. The average primary root lengths on day 8 for WT and

bzip18 were 1.02 ± 0.1 cm and 0.95 ± 0.11 cm (p = 0.15). Further, preliminary nuclear size data was collected from *bzip18* mutant lower epidermal cotyledon pavement cells (by Gareth Hyam). Figure 5.12b shows that the average length of *bzip18* (8.81 ± 0.5 μm) mutant cotyledon nuclei was significantly (p = 0.048) shorter than WT (10.05 ± 0.34 μm). Nuclear width (5.40 ± 0.5 μm) was similar (p = 0.72) to that of WT (5.48 ± 0.14 μm). However, the CI of *bzip18* (0.60 ± 0.02) mutant cotyledon nuclei was significantly higher (p = 0.007) than WT (0.49 ± 0.004, figure 5.12c). Thus, the *bzip18* cotyledon nuclei were significantly shorter and more circular compared to WT. Nuclear morphology changes in other cell types including leaf trichome, guard cells and root hair and cortex cells will be studied for the *bzip18* line in the future (Chapter 6 section 6.3.3).

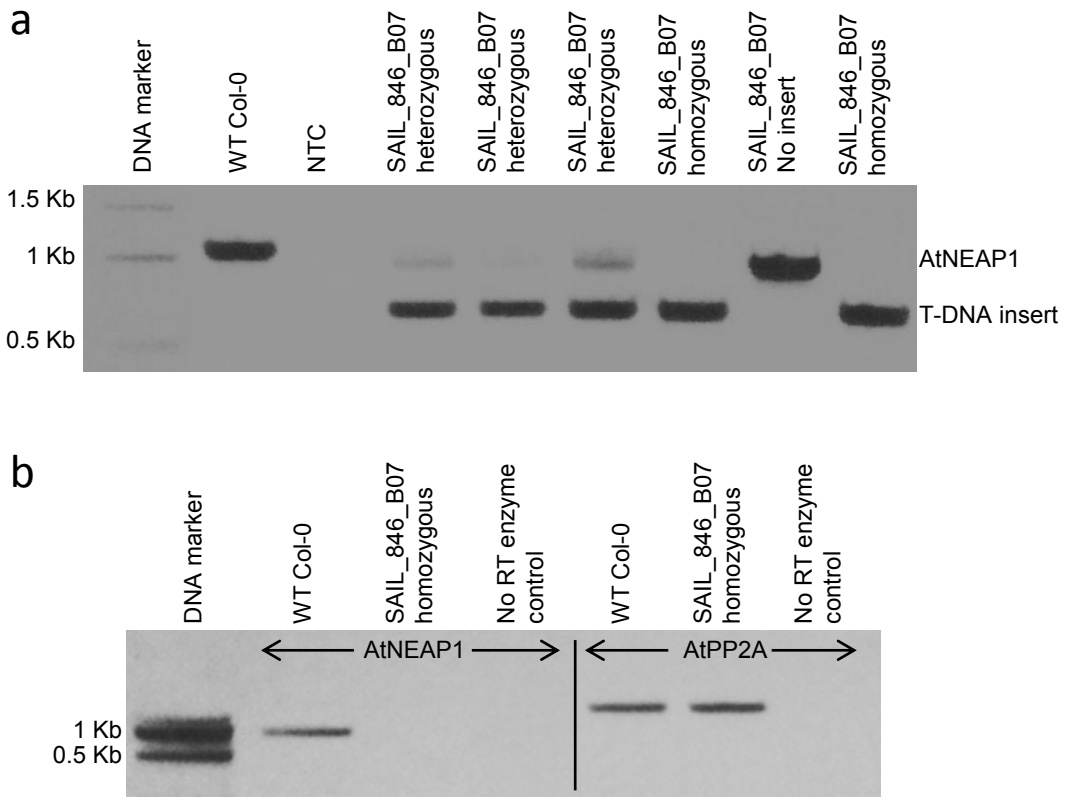

Figure 5.1: Characterisation of an AtNEAP1 knockout T-DNA line SAIL_846_B07.

a. Genotyping PCR showing AtNEAP1 genomic DNA (gDNA, ~1 Kb) in WT Col-0 (lanes 2 and 8), T-DNA insertion in AtNEAP1 (~0.7 Kb) in homozygous lines (lanes 7 and 9), and both the bands in heterozygous lines (lanes 4, 5 and 6). Lane 3 represents the non template control (NTC). Lane 1 shows the DNA marker. PCR reaction contained three primers, two AtNEAP1 gDNA primers flanking the T-DNA insertion site and one primer on the border of the T-DNA insert.

b. Semi-quantitative RT-PCR using cDNA primers for AtNEAP1 (~1 Kb) and control gene AtPP2A (~1.2 Kb). Showing AtNEAP1 mRNA levels present in WT Col-0 (lane 2) and absent in homozygous SAIL_846_B07 line (lane 3). AtPP2A mRNA levels seen relatively unchanged between the WT Col-0 (lane 5) and homozygous SAIL_846_B07 line (lane 6). Lanes 4 and 7 represent reverse transcriptase (RT) enzyme controls. Lane 1 shows the DNA marker.

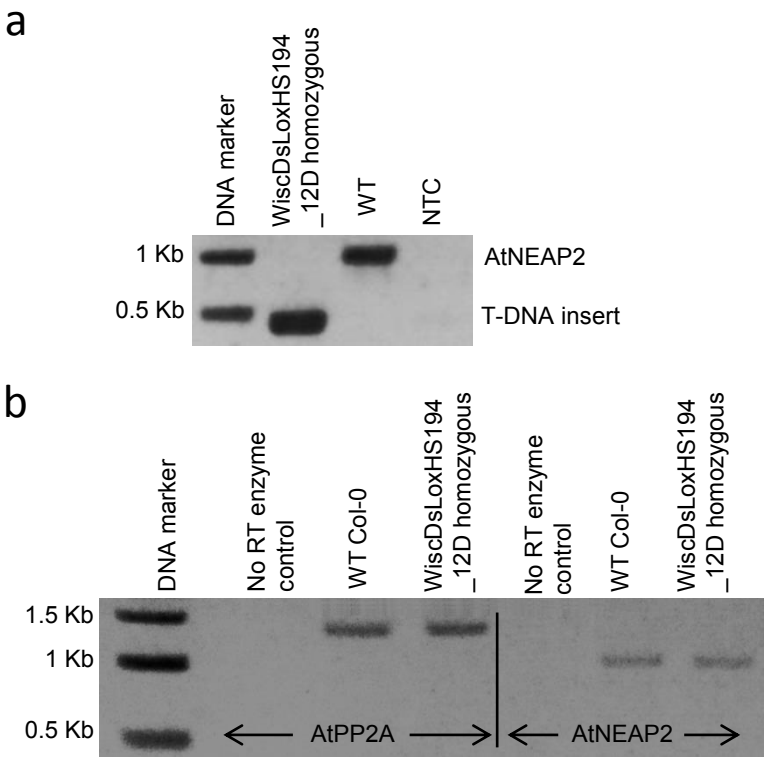

Figure 5.2: Characterisation of AtNEAP2 T-DNA line WiscDsLoxHS194_12D.

a. Genotyping PCR showing AtNEAP2 gDNA (~1 Kb) in WT Col-0 (lane 3) and T-DNA insertion in AtNEAP2 (~0.5 Kb) in a homozygous WiscDsLoxHS194_12D line (lane 2). Lane 4 represents the NTC. Lane 1 shows the DNA marker. PCR reaction contained three primers, two AtNEAP2 gDNA primers flanking the T-DNA insertion site and one primer on the border of the T-DNA insert.

b. Semi-quantitative RT-PCR using cDNA primers for AtNEAP2 (~1 Kb) and control gene AtPP2A (~1.2 Kb). Showing AtNEAP2 mRNA levels comparitively unchanged between WT Col-0 (lane 3) and homozygous WiscDsLoxHS194_12D line (lane 4). AtPP2A mRNA levels appear unchanged between the WT Col-0 (lane 6) and homozygous WiscDsLoxHS194_12D line (lane 7). Lanes 2 and 5 represent no RT enzyme controls. Lane 1 shows the DNA marker.

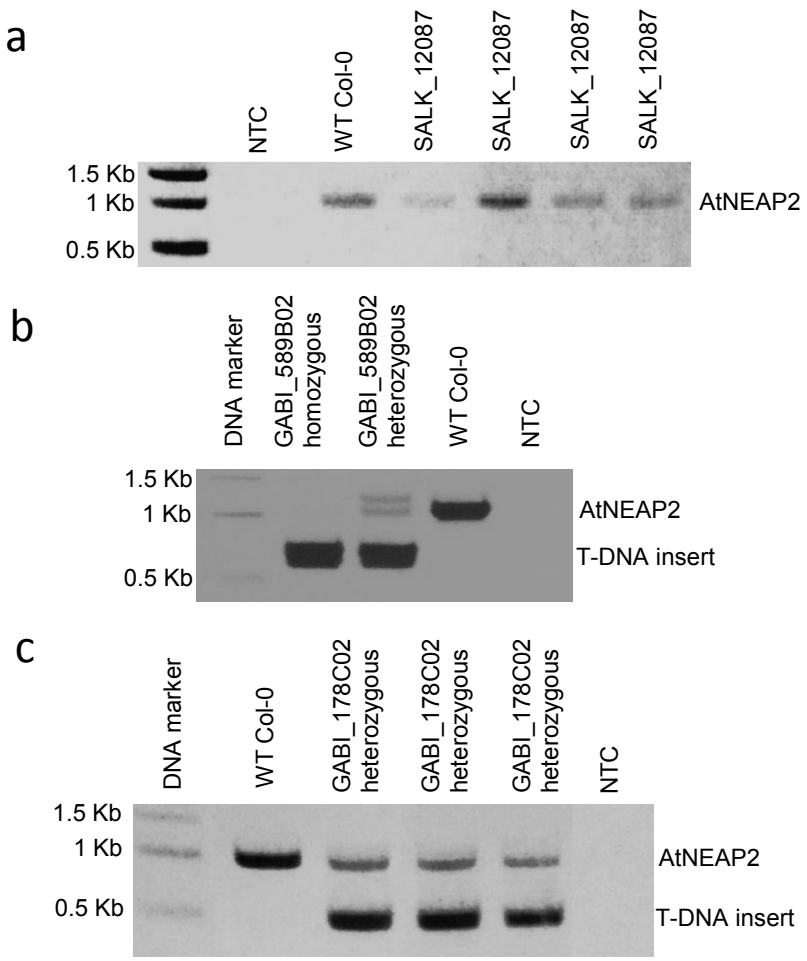

Figure 5.3: Characterisation of AtNEAP2 T-DNA lines.

a. Genotyping PCR showing AtNEAP2 gDNA (~1 Kb) in WT Col-0 (lane 3) and SALK_12087 lines (lanes 4, 5, 6 and 7). None of the SALK_12087 lines (lanes 4-7) contained a T-DNA insertion in AtNEAP2 (expected ~0.5 Kb). Lane 2 represents the NTC. Lane 1 shows the DNA marker.
b. Genotyping PCR showing AtNEAP2 gDNA (~1 Kb) in WT Col-0 (lane 4), T-DNA insertion in AtNEAP2 gene (~0.7 Kb) in a GABI_589B02 homozygous line (lane 2) and both the bands in a heterozygous line (lane 3). Lane 5 represents the NTC. Lane 1 shows the DNA marker.
c. Genotyping PCR showing AtNEAP2 gDNA (~1 Kb) in WT Col-0 (lane 2). GABI_178C02 heterozygous T-DNA insertion lines (lanes 3, 4 and 5) show both the AtNEAP2 gDNA (~1 Kb) and a T-DNA insertion in AtNEAP2 (~0.5 Kb). Lane 6 represents the NTC. Lane 1 shows the DNA marker.

Genotyping PCR reaction contained three primers, two AtNEAP2 gDNA primers flanking the T-DNA insertion site and one primer on the border of the T-DNA insert.

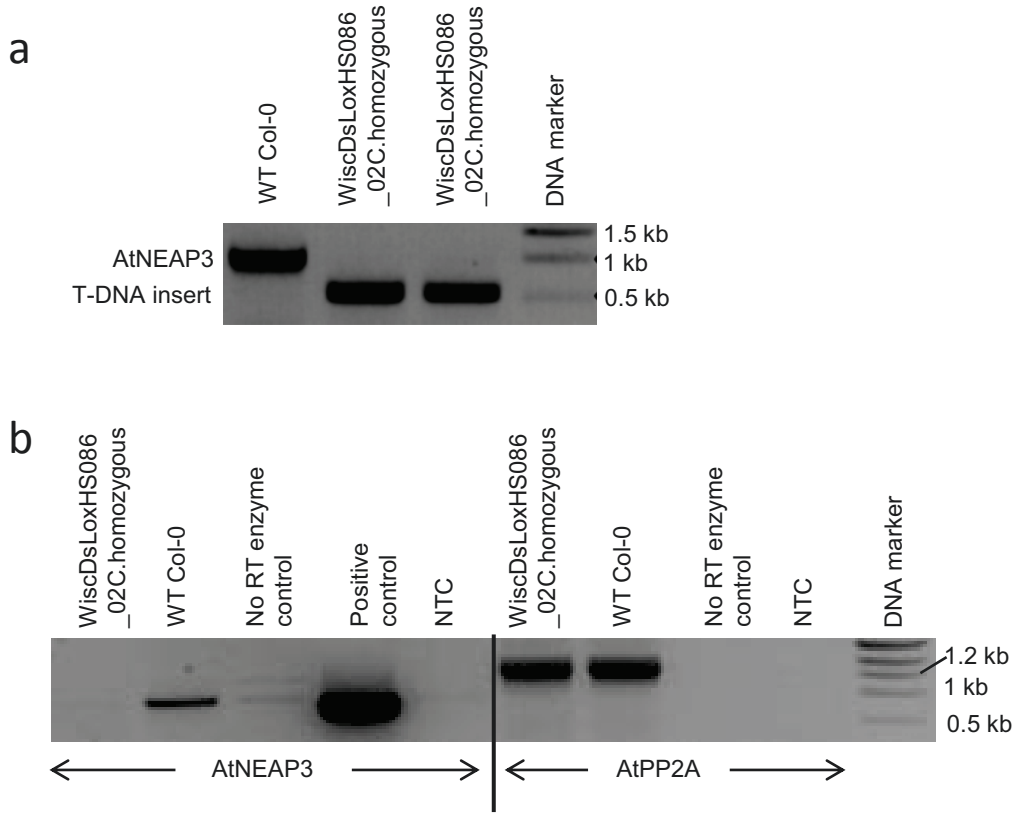

Figure 5.4: Characterisation of an AtNEAP3 knockout T-DNA line WiscDsLoxHS086_02C.

a. Genotyping PCR showing AtNEAP3 genomic DNA (~1 Kb) in WT Col-0 (lane 1) and T-DNA insertion in AtNEAP3 gene (~0.5 Kb) in homozygous lines (lanes 2 and 3). Lane 4 shows the DNA marker. PCR reaction contained three primers, two AtNEAP3 gDNA primers flanking the T-DNA insertion site and one primer on the border of the T-DNA insert.

b. Semi-quantitative RT-PCR using cDNA primers for AtNEAP3 (~1 Kb) and control gene AtPP2A (~1.2 Kb). Showing AtNEAP3 mRNA levels present in WT Col-0 (lane 2) and absent in homozygous WiscDsLoxHS086_02C line (lane 1). AtPP2A mRNA levels seen relatively unchanged between the WT Col-0 (lane 7) and homozygous WiscDsLoxHS086_02C line (lane 6). Lanes 3 and 8 represent no RT enzyme controls. Lane 4 represents a positive AtNEAP3 cDNA control. Lanes 5 and 9 represent the NTC. Lane 10 shows the DNA marker.

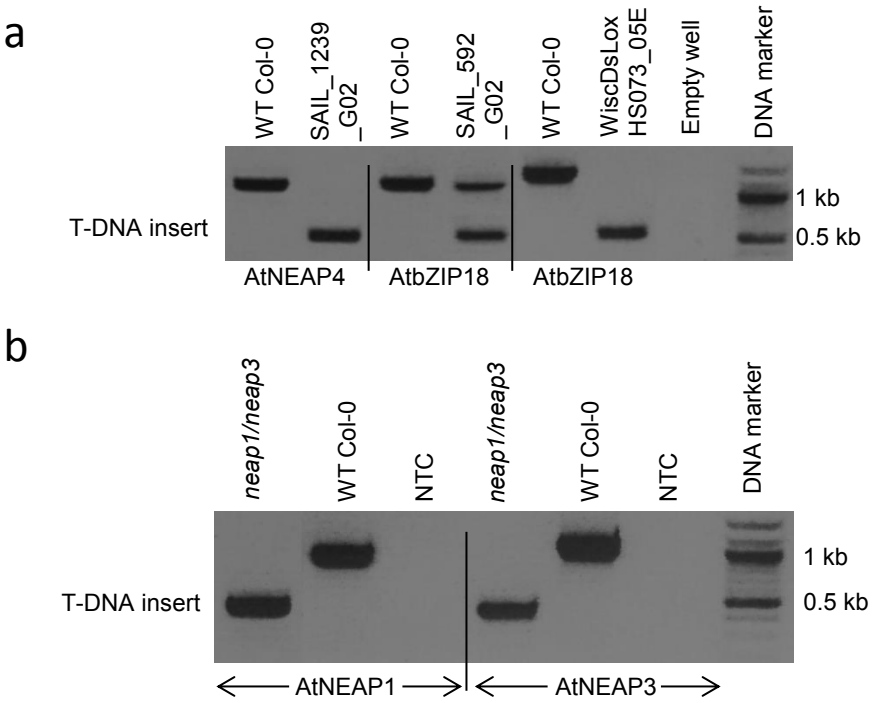

Figure 5.5: Characterisation of AtNEAP4 (SAIL_1239_G02), AtbZIP18 (SAIL_592_G02 and WiscDsLoxHS073_05E), and *neap1/neap3* double (SAIL_846_B07/WiscDsLoxHS086_02C) mutant T-DNA lines.

a. Genotyping PCR showing AtNEAP4 gDNA (~1 Kb) in WT Col-0 (lane 1) and T-DNA insertion in AtNEAP4 (~0.5 Kb) in a homozygous SAIL_1239_G02 line (lane 2). Followed by AtbZIP18 gDNA (~1 Kb) in WT Col-0 (lane 3). A heterozygous SAIL_592_G02 line (lane 4) shows both AtbZIP18 gDNA and a T-DNA insertion (~0.5 Kb). Lastly, AtbZIP18 gDNA (~1 Kb) seen in WT Col-0 (lane 5) and a T-DNA insertion (~0.5 Kb) in AtbZIP18 gene in a homozygous WiscDsLoxHS073_05E line (lane 6). Lane 8 shows the DNA marker.
b. Genotyping PCR showing AtNEAP1 gDNA (~1 Kb) in WT Col-0 (lane 2) and homozygous insertion in AtNEAP1 (~0.5 Kb) in a *neap1/neap3* double mutant line (lane 1), followed by AtNEAP3 gDNA (~1 Kb) in WT Col-0 (lane 5) and homozygous insertion in AtNEAP3 (~0.5 Kb) in the *neap1/neap3* double mutant line (lane 4). Lanes 3 and 6 represent the NTC. Lane 7 shows the DNA marker.

Each genotyping PCR reaction contained three primers, two gDNA primers for the gene of interest (e.g. AtNEAP4, AtbZIP18, AtNEAP1 and AtNEAP3) flanking the T-DNA insertion site and one primer on the border of the T-DNA insert.

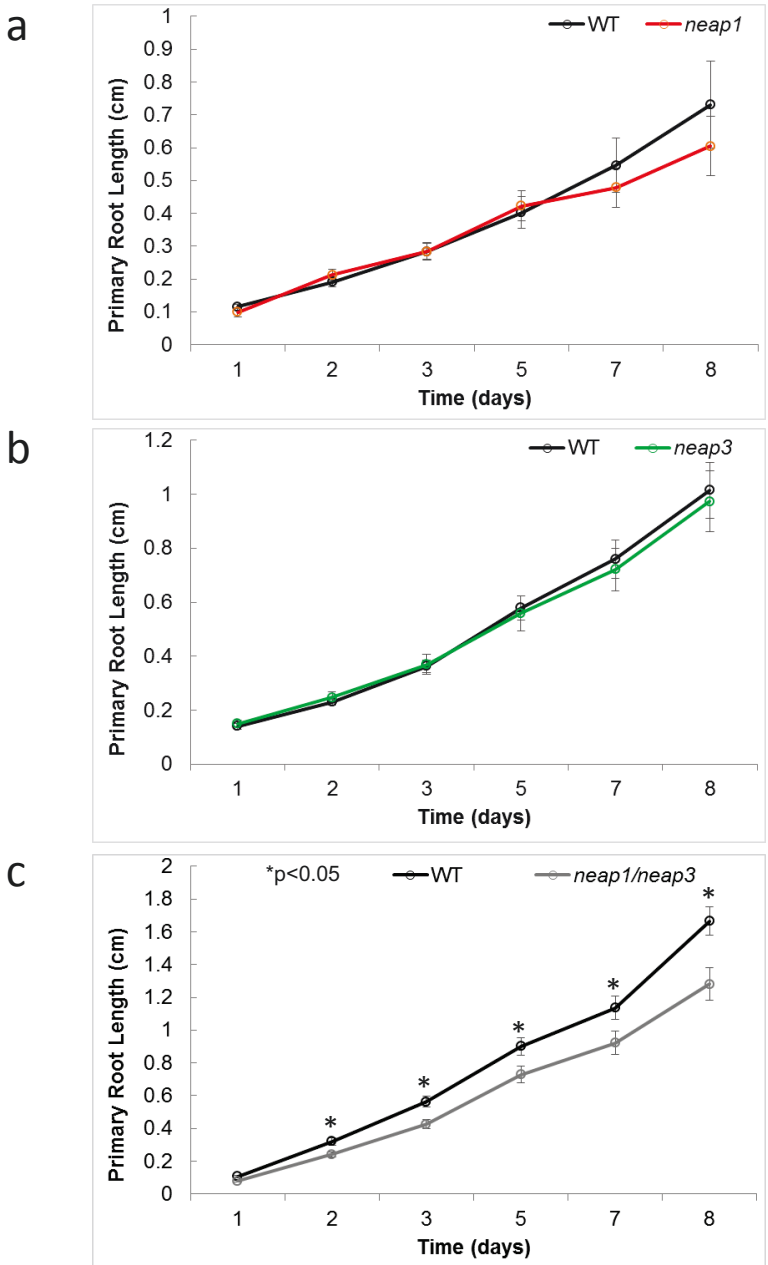

Figure 5.6: Root growth assays comparing primary root lengths of *neap1*, *neap3* and *neap1/neap3* double mutant lines versus WT Col-0 in 1 to 8 day old seedlings.

a. Graph shows that there was no difference in primary root lengths of *neap1* mutant (red) seedlings compared to the WT Col-0 (black) between 1 to 5 days. *neap1* root growth was slower than WT Col-0 on days 6 and 7, however the difference was not statistically significant.

b. Graph shows that there was no difference in primary root lengths of *neap3* mutant (green) seedlings compared to WT Col-0 (black) between 1 to 8 days.

c. Graph shows that the lengths of *neap1/neap3* mutant (grey) primary roots were significantly shorter than WT Col-0 (black) in 2 to 8 day old seedlings.

All values were expressed as mean ± standard error of mean (SEM). Unpaired t test was performed, where *p<0.05 was statistically significant (n = 30).

a

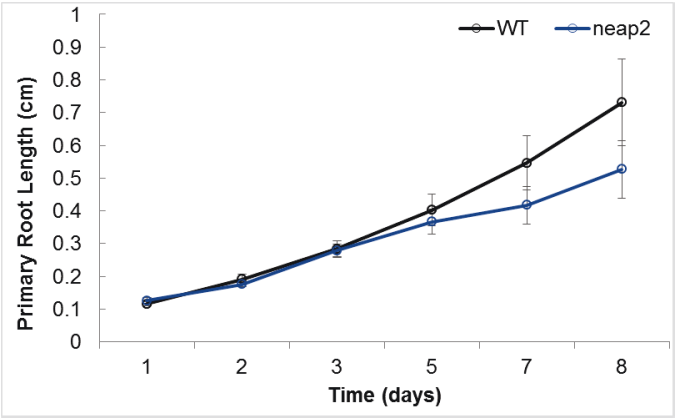

b

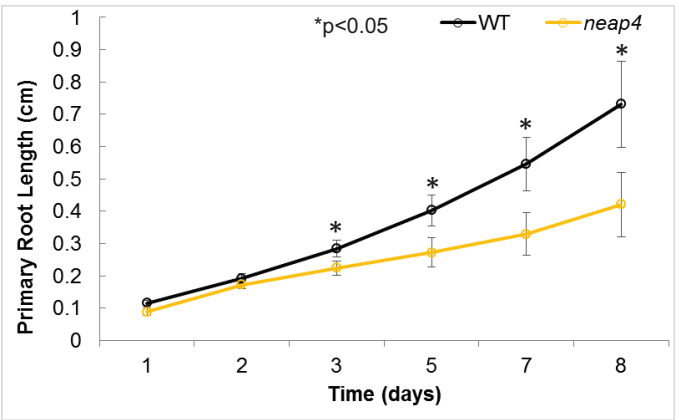

Figure 5.7: : Root growth assays comparing primary root lengths of *neap2* and *neap4* mutant lines versus WT Col-0 in 1 to 8 day old seedlings.

a. Graph shows that there was no difference in primary root lengths of *neap2* mutant (blue) seedlings compared to the WT Col-0 (black) between 1 to 5 days. *neap2* root growth was slower than WT Col-0 on days 6 and 7, however the difference was not statistically significant.

b. Graph shows that the lengths of *neap4* mutant (yellow) primary roots were significantly shorter than WT Col-0 (black) in 3 to 8 day old seedlings.

All values were expressed as mean ± SEM. Unpaired t test was performed, where *p<0.05 was statistically significant (n = 30).

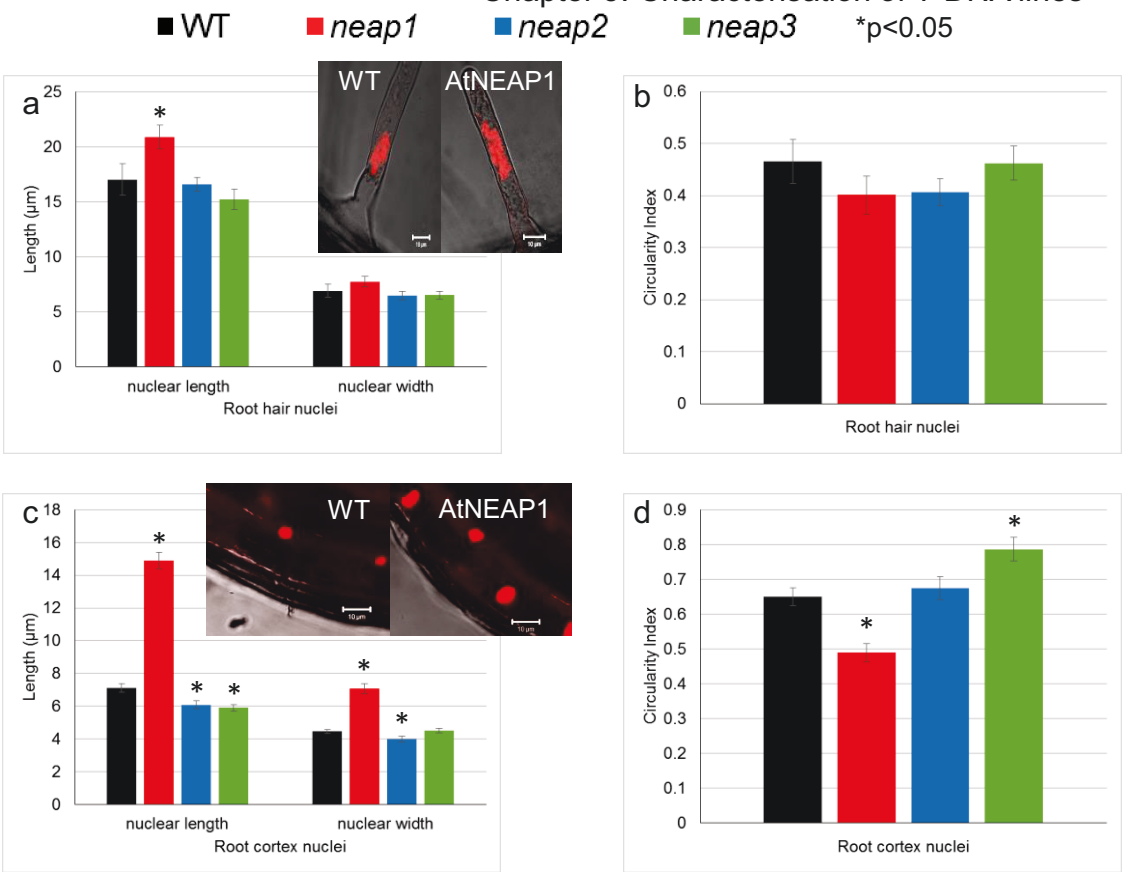

Figure 5.8: Analysis of nuclear size and roundedness in 10 day old roots of *neap1* (red), *neap2* (blue) and *neap3* (green) mutant lines in comparison to WT Col-0 (black). Circularity index (CI) is a measure of nuclear roundedness calculated as the ratio of nuclear width to length. A CI of 1 indicates a perfectly round nucleus whereas a value close to zero denotes a highly elongated nucleus.

a. *neap1* mutant root hair nuclei were significantly longer and wider compared to WT, however the increase in width was not statistically significant. Lengths and widths of *neap2* and *neap3* mutant root hair nuclei were similar compared to WT.

b. The CI of *neap1*, *neap2* and *neap3* root hair nuclei were not different from the WT.

c. *neap1* mutant root cortex nuclei were significantly larger (increased length and width) while *neap2* mutant root cortex nuclei were significantly smaller (decreased length and width) compared to WT. *neap3* mutant root cortex nuclei were significantly longer while their width was similar to WT.

d. The CI of *neap1* mutant root cortex nuclei was significantly lower indicating highly elongated nuclei compared to WT. On the contrary the CI of *neap3* mutant root cortex nuclei was significantly higher indicating increased roundedness of nuclei compared to WT. The CI of *neap2* mutant root cortex nuclei was similar to WT.

All values were expressed as mean ± SEM. Unpaired t test was performed, where *p<0.05 was statistically significant (n = 30). This data was collected by Marlene Salvi.

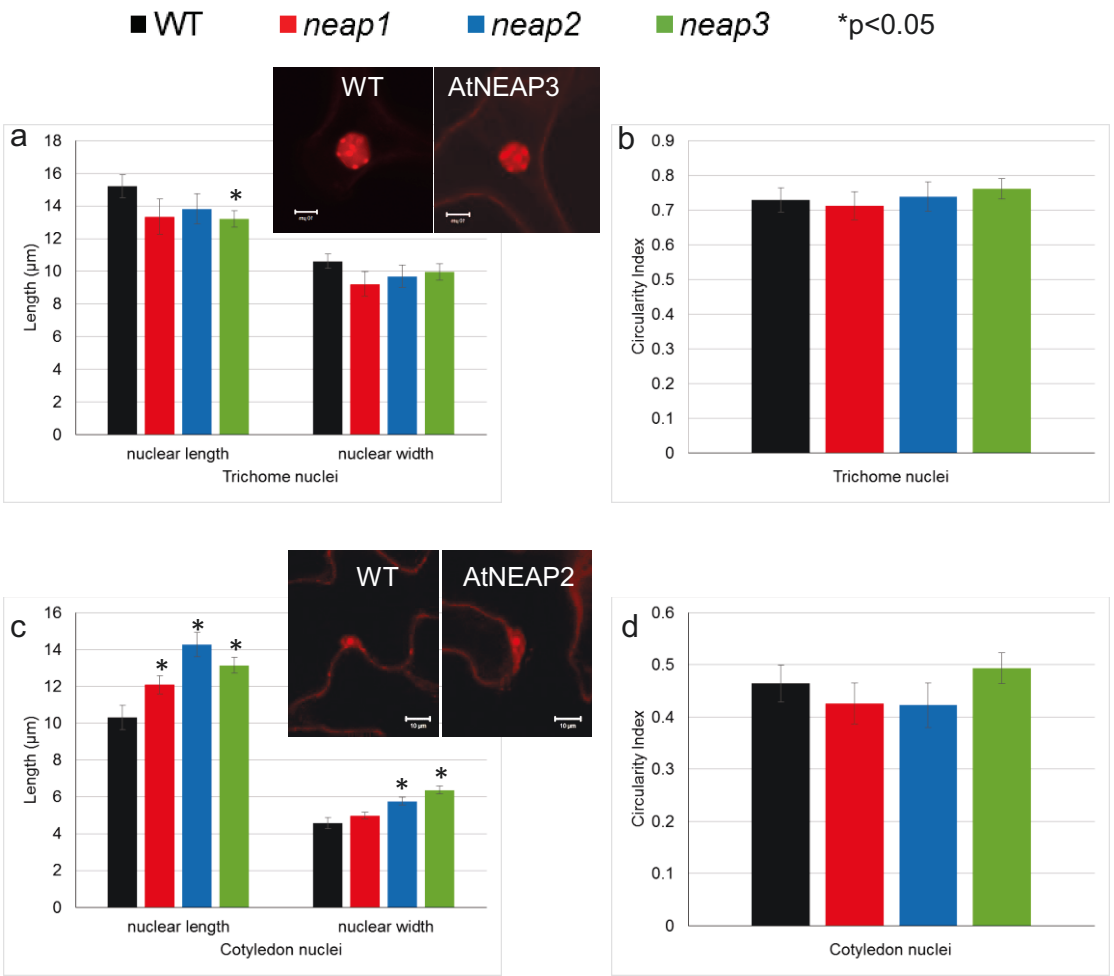

Figure 5.9: Analysis of nuclear size and roundedness in 10 day old cotyledons and leaf trichomes of *neap1* (red), *neap2* (blue) and *neap3* (green) mutant lines in comparison to WT Col-0 (black). Circularity index (CI) is a measure of nuclear roundedness calculated as the ratio of nuclear width to length. A CI of 1 indicates a perfectly round nucleus whereas a value close to zero denotes a highly elongated nucleus.

a. Lengths and widths of *neap1* and *neap2* mutant leaf trichome nuclei were similar compared to WT. *neap3* mutant leaf trichome nuclei were significantly longer whereas nuclear width was similar compared to WT.

b. The CI of *neap1*, *neap2* and *neap3* leaf trichome nuclei were not different from the WT.

c. *neap1* mutant cotyledon nuclei were significantly longer whereas nuclear width was similar compared to WT. *neap2* and *neap3* mutant cotyledon nuclei were significantly larger (increased length and width) compared to WT.

d. The CI of *neap1*, *neap2* and *neap3* cotyledon nuclei were not different from WT.

All values were expressed as mean ± SEM. Unpaired t test was performed, where *p<0.05 was statistically significant (n = 30). This data was collected by Marlene Salvi.

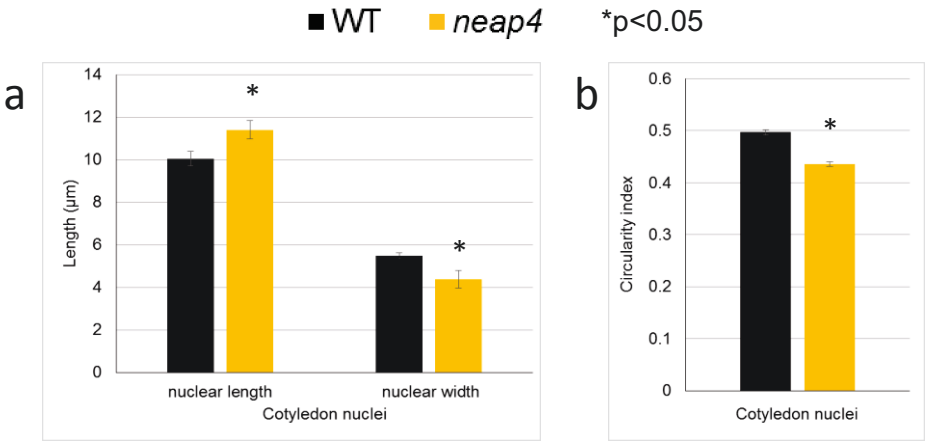

Figure 5.10: Analysis of nuclear size and roundedness in 10 day old cotyledons of *neap4* (yellow) mutant line in comparison to WT Col-0 (black). Circularity index (CI) is a measure of nuclear roundedness calculated as the ratio of nuclear width to length. A CI of 1 indicates a perfectly round nucleus whereas a value close to zero denotes a highly elongated nucleus.

a. *neap4* mutant cotyledon nuclei were significantly larger (increased length and width) compared to WT.

b. The CI of *neap4* mutant cotyledon nuclei was significantly reduced indicating highly elongated nuclei compared to WT.

All values were expressed as mean ± SEM. Unpaired t test was performed, where *p<0.05 was statistically significant (n = 30). This data was collected by Gareth Hyam.

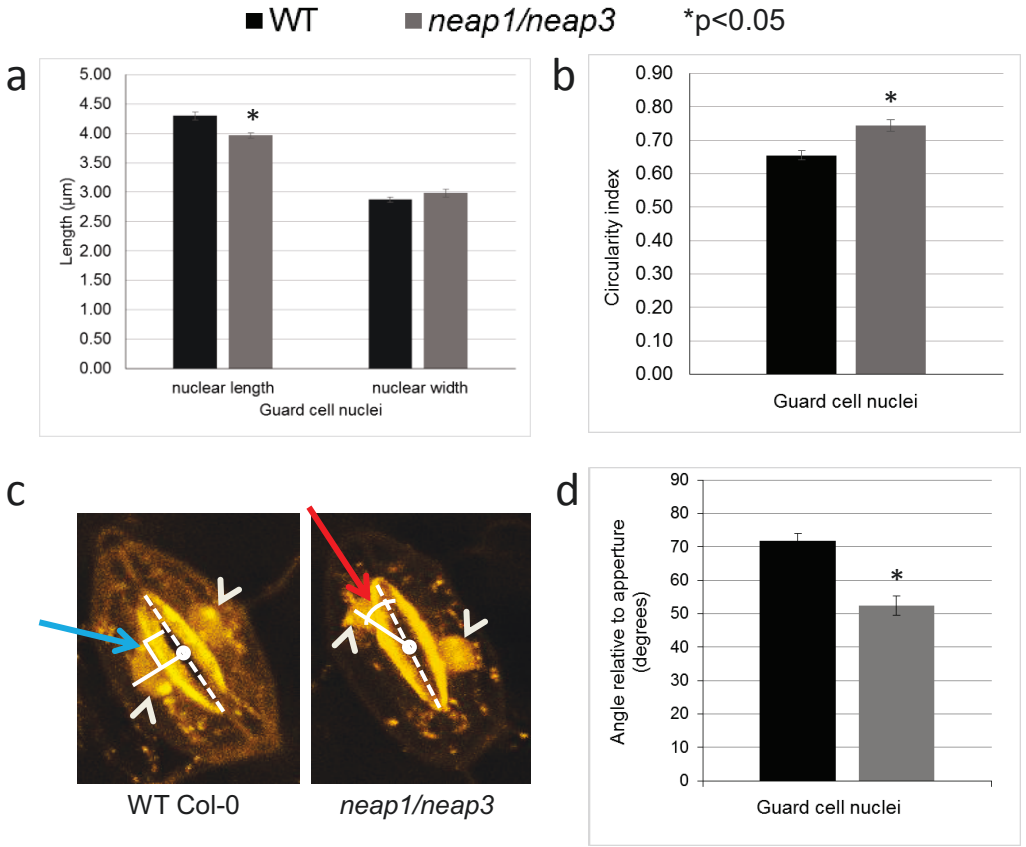

Figure 5.11: Analysis of nuclear size, roundedness and nuclear positioning relative to the stomatal apperture in 10 day old leaf guard cells of *neap1/neap3* (grey) mutant line in comparison to WT Col-0 (black). Circularity index (CI) is a measure of nuclear roundedness calculated as the ratio of nuclear width to length. A CI of 1 indicates a perfectly round nucleus whereas a value close to zero denotes a highly elongated nucleus.

a. *neap1/neap3* mutant guard cell nuclei were significantly shorter whereas nuclear width was similar compared to WT.

b. The CI of *neap1/neap3* mutant guard cell nuclei was significantly increased indicating an increase in nuclear roundedness compared to WT.

c. Confocal micrographs show that position of guard cell nuclei (white arrows) in WT Col-0 is nearly perpendicular (blue arrow) to the longitudinal plane (dotted white line) of the stomatal pore whereas *neap1/neap3* mutant nuclei lie at a smaller angle (red arrow).

d. Graph shows the relative angle of nuclear positioning to the apperture is significantly smaller in *neap1/neap3* mutant (grey) nuclei compared to WT Col-0 (black).

All values were expressed as mean ± SEM. Unpaired t test was performed, where *p<0.05 was statistically significant (n = 40). This data was collected by Katja Graumann.

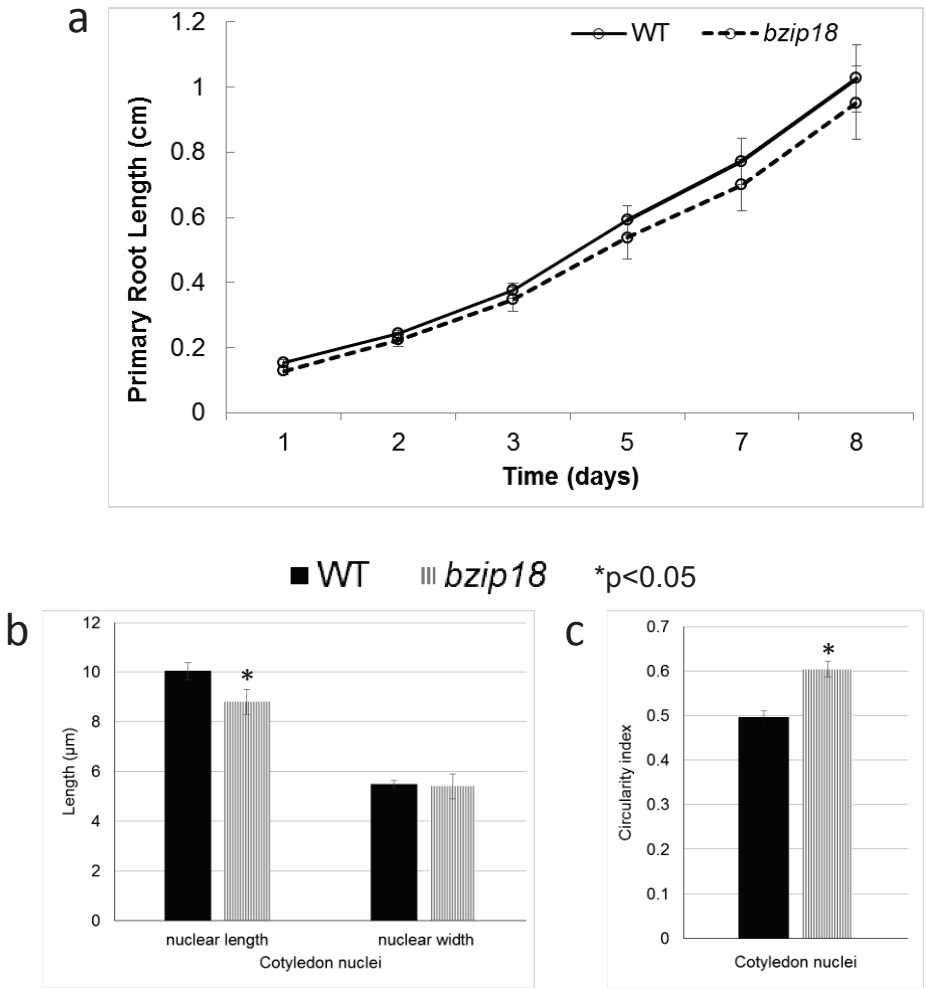

Figure 5.12: Phenotypic characterisation of *bzip18* mutant T-DNA line versus WT Col-0.

a. Root growth assay shows that there was no difference in primary root lengths of *bzip18* mutant T-DNA line (dotted curve) compared to WT Col-0 (black curve) between 1 to 8 days.
b. Analysis of nuclear size in 10 day old cotyledons shows that the mean length of *bzip18* mutant (grey, striped) cotyledon nuclei was significantly shorter compared to WT (black). Their mean width was similar to WT.
c. Analysis of nuclear roundedness in 10 day old cotyledons shows that the CI of *bzip18* mutant (grey, striped) cotyledon nuclei was significantly greater indicating increased roundedness of nuclei compared to WT Col-0 (black).

All values were expressed as mean ± SEM. Unpaired t test was performed, where *p<0.05 was statistically significant (n = 30). The nuclear size measurement data was collected by Gareth Hyam (b and c).

5.4 Discussion

5.4.1 Identification of KO AtNEAP and AtbZIP18 mutant lines

As described in section 5.3.1, genotyping PCR was used for identification of homozygous T-DNA insertion lines. The SAIL_846_B07 (*neap1*) line was identified as a homozygous line (figure 5.1a). Semi-quantitative RT-PCR showed that *neap1* had no AtNEAP1 mRNA (figure 5.1b). As the insertion was known to be in an intronic region of AtNEAP1, the absence of mRNA indicates that the T-DNA insertion disrupted the intron splicing machinery in the cell.

Further, WiscDsLoxHS194_12D was genotyped to contain a homozygous insertion in the 5' UTR of AtNEAP2 (figure 5.2a). However, the insertion had no effect on AtNEAP2 mRNA levels (figure 5.2b). Mutations in the 5' UTR have been shown to affect mRNA transcription of the target gene, as well as protein translation (Wilkie et al. 2003, Lytle et al. 2007). In this instance while mRNA KD was not seen, changes in endogenous protein levels could not be assayed due to inability to detect low levels of endogenous AtNEAP2 on a Western Blot. Genotyping a SALK_12087 line showed no insertion in the AtNEAP2 gene (figure 5.3a) suggesting the insertion may have been lost during gamete production by the DNA repair machinery of the cell.

Two more lines GABI_589B02 (*neap2*) and GABI_178C02 were genotyped, and found to contain a homozygous and heterozygous T-DNA insertion in their 5' UTR and intronic regions respectively (figure 5.3b and c). Whether the T-DNA insertion affected mRNA levels could not be ascertained due to lack of time to perform RT-PCR. The progeny of the heterozygous GABI_178C02 line is yet to be genotyped (Chapter 6 section 6.3.3).

A WiscDsLoxHS086_02C (*neap3*) line was identified to contain a homozygous T-DNA insertion in one of the exons of AtNEAP3 (figure 5.4a). RT-PCR also confirmed absence of AtNEAP3 mRNA (figure 5.4b) indicating that the T-DNA insertion disrupted mRNA transcription. A SAIL_1239_G02 (*neap4*) was genotyped and confirmed to contain a homozygous insertion in an intronic

region of AtNEAP4 (figure 5.5a). However mRNA KD has not yet been confirmed by RT-PCR (Chapter 6 section 6.3.3). Genotyping also helped identify a homozygous WiscDsLoxHS073_05E (*bzip18*) line and a heterozygous SAIL_592_G02 line containing a T-DNA insertion in an exon and intron of AtbZIP18 gene respectively (figure 5.5a). RT-PCR and genotyping of SAIL_592_G02 progeny will be done in the future. In summary, *neap1* and *neap3* lines were confirmed to be mRNA KO lines, while *neap2*, *neap4* and *bzip18* mRNA KD remain to be confirmed. A *neap1/neap3* double homozygous mutant line was also successfully generated by crossing the *neap1* and *neap3* lines (figure 5.5b). More double and triple KO lines will be generated by crossing the available *neap1*, *neap2*, *neap3* and *neap4* lines in different combinations to address redundancy of gene function (section 5.4.2 and Chapter 6 section 6.3.3).

5.4.2 Growth defects in AtNEAP and AtbZIP18 mutant lines

As described in section 5.3.2, *neap1*, *neap2*, *neap3*, *neap4* and *neap1/neap3* lines were phenotypically normal, capable of successful seed germination, root, leaf and flower development and had viable pollen capable of seed production. Normal growth phenotype in mutant lines suggested that loss of function of a single gene (or two in *neap1/neap3*) may be compensated by other gene products within the family.

Irregularities in primary root growth were monitored as an indicator of abnormal nuclear functions. Normal root growth is dependent on non-defective cell division and cell expansion which is limited by nuclear expansion (Scheres et al. 2002). Defects in nuclear size could alter the ability of the cell to expand and affect overall tissue growth. Single gene mutant lines *neap1*, *neap2* and *neap3* showed no effect on the rate of primary root growth between 1 to 8 days (figure 5.6a, 5.7 and 5.6b). Interestingly, the *neap1/neap3* line showed significantly slower growth of primary roots between 1 to 8 days. Thus loss of AtNEAP1 or AtNEAP3 on their own did not alter root growth probably indicating redundancy of function in the single mutants. Expression of AtNEAP1 and AtNEAP2 was found to be at medium levels in roots, however this data was unavailable for NEAP3 (Chapter 3 figures 3.6, 3.7 and 3.8). That loss of AtNEAP1 and

AtNEAP3 affected root growth suggests the two genes may function in an additive manner. This supports future strategy to generate more double and triple KO lines to assess their effects on root length phenotypes. As discussed earlier in this section, the changes in root growth may be a result of altered nuclear size and has been explored is section 5.4.3.1.

The *neap4* line showed significantly slower primary root growth between 3 to 8 days (figure 5.7b), suggesting that AtNEAP4 may perform functions that were not complemented by AtNEAP1, AtNEAP2 and AtNEAP3. It is important to note here that AtNEAP4 peptide sequence (112 amino acid) is approximately one third the size of other AtNEAP proteins (> than 335 amino acids) and lacks the extensive CC regions of AtNEAP1, AtNEAP2 or AtNEAP3 (Chapter 3 section 3.4.1). Thus AtNEAP4 may be involved in functions not shared by the rest of the family. Unfortunately, AtNEAP4 mRNA expression in root tissues was not available from Genevestigator or the BAR Arabidopsis eFP browser.

Similar to *neap1*, *neap2* and *neap3;* the *bzip18* mutant line showed no effect on the rate of primary root growth between 1 to 8 days (figure 5.12a), suggesting functional redundancy compensating for loss of single gene function. Expression of AtbZIP18 in root tissues was medium to low in Genevestigator and BAR Arabidopsis eFP browser (Chapter 4 figures 4.26 and 4.27) suggesting that AtbZIP18 may not have a role in root growth.

5.4.3 Nuclear morphology of AtNEAP and AtbZIP18 mutant lines

Plant nuclei have varied shapes and sizes including spherical, spindle shaped and cylindrical depending on the tissue type (Chytilova et al. 2000). For instance, epidermal leaf guard cells have some of the smallest and circular shaped nuclei, while pavement cells and trichomes have large and spindle shaped nuclei (Chytilova et al. 1999). Nuclei in root epidermal and cortex cells are spindle-form while vascular tissues have rod shaped nuclei (Chytilova et al. 1999). In most cells, nuclei are usually circular or oval, centrally located and mobile inside the cytoplasm (Graumann and Evans 2013). Nuclear morphology is regulated by interactions between nucleoskeletal and cytoskeletal

components facilitated by SUN-KASH LINC complexes in metazoans as well as plants (Jevtic et al. 2014, Tamura et al. 2015). SUN, KASH, NPC components and proteins components of the lamina such as the metazoan lamins and lamin binding INM proteins and plant NMCP proteins have been shown to affect nuclear morphology features such as size, shape and positioning (Ciska and Moreno Diaz de la Espina 2014, Davidson and Lammerding 2014, Tamura et al. 2015). In this section changes in nuclear morphology characteristics of several AtNEAP mutant lines are discussed in various cell types including lower epidermal cotyledon pavement cells, epidermal root hair and cortex cells, leaf trichomes and guard cells.

5.4.3.1 Nuclear size

While the average maximum length of *neap1* mutant nuclei was significantly increased in cotyledon cells, *neap2* and *neap3* single mutant cotyledon nuclei showed an increase in overall nuclear size (figure 5.9c). Cotyledons of *neap4* showed an increase in average nuclear length and a simultaneous decrease in average nuclear width (figure 5.10a). Thus AtNEAP1, AtNEAP2, AtNEAP3 and AtNEAP4 appear to have a role in regulating nuclear size and maintaining nuclear compactness. Expression of AtNEAP1 and AtNEAP2 mRNA was low to medium in cotyledons on arrays available from Genevestigator and BAR Arabidopsis eFP browser (Chapter 3 figures 3.6, 3.7 and 3.8). This information was not available for AtNEAP3 and AtNEAP4. In the *bzip18* line, cotyledon nuclei showed no differences in nuclear size (figure 5.12b) suggesting that the effect of loss of AtbZIP18 function may have been compensated by other gene products. On the other hand AtbZIP18 is expressed at very low levels in cotyledons and may have no role in cotyledon nuclear size (Chapter 4 figure 4.27). As discussed in section 5.4.2, AtbZIP18 also had no effect on primary root growth suggesting it does not have a function in root epidermal cell and nuclear expansion (figure 5.12a).

The average maximum length achieved by *neap1* mutant nuclei was significantly increased in root hair whereas *neap2* and *neap3* mutant root hair nuclei showed no change in nuclear size (figure 5.8a). Also *neap1* root cortex nuclei showed an overall increase in size, whereas *neap2* nuclei were

significantly smaller and *neap3* nuclei had a significantly reduced average maximum length (figure 5.8c). It appears that AtNEAP1 is important for nuclear compactness in root hair and cortex whereas AtNEAP2 and AtNEAP3 have functions of nuclear expansion in the root cortex. The increased size of *neap1* mutant root hair and root cortex nuclei may explain why root growth was not affected in the *neap1* mutant (figure 5.6a). Although the *neap2* mutant line had smaller nuclei in root cortex, this reduction in nuclear size was insufficient to affect cell expansion and may explain no effect on the growth rate of the primary root growth (figure 5.7a). Root cortex nuclei in the *neap3* mutant showed significantly reduced length, which affect nuclear and cell expansion thus affecting root growth seen in figure 5.6b.

While *neap1* and *neap2* leaf trichome nuclei showed no changes in size, the average maximum length achieved by *neap3* mutant nuclei was significantly reduced (figure 5.9a) suggesting a role for AtNEAP3 in nuclear expansion. Cell and nuclear size in leaf trichome cells is sensitive to its endoreduplication state (Sugimoto-Shirasu et al. 2005). Endoreduplication defects manifest in the form of abnormal nuclear morphology as well as malformed trichome cells (Dittmer et al. 2007). That AtNEAP3 KO trichome nuclei show increased nuclear expansion may suggest a role for AtNEAP3 in endoreduplication.

In a preliminary examination of guard cells, the nuclei of *neap1/neap3* double mutant showed shortening of average nuclear length (figure 5.11a). Whereas *neap1* mutant nuclei have increased size in cotyledon, root hair and cortex cells, *neap3* mutant nuclei show reduced nuclear expansion in root cortex and trichomes (discussed above). This may suggest that the two genes are antagonistic in function with the effect of the AtNEAP3 mutation being dominant over AtNEAP1 in the double mutant.

The contradictory phenotypes of increased cotyledon nuclear size in *neap2* and *neap3* versus reduced nuclear size in *neap2* and *neap3* root cortex and *neap3* leaf trichrome suggest tissue-specific differential function of AtNEAP2 and AtNEAP3 in regulating nuclear size. The tissue specific functions may be explained by differential levels of expression of AtNEAP mRNA in different tissues (Chapter 3 figures 3.6, 3.7 and 3.8) and different protein-protein interactions in different tissues. In summary at least one NEAP protein has the

function of regulating nuclear size in one or more of the five different tissue types studied.

Several NE components including proteins associated with the SUN-KASH LINC complexes, components of the lamina and NPC have been shown to have an important function in regulating nuclear size (Jevtic et al. 2014). In plants, several NMCP proteins have been shown to be regulators of nuclear size (Dittmer et al. 2007, Sakamoto and Takagi 2013, Goto et al. 2014). The single *linc1* and *linc2* as well as the *linc1/linc2* double mutant show reduction in nuclear size in leaf epidermal and pavement cells, root epidermal, cortex and root hairs and anther filament cells (Dittmer et al. 2007). Nuclear area was also significantly reduced in *linc1*, *linc4* and the *linc1/linc4* double mutant compared to WT, and to *linc2*, *linc3* and the *linc2/linc3* double mutant (Sakamoto and Takagi 2013, Wang et al. 2013). NMCP1 and NMCP4 have been shown to interact with a novel INM protein, KAKU4 and several *kaku4* mutant plants also show smaller nuclei compared to WT (Goto et al. 2014). NMCP1 and KAKU4 overexpression independently led to nuclear membrane overgrowth and deformation (Goto et al. 2014). *A. thaliana* mid-SUN domain double mutant *sun4/sun5* as well as a KASH domain *tik* mutant showed smaller nuclei compared to WT (Graumann et al. 2014). While all the above mutants have shown a reduction in nuclear size, the NEAP family is peculiar in that AtNEAP1 disruption has led to increase in nuclear size in most tissues, whereas AtNEAP2 and AtNEAP3 disruption has led to a cotyledon-specific increase while decreasing nuclear size in trichome and root cortex cells.

5.4.3.2 Nuclear shape

Single mutant *neap1*, *neap2* and *neap3* cotyledon nuclei had no effect on their circularity (figure 5.9d). While the cotyledon nuclei of *neap4* mutant line were highly elongated those of the single mutant *bzip18* line were highly circular suggesting participation in antagonistic functions (figures 5.10b and 5.12b). The circularity of single mutant *neap1*, *neap2* and *neap3* nuclei also remained unaltered in root hair (figure 5.8b) and leaf trichome cells (figure 5.9b) suggesting that the NEAP family has no control over nuclear shape in root hair and leaf trichomes. In root cortex cells, *neap1* nuclei were highly elongated,

neap2 nuclei showed no change and *neap3* nuclei were significantly more circular relative to WT (figure 5.8d), suggesting antagonism between the functions of AtNEAP1 and AtNEAP3 similar to that seen in nuclear size (section 5.4.3.1). Guard cells in the *neap1/neap3* mutant line showed highly circular nuclei (figure 5.11b), suggesting that the effect of the mutation in AtNEAP3 gene on nuclear shape (seen in root cortex) was dominant in the double mutant consistent with a similar dominant effect of AtNEAP3 seen on nuclear size (section 5.4.3.1). The circularity of guard cell nuclei in the *neap1* and *neap3* single mutants remains to be studied.

In plants, the disruption of SUN domain and KASH domain proteins, such as AtSUN1/AtSUN2 and AtWIP1/AtWIP2 caused an increased roundedness of *A. thaliana* nuclei (Oda and Fukuda 2011, Zhou et al. 2012). The loss of mid-SUN protein AtSUN3 also led to significantly rounded nuclei (Graumann et al. 2014). The *linc1, linc2* and *linc1 linc2* mutants showed a homogenous increase in roundedness in leaf epidermal and pavement cells, root epidermal, cortex and root hairs and anther filament cells (Dittmer et al. 2007). All NMCP mutants, showed an increase in nuclear roundedness in leaf and root epidermal cells except *linc3*, which had significantly rounded nuclei in root epidermal cells but not leaf cells (Sakamoto and Takagi 2013). Several *kaku4* mutant plants also had more spherical nuclei compared to WT (Goto et al. 2014). Interestingly, AtNEAP proteins have been shown to interact with the classical as well as the mid-SUN domain proteins (Chapter 4 figures 4.18 and 4.24b). They have also been suggested to interact with NMCP1 (Chapter 4 section 4.4.2). The interaction of NEAP proteins with the two SUN families and the NMCP family and their similarity in functions of nuclear shape and morphology suggests that they may associate with the same LINC complexes at the NE. Also the functions of AtNEAP proteins in nuclear shape were consistent with that seen for several LINC complex and lamina associated components in animal systems.

Several metazoan NE associated proteins including components of the lamina, NPC's as well as SUN and KASH domain proteins have been shown to affect the circularity of nuclei (Jevtic et al. 2014). As seen in Hutchinson-Gilford progeria syndrome, the expression of permanently farnesylated mutant lamin A

in mouse keratinocytes and human fibroblasts led to nuclear morphological defects including increased roundedness that was reversed by treatment with inhibitors of farnesylation (Wang et al. 2010, Bifulco et al. 2013). Similarly expression of several lamin A mutations cause mis-shaped nuclei in human and mouse fibroblasts (Ibrahim et al. 2013). Interestingly, the mechanism of misshaped nuclei in lamin A mutant fibroblasts was shown to be mediated by the over-accumulation of SUN1 (Chen et al. 2012). Misshaped and elongated nuclei were caused in lamin B1 and B2 deficient neurons respectively (Coffinier et al. 2011). Defects in lamina-associated INM proteins LEM2 and LEM4 were also responsible for mis-shaped nuclei (Ulbert et al. 2006, Asencio et al. 2012). Thus the lamin-like protein structure of NEAP proteins and their interaction with the two SUN- domain families fits well with its functions in regulating nuclear morphology.

5.4.3.3 Nuclear positioning

The guard cell nuclear data collected for *neap1/neap3* was also used to study positioning of nuclei in guard cells. As described in section 5.3.3, WT nuclei of guard cells are positioned very close to the centre of the longitudinal plane of the stomatal aperture (figure 5.11c and d). Whereas *neap1/neap3* mutant nuclei fail to position close to the centre and lie significantly further from the centre of the longitudinal plane (figure 5.11c and d) indicating defective positioning in *neap1/neap3* guard cell nuclei. This suggests that AtNEAP1 and/or AtNEAP3 have an important function of positioning nuclei accurately in guard cells. Interestingly, AtNEAP1 mRNA has been shown to be upregulated in guard cells on two independent microarrays available on Genevestigator and the BAR Arabidopsis eFP browser respectively (Chapter 3 section 3.3.3, figures 3.6b and 3.7). Thus the up-regulation of AtNEAP1 may be important for guard cell specific function of nuclear positioning. Analysis of single mutant lines *neap1* and *neap3* may allow association of one or both genes with nuclear positioning in guard cells (Chapter 6 section 6.3.3). Guard cell nuclear positioning in other single mutant lines *neap2*, *neap4* and *bzip18* as well as any double, triple or quadruple mutant lines generated in the future remain to be analysed (Chapter 6 section 6.3.3).

A plant-specific KASH protein AtSINE1 largely expressed in guard cells has previously been shown to be important for positioning nuclei centrally in guard cells by associating with the actin cytoskeleton (Zhou et al. 2014). A *sun1-KO/sun2-KD* mutant also showed aberrant nuclear positioning in *A. thaliana* guard cells (Zhou et al. 2014). As AtNEAP proteins are known to interact with AtSUN1 and AtSUN2 (Chapter 4 section 4.4.3), their common functions in guard cell nuclear positioning may suggest association of AtNEAP1 and/or AtNEAP3 with the SUN1-SINE1 and SUN2-SINE1 containing LINC complexes. Nuclear positioning in mammalian systems has also been associated with mutations in SUN and/or KASH proteins in secretory epithelial, skeletal muscle and retinal cells (Lei et al. 2009, Roux et al. 2009, Yu et al. 2011). Several disease causing mutations of lamins also show defects in nuclear anchorage and movement in skeletal muscle and neuronal cells (Ji et al. 2007, Folker et al. 2011). Thus the role of AtNEAP proteins in nuclear positioning is also similar to functions of other LINC complex and lamina associated components in plant and animal systems.

5.5 Conclusions

Reverse genetics analysis of T-DNA lines has been used to aid the understanding of NEAP function *in planta*. Unlike any other single mutant line studied, the slowed rate of growth of the primary root in the *neap4* line suggested a function for AtNEAP4 in normal root growth. The reduction in growth rate of the primary root after loss of multiple genes of AtNEAP1, AtNEAP2 and AtNEAP3, for instance in the *neap1/neap3* mutant, not seen in single KO lines suggests redundancy of function within the AtNEAP family.

Analysis of T-DNA lines suggested that AtNEAP proteins are involved in regulating nuclear morphology characteristics of nuclear shape and circularity. The increase in nuclear size in certain tissues such as large nuclei in *neap1* root cortex, and *neap2* and *neap3* cotyledons and the reduction in size of *neap2* root cortex nuclei suggested not only differential functions of the different AtNEAP genes but also varying functions for individual genes in different tissue types. Differential gene function was also evident in highly elongated *neap1* root cortex nuclei as opposed to their highly circular counterparts in *neap3* root cortex. AtNEAP4 and AtbZIP18 were also suggested to have a role in regulating nuclear circularity as seen in the highly elongated *neap4* and highly circular *bzip18* mutant cotyledon nuclei.

AtNEAP proteins were also suggested to have a function in positioning nuclei in guard cells as evident in the *neap1/neap3* line. More lines are required to be analysed to understand the role of individual AtNEAP genes in nuclear positioning.

In summary, several AtNEAP genes were shown to have important functions in regulation of nuclear morphology characteristics such as size, shape and positioning. More lines containing mutations in multiple AtNEAP genes including double, triple and quadruple mutant lines are required to be generated and analysed using the assays developed in this chapter (Chapter 6 section 6.3.3).

Chapter 6
General Discussion and Future Work

Chapter 6
General Discussion and Future Work

The work described in this thesis provides novel insights about the protein structure, interactions and functions of the NEAP family. These proteins belong to a previously unknown plant-specific family annotated as IF-like and shown to be localised at the nuclear periphery (Chapter 3 section 3.3.4). Their phylogenetic distribution is restricted to the angiosperm clade (Chapter 3 section 3.3.2). Their expression *in planta,* although ubiquitous, is specifically upregulated in embryo, inflorescence and guard cells (Chapter 3 section 3.3.3). Detection of AtNEAP1, AtNEAP2 and AtNEAP3, predicted to have relative molecular masses of 41kDa, 38kDa and 39kDa, was at an apparent lower molecular mass of approximately 34kDa, 33kDa and 38kDa respectively (Chapter 3 section 3.3.6). The extensively CC nature of the NEAP proteins was potentially responsible for their insolubility under high ionic salt and Triton X-100 treatment in common with other IF-like proteins (Chapter 3 section 3.4.5, (Aebi et al. 1986, Foisner and Gerace 1993, Masuda et al. 1997, Ciska et al. 2013). The predicted NLS was found to be important for nuclear import and the TM domain was essential for membrane anchoring (Chapter 3 section 3.3.5). FRAP showed that the NEAP proteins were highly immobilised as part of stable protein complexes at the NE (Chapter 3 section 3.3.7). Further, NEAP proteins were shown to interact with each other as well as with the classical and mid-SUN domain proteins (Chapter 4 section 4.4.1 and 4.4.3). Presence of NEAP proteins also dislocated NMCP1 from the nuclear periphery to the nucleoplasm (Chapter 4 section 4.4.2). Finally, a bZIP TF was identified as a novel interactor of AtNEAP1 (Chapter 4 section 4.3.6) Insertion mutants of the NEAP family showed shortened

primary root growth in the *neap1/neap3* and *neap4* mutants (Chapter 5 section 5.4.2). T-DNA insertion lines also showed altered nuclear size as shown by an increase in *neap1* root cortex and *neap2* and *neap3* cotyledon nuclei and an increase in length of *neap1* root hair and *neap1* and *neap4* cotyledon nuclei (Chapter 5 section 5.4.3.1). NEAP mutants also showed altered nuclear circularity as shown by highly elongated nuclei of *neap1* root cortex and *neap4* cotyledon (Chapter 5 section 5.4.3.2). In other cases NEAP mutants had more circular nuclei as seen in *neap3* root cortex and *neap1/neap3* guard cells (Chapter 5 section 5.4.3.2). The *neap1/neap3* mutant line also showed aberrant positioning of nuclei in guard cells (Chapter 5 section 5.4.3.3). The significance of these changes in nuclear morphology has already been discussed in Chapter 5 (section 5.4.3). Thus the NEAP proteins are angiosperm-specific nuclear IF-like proteins stably anchored at the NE with potential functions in regulating nuclear morphology. In this chapter the role of NEAP proteins at the NE is discussed and their potential role as components of the plant lamina is explored.

6.1 NEAP proteins are novel INM intrinsic proteins

Although confocal microscopy showed that the AtNEAP proteins were localised at the nuclear periphery, its limited resolution restricted identification of INM or ONM specific localisation (Chapter 3 section 3.4.4). However multiple lines of evidence point towards INM rather than ONM localisation. The presence of an active NLS suggested requirement for import into the nucleus. Overexpressed AtNEAP proteins accumulate in the nucleoplasm rather than cytoplasm suggests localisation at the INM-nucleoplasmic interface (Chapter 4 figure 4.3). Nucleoplasmic localisation of the TM domain deletion mutant protein indicated a functional TM domain responsible for anchoring at the INM (Chapter 3 figure 3.11d). In

addition, interaction with AtbZIP18 TF which is likely to be localised to the nucleus also suggests intra-nuclear NEAP localisation (Chapter 4 section 4.3.6). Further evidence of the membrane topology of AtNEAP proteins was provided by the NEAP-SUN interaction using apFRET (Chapter 4 section 4.4.3). The interaction of AtNEAP-FP with AtSUN1/2-FP not only indicated close proximity of the C-terminal FP proteins but also their co-localisation in the periplasmic space of the NE where the C-terminus of AtSUN protein is known to be localised. Thus AtNEAP proteins are likely to be tail anchored at the INM via their C-terminal TM domain while their large CC domains remain in the nucleoplasm. Deletion of the SUN domain did not disrupt NEAP-SUN interaction, thus ruling out the possibility of AtNEAP proteins being KASH domain proteins (Chapter 4 figure 4.21).

In plants, a very small number of INM proteins have been characterised. These include calcium pumping ATPases, cation channel proteins such as the *Medicago trunculata* doesn't make infection 1 (DMI1) and its *Lotus japanicus* homologues, Castor and Pollux and the classical SUN domain proteins (Riely et al. 2007, Charpentier et al. 2008, Graumann et al. 2010, Graumann and Evans 2013, Fedorenko and Marchenko 2014). Mid SUN domain proteins which are enriched in the ER also localise to the NE, however their INM or ONM specificity remains unknown (Graumann et al. 2014). AtSUN3 has been hypothesized to localise to INM on the basis of its interaction with a transcription factor using MYTH (Vanrobays et al. unpublished). Interestingly NEAP proteins have been shown to interact with the classical as well as mid-SUN domain proteins in this study which may act as potential means of linkage to plant SUN-KASH LINC complexes. Thus identification of the NEAP protein family as novel INM components significantly adds to the limited knowledge of the plant INM proteome and furthers our understanding of the functions of the plant NE.

In contrast the opisthokont INM is enriched with more than 80 proteins (Schirmer et al. 2003, Korfali et al. 2012). These include the SUN domain proteins conserved in plants, the lamin B receptor (LBR) and the LAP2, Emerin, Man1 (LEM) domain containing proteins absent in plants (Chapter

1 section 1.2.2). LEM domain proteins contain the LEM domain which binds barrier to auto integration factor (BAF), a chromatin interacting protein (Brachner and Foisner 2011). The LEM-BAF interaction is highly conserved in metazoans but both these proteins are absent in plants (Margalit et al. 2007, Graumann and Evans 2013). LEM domain proteins also contain nucleoplasmic lamin binding domains, owing to which they are often described as components of the nuclear lamina (Barton et al. 2014). Except LAP2α and Ankyrin repeat and LEM domain containing 1 (ANKLE1), all other LEM domain proteins contain one or more TM domains that anchor them to the INM (Brachner and Foisner 2014). Some LEM domain proteins such as emerin, LAP2β/γ and LEMD1 are C-terminally anchored at the INM similar to the AtNEAP proteins (Berk et al. 2013, Brachner and Foisner 2014). The nucleoplasmic region of human emerin, a 245 aa long protein, contains an N-terminal (2-54 aa) LEM domain and a centrally positioned (115-171 aa) NLS (Wolff et al. 2001). Likewise the nucleoplasmic region of human LAP2β, a 454 aa long protein, contains the N-terminal (1-85 aa) chromatin binding LEM domain as well as the lamin binding (298-373 aa) domain important for INM targeting (Furukawa et al. 1998, Gant et al. 1999). LAP2γ, the shorter isoform is 344 aa long and also contains the N-terminal LEM domain and a section of the lamin binding domain (Furukawa et al. 1998). Human LEMD1 has 6 testis specific isoforms, ranging from 29 aa to 181 aa in length, two of which contain both the N-terminal LEM domain and the C-terminal TM domain (Yuki et al. 2004, Magrane and Consortium 2011). NEAP proteins are C-terminally anchored at the INM but do not contain the LEM or other recognisable domains (Chapter 3 section 3.4.1). Also, none of the LEM domain proteins contain the extensive CC regions seen in NEAP proteins (Magrane and Consortium 2011, Berk et al. 2013, Brachner and Foisner 2014). LEM domain proteins have the important function of tethering chromatin to the nuclear periphery and of gene regulation (Brachner and Foisner 2011). There are also possible functional similarities between the NEAP and LEM domain proteins. As discussed in

Chapter 4 section 4.4.4, AtNEAP1 has been shown to interact with a transcription factor AtbZIP18 which contains a bZIP motif known to bind DNA and regulate gene expression (Jakoby et al. 2002). In the absence of the LEM domain and BAF in plants, AtNEAP proteins could be potential functional alternatives to LEM domain proteins capable of tethering chromatin to the NE.

Apart from SUN domain proteins and components of NPC's, there is no sequence conservation for any of the opisthokont NE associated proteins including the ONM KASH proteins, the INM LEM domain proteins or the nuclear lamins in plants. Despite lack of sequence of sequence homology several proteins such as WIP, SINE and TIK have been shown to be functional KASH proteins in plants (Zhou et al. 2012, Graumann et al. 2014, Zhou et al. 2014). Likewise, the NMCP family has been suggested to be lamin-like analogues in plants (Ciska et al. 2013). Thus the identification of the novel family of NEAP proteins could add to one of the functions of the INM proteins missing in plants.

6.2 NEAP proteins are putative components of the plant lamina

As described in section 6.1, NEAP proteins are C-terminally anchored at the INM. This section discusses their IF-like characteristics which make them potential structural molecules. Firstly, AtNEAP1 is annotated as alpha helical intermediate filament (IF)-like in the Arabidopsis information resource (TAIR). One NEAP1 cDNA transcript was identified in an IF antibody screen (Colter and Saunders 1996). IF proteins organise into ~10nm filaments that form important structural components inside the nucleus, at the nuclear periphery and the cytoplasm (Gruenbaum and Aebi 2014, Snider and Omary 2014). IF proteins are also biochemically stable, nuclear IF proteins like metazoan lamins and IF-like plant NMCPs which are insoluble in high ionic salt and Triton X-100 buffers were only

solubilised with addition of urea to the buffers (Aebi et al. 1986, Foisner and Gerace 1993, Masuda et al. 1997, Ciska et al. 2013). The resistance of AtNEAP proteins to biochemical extraction and its reversal by treatment with urea suggests IF-like biochemical characteristics (Chapter 3 section 3.4.5).

Further AtNEAP protein structure has several similarities to other nuclear IF proteins like lamins and NMCP proteins. They have a central CC rod domain, followed by an NLS similar to lamins and NMCP proteins (Chapter 3 sections 3.4.1 and 3.4.4). AtNEAP proteins also have a hydrophobic C-terminus which allows membrane association (Chapter 3 section 3.4.4). Although both lamins and NMCP proteins are concentrated at the nuclear periphery, they do not contain a TM domain (Dechat et al. 2010, Burke and Stewart 2013, Ciska and Moreno Diaz de la Espina 2014). The lamin C-terminus however, is modified post-translationally by farnesylation, making it hydrophobic and has been shown to be important for its INM association (Holtz et al. 1989, Firmbach-Kraft and Stick 1993, Maske and Vaux 2004, Jung et al. 2013, Simon and Wilson 2013). The farnesylated C-terminus of A-type lamins is cleaved post incorporation into the lamina whereas B-type lamins remain permanently farnesylated (Adam and Goldman 2012). Association of NMCP proteins to the nuclear periphery has been shown to be regulated by two regions, a conserved sequence R/QYNLRR/H linked to the active NLS and its N-terminal region including the beginning of the CC domain (Kimura et al. 2010). Similar to NMCP1 the N-terminal region of AtNEAP3 containing the CC domain was also found to be essential for its NE association (Chapter 3 section 3.4.4).

Although NEAP proteins show structural and biochemical similarities to nuclear IF proteins, whether they form part of the nucleoskeletal network *in planta* is not known. Structural components of the lamina have been shown to be highly immobilised into stable networks represented by low rate of recoveries in FRAP assays. FRAP in Chapter 3 section 3.3.7 showed low mobilities of AtNEAP1 and AtNEAP2 (~ 20% mobile) similar to other lamina components such as ~ 20% mobile lamin A (Gilchrist et al.

2004) and ~ 25% mobile NMCP1 (Graumann 2014). However, the mobility of YFP-NEAP3 (~ 46% mobile) was comparable to that of INM proteins like SUN1 (~ 49% mobile), SUN2 (~ 54% mobile) and LBR-GFP (~ 40% mobile) *in vivo* (Ellenberg et al. 1997, Graumann et al. 2010). The low mobility of NEAP proteins suggested their involvement in stable interaction networks, which could be potential components of the plant nucleoskeleton or lamina. In Chapter 4 section 4.4.1, AtNEAP2 and AtNEAP3 were shown to interact with themselves and with each other and AtNEAP1 forming homomeric and heteromeric complexes. However despite NEAP-NEAP interactions and their IF-like properties whether NEAP proteins assemble into filamentous structures remains to be studied. As described in chapter 1 section 1.2.1, the assembly of lamin filaments involves formation of homodimers, which form polymeric strings that further associate laterally to form the protofilament (Burke and Stewart 2013). The homomers formed by NEAP proteins could associate with themselves and extend into polymeric filaments. Similar to NEAP proteins, A and B type lamins are capable of interacting with self and each other, however, *in vivo* they preferentially polymerise into separate homomeric networks that cross interact with each other (Goldberg et al. 2008). Interaction of AtNEAP proteins with each other suggests that the AtNEAP homomeric filaments may interact with each other, forming a complex overlapping network.

Expression of AtNEAP proteins affected the localisation of AtNMCP1 at the nuclear periphery and vice versa, AtNMCP1 caused dislocation of AtNEAP proteins from the nuclear periphery (Chapter 4, section 4.4.2). Whether this effect was caused by direct interaction of NEAP and NMCP proteins or indirectly due to competition for common interaction partners such as SUN1 and SUN2 is not known. The plant nucleoskeleton is formed of two types of filaments, 10-13nm wide parallel filaments cross-linked by 5-8 nm wide filaments (Li and Roux 1992, Blumenthal et al. 2004, Fiserova et al. 2009). The presence of two kinds of filaments may be explained by the presence of two varieties of lamina proteins, the

NEAP and NMCP protein families for instance, leading to different filament thickness. Similar to metazoan lamins and plant NMCP proteins, NEAP proteins have been shown to interact with members of the classical SUN domain family (Haque et al. 2006, Graumann 2014).

Several components of the metazoan lamina including the lamins and the LEM domain family tether chromatin to the nuclear periphery (Dechat et al. 2010). In plants chromatin binding nucleoskeletal proteins remain unknown. Although NMCP proteins associate with chromatin during cell division, whether they interact directly or via other chromatin binding proteins is unknown (Kimura et al. 2010, Sakamoto and Takagi 2013). As previously discussed, AtbZIP18, a transcription factor containing a DNA binding basic leucine zipper domain was identified in this study as a novel interactor of AtNEAP1 (Chapter 4 section 4.4.4). Thus if NEAP proteins were nuclear IF-like proteins forming putative components of the plant nucleoskeleton, AtbZIP18 could be the first chromatin binding nucleoskeletal tether to be described in plants.

6.3 Future work

6.3.1 Characterisation of AtNEAP4

All work in this thesis has focussed on AtNEAP1, AtNEAP2 and AtNEAP3, as AtNEAP4 was not cloned during the period of this thesis. A synthetic AtNEAP4 cDNA construct was ordered and is available for cloning using Gateway technology into several FP containing vectors of choice. Once cloning is successful, nuclear or peripheral localisation of AtNEAP4 can be confirmed. Use of FRAP will permit comparison of its mobility with the rest of the NEAP family. The AtNEAP4-FP construct will permit analysis of its interactions with itself, with members of the NEAP family and other nuclear proteins such as the SUN and NMCP proteins using apFRET and MYTH. Expression of AtNEAP4 in various tissues such as leaves, flowers and siliques can be explored using semi-quantitative RT-PCR.

6.3.2 NEAP interactions with other nuclear proteins

All positive NEAP-protein interactions observed using apFRET and MYTH are summarised in Chapter 4 table 4.1. Several NEAP-NEAP interactions were identified using apFRET but remain to be confirmed using MYTH. These include interactions between AtNEAP2-AtNEAP2, AtNEAP2-AtNEAP3 and AtNEAP3-AtNEAP3. In this study AtNEAP3 was co-localised with AtNEAP3ΔCC1, AtNEAP3ΔCC2 and AtNEAP3ΔNLS (Chapter 4 figure 4.7). Key domains involved in interaction between the deletion mutants and AtNEAP3 can be studied using apFRET and MYTH. AtNEAP3ΔTM and AtNEAP3 did not co-localise at the NE (Chapter 4 figure 4.7), in which case MYTH could be used to study if they interact *ex vivo*.

AtNEAP1, AtNEAP2 and AtNEAP3 were shown to interact with AtSUN1 and AtSUN2 *in planta* (Chapter 4 figure 4.18). AtNEAP2 was shown to interact with AtSUN1 and AtSUN2 as well as the mid-SUN domain family using MYTH (Chapter 4 figure 4.24b). Interactions of AtNEAP1 and

AtNEAP3 with the classical and mid-SUN domain proteins remain to be tested using this technique (Chapter 4 table 4.2). The NEAP and mid-SUN domain proteins remain to be co-localised *in planta* and if co-localisation is demonstrated, their interactions could be confirmed using apFRET.

In order to identify which NEAP protein domains are actively involved in interaction with the classical SUN domain proteins, the AtNEAP3 domain deletion mutants AtNEAP3ΔCC1, AtNEAP3ΔCC2, AtNEAP3ΔNLS and AtNEAP3ΔTM can be co-expressed with AtSUN1 and AtSUN2 and tested for interaction using apFRET and MYTH. AtSUN2 domain deletion mutants AtSUN2ΔCC and AtSUN2ΔSUN were co-localised with AtNEAP1, AtNEAP2 and AtNEAP3 and also shown to interact using apFRET (Chapter 4 figures 4.19, 4.20 and 4.21). These interactions remain to be confirmed using MYTH. AtSUN2ΔN also co-localised with AtNEAP1, AtNEAP2 and AtNEAP3 (Chapter 4 figure 4.22), their interactions could be explored using apFRET and MYTH. A construct containing the first 264 amino acids of the N-terminus of AtSUN2 did not co-localise at the NE with AtNEAP proteins (Chapter 4 figure 4.23). Although apFRET cannot be performed in the absence of co-localisation at the nuclear periphery, their interaction can be tested using MYTH. AtNEAP4 can also be included in the above analysis. However, the SUN2 domain deletion mutants did not provide conclusive results for the domain involved in NEAP-SUN interaction (Chapter 4 section 4.3.3). Further domain deletions of AtSUN2 protein need to be made and studied to investigate the linker domains between TM and CC domain, and between CC and SUN domain.

AtNEAP proteins did not co-localise with AtNMCP1 at the nuclear periphery (Chapter 4 figures 4.8 and 4.9), hence apFRET could not be carried out. An indication of their interaction *in planta* may be obtained by studying changes in their mobility using FRAP when co-expressed with each other. Interactions can also be tested using MYTH. Similarly AtbZIP18 was identified as an interactor of AtNEAP1 using MYTH (Chapter 4 section 4.4.4). AtNEAP1, AtNEAP2 and AtNEAP3 co-localised with AtbZIP18 in the nucleoplasm but not at the nuclear periphery and

hence, apFRET could not be carried out (Chapter 4 figure 4.25). FRAP and MYTH can allow testing these interactions.

6.3.3 Characterisation of T-DNA lines

All T-DNA insertion lines characterised during this study are summarised in Chapter 5 table 5.1, which shows that the NEAP2 line GABI_178C02 and the bZIP18 line SAIL_592_A12 were genotyped as heterozygous. Genotyping the progeny from the heterozygous parent should allow identification of one homozygous seedling in every 4 offspring. Table 5.1 also shows that mRNA knockdown in the NEAP2 T-DNA lines GABI_589B02 and GABI_178C02, the NEAP4 line SAIL_1239_G02 and the bZIP18 lines SAIL_592_A12 and WiscDsLoxHs073_05E remains to be confirmed using semi-quantitative RT-PCR. In order to tackle the inability to detect NEAP4 mRNA in whole seedlings, specific tissues such as leaves, flowers and siliques could be used to extract NEAP4 mRNA.

For this study, *neap1*, *neap2*, *neap3* and *neap4* lines were crossed in multiple combinations. A double homozygous *neap1/neap3* line was also genotyped and used for crosses with the single mutants. At the time of writing this section the following heterozygous mutant lines had been genotyped; *neap3/neap4*, *neap1/neap2/neap3* and *neap1/neap3/neap4*. Genotyping the progeny of these heterozygous mutants would allow identification of double homozygous lines *neap1/neap2*, *neap2/neap3*, *neap3/neap4*, *neap1/neap4* and triple homozygous lines *neap1/neap2/neap3* and *neap1/neap3/neap4*. The two triple homozygous lines can then be crossed to obtain the quadruple mutant. Crossing the *bzip18* lines with single, double, triple and quadruple NEAP mutant lines would allow identification of common functional pathways that the proteins are involved *in vivo*. Analysis of all available lines can then be performed using the phenotyping assays described in Chapter 5, such as primary root growth; nuclear size and circularity in leaf, trichome, guard cells, cotyledon, root hair and cortex; and nuclear positioning in guard cells.

The loss of function phenotypes of the NEAP mutant T-DNA lines can be rescued by introducing the absent NEAP-FP protein using a floral dipping stable transformation technique. Floral dipping using a nuclear label such as H2B-CFP would allow live cell imaging of stable *A. thaliana* mutant lines and studying changes in nuclear movement *in planta*.

6.3.4 Other experiments

Several new experiments can be proposed to further investigate the NEAP family of proteins. These include cloning of the NEAP genes under their respective native promoters along with a FP tag for detection and localisation using confocal as well as electron microscopy. Immunogold labelling could be done using commercially available YFP antibodies or novel NEAP specific antibodies. If NEAP specific antibodies were generated, these could be useful for detection of native NEAP proteins from *A. thaliana* extracts on Western Blots. Proteomic pull down of NEAP proteins and any associated DNA fragments could be carried out to identify NEAP interacting DNA sequences using a technique called Chromatin immunoprecipitation (ChIP). This could also be employed to study what AtbZIP18 interacts with and thus what gene regulation processes the NEAPs are involved in. Using the floral dipping technique, several *A. thaliana* lines stably expressing NEAP-FP proteins could be generated to study NEAP behaviour during cell division.

References

References

Aaronson, R. P., Blobel, G., 1975. Isolation of nuclear pore complexes in association with a lamina. Proc Natl Acad Sci U S A. 72, 1007-11.

Abe, M., Kobayashi, Y., Yamamoto, S., Daimon, Y., Yamaguchi, A., Ikeda, Y., Ichinoki, H., Notaguchi, M., Goto, K., Araki, T., 2005. FD, a bZIP protein mediating signals from the floral pathway integrator FT at the shoot apex. Science. 309, 1052-6.

Adam, S. A., Goldman, R. D., 2012. Insights into the differences between the A- and B-type nuclear lamins. Adv Biol Regul. 52, 108-13.

Aebi, U., Cohn, J., Buhle, L., Gerace, L., 1986. The nuclear lamina is a meshwork of intermediate-type filaments. Nature. 323, 560-4.

Allen, J. L., Douglas, M. G., 1989. Organization of the nuclear pore complex in *Saccharomyces cerevisiae*. J Ultrastruct Mol Struct Res. 102, 95-108.

Alonso, J. M., Stepanova, A. N., Leisse, T. J., Kim, C. J., Chen, H., Shinn, P., Stevenson, D. K., Zimmerman, J., Barajas, P., Cheuk, R., Gadrinab, C., Heller, C., Jeske, A., Koesema, E., Meyers, C. C., Parker, H., Prednis, L., Ansari, Y., Choy, N., Deen, H., Geralt, M., Hazari, N., Hom, E., Karnes, M., Mulholland, C., Ndubaku, R., Schmidt, I., Guzman, P., Aguilar-Henonin, L., Schmid, M., Weigel, D., Carter, D. E., Marchand, T., Risseeuw, E., Brogden, D., Zeko, A., Crosby, W. L., Berry, C. C., Ecker, J. R., 2003. Genome-wide insertional mutagenesis of *Arabidopsis thaliana*. Science. 301, 653-7.

Alonso, R., Onate-Sanchez, L., Weltmeier, F., Ehlert, A., Diaz, I., Dietrich, K., Vicente-Carbajosa, J., Droge-Laser, W., 2009. A pivotal role of the basic leucine zipper transcription factor bZIP53 in the regulation of *Arabidopsis* seed maturation gene expression based on heterodimerization and protein complex formation. Plant Cell. 21, 1747-61.

Amoutzias, G. D., Veron, A. S., Weiner, J., 3rd, Robinson-Rechavi, M., Bornberg-Bauer, E., Oliver, S. G., Robertson, D. L., 2007. One billion years of bZIP transcription factor evolution: conservation and change in dimerization and DNA-binding site specificity. Mol Biol Evol. 24, 827-35.

Apel, E. D., Lewis, R. M., Grady, R. M., Sanes, J. R., 2000. Syne-1, a dystrophin- and Klarsicht-related protein associated with synaptic nuclei at the neuromuscular junction. J Biol Chem. 275, 31986-95.

Arlucea, J., Andrade, R., Alonso, R., Arechaga, J., 1998. The nuclear basket of the nuclear pore complex is part of a higher-order filamentous network that is related to chromatin. J Struct Biol. 124, 51-8.

Asencio, C., Davidson, I. F., Santarella-Mellwig, R., Ly-Hartig, T. B., Mall, M., Wallenfang, M. R., Mattaj, I. W., Gorjanacz, M., 2012. Coordination of kinase and phosphatase activities by Lem4 enables nuclear envelope reassembly during mitosis. Cell. 150, 122-35.

Azuma, Y., Dasso, M., 2000. The role of Ran in nuclear function. Curr Opin Cell Biol. 12, 302-7.

Bao, X., Zhang, W., Krencik, R., Deng, H., Wang, Y., Girton, J., Johansen, J., Johansen, K. M., 2005. The JIL-1 kinase interacts with lamin Dm0 and regulates nuclear lamina morphology of *Drosophila* nurse cells. J Cell Sci. 118, 5079-87.

Barton, L. J., Wilmington, S. R., Martin, M. J., Skopec, H. M., Lovander, K. E., Pinto, B. S., Geyer, P. K., 2014. Unique and shared functions of nuclear lamina LEM domain proteins in *Drosophila*. Genetics. 197, 653-65.

Batsios, P., Peter, T., Baumann, O., Stick, R., Meyer, I., Graf, R., 2012. A lamin in lower eukaryotes? Nucleus. 3, 237-43.

Ben-Harush, K., Wiesel, N., Frenkiel-Krispin, D., Moeller, D., Soreq, E., Aebi, U., Herrmann, H., Gruenbaum, Y., Medalia, O., 2009. The supramolecular organization of the *C. elegans* nuclear lamin filament. J Mol Biol. 386, 1392-402.

Berk, J. M., Tifft, K. E., Wilson, K. L., 2013. The nuclear envelope LEM-domain protein emerin. Nucleus. 4, 298-314.

Bernard, P., Couturier, M., 1992. Cell killing by the F plasmid CcdB protein involves poisoning of DNA-topoisomerase II complexes. J Mol Biol. 226, 735-45.

Bifulco, M., D'Alessandro, A., Paladino, S., Malfitano, A. M., Notarnicola, M., Caruso, M. G., Laezza, C., 2013. N6-isopentenyladenosine improves nuclear shape in fibroblasts from humans with progeroid syndromes by inhibiting the farnesylation of prelamin A. FEBS J. 280, 6223-32.

Blumenthal, S. S., Clark, G. B., Roux, S. J., 2004. Biochemical and immunological characterization of pea nuclear intermediate filament proteins. Planta. 218, 965-75.

Brachner, A., Foisner, R., 2011. Evolvement of LEM proteins as chromatin tethers at the nuclear periphery. Biochem Soc Trans. 39, 1735-41.

Brachner, A., Foisner, R., 2014. Lamina-associated polypeptide (LAP)2alpha and other LEM proteins in cancer biology. Adv Exp Med Biol. 773, 143-63.

Bupp, J. M., Martin, A. E., Stensrud, E. S., Jaspersen, S. L., 2007. Telomere anchoring at the nuclear periphery requires the budding yeast Sad1-UNC-84 domain protein Mps3. J Cell Biol. 179, 845-54.

Burke, B., Stewart, C. L., 2013. The nuclear lamins: flexibility in function. Nat Rev Mol Cell Biol. 14, 13-24.

Calikowski, T. T., Meulia, T., Meier, I., 2003. A proteomic study of the *Arabidopsis* nuclear matrix. J Cell Biochem. 90, 361-78.

Callan, H. G., Tomlin, S. G., 1950. Experimental studies on amphibian oocyte nuclei. I. Investigation of the structure of the nuclear membrane by means of the electron microscope. Proc R Soc Lond B Biol Sci. 137, 367-78.

Cau, P., Navarro, C., Harhouri, K., Roll, P., Sigaudy, S., Kaspi, E., Perrin, S., De Sandre-Giovannoli, A., Levy, N., 2014. Nuclear matrix, nuclear envelope and premature aging syndromes in a translational research perspective. Semin Cell Dev Biol.

Chang, W., Worman, H. J., Gundersen, G. G. (2015). Accessorizing and anchoring the LINC complex for multifunctionality. J Cell Biol. 208 (1): 11-22. Charpentier, M., Bredemeier, R., Wanner, G., Takeda, N., Schleiff, E., Parniske, M., 2008. *Lotus japonicus* CASTOR and POLLUX are ion channels essential for perinuclear calcium spiking in legume root endosymbiosis. Plant Cell. 20, 3467-79.

Chen, C. Y., Chi, Y. H., Mutalif, R. A., Starost, M. F., Myers, T. G., Anderson, S. A., Stewart, C. L., Jeang, K. T., 2012. Accumulation of the inner nuclear envelope protein SUN1 is pathogenic in progeric and dystrophic laminopathies. Cell. 149, 565-77.

Cheung, A. Y., Reddy, A. S., 2012. Nuclear architecture and dynamics: territories, nuclear bodies, and nucleocytoplasmic trafficking. Plant Physiol. 158, 23-5.

Chook, Y. M., Blobel, G., 2001. Karyopherins and nuclear import. Curr Opin Struct Biol. 11, 703-15.

Chytilova, E., Macas, J., Galbraith, D. W., 1999. Green fluorescent protein targeted to the nucleus, a transgenic phenotype useful for studies in plant biology. Annals of Botany. 83, 645-654.

Chytilova, E., Macas, J., Sliwinska, E., Rafelski, S. M., Lambert, G. M., Galbraith, D. W., 2000. Nuclear dynamics in *Arabidopsis thaliana.* Mol Biol Cell. 11, 2733-41.

Ciska, M., Masuda, K., Moreno Diaz de la Espina, S., 2013. Lamin-like analogues in plants: the characterization of NMCP1 in *Allium cepa*. J Exp Bot. 64, 1553-64.

Ciska, M., Moreno Diaz de la Espina, S., 2014. The intriguing plant nuclear lamina. Front Plant Sci. 5, 166.

Coffinier, C., Jung, H. J., Nobumori, C., Chang, S., Tu, Y., Barnes, R. H., 2nd, Yoshinaga, Y., de Jong, P. J., Vergnes, L., Reue, K., Fong, L. G., Young, S. G., 2011. Deficiencies in lamin B1 and lamin B2 cause neurodevelopmental defects and distinct nuclear shape abnormalities in neurons. Mol Biol Cell. 22, 4683-93.

Cohen, M., Tzur, Y. B., Neufeld, E., Feinstein, N., Delannoy, M. R., Wilson, K. L., Gruenbaum, Y., 2002. Transmission electron microscope studies of the nuclear envelope in *Caenorhabditis elegans* embryos. J Struct Biol. 140, 232-40.

Colter, M. E., Saunders, M. J., *Arabidopsis thaliana* intermediate filament-related plant cDNA clones isolated by IFA screening of a flower expression library

EMBL/GenBank/DDBJ databases 1996.

Cremer, T., Cremer, M., Dietzel, S., Muller, S., Solovei, I., Fakan, S., 2006. Chromosome territories--a functional nuclear landscape. Curr Opin Cell Biol. 18, 307-16.

Crisp, M., Liu, Q., Roux, K., Rattner, J. B., Shanahan, C., Burke, B., Stahl, P. D., Hodzic, D., 2006. Coupling of the nucleus and cytoplasm: role of the LINC complex. J Cell Biol. 172, 41-53.

Cruz, J. R., de la Torre, C., Moreno Diaz de la Espina, S., 2008. Nuclear actin in plants. Cell Biol Int. 32, 584-7.

Cserzo, M., Wallin, E., Simon, I., von Heijne, G., Elofsson, A., 1997. Prediction of transmembrane alpha-helices in prokaryotic membrane proteins: the dense alignment surface method. Protein Eng. 10, 673-6.

Czechowski, T., Stitt, M., Altmann, T., Udvardi, M. K., Scheible, W. R., 2005. Genome-wide identification and testing of superior reference genes for transcript normalization in *Arabidopsis*. Plant Physiol. 139, 5-17.

Daigle, N., Beaudouin, J., Hartnell, L., Imreh, G., Hallberg, E., Lippincott-Schwartz, J., Ellenberg, J., 2001. Nuclear pore complexes form immobile networks and have a very low turnover in live mammalian cells. J Cell Biol. 154, 71-84.

Daneholt, B., 2001. Assembly and transport of a premessenger RNP particle. Proc Natl Acad Sci U S A. 98, 7012-7.

Davidson, P. M., Lammerding, J., 2014. Broken nuclei--lamins, nuclear mechanics, and disease. Trends Cell Biol. 24, 247-56.

De Ruijter, N. C., Ketelaar, T., Blumenthal, S. S., Emons, A. M., Schel, J. H., 2000. Spectrin-like proteins in plant nuclei. Cell Biol Int. 24, 427-38.

Dechat, T., Adam, S. A., Taimen, P., Shimi, T., Goldman, R. D., 2010. Nuclear Lamins. Cold Spring Harbor Perspectives in Biology. 2.

DeGrasse, J. A., DuBois, K. N., Devos, D., Siegel, T. N., Sali, A., Field, M. C., Rout, M. P., Chait, B. T., 2009. Evidence for a shared nuclear pore complex architecture that is conserved from the last common eukaryotic ancestor. Mol Cell Proteomics. 8, 2119-30.

Delorenzi, M., Speed, T., 2002. An HMM model for coiled-coil domains and a comparison with PSSM-based predictions. Bioinformatics. 18, 617-25.

Denning, D. P., Patel, S. S., Uversky, V., Fink, A. L., Rexach, M., 2003. Disorder in the nuclear pore complex: the FG repeat regions of nucleoporins are natively unfolded. Proc Natl Acad Sci U S A. 100, 2450-5.

Ding, D., Muthuswamy, S., Meier, I., 2012. Functional interaction between the *Arabidopsis* orthologs of spindle assembly checkpoint proteins MAD1 and MAD2 and the nucleoporin NUA. Plant Mol Biol. 79, 203-16.

Ding, X., Xu, R., Yu, J., Xu, T., Zhuang, Y., Han, M., 2007. SUN1 is required for telomere attachment to nuclear envelope and gametogenesis in mice. Dev Cell. 12, 863-72.

Dittmer, T. A., Stacey, N. J., Sugimoto-Shirasu, K., Richards, E. J., 2007. LITTLE NUCLEI genes affecting nuclear morphology in *Arabidopsis thaliana*. Plant Cell. 19, 2793-803.

DuBois, K. N., Alsford, S., Holden, J. M., Buisson, J., Swiderski, M., Bart, J. M., Ratushny, A. V., Wan, Y., Bastin, P., Barry, J. D., Navarro, M., Horn, D., Aitchison, J. D., Rout, M. P., Field, M. C., 2012. NUP-1 Is a large coiled-coil nucleoskeletal protein in trypanosomes with lamin-like functions. PLoS Biol. 10, e1001287.

E, Z. G., Zhang, Y. P., Zhou, J. H., Wang, L., 2014. Mini review roles of the bZIP gene family in rice. Genet Mol Res. 13, 3025-36.

Elhanany-Tamir, H., Yu, Y. V., Shnayder, M., Jain, A., Welte, M., Volk, T., 2012. Organelle positioning in muscles requires cooperation between two KASH proteins and microtubules. J Cell Biol. 198, 833-46.

Ellenberg, J., Siggia, E. D., Moreira, J. E., Smith, C. L., Presley, J. F., Worman, H. J., Lippincott-Schwartz, J., 1997. Nuclear membrane dynamics and reassembly in living cells: targeting of an inner nuclear membrane protein in interphase and mitosis. J Cell Biol. 138, 1193-206.

Evans, D. E., Pawar, V., Smith, S. J., Graumann, K., 2014. Protein interactions at the higher plant nuclear envelope: evidence for a linker of nucleoskeleton and cytoskeleton complex. Front Plant Sci. 5, 183.

Fahrenkrog, B., Koser, J., Aebi, U., 2004. The nuclear pore complex: a jack of all trades? Trends Biochem Sci. 29, 175-82.

Fawcett, D. W., 1966. On the occurrence of a fibrous lamina on the inner aspect of the nuclear envelope in certain cells of vertebrates. Am J Anat. 119, 129-45.

Fedorenko, O. A., Marchenko, S. M., 2014. Ion channels of the nuclear membrane of hippocampal neurons. Hippocampus. 24, 869-76.

Firmbach-Kraft, I., Stick, R., 1993. The role of CaaX-dependent modifications in membrane association of *Xenopus* nuclear lamin B3 during meiosis and the fate of B3 in transfected mitotic cells. J Cell Biol. 123, 1661-70.

Fiserova, J., Kiseleva, E., Goldberg, M. W., 2009. Nuclear envelope and nuclear pore complex structure and organization in tobacco BY-2 cells. Plant J. 59, 243-55.

Foisner, R., Gerace, L., 1993. Integral membrane proteins of the nuclear envelope interact with lamins and chromosomes, and binding is modulated by mitotic phosphorylation. Cell. 73, 1267-79.

Folker, E. S., Ostlund, C., Luxton, G. W., Worman, H. J., Gundersen, G. G., 2011. Lamin A variants that cause striated muscle disease are defective in anchoring transmembrane actin-associated nuclear lines for nuclear movement. Proc Natl Acad Sci U S A. 108, 131-6.

Foster, R., Izawa, T., Chua, N. H., 1994. Plant bZIP proteins gather at ACGT elements. FASEB J. 8, 192-200.

Franke, W. W., Scheer, U., Krohne, G., Jarasch, E. D., 1981. The nuclear envelope and the architecture of the nuclear periphery. J Cell Biol. 91, 39s-50s.

Fridkin, A., Mills, E., Margalit, A., Neufeld, E., Lee, K. K., Feinstein, N., Cohen, M., Wilson, K. L., Gruenbaum, Y., 2004. Matefin, a *Caenorhabditis elegans* germ line-specific SUN-domain nuclear membrane protein, is essential for early embryonic and germ cell development. Proc Natl Acad Sci U S A. 101, 6987-92.

Fridkin, A., Penkner, A., Jantsch, V., Gruenbaum, Y., 2009. SUN-domain and KASH-domain proteins during development, meiosis and disease. Cell Mol Life Sci. 66, 1518-33.

Fridolfsson, H. N., Ly, N., Meyerzon, M., Starr, D. A., 2010. UNC-83 coordinates kinesin-1 and dynein activities at the nuclear envelope during nuclear migration. Dev Biol. 338, 237-50.

Fridolfsson, H. N., Starr, D. A., 2010. Kinesin-1 and dynein at the nuclear envelope mediate the bidirectional migrations of nuclei. Journal of Cell Biology. 191, 115-28.

Friederichs, J. M., Gardner, J. M., Smoyer, C. J., Whetstine, C. R., Gogol, M., Slaughter, B. D., Jaspersen, S. L., 2012. Genetic analysis of Mps3 SUN domain mutants in *Saccharomyces cerevisiae* reveals an interaction with the SUN-like protein Slp1. G3 (Bethesda). 2, 1703-18.

Fukazawa, J., Sakai, T., Ishida, S., Yamaguchi, I., Kamiya, Y., Takahashi, Y., 2000. Repression of shoot growth, a bZIP transcriptional activator, regulates cell elongation by controlling the level of gibberellins. Plant Cell. 12, 901-15.

Furukawa, K., Fritze, C. E., Gerace, L., 1998. The major nuclear envelope targeting domain of LAP2 coincides with its lamin binding region but is distinct from its chromatin interaction domain. J Biol Chem. 273, 4213-9.

Gant, T. M., Harris, C. A., Wilson, K. L., 1999. Roles of LAP2 proteins in nuclear assembly and DNA replication: truncated LAP2beta proteins alter lamina assembly, envelope formation, nuclear size, and DNA replication efficiency in *Xenopus laevis* extracts. J Cell Biol. 144, 1083-96.

Gardner, J. M., Smoyer, C. J., Stensrud, E. S., Alexander, R., Gogol, M., Wiegraebe, W., Jaspersen, S. L., 2011. Targeting of the SUN protein Mps3 to the inner nuclear membrane by the histone variant H2A.Z. J Cell Biol. 193, 489-507.

Gattolin, S., Sorieul, M., Frigerio, L., 2011. Mapping of tonoplast intrinsic proteins in maturing and germinating Arabidopsis seeds reveals dual localization of embryonic TIPs to the tonoplast and plasma membrane. Mol Plant. 4, 180-9.

Gattolin, S., Sorieul, M., Hunter, P. R., Khonsari, R. H., Frigerio, L., 2009. *In vivo* imaging of the tonoplast intrinsic protein family in Arabidopsis roots. BMC Plant Biol. 9, 133.

Gerace, L., Burke, B., 1988. Functional organization of the nuclear envelope. Annu Rev Cell Biol. 4, 335-74.

Gilchrist, S., Gilbert, N., Perry, P., Ostlund, C., Worman, H. J., Bickmore, W. A., 2004. Altered protein dynamics of disease-associated lamin A mutants. BMC Cell Biol. 5, 46.

Gindullis, F., Peffer, N. J., Meier, I., 1999. MAF1, a novel plant protein interacting with matrix attachment region binding protein MFP1, is located at the nuclear envelope. Plant Cell. 11, 1755-68.

Glover, J. N., Harrison, S. C., 1995. Crystal structure of the heterodimeric bZIP transcription factor c-Fos-c-Jun bound to DNA. Nature. 373, 257-61.

Goldberg, M. W., Allen, T. D., 1996. The nuclear pore complex and lamina: three-dimensional structures and interactions determined by field emission in-lens scanning electron microscopy. J Mol Biol. 257, 848-65.

Goldberg, M. W., Fiserova, J., Huttenlauch, I., Stick, R., 2008a. A new model for nuclear lamina organization. Biochem Soc Trans. 36, 1339-43.

Goldberg, M. W., Huttenlauch, I., Hutchison, C. J., Stick, R., 2008b. Filaments made from A- and B-type lamins differ in structure and organization. J Cell Sci. 121, 215-25.

Gonzalez-Suarez, I., Redwood, A. B., Perkins, S. M., Vermolen, B., Lichtensztejin, D., Grotsky, D. A., Morgado-Palacin, L., Gapud, E. J., Sleckman, B. P., Sullivan, T., Sage, J., Stewart, C. L., Mai, S., Gonzalo, S., 2009. Novel roles for A-type lamins in telomere biology and the DNA damage response pathway. EMBO J. 28, 2414-27.

Gorlich, D., Kutay, U., 1999. Transport between the cell nucleus and the cytoplasm. Annu Rev Cell Dev Biol. 15, 607-60.

Goshima, G., Saitoh, S., Yanagida, M., 1999. Proper metaphase spindle length is determined by centromere proteins Mis12 and Mis6 required for faithful chromosome segregation. Genes Dev. 13, 1664-77.

Goto, C., Tamura, K., Fukao, Y., Shimada, T., Hara-Nishimura, I., 2014. The novel nuclear envelope protein KAKU4 modulates nuclear morphology in *Arabidopsis*. Plant Cell. 26, 2143-2155.

Graumann, K., 2014. Evidence for LINC1-SUN associations at the plant nuclear periphery. PLoS One. 9, e93406.

Graumann, K., Evans, D. E., 2010. Plant SUN domain proteins: components of putative plant LINC complexes? Plant Signal Behav. 5, 154-6.

Graumann, K., Evans, D. E., 2011. Nuclear envelope dynamics during plant cell division suggest common mechanisms between kingdoms. Biochem J. 435, 661-7.

Graumann, K., Evans, D. E., The nuclear envelope — structure and protein interactions. Annual Plant Reviews. John Wiley & Sons Ltd, 2013, pp. 19-55.

Graumann, K., Irons, S. L., Runions, J., Evans, D. E., 2007. Retention and mobility of the mammalian lamin B receptor in the plant nuclear envelope. Biol Cell. 99, 553-62.

Graumann, K., Runions, J., Evans, D. E., 2010. Characterization of SUN-domain proteins at the higher plant nuclear envelope. Plant J. 61, 134-44.

Graumann, K., Vanrobays, E., Tutois, S., Probst, A. V., Evans, D. E., Tatout, C., 2014. Characterization of two distinct subfamilies of SUN-domain proteins in *Arabidopsis* and their interactions with the novel KASH-domain protein AtTIK. J Exp Bot. 65, 6499-512.

Gruenbaum, Y., Aebi, U., 2014. Intermediate filaments: a dynamic network that controls cell mechanics. F1000Prime Rep. 6, 54.

Gruenbaum, Y., Margalit, A., Goldman, R. D., Shumaker, D. K., Wilson, K. L., 2005. The nuclear lamina comes of age. Nat Rev Mol Cell Biol. 6, 21-31.

Guttinger, S., Laurell, E., Kutay, U., 2009. Orchestrating nuclear envelope disassembly and reassembly during mitosis. Nat Rev Mol Cell Biol. 10, 178-91.

Haque, F., Lloyd, D. J., Smallwood, D. T., Dent, C. L., Shanahan, C. M., Fry, A. M., Trembath, R. C., Shackleton, S., 2006. SUN1 interacts with nuclear lamin A and cytoplasmic nesprins to provide a physical connection between the nuclear lamina and the cytoskeleton. Mol Cell Biol. 26, 3738-51.

Haque, F., Mazzeo, D., Patel, J. T., Smallwood, D. T., Ellis, J. A., Shanahan, C. M., Shackleton, S., 2010. Mammalian SUN protein interaction networks at the inner nuclear membrane and their role in laminopathy disease processes. J Biol Chem. 285, 3487-98.

Harel, A., Forbes, D. J., 2004. Importin beta: conducting a much larger cellular symphony. Mol Cell. 16, 319-30.

Hatch, E., Hetzer, M., 2014. Breaching the nuclear envelope in development and disease. J Cell Biol. 205, 133-41.

Heitlinger, E., Peter, M., Lustig, A., Villiger, W., Nigg, E. A., Aebi, U., 1992. The role of the head and tail domain in lamin structure and assembly: analysis of bacterially expressed chicken lamin A and truncated B2 lamins. J Struct Biol. 108, 74-89.

Hetzer, M. W., Walther, T. C., Mattaj, I. W., 2005. Pushing the envelope: structure, function, and dynamics of the nuclear periphery. Annu Rev Cell Dev Biol. 21, 347-80.

Hiraoka, Y., Dernburg, A. F., 2009. The SUN rises on meiotic chromosome dynamics. Dev Cell. 17, 598-605.

Hirota, T., Lipp, J. J., Toh, B. H., Peters, J. M., 2005. Histone H3 serine 10 phosphorylation by Aurora B causes HP1 dissociation from heterochromatin. Nature. 438, 1176-80.

Holden, J. M., Koreny, L., Obado, S., Ratushny, A. V., Chen, W. M., Chiang, J. H., Kelly, S., Chait, B. T., Aitchison, J. D., Rout, M. P., Field, M. C., 2014. Nuclear pore complex evolution: a trypanosome Mlp analogue functions in chromosomal segregation but lacks transcriptional barrier activity. Mol Biol Cell. 25, 1421-36.

Holtz, D., Tanaka, R. A., Hartwig, J., McKeon, F., 1989. The CaaX motif of lamin A functions in conjunction with the nuclear localization signal to target assembly to the nuclear envelope. Cell. 59, 969-77.

Hooper, C. M., Tanz, S. K., Castleden, I. R., Vacher, M. A., Small, I. D., Millar, A. H., 2014. SUBAcon: a consensus algorithm for unifying the subcellular localization data of the *Arabidopsis* proteome. Bioinformatics. 30, 3356-64.

Horn, H. F., Brownstein, Z., Lenz, D. R., Shivatzki, S., Dror, A. A., Dagan-Rosenfeld, O., Friedman, L. M., Roux, K. J., Kozlov, S., Jeang, K. T., Frydman, M., Burke, B., Stewart, C. L., Avraham, K. B., 2013. The LINC complex is essential for hearing. J Clin Invest. 123, 740-50.

Hou, H., Zhou, Z., Wang, Y., Wang, J., Kallgren, S. P., Kurchuk, T., Miller, E. A., Chang, F., Jia, S., 2012. Csi1 links centromeres to the nuclear envelope for centromere clustering. J Cell Biol. 199, 735-44.

Hruz, T., Laule, O., Szabo, G., Wessendorp, F., Bleuler, S., Oertle, L., Widmayer, P., Gruissem, W., Zimmermann, P., 2008. Genevestigator v3: a reference expression database for the meta-analysis of transcriptomes. Adv Bioinformatics. 2008, 420747.

Hsieh, W. P., Hsieh, H. L., Wu, S. H., 2012. *Arabidopsis* bZIP16 transcription factor integrates light and hormone signaling pathways to regulate early seedling development. Plant Cell. 24, 3997-4011.

Hurst, H. C., 1994. Transcription factors. 1: bZIP proteins. Protein Profile. 1, 123-68.

Hutten, S., Flotho, A., Melchior, F., Kehlenbach, R. H., 2008. The Nup358-RanGAP complex is required for efficient importin alpha/beta-dependent nuclear import. Mol Biol Cell. 19, 2300-10.

Ibrahim, M. X., Sayin, V. I., Akula, M. K., Liu, M., Fong, L. G., Young, S. G., Bergo, M. O., 2013. Targeting isoprenylcysteine methylation ameliorates disease in a mouse model of progeria. Science. 340, 1330-3.

Jakoby, M., Weisshaar, B., Droge-Laser, W., Vicente-Carbajosa, J., Tiedemann, J., Kroj, T., Parcy, F., 2002. bZIP transcription factors in *Arabidopsis*. Trends Plant Sci. 7, 106-11.

Jevtic, P., Edens, L. J., Vukovic, L. D., Levy, D. L., 2014. Sizing and shaping the nucleus: mechanisms and significance. Curr Opin Cell Biol. 28, 16-27.

Ji, J. Y., Lee, R. T., Vergnes, L., Fong, L. G., Stewart, C. L., Reue, K., Young, S. G., Zhang, Q., Shanahan, C. M., Lammerding, J., 2007. Cell nuclei spin in the absence of lamin b1. J Biol Chem. 282, 20015-26.

Jung, H. J., Nobumori, C., Goulbourne, C. N., Tu, Y., Lee, J. M., Tatar, A., Wu, D., Yoshinaga, Y., de Jong, P. J., Coffinier, C., Fong, L. G., Young, S. G., 2013. Farnesylation of lamin B1 is important for retention of nuclear chromatin during neuronal migration. Proc Natl Acad Sci U S A. 110, E1923-32.

Kandasamy, M. K., McKinney, E. C., Meagher, R. B., 2002. Plant profilin isovariants are distinctly regulated in vegetative and reproductive tissues. Cell Motil Cytoskeleton. 52, 22-32.

Kapinos, L. E., Schumacher, J., Mucke, N., Machaidze, G., Burkhard, P., Aebi, U., Strelkov, S. V., Herrmann, H., 2010. Characterization of the head-to-tail overlap complexes formed by human lamin A, B1 and B2 "half-minilamin" dimers. J Mol Biol. 396, 719-31.

Karpova, T., McNally, J. G., 2006. Detecting protein-protein interactions with CFP-YFP FRET by acceptor photobleaching. Curr Protoc Cytom. Chapter 12, Unit12 7.

Kaufmann, A., Heinemann, F., Radmacher, M., Stick, R., 2011. Amphibian oocyte nuclei expressing lamin A with the progeria mutation E145K exhibit an increased elastic modulus. Nucleus. 2, 310-9.

Kimura, Y., Fujino, K., Ogawa, K., Masuda, K., 2014. Localization of *Daucus carota* NMCP1 to the nuclear periphery: the role of the N-terminal region and an NLS-linked sequence motif, RYNLRR, in the tail domain. Front Plant Sci. 5, 62.

Kimura, Y., Kuroda, C., Masuda, K., 2010. Differential nuclear envelope assembly at the end of mitosis in suspension-cultured *Apium graveolens* cells. Chromosoma. 119, 195-204.

Kiseleva, E., Allen, T. D., Rutherford, S., Bucci, M., Wente, S. R., Goldberg, M. W., 2004. Yeast nuclear pore complexes have a cytoplasmic ring and internal filaments. J Struct Biol. 145, 272-88.

Kiseleva, E., Rutherford, S., Cotter, L. M., Allen, T. D., Goldberg, M. W., 2001. Steps of nuclear pore complex disassembly and reassembly during mitosis in early *Drosophila* embryos. J Cell Sci. 114, 3607-18.

Kleinboelting, N., Huep, G., Kloetgen, A., Viehoever, P., Weisshaar, B., 2012. GABI-Kat SimpleSearch: new features of the *Arabidopsis thaliana* T-DNA mutant database. Nucleic Acids Res. 40, D1211-5.

Korfali, N., Wilkie, G. S., Swanson, S. K., Srsen, V., de Las Heras, J., Batrakou, D. G., Malik, P., Zuleger, N., Kerr, A. R., Florens, L., Schirmer, E. C., 2012. The nuclear envelope proteome differs notably between tissues. Nucleus. 3, 552-64.

Kosugi, S., Hasebe, M., Tomita, M., Yanagawa, H., 2009. Systematic identification of cell cycle-dependent yeast nucleocytoplasmic shuttling proteins by prediction of composite motifs. Proc Natl Acad Sci U S A. 106, 10171-6.

Kracklauer, M. P., Banks, S. M., Xie, X., Wu, Y., Fischer, J. A., 2007. *Drosophila* klaroid encodes a SUN domain protein required for Klarsicht localization to the nuclear envelope and nuclear migration in the eye. Fly (Austin). 1, 75-85.

Kruger, A., Batsios, P., Baumann, O., Luckert, E., Schwarz, H., Stick, R., Meyer, I., Graf, R., 2012. Characterization of NE81, the first lamin-like nucleoskeleton protein in a unicellular organism. Mol Biol Cell. 23, 360-70.

Kuga, T., Nozaki, N., Matsushita, K., Nomura, F., Tomonaga, T., 2010. Phosphorylation statuses at different residues of lamin B2, B1, and A/C dynamically and independently change throughout the cell cycle. Exp Cell Res. 316, 2301-12.

Lamesch, P., Berardini, T. Z., Li, D., Swarbreck, D., Wilks, C., Sasidharan, R., Muller, R., Dreher, K., Alexander, D. L., Garcia-Hernandez, M., Karthikeyan, A. S., Lee, C. H., Nelson, W. D., Ploetz, L., Singh, S., Wensel, A., Huala, E., 2012. The *Arabidopsis* Information Resource (TAIR): improved gene annotation and new tools. Nucleic Acids Res. 40, D1202-10.

Lee, K. K., Starr, D., Cohen, M., Liu, J., Han, M., Wilson, K. L., Gruenbaum, Y., 2002. Lamin-dependent localization of UNC-84, a protein required for nuclear migration in Caenorhabditis elegans. Mol Biol Cell. 13, 892-901.

Lei, K., Zhang, X., Ding, X., Guo, X., Chen, M., Zhu, B., Xu, T., Zhuang, Y., Xu, R., Han, M., 2009. SUN1 and SUN2 play critical but partially redundant roles in anchoring nuclei in skeletal muscle cells in mice. Proc Natl Acad Sci U S A. 106, 10207-12.

Lenz-Bohme, B., Wismar, J., Fuchs, S., Reifegerste, R., Buchner, E., Betz, H., Schmitt, B., 1997. Insertional mutation of the *Drosophila* nuclear lamin Dm0 gene results in defective nuclear envelopes, clustering of nuclear pore complexes, and accumulation of annulate lamellae. J Cell Biol. 137, 1001-16.

Letunic, I., Doerks, T., Bork, P., 2012. SMART 7: recent updates to the protein domain annotation resource. Nucleic Acids Res. 40, D302-5.

Li, H., Roux, S. J., 1992. Casein kinase II protein kinase is bound to lamina-matrix and phosphorylates lamin-like protein in isolated pea nuclei. Proc Natl Acad Sci U S A. 89, 8434-8.

Liu, J., Chen, N., Chen, F., Cai, B., Dal Santo, S., Tornielli, G. B., Pezzotti, M., Cheng, Z. M., 2014. Genome-wide analysis and expression profile of the bZIP transcription factor gene family in grapevine (*Vitis vinifera*). BMC Genomics. 15, 281.

Liu, J., Rolef Ben-Shahar, T., Riemer, D., Treinin, M., Spann, P., Weber, K., Fire, A., Gruenbaum, Y., 2000. Essential roles for *Caenorhabditis elegans* lamin gene in nuclear organization, cell cycle progression, and spatial organization of nuclear pore complexes. Mol Biol Cell. 11, 3937-47.

Liu, Q., Pante, N., Misteli, T., Elsagga, M., Crisp, M., Hodzic, D., Burke, B., Roux, K. J., 2007. Functional association of Sun1 with nuclear pore complexes. J Cell Biol. 178, 785-98.

Llorca, C. M., Potschin, M., Zentgraf, U., 2014. bZIPs and WRKYs: two large transcription factor families executing two different functional strategies. Front Plant Sci. 5, 169.

Lombardi, M. L., Jaalouk, D. E., Shanahan, C. M., Burke, B., Roux, K. J., Lammerding, J., 2011. The interaction between nesprins and sun proteins at the nuclear envelope is critical for force transmission between the nucleus and cytoskeleton. J Biol Chem. 286, 26743-53.

Lu, T., Identification of a plant nuclear envelope associated protein and its characterisation. M.Phil. Oxford Brookes University, Oxford, 2011.

Lu, W., Schneider, M., Neumann, S., Jaeger, V. M., Taranum, S., Munck, M., Cartwright, S., Richardson, C., Carthew, J., Noh, K., Goldberg, M., Noegel, A. A., Karakesisoglou, I., 2012. Nesprin interchain associations control nuclear size. Cell Mol Life Sci. 69, 3493-509.

Lupas, A., Van Dyke, M., Stock, J., 1991. Predicting coiled coils from protein sequences. Science. 252, 1162-4.

Lussi, Y. C., Hugi, I., Laurell, E., Kutay, U., Fahrenkrog, B., 2011. The nucleoporin Nup88 is interacting with nuclear lamin A. Mol Biol Cell. 22, 1080-90.

Luxton, G. W., Gomes, E. R., Folker, E. S., Vintinner, E., Gundersen, G. G., 2010. Linear arrays of nuclear envelope proteins harness retrograde actin flow for nuclear movement. Science. 329, 956-9.

Luxton, G. W., Starr, D. A., 2014. KASHing up with the nucleus: novel functional roles of KASH proteins at the cytoplasmic surface of the nucleus. Curr Opin Cell Biol. 28, 69-75.

Lytle, J. R., Yario, T. A., Steitz, J. A., 2007. Target mRNAs are repressed as efficiently by microRNA-binding sites in the 5' UTR as in the 3' UTR. Proc Natl Acad Sci U S A. 104, 9667-72.

Macara, I. G., 2001. Transport into and out of the nucleus. Microbiol Mol Biol Rev. 65, 570-94, table of contents.

Maeshima, K., Yahata, K., Sasaki, Y., Nakatomi, R., Tachibana, T., Hashikawa, T., Imamoto, F., Imamoto, N., 2006. Cell-cycle-dependent dynamics of nuclear pores: pore-free islands and lamins. J Cell Sci. 119, 4442-51.

Magrane, M., Consortium, U., 2011. UniProt Knowledgebase: a hub of integrated protein data. Database (Oxford). 2011, bar009.

Malone, C. J., Fixsen, W. D., Horvitz, H. R., Han, M., 1999. UNC-84 localizes to the nuclear envelope and is required for nuclear migration and anchoring during *C. elegans* development. Development. 126, 3171-81.

Margalit, A., Brachner, A., Gotzmann, J., Foisner, R., Gruenbaum, Y., 2007a. Barrier-to-autointegration factor--a BAFfling little protein. Trends Cell Biol. 17, 202-8.

Margalit, A., Neufeld, E., Feinstein, N., Wilson, K. L., Podbilewicz, B., Gruenbaum, Y., 2007b. Barrier to autointegration factor blocks premature cell fusion and maintains adult muscle integrity in C. elegans. J Cell Biol. 178, 661-73.

Martin, K., Kopperud, K., Chakrabarty, R., Banerjee, R., Brooks, R., Goodin, M. M., 2009. Transient expression in *Nicotiana benthamiana* fluorescent marker lines provides enhanced definition of protein localization, movement and interactions in planta. Plant J. 59, 150-62.

Maske, C. P., Vaux, D. J., 2004. CAAX-dependent modifications of the lamin proteins in the organization of the nuclear periphery. Symp Soc Exp Biol. 317-28.

Masuda, K., Xu, Z. J., Takahashi, S., Ito, A., Ono, M., Nomura, K., Inoue, M., 1997. Peripheral framework of carrot cell nucleus contains a novel protein predicted to exhibit a long alpha-helical domain. Exp Cell Res. 232, 173-81.

McDonnell, A. V., Jiang, T., Keating, A. E., Berger, B., 2006. Paircoil2: improved prediction of coiled coils from sequence. Bioinformatics. 22, 356-8.

McGee, M. D., Rillo, R., Anderson, A. S., Starr, D. A., 2006. UNC-83 IS a KASH protein required for nuclear migration and is recruited to the outer nuclear membrane by a physical interaction with the SUN protein UNC-84. Mol Biol Cell. 17, 1790-801.

McNulty, A. K., Saunders, M. J., 1992. Purification and immunological detection of pea nuclear intermediate filaments: evidence for plant nuclear lamins. J Cell Sci. 103 (Pt 2), 407-14.

Meier, I., 2007. Composition of the plant nuclear envelope: theme and variations. J Exp Bot. 58, 27-34.

Meier, I., Phelan, T., Gruissem, W., Spiker, S., Schneider, D., 1996. MFP1, a novel plant filament-like protein with affinity for matrix attachment region DNA. Plant Cell. 8, 2105-15.

Mestyan, I., Kellermayer, M., Roger, W., Mezofi, B., 1988. Analysis of Triton X-100 insoluble proteins of human chorionic and amniotic tissues with special emphasis on intermediate filaments. Acta Biochim Biophys Hung. 23, 187-93.

Meyerzon, M., Fridolfsson, H. N., Ly, N., McNally, F. J., Starr, D. A., 2009a. UNC-83 is a nuclear-specific cargo adaptor for kinesin-1-mediated nuclear migration. Development. 136, 2725-33.

Meyerzon, M., Gao, Z., Liu, J., Wu, J. C., Malone, C. J., Starr, D. A., 2009b. Centrosome attachment to the *C. elegans* male pronucleus is dependent on the surface area of the nuclear envelope. Dev Biol. 327, 433-46.

Miller, M., Shuman, J. D., Sebastian, T., Dauter, Z., Johnson, P. F., 2003. Structural basis for DNA recognition by the basic region leucine zipper transcription factor CCAAT/enhancer-binding protein alpha. J Biol Chem. 278, 15178-84.

Minguez, A., Moreno Diaz de la Espina, S., 1993. Immunological characterization of lamins in the nuclear matrix of onion cells. J Cell Sci. 106 (Pt 1), 431-9.

Minn, I. L., Rolls, M. M., Hanna-Rose, W., Malone, C. J., 2009. SUN-1 and ZYG-12, mediators of centrosome-nucleus attachment, are a functional SUN/KASH pair in *Caenorhabditis elegans*. Molecular Biology of the Cell. 20, 4586-95.

Mohr, D., Frey, S., Fischer, T., Guttler, T., Gorlich, D., 2009. Characterisation of the passive permeability barrier of nuclear pore complexes. EMBO J. 28, 2541-53.

Morgan, J. T., Pfeiffer, E. R., Thirkill, T. L., Kumar, P., Peng, G., Fridolfsson, H. N., Douglas, G. C., Starr, D. A., Barakat, A. I., 2011. Nesprin-3 regulates endothelial cell morphology, perinuclear cytoskeletal architecture, and flow-induced polarization. Mol Biol Cell. 22, 4324-34.

Moriguchi, K., Suzuki, T., Ito, Y., Yamazaki, Y., Niwa, Y., Kurata, N., 2005. Functional isolation of novel nuclear proteins showing a variety of subnuclear localizations. Plant Cell. 17, 389-403.

Murphy, S. P., Gumber, H. K., Mao, Y., Bass, H. W., 2014. A dynamic meiotic SUN belt includes the zygotene-stage telomere bouquet and is disrupted in chromosome segregation mutants of maize (*Zea mays* L.). Front Plant Sci. 5, 314.

Murphy, S. P., Simmons, C. R., Bass, H. W., 2010. Structure and expression of the maize (*Zea mays* L.) SUN-domain protein gene family: evidence for the existence of two divergent classes of SUN proteins in plants. BMC Plant Biol. 10, 269.

Nagai, R., 1993. Regulation of intracellular movements in plant-cells by environmental stimuli. International Review of Cytology - a Survey of Cell Biology, Vol 145. 145, 251-310.

Nakano, H., Funasaka, T., Hashizume, C., Wong, R. W., 2010. Nucleoporin translocated promoter region (Tpr) associates with dynein complex, preventing chromosome lagging formation during mitosis. J Biol Chem. 285, 10841-9.

Newport, J. W., Forbes, D. J., 1987. The nucleus: structure, function, and dynamics. Annu Rev Biochem. 56, 535-65.

Nguyen Ba, A. N., Pogoutse, A., Provart, N., Moses, A. M., 2009. NLStradamus: a simple Hidden Markov Model for nuclear localization signal prediction. BMC Bioinformatics. 10, 202.

Niepel, M., Strambio-de-Castillia, C., Fasolo, J., Chait, B. T., Rout, M. P., 2005. The nuclear pore complex-associated protein, Mlp2p, binds to the yeast spindle pole body and promotes its efficient assembly. J Cell Biol. 170, 225-35.

Nigg, E. A., 1992. Assembly-disassembly of the nuclear lamina. Curr Opin Cell Biol. 4, 105-9.

Nijhawan, A., Jain, M., Tyagi, A. K., Khurana, J. P., 2008. Genomic survey and gene expression analysis of the basic leucine zipper transcription factor family in rice. Plant Physiol. 146, 333-50.

Nitta, R. T., Jameson, S. A., Kudlow, B. A., Conlan, L. A., Kennedy, B. K., 2006. Stabilization of the retinoblastoma protein by A-type nuclear lamins is required for INK4A-mediated cell cycle arrest. Mol Cell Biol. 26, 5360-72.

Oda, Y., Fukuda, H., 2011. Dynamics of Arabidopsis SUN proteins during mitosis and their involvement in nuclear shaping. Plant J. 66, 629-41.

Okada, Y., Suzuki, T., Sunden, Y., Orba, Y., Kose, S., Imamoto, N., Takahashi, H., Tanaka, S., Hall, W. W., Nagashima, K., Sawa, H., 2005. Dissociation of heterochromatin protein 1 from

lamin B receptor induced by human polyomavirus agnoprotein: role in nuclear egress of viral particles. EMBO Rep. 6, 452-7.

Olins, A. L., Rhodes, G., Welch, D. B., Zwerger, M., Olins, D. E., 2010. Lamin B receptor: multi-tasking at the nuclear envelope. Nucleus. 1, 53-70.

Pante, N., Kann, M., 2002. Nuclear pore complex is able to transport macromolecules with diameters of about 39 nm. Mol Biol Cell. 13, 425-34.

Parry, D. A., Fraser, R. D., Squire, J. M., 2008. Fifty years of coiled-coils and alpha-helical bundles: a close relationship between sequence and structure. J Struct Biol. 163, 258-69.

Pendle, A. F., Clark, G. P., Boon, R., Lewandowska, D., Lam, Y. W., Andersen, J., Mann, M., Lamond, A. I., Brown, J. W., Shaw, P. J., 2005. Proteomic analysis of the *Arabidopsis* nucleolus suggests novel nucleolar functions. Mol Biol Cell. 16, 260-9.

Perez-Munive, C., Moreno Diaz de la Espina, S., 2011. Nuclear spectrin-like proteins are structural actin-binding proteins in plants. Biol Cell. 103, 145-57.

Peric-Hupkes, D., van Steensel, B., 2010. Role of the nuclear lamina in genome organization and gene expression. Cold Spring Harb Symp Quant Biol. 75, 517-24.

Proost, S., Van Bel, M., Sterck, L., Billiau, K., Van Parys, T., Van de Peer, Y., Vandepoele, K., 2009. PLAZA: a comparative genomics resource to study gene and genome evolution in plants. Plant Cell. 21, 3718-31.

Quimby, B. B., Dasso, M., 2003. The small GTPase Ran: interpreting the signs. Curr Opin Cell Biol. 15, 338-44.

Rajgor, D., Shanahan, C. M., 2013. Nesprins: from the nuclear envelope and beyond. Expert Rev Mol Med. 15, e5.

Razafsky, D., Hodzic, D., 2009. Bringing KASH under the SUN: the many faces of nucleo-cytoskeletal connections. Journal of Cell Biology. 186, 461-72.

Reddy, K. L., Singh, H., 2008. Using molecular tethering to analyze the role of nuclear compartmentalization in the regulation of mammalian gene activity. Methods. 45, 242-51.

Riely, B. K., Lougnon, G., Ane, J. M., Cook, D. R., 2007. The symbiotic ion channel homolog DMI1 is localized in the nuclear membrane of *Medicago truncatula* roots. Plant J. 49, 208-16.

Ringli, C., Keller, B., 1998. Specific interaction of the tomato bZIP transcription factor VSF-1 with a non-palindromic DNA sequence that controls vascular gene expression. Plant Mol Biol. 37, 977-88.

Rose, A., Meier, I., 2001. A domain unique to plant RanGAP is responsible for its targeting to the plant nuclear rim. Proc Natl Acad Sci U S A. 98, 15377-82.

Rose, A., Patel, S., Meier, I., 2004. The plant nuclear envelope. Planta. 218, 327-36.

Roux, K. J., Crisp, M. L., Liu, Q., Kim, D., Kozlov, S., Stewart, C. L., Burke, B., 2009. Nesprin 4 is an outer nuclear membrane protein that can induce kinesin-mediated cell polarization. Proc Natl Acad Sci U S A. 106, 2194-9.

Ruzicka, D. R., Kandasamy, M. K., McKinney, E. C., Burgos-Rivera, B., Meagher, R. B., 2007. The ancient subclasses of *Arabidopsis* Actin Depolymerizing Factor genes exhibit novel and differential expression. Plant J. 52, 460-72.

Sakamoto, Y., Takagi, S., 2013. LITTLE NUCLEI 1 and 4 regulate nuclear morphology in *Arabidopsis thaliana*. Plant Cell Physiol. 54, 622-33.

Sambrook, M. G. a. J., Molecular Cloning: A Laboratory Manual (Fourth Edition). Cold Spring Harbor Laboratory Press, 2012.

Scheres, B., Benfey, P., Dolan, L., 2002. Root development. *Arabidopsis* Book. 1, e0101.

Schirmer, E. C., Florens, L., Guan, T., Yates, J. R., 3rd, Gerace, L., 2003. Nuclear membrane proteins with potential disease links found by subtractive proteomics. Science. 301, 1380-2.

Schmid, M., Davison, T. S., Henz, S. R., Pape, U. J., Demar, M., Vingron, M., Scholkopf, B., Weigel, D., Lohmann, J. U., 2005. A gene expression map of *Arabidopsis thaliana* development. Nat Genet. 37, 501-6.

Schneider, C. A., Rasband, W. S., Eliceiri, K. W., 2012. NIH Image to ImageJ: 25 years of image analysis. Nat Methods. 9, 671-5.

Schumacher, M. A., Goodman, R. H., Brennan, R. G., 2000. The structure of a CREB bZIP.somatostatin CRE complex reveals the basis for selective dimerization and divalent cation-enhanced DNA binding. J Biol Chem. 275, 35242-7.

Schwacke, R., Schneider, A., van der Graaff, E., Fischer, K., Catoni, E., Desimone, M., Frommer, W. B., Flugge, U. I., Kunze, R., 2003. ARAMEMNON, a novel database for *Arabidopsis* integral membrane proteins. Plant Physiol. 131, 16-26.

Shaikhali, J., Noren, L., de Dios Barajas-Lopez, J., Srivastava, V., Konig, J., Sauer, U. H., Wingsle, G., Dietz, K. J., Strand, A., 2012. Redox-mediated mechanisms regulate DNA binding activity of the G-group of basic region leucine zipper (bZIP) transcription factors in *Arabidopsis*. J Biol Chem. 287, 27510-25.

Shimamura, M., Brown, R. C., Lemmon, B. E., Akashi, T., Mizuno, K., Nishihara, N., Tomizawa, K., Yoshimoto, K., Deguchi, H., Hosoya, H., Horio, T., Mineyuki, Y., 2004. Gamma-tubulin in

basal land plants: characterization, localization, and implication in the evolution of acentriolar microtubule organizing centers. Plant Cell. 16, 45-59.

Shumaker, D. K., Solimando, L., Sengupta, K., Shimi, T., Adam, S. A., Grunwald, A., Strelkov, S. V., Aebi, U., Cardoso, M. C., Goldman, R. D., 2008. The highly conserved nuclear lamin Ig-fold binds to PCNA: its role in DNA replication. J Cell Biol. 181, 269-80.

Sievers, F., Higgins, D. G., 2014. Clustal omega. Curr Protoc Bioinformatics. 48, 3 13 1-3 13 16.

Simon, D. N., Wilson, K. L., 2013. Partners and post-translational modifications of nuclear lamins. Chromosoma. 122, 13-31.

Skalamera, D., Heath, M. C., 1998. Changes in the cytoskeleton accompanying infection-induced nuclear movements and the hypersensitive response in plant cells invaded by rust fungi. Plant J. 16, 191-200.

Smith, A. E., Slepchenko, B. M., Schaff, J. C., Loew, L. M., Macara, I. G., 2002. Systems analysis of Ran transport. Science. 295, 488-91.

Smykowski, A., Zimmermann, P., Zentgraf, U., 2010. G-Box binding factor1 reduces CATALASE2 expression and regulates the onset of leaf senescence in *Arabidopsis*. Plant Physiol. 153, 1321-31.

Smythe, C., Jenkins, H. E., Hutchison, C. J., 2000. Incorporation of the nuclear pore basket protein nup153 into nuclear pore structures is dependent upon lamina assembly: evidence from cell-free extracts of *Xenopus* eggs. EMBO J. 19, 3918-31.

Snider, J., Kittanakom, S., Curak, J., Stagljar, I., 2010a. Split-ubiquitin based membrane yeast two-hybrid (MYTH) system: a powerful tool for identifying protein-protein interactions. J Vis Exp.

Snider, J., Kittanakom, S., Damjanovic, D., Curak, J., Wong, V., Stagljar, I., 2010b. Detecting interactions with membrane proteins using a membrane two-hybrid assay in yeast. Nat Protoc. 5, 1281-93.

Snider, N. T., Omary, M. B., 2014. Post-translational modifications of intermediate filament proteins: mechanisms and functions. Nat Rev Mol Cell Biol. 15, 163-77.

Sohaskey, M. L., Jiang, Y., Zhao, J. J., Mohr, A., Roemer, F., Harland, R. M., 2010. Osteopotentia regulates osteoblast maturation, bone formation, and skeletal integrity in mice. J Cell Biol. 189, 511-25.

Solovei, I., Wang, A. S., Thanisch, K., Schmidt, C. S., Krebs, S., Zwerger, M., Cohen, T. V., Devys, D., Foisner, R., Peichl, L., Herrmann, H., Blum, H., Engelkamp, D., Stewart, C. L., Leonhardt, H., Joffe, B., 2013. LBR and lamin A/C sequentially tether peripheral heterochromatin and inversely regulate differentiation. Cell. 152, 584-98.

Sosa, B. A., Rothballer, A., Kutay, U., Schwartz, T. U., 2012. LINC complexes form by binding of three KASH peptides to domain interfaces of trimeric SUN proteins. Cell. 149, 1035-47.

Sparkes, I. A., Graumann, K., Martiniere, A., Schoberer, J., Wang, P., Osterrieder, A., 2011. Bleach it, switch it, bounce it, pull it: using lasers to reveal plant cell dynamics. J Exp Bot. 62, 1-7.

Sparkes, I. A., Runions, J., Kearns, A., Hawes, C., 2006. Rapid, transient expression of fluorescent fusion proteins in tobacco plants and generation of stably transformed plants. Nat Protoc. 1, 2019-25.

Staehelin, L. A., 1997. The plant ER: a dynamic organelle composed of a large number of discrete functional domains. Plant J. 11, 1151-65.

Starr, D. A., 2009. A nuclear-envelope bridge positions nuclei and moves chromosomes. J Cell Sci. 122, 577-86.

Starr, D. A., Fischer, J. A., 2005. KASH 'n Karry: the KASH domain family of cargo-specific cytoskeletal adaptor proteins. Bioessays. 27, 1136-46.

Starr, D. A., Fridolfsson, H. N., 2010. Interactions between nuclei and the cytoskeleton are mediated by SUN-KASH nuclear-envelope bridges. Annu Rev Cell Dev Biol. 26, 421-44.

Starr, D. A., Han, M., 2005. A genetic approach to study the role of nuclear envelope components in nuclear positioning. Novartis Found Symp. 264, 208-19; discussion 219-230.

Strelkov, S. V., Schumacher, J., Burkhard, P., Aebi, U., Herrmann, H., 2004. Crystal structure of the human lamin A coil 2B dimer: implications for the head-to-tail association of nuclear lamins. J Mol Biol. 343, 1067-80.

Stuurman, N., Heins, S., Aebi, U., 1998. Nuclear lamins: their structure, assembly, and interactions. J Struct Biol. 122, 42-66.

Sugimoto-Shirasu, K., Roberts, G. R., Stacey, N. J., McCann, M. C., Maxwell, A., Roberts, K., 2005. RHL1 is an essential component of the plant DNA topoisomerase VI complex and is required for ploidy-dependent cell growth. Proc Natl Acad Sci U S A. 102, 18736-41.

Sugimoto, K., Tasaka, H., Dotsu, M., 2001. Molecular behavior in living mitotic cells of human centromere heterochromatin protein HPLalpha ectopically expressed as a fusion to red fluorescent protein. Cell Struct Funct. 26, 705-18.

Sulston, J. E., Horvitz, H. R., 1981. Abnormal cell lineages in mutants of the nematode *Caenorhabditis elegans*. Dev Biol. 82, 41-55.

Tamura, K., Fukao, Y., Iwamoto, M., Haraguchi, T., Hara-Nishimura, I., 2010. Identification and characterization of nuclear pore complex components in *Arabidopsis thaliana*. Plant Cell. 22, 4084-97.

Tamura, K., Hara-Nishimura, I., 2011. Involvement of the nuclear pore complex in morphology of the plant nucleus. Nucleus. 2, 168-72.

Tamura, K., Hara-Nishimura, I., 2013. The molecular architecture of the plant nuclear pore complex. J Exp Bot. 64, 823-32.

Tamura, K., Hara-Nishimura, I., 2014. Functional insights of nucleocytoplasmic transport in plants. Front Plant Sci. 5, 118.

Tamura, K., Goto, C., Hara-Nishimura, I. (2015). Recent advances in understanding plant nuclear envelope proteins involved in nuclear morphology. J Exp Bot. 66 (6): 1641-7.

Tamura, K., Iwabuchi, K., Fukao, Y., Kondo, M., Okamoto, K., Ueda, H., Nishimura, M., Hara-Nishimura, I., 2013. Myosin XI-i links the nuclear membrane to the cytoskeleton to control nuclear movement and shape in *Arabidopsis*. Curr Biol. 23, 1776-81.

Tanz, S. K., Castleden, I., Hooper, C. M., Vacher, M., Small, I., Millar, H. A., 2013. SUBA3: a database for integrating experimentation and prediction to define the SUBcellular location of proteins in *Arabidopsis*. Nucleic Acids Res. 41, D1185-91.

Tapley, E. C., Ly, N., Starr, D. A., 2011. Multiple mechanisms actively target the SUN protein UNC-84 to the inner nuclear membrane. Mol Biol Cell. 22, 1739-52.

Taranum, S., Sur, I., Muller, R., Lu, W., Rashmi, R. N., Munck, M., Neumann, S., Karakesisoglou, I., Noegel, A. A., 2012. Cytoskeletal interactions at the nuclear envelope mediated by nesprins. Int J Cell Biol. 2012, 736524.

Technau, M., Roth, S., 2008. The *Drosophila* KASH domain proteins Msp-300 and Klarsicht and the SUN domain protein Klaroid have no essential function during oogenesis. Fly (Austin). 2, 82-91.

Toufighi, K., Brady, S. M., Austin, R., Ly, E., Provart, N. J., 2005. The Botany Array Resource: e-Northerns, Expression Angling, and promoter analyses. Plant J. 43, 153-63.

Tran, E. J., King, M. C., Corbett, A. H., 2014. Macromolecular transport between the nucleus and the cytoplasm: Advances in mechanism and emerging links to disease. Biochim Biophys Acta.

Ulbert, S., Antonin, W., Platani, M., Mattaj, I. W., 2006. The inner nuclear membrane protein Lem2 is critical for normal nuclear envelope morphology. FEBS Lett. 580, 6435-41.

Van Bel, M., Proost, S., Wischnitzki, E., Movahedi, S., Scheerlinck, C., Van de Peer, Y., Vandepoele, K., 2012. Dissecting plant genomes with the PLAZA comparative genomics platform. Plant Physiol. 158, 590-600.

Van Damme, D., Bouget, F. Y., Van Poucke, K., Inze, D., Geelen, D., 2004. Molecular dissection of plant cytokinesis and phragmoplast structure: a survey of GFP-tagged proteins. Plant J. 40, 386-98.

Varas, J., Graumann, K., Osman, K., Pradillo, M., Evans, D. E., Santos, J. L., Armstrong, S. J., 2015. Absence of SUN1 and SUN2 proteins in *Arabidopsis thaliana* leads to a delay in meiotic progression and defects in synapsis and recombination. Plant J. 81, 329-46.

Vinciguerra, P., Iglesias, N., Camblong, J., Zenklusen, D., Stutz, F., 2005. Perinuclear Mlp proteins downregulate gene expression in response to a defect in mRNA export. EMBO J. 24, 813-23.

Voeltz, G. K., Rolls, M. M., Rapoport, T. A., 2002. Structural organization of the endoplasmic reticulum. EMBO Rep. 3, 944-50.

Walther, T. C., Fornerod, M., Pickersgill, H., Goldberg, M., Allen, T. D., Mattaj, I. W., 2001. The nucleoporin Nup153 is required for nuclear pore basket formation, nuclear pore complex anchoring and import of a subset of nuclear proteins. EMBO J. 20, 5703-14.

Wang, F., Higgins, J. M., 2013. Histone modifications and mitosis: countermarks, landmarks, and bookmarks. Trends Cell Biol. 23, 175-84.

Wang, H., Dittmer, T. A., Richards, E. J., 2013. *Arabidopsis* CROWDED NUCLEI (CRWN) proteins are required for nuclear size control and heterochromatin organization. BMC Plant Biol. 13, 200.

Wang, J., Zhou, J., Zhang, B., Vanitha, J., Ramachandran, S., Jiang, S. Y., 2011. Genome-wide expansion and expression divergence of the basic leucine zipper transcription factors in higher plants with an emphasis on sorghum. J Integr Plant Biol. 53, 212-31.

Wang, Y., Ostlund, C., Worman, H. J., 2010. Blocking protein farnesylation improves nuclear shape abnormalities in keratinocytes of mice expressing the prelamin A variant in Hutchinson-Gilford progeria syndrome. Nucleus. 1, 432-9.

Wang, Y., Zhang, W. Z., Song, L. F., Zou, J. J., Su, Z., Wu, W. H., 2008. Transcriptome analyses show changes in gene expression to accompany pollen germination and tube growth in *Arabidopsis*. Plant Physiol. 148, 1201-11.

Wei, K., Chen, J., Wang, Y., Chen, Y., Chen, S., Lin, Y., Pan, S., Zhong, X., Xie, D., 2012. Genome-wide analysis of bZIP-encoding genes in maize. DNA Res. 19, 463-76.

Weis, K., 2003. Regulating access to the genome: nucleocytoplasmic transport throughout the cell cycle. Cell. 112, 441-51.

Wilhelmsen, K., Ketema, M., Truong, H., Sonnenberg, A., 2006. KASH-domain proteins in nuclear migration, anchorage and other processes. J Cell Sci. 119, 5021-9.

Wilhelmsen, K., Litjens, S. H., Kuikman, I., Tshimbalanga, N., Janssen, H., van den Bout, I., Raymond, K., Sonnenberg, A., 2005. Nesprin-3, a novel outer nuclear membrane protein, associates with the cytoskeletal linker protein plectin. J Cell Biol. 171, 799-810.

Wilkie, G. S., Dickson, K. S., Gray, N. K., 2003. Regulation of mRNA translation by 5'- and 3'-UTR-binding factors. Trends Biochem Sci. 28, 182-8.

Wilson, K. L., Foisner, R., 2010. Lamin-binding Proteins. Cold Spring Harb Perspect Biol. 2, a000554.

Winter, D., Vinegar, B., Nahal, H., Ammar, R., Wilson, G. V., Provart, N. J., 2007. An "Electronic Fluorescent Pictograph" browser for exploring and analyzing large-scale biological data sets. PLoS One. 2, e718.

Woglar, A., Jantsch, V., 2014. Chromosome movement in meiosis I prophase of *Caenorhabditis elegans*. Chromosoma. 123, 15-24.

Wolff, N., Gilquin, B., Courchay, K., Callebaut, I., Worman, H. J., Zinn-Justin, S., 2001. Structural analysis of emerin, an inner nuclear membrane protein mutated in X-linked Emery-Dreifuss muscular dystrophy. FEBS Lett. 501, 171-6.

Worman, H. J., Yuan, J., Blobel, G., Georgatos, S. D., 1988. A lamin B receptor in the nuclear envelope. Proc Natl Acad Sci U S A. 85, 8531-4.

Wozniak, R. W., Rout, M. P., Aitchison, J. D., 1998. Karyopherins and kissing cousins. Trends Cell Biol. 8, 184-8.

Xu, X. M., Meulia, T., Meier, I., 2007. Anchorage of plant RanGAP to the nuclear envelope involves novel nuclear-pore-associated proteins. Curr Biol. 17, 1157-63.

Yamada, K., Lim, J., Dale, J. M., Chen, H., Shinn, P., Palm, C. J., Southwick, A. M., Wu, H. C., Kim, C., Nguyen, M., Pham, P., Cheuk, R., Karlin-Newmann, G., Liu, S. X., Lam, B., Sakano, H., Wu, T., Yu, G., Miranda, M., Quach, H. L., Tripp, M., Chang, C. H., Lee, J. M., Toriumi, M., Chan, M. M., Tang, C. C., Onodera, C. S., Deng, J. M., Akiyama, K., Ansari, Y., Arakawa, T., Banh, J., Banno, F., Bowser, L., Brooks, S., Carninci, P., Chao, Q., Choy, N., Enju, A., Goldsmith, A. D., Gurjal, M., Hansen, N. F., Hayashizaki, Y., Johnson-Hopson, C., Hsuan, V. W., Iida, K., Karnes, M., Khan, S., Koesema, E., Ishida, J., Jiang, P. X., Jones, T., Kawai, J., Kamiya, A., Meyers, C., Nakajima, M., Narusaka, M., Seki, M., Sakurai, T., Satou, M., Tamse, R., Vaysberg, M., Wallender, E. K., Wong, C., Yamamura, Y., Yuan, S., Shinozaki, K., Davis, R.

W., Theologis, A., Ecker, J. R., 2003. Empirical analysis of transcriptional activity in the *Arabidopsis* genome. Science. 302, 842-6.

Yin, Y., Zhu, Q., Dai, S., Lamb, C., Beachy, R. N., 1997. RF2a, a bZIP transcriptional activator of the phloem-specific rice tungro bacilliform virus promoter, functions in vascular development. EMBO J. 16, 5247-59.

Yu, J., Lei, K., Zhou, M., Craft, C. M., Xu, G., Xu, T., Zhuang, Y., Xu, R., Han, M., 2011. KASH protein Syne-2/Nesprin-2 and SUN proteins SUN1/2 mediate nuclear migration during mammalian retinal development. Hum Mol Genet. 20, 1061-73.

Yuki, D., Lin, Y. M., Fujii, Y., Nakamura, Y., Furukawa, Y., 2004. Isolation of LEM domain-containing 1, a novel testis-specific gene expressed in colorectal cancers. Oncol Rep. 12, 275-80.

Zastrow, M. S., Flaherty, D. B., Benian, G. M., Wilson, K. L., 2006. Nuclear titin interacts with A- and B-type lamins *in vitro* and *in vivo*. J Cell Sci. 119, 239-49.

Zhang, J., Sarge, K. D., 2008. Mel-18 interacts with RanGAP1 and inhibits its sumoylation. Biochem Biophys Res Commun. 375, 252-5.

Zhang, Q., Ragnauth, C., Greener, M. J., Shanahan, C. M., Roberts, R. G., 2002. The nesprins are giant actin-binding proteins, orthologous to *Drosophila melanogaster* muscle protein MSP-300. Genomics. 80, 473-81.

Zhang, X., Lei, K., Yuan, X., Wu, X., Zhuang, Y., Xu, T., Xu, R., Han, M., 2009. SUN1/2 and Syne/Nesprin-1/2 complexes connect centrosome to the nucleus during neurogenesis and neuronal migration in mice. Neuron. 64, 173-87.

Zhang, X., Xu, R., Zhu, B., Yang, X., Ding, X., Duan, S., Xu, T., Zhuang, Y., Han, M., 2007. Syne-1 and Syne-2 play crucial roles in myonuclear anchorage and motor neuron innervation. Development. 134, 901-8.

Zhou, X., Graumann, K., Evans, D. E., Meier, I., 2012a. Novel plant SUN-KASH bridges are involved in RanGAP anchoring and nuclear shape determination. J Cell Biol. 196, 203-11.

Zhou, X., Graumann, K., Wirthmueller, L., Jones, J. D., Meier, I., 2014. Identification of unique SUN-interacting nuclear envelope proteins with diverse functions in plants. J Cell Biol. 205, 677-92.

Zhou, Z., Du, X., Cai, Z., Song, X., Zhang, H., Mizuno, T., Suzuki, E., Yee, M. R., Berezov, A., Murali, R., Wu, S. L., Karger, B. L., Greene, M. I., Wang, Q., 2012b. Structure of Sad1-UNC84 homology (SUN) domain defines features of molecular bridge in nuclear envelope. J Biol Chem. 287, 5317-26.

Appendix I

Publication

Evans, D., Pawar Menon, V., Smith, S. and Graumann, K. (2014) 'Protein interactions at the higher plant nuclear envelope: evidence for a linker of nucleoskeleton and cytoskeleton complex', Frontiers in Plant Science, 5 pp. 1-5. https://www.frontiersin.org/articles/10.3389/fpls.2014.00183/full. DOI 10.3389/fpls.2014.00183

Appendix II

Presentations

Oral presentations

Vidya Pawar, Katja Graumann and David Evans (2014). A novel family of Nuclear Envelope Associated Coiled-coil Proteins in *Arabidopsis thaliana.* Oral presentation. The Society for Experimental Biology Annual Main Meeting, Manchester, UK.

Vidya Pawar, Katja Graumann and David Evans (2013). A novel family of Nuclear Envelope Associated Proteins in *Arabidopsis thaliana.* Oral presentation. The Society for Experimental Biology Annual Main Meeting, Valencia, Spain

Vidya Pawar, Katja Graumann and David Evans (2013). A novel family of Nuclear Envelope Associated Proteins in *Arabidopsis thaliana.* Oral presentation. International Plant Nucleus Consortium Meeting, Oxford, UK

Vidya Pawar, Ting Lu, John Runions, Katja Graumann and David Evans (2012). Characterisation of a novel family of plant-specific Nuclear Envelope associated proteins in *A. thaliana*. Young Researcher Symposium Protein-protein Interaction Network, Leeds, UK

Poster presentations

Vidya Pawar, Katja Graumann and David Evans (2014). A novel family of Nuclear Envelope Associated Proteins in *Arabidopsis thaliana.* Oral presentation. School of Life Sciences Postgraduate Symposium, Oxford Brookes University, Oxford, UK

Vidya Pawar, Ting Lu, John Runions, Katja Graumann and David Evans (2012). Characterisation of novel Nuclear Envelope Associated Proteins in *A. thaliana*. The Society for Experimental Biology Annual Main Meeting, Salzburg, Austria.

Appendix III

Sequencing Alignments

Query: NEAP3delCC1, Primer_RN3dNLSa

```
Query  1    ATGCCAACTTCTGTTAGTCTAAGAGAGGATGATCCTTTTGTGAAGGAATTGGCTGATATC  60
            ||||||||||||||||||||||||||||||||||||||||||||||||||||||||||||
Sbjct  449  ATGCCAACTTCTGTTAGTCTAAGAGAGGATGATCCTTTTGTGAAGGAATTGGCTGATATC  390

Query  61   AAATCACAGCTAGCAGCAACACATGCAACTGCAGAGGCAAGTGCTTTGTCAGCTGAATCA  120
            ||||||||||||||||||||||||||||||||||||||||||||||||||||||||||||
Sbjct  389  AAATCACAGCTAGCAGCAACACATGCAACTGCAGAGGCAAGTGCTTTGTCAGCTGAATCA  330

Query  121  GCACATTCTCATTGTAGAGTGCTTTCGAAACAATTGCATGAGAGGACCGGTTCTTTGAAA  180
            ||||||||||||||||||||||||||||||||||||||||||||||||||||||||||||
Sbjct  329  GCACATTCTCATTGTAGAGTGCTTTCGAAACAATTGCATGAGAGGACCGGTTCTTTGAAA  270

Query  181  GAGCATGAGGACCAAGTAACTAGACTTGGTGAGCAGCTAGAGAATCTAAGAAAGGAGCTG  240
            ||||||||||||||||||||||||||||||||||||||||||||||||||||||||||||
Sbjct  269  GAGCATGAGGACCAAGTAACTAGACTTGGTGAGCAGCTAGAGAATCTAAGAAAGGAGCTG  210

Query  241  CGAGTTAGAGAATCTTCACAGAAGCAGCTAAGAGATGAGCTTTTGAAAGTTGAAGGTGAC  300
            ||||||||||||||||||||||||||||||||||||||||||||||||||||||||||||
Sbjct  209  CGAGTTAGAGAATCTTCACAGAAGCAGCTAAGAGATGAGCTTTTGAAAGTTGAAGGTGAC  150

Query  301  ATTATGCGGGCTGTATCAGTGGTCAAGACCAAGGAGAACTCTGAGGTGCGGAACATGCTA  360
            ||||||||||||||||||||||||||||||||||||||||||||||||||||||||||||
Sbjct  149  ATTATGCGGGCTGTATCAGTGGTCAAGACCAAGGAGAACTCTGAGGTGCGGAACATGCTA  90

Query  361  AATGAAGATACTCCAAAGAATTCTGAAAGAATCAACAAACTTTTGACGGCTAAAGATGAT  420
            ||||||||||||||||||||||||||||||||||||||||||||||||||||||||||||
Sbjct  89   AATGAAGATACTCCAAAGAATTCTGAAAGAATCAACAAACTTTTGACGGCTAAAGATGA-  31

Query  421  GAAATTGCAAG-ACTGAG-AGA  440
            ||||| ||||| |||||| |||
Sbjct  30   GAAAT-GCAAGGACTGAGGAGA  10
```

Query: NEAP3delCC1, Primer_FN3dCC2a

```
Query  355  ATGCTAAATGAAGATACTCCAAAGAATTCTGAAAGAATCAACAAACTTTTGACGGCTAAA  414
            ||||| ||||||||||||||||||||||||||||||||||||||||||||||||||||||
Sbjct  20   ATGCT-AATGAAGATACTCCAAAGAATTCTGAAAGAATCAACAAACTTTTGACGGCTAAA  78

Query  415  GATGATGAAATTGCAAGACTGAGAGATGAACTGAAGATTATATCGGCTCACTGGAGGTTT  474
            ||||||||||||||||||||||||||||||||||||||||||||||||||||||||||||
Sbjct  79   GATGATGAAATTGCAAGACTGAGAGATGAACTGAAGATTATATCGGCTCACTGGAGGTTT  138

Query  475  AAGACCAAGGAATTAGAAGATCAGGTGGAGAATCAAAGGAGAATTGATCAGGAGCTGAAG  534
            ||||||||||||||||||||||||||||||||||||||||||||||||||||||||||||
Sbjct  139  AAGACCAAGGAATTAGAAGATCAGGTGGAGAATCAAAGGAGAATTGATCAGGAGCTGAAG  198

Query  535  AAGAAGGTGCTGAAGTTAGAATTTTGCCTACGAGAAACACGCATCCAAACTCGAAAACTT  594
            ||||||||||||||||||||||||||||||||||||||||||||||||||||||||||||
Sbjct  199  AAGAAGGTGCTGAAGTTAGAATTTTGCCTACGAGAAACACGCATCCAAACTCGAAAACTT  258

Query  595  CAAAAGATGGGAGAGCGAAACGATGTGGCAATACAAGAACTCAAGGAGCAATTGGCTGCa  654
            ||||||||||||||||||||||||||||||||||||||||||||||||||||||||||||
Sbjct  259  CAAAAGATGGGAGAGCGAAACGATGTGGCAATACAAGAACTCAAGGAGCAATTGGCTGCA  318

Query  655  aaaaaaCAGCATGAAGCTGATCATTCTAGCAACCAAAACTTGTGGGACAAATCAGGTTTC  714
            ||||||||||||||||||||||||||||||||||||||||||||||||||||||||||||
Sbjct  319  AAAAAACAGCATGAAGCTGATCATTCTAGCAACCAAAACTTGTGGGACAAATCAGGTTTC  378

Query  715  AAGATTGTTGTCTCCATGTCAATGCTGATATTAGTTGCGTTTTCTAGGCGT  765
            |||||||||||||||||||||||||||||||||||||||||||||||||||
Sbjct  379  AAGATTGTTGTCTCCATGTCAATGCTGATATTAGTTGCGTTTTCTAGGCGT  429
```

Conclusions:
The reverse primer has sequenced cleanly from start to upto 419bp of query, and the forward primer has clean sequencing from 361bp of query onwards to the end of query. No mutations.

Query: NEAP3delCC2, Primer_RN3dNLSa

```
Query  1    ATGCCAACTTCTGTTAGTCTAAGAGAGGATGATCCTTTGTTGAAGGATTTGAGTGAGAAG  60
            ||||||||||||||||||||||||||||||||||||||||||||||||||||||||||||
Sbjct  506  ATGCCAACTTCTGTTAGTCTAAGAGAGGATGATCCTTTGTTGAAGGATTTGAGTGAGAAG  447

Query  61   AAGCAGAGTTTCAGGAGAAATGTGGTGTCTTTGGCCACTGAGTTGAAAGAAGCGAGGACT  120
            ||||||||||||||||||||||||||||||||||||||||||||||||||||||||||||
Sbjct  446  AAGCAGAGTTTCAGGAGAAATGTGGTGTCTTTGGCCACTGAGTTGAAAGAAGCGAGGACT  387

Query  121  CGTCTTGCGGAACAGGAGCGGTCGTGTTCAAAAGAAGCTATGTCCAGGCAGGAGGCAGAA  180
            ||||||||||||||||||||||||||||||||||||||||||||||||||||||||||||
Sbjct  386  CGTCTTGCGGAACAGGAGCGGTCGTGTTCAAAAGAAGCTATGTCCAGGCAGGAGGCAGAA  327

Query  181  ACAAGAGTTAAGAGAATGGAAGATGAAATGCATGAACTTGCCAAGGAACTAAACGAGAAA  240
            ||||||||||||||||||||||||||||||||||||||||||||||||||||||||||||
Sbjct  326  ACAAGAGTTAAGAGAATGGAAGATGAAATGCATGAACTTGCCAAGGAACTAAACGAGAAA  267

Query  241  GTTGAGCAGATTCGTGCTTCGGATGTTGCTACTGAGAAGTTTGTGAAGGAATTGGCTGAT  300
            ||||||||||||||||||||||||||||||||||||||||||||||||||||||||||||
Sbjct  266  GTTGAGCAGATTCGTGCTTCGGATGTTGCTACTGAGAAGTTTGTGAAGGAATTGGCTGAT  207

Query  301  ATCAAATCACAGCTAGCAGCAACACATGCAACTGCAGAGGCAAGTGCTTTGTCAGCTGAA  360
            ||||||||||||||||||||||||||||||||||||||||||||||||||||||||||||
Sbjct  206  ATCAAATCACAGCTAGCAGCAACACATGCAACTGCAGAGGCAAGTGCTTTGTCAGCTGAA  147

Query  361  TCAGCACATGTATCAGTGGTCAAGACCAAGGAGAACTCTGAGGTGCGGAACATGCTAAAT  420
            ||||||||||||||||||||||||||||||||||||||||||||||||||||||||||||
Sbjct  146  TCAGCACATGTATCAGTGGTCAAGACCAAGGAGAACTCTGAGGTGCGGAACATGCTAAAT  87

Query  421  GAAGATACTCCAAAGAATTCTGAAAGAATCAACAAACTTTTGACGGCTAAAGATGATGAA  480
            ||||||||||||||||||||||||||||||||||||||||||||||||||||||||||||
Sbjct  86   GAAGATACTCCAAAGAATTCTGAAAGAATCAACAAACTTTTGACGGCTAAAGATGATGAA  27

Query  481  ATTGCAAGACTGAGAGA  497
            || ||||||| ||||||
Sbjct  26   AT-GCAAGACGGAGAGA  11
```

Query: NEAP3delCC2, Primer_FN3dCC2a

```
Query  412  ATGCTAAATGAAGATACTCCAAAGAATTCTGAAAGAATCAACAAACTTTTGACGGCTAAA  471
            ||||| |||| ||||||||||||||||||||||||||||||||||||||||||||||||||
Sbjct  22   ATGCT-AATG-AGATACTCCAAAGAATTCTGAAAGAATCAACAAACTTTTGACGGCTAAA  79

Query  472  GATGATGAAATTGCAAGACTGAGAGATGAACTGAAGATTATATCGGCTCACTGGAGGTTT  531
            ||||||||||||||||||||||||||||||||||||||||||||||||||||||||||||
Sbjct  80   GATGATGAAATTGCAAGACTGAGAGATGAACTGAAGATTATATCGGCTCACTGGAGGTTT  139

Query  532  AAGACCAAGGAATTAGAAGATCAGGTGGAGAATCAAAGGAGAATTGATCAGGAGCTGAAG  591
            ||||||||||||||||||||||||||||||||||||||||||||||||||||||||||||
Sbjct  140  AAGACCAAGGAATTAGAAGATCAGGTGGAGAATCAAAGGAGAATTGATCAGGAGCTGAAG  199

Query  592  AAGAAGGTGCTGAAGTTAGAATTTTGCCTACGAGAAACACGCATCCAAACTCGAAAACTT  651
            ||||||||||||||||||||||||||||||||||||||||||||||||||||||||||||
Sbjct  200  AAGAAGGTGCTGAAGTTAGAATTTTGCCTACGAGAAACACGCATCCAAACTCGAAAACTT  259

Query  652  CAAAAGATGGGAGAGCGAAACGATGTGGCAATACAAGAACTCAAGGAGCAATTGGCTGCa  711
            ||||||||||||||||||||||||||||||||||||||||||||||||||||||||||||
Sbjct  260  CAAAAGATGGGAGAGCGAAACGATGTGGCAATACAAGAACTCAAGGAGCAATTGGCTGCA  319

Query  712  aaaaaaCAGCATGAAGCTGATCATTCTAGCAACCAAAACTTGTGGGACAAATCAGGTTTC  771
            ||||||||||||||||||||||||||||||||||||||||||||||||||||||||||||
Sbjct  320  AAAAAACAGCATGAAGCTGATCATTCTAGCAACCAAAACTTGTGGGACAAATCAGGTTTC  379

Query  772  AAGATTGTTGTCTCCATGTCAATGCTGATATTAGTTGCGTTTTCTAGGCGT  822
            ||||||||||||||||||||||||||||||||||||||||||||||||||
Sbjct  380  AAGATTGTTGTCTCCATGTCAATGCTGATATTAGTTGCGTTTTCTAGGCGT  430
```

Conclusions: No mutations in NEAP3delCC2. Reverse primer shows clean read from start to 481 bp, and forward primer shows overlapping clean read from 423 bp to end of query.

Query: NEAP3delNLS, Primer_RN3dNLSa

```
Query  1    ATGCCAACTTCTGTTAGTCTAAGAGAGGATGATCCTTTGTTGAAGGATTTGAGTGAGAAG  60
           ||||||||||||||||||||||||||||||||||||||||||||||||||||||||||||||
Sbjct  691  ATGCCAACTTCTGTTAGTCTAAGAGAGGATGATCCTTTGTTGAAGGATTTGAGTGAGAAG  632

Query  61   AAGCAGAGTTTCAGGAGAAATGTGGTGTCTTTGGCCACTGAGTTGAAAGAAGCGAGGACT  120
           ||||||||||||||||||||||||||||||||||||||||||||||||||||||||||||||
Sbjct  631  AAGCAGAGTTTCAGGAGAAATGTGGTGTCTTTGGCCACTGAGTTGAAAGAAGCGAGGACT  572

Query  121  CGTCTTGCGGAACAGGAGCGGTCGTGTTCAAAAGAAGCTATGTCCAGGCAGGAGGCAGAA  180
           ||||||||||||||||||||||||||||||||||||||||||||||||||||||||||||||
Sbjct  571  CGTCTTGCGGAACAGGAGCGGTCGTGTTCAAAAGAAGCTATGTCCAGGCAGGAGGCAGAA  512

Query  181  ACAAGAGTTAAGAGAATGGAAGATGAAATGCATGAACTTGCCAAGGAACTAAACGAGAAA  240
           ||||||||||||||||||||||||||||||||||||||||||||||||||||||||||||||
Sbjct  511  ACAAGAGTTAAGAGAATGGAAGATGAAATGCATGAACTTGCCAAGGAACTAAACGAGAAA  452

Query  241  GTTGAGCAGATTCGTGCTTCGGATGTTGCTACTGAGAAGTTTGTGAAGGAATTGGCTGAT  300
           ||||||||||||||||||||||||||||||||||||||||||||||||||||||||||||||
Sbjct  451  GTTGAGCAGATTCGTGCTTCGGATGTTGCTACTGAGAAGTTTGTGAAGGAATTGGCTGAT  392

Query  301  ATCAAATCACAGCTAGCAGCAACACATGCAACTGCAGAGGCAAGTGCTTTGTCAGCTGAA  360
           ||||||||||||||||||||||||||||||||||||||||||||||||||||||||||||||
Sbjct  391  ATCAAATCACAGCTAGCAGCAACACATGCAACTGCAGAGGCAAGTGCTTTGTCAGCTGAA  332

Query  361  TCAGCACATTCTCATTGTAGAGTGCTTTCGAAACAATTGCATGAGAGGACCGGTTCTTTG  420
           ||||||||||||||||||||||||||||||||||||||||||||||||||||||||||||||
Sbjct  331  TCAGCACATTCTCATTGTAGAGTGCTTTCGAAACAATTGCATGAGAGGACCGGTTCTTTG  272

Query  421  AAAGAGCATGAGGACCAAGTAACTAGACTTGGTGAGCAGCTAGAGAATCTAAGAAAGGAG  480
           ||||||||||||||||||||||||||||||||||||||||||||||||||||||||||||||
Sbjct  271  AAAGAGCATGAGGACCAAGTAACTAGACTTGGTGAGCAGCTAGAGAATCTAAGAAAGGAG  212

Query  481  CTGCGAGTTAGAGAATCTTCACAGAAGCAGCTAAGAGATGAGCTTTTGAAAGTTGAAGGT  540
           ||||||||||||||||||||||||||||||||||||||||||||||||||||||||||||||
Sbjct  211  CTGCGAGTTAGAGAATCTTCACAGAAGCAGCTAAGAGATGAGCTTTTGAAAGTTGAAGGT  152

Query  541  GACATTATGCGGGCTGTATCAGTGGTCAAGACCAAGGAGAACTCTGAGGTGCGGAACATG  600
           ||||||||||||||||||||||||||||||||||||||||||||||||||||||||||||||
Sbjct  151  GACATTATGCGGGCTGTATCAGTGGTCAAGACCAAGGAGAACTCTGAGGTGCGGAACATG  92

Query  601  CTAAATGAAGATACTCCAAAGAATTCTGAAAGAATCAACAAACTTTTGACGGCTAAAGAT  660
           ||||||||||||||||||||||||||||||||||||||||||||||||||||||||||||||
Sbjct  91   CTAAATGAAGATACTCCAAAGAATTCTGAAAGAATCAACAAACTTTTGACGGCTAAAGAT  32

Query  661  GATGAAATTGCAAGACTGAGAGA  683
           || ||||| |||||||| |||||
Sbjct  31   GA-GAAAT-GCAAGACT-AGAGA  12
```

Query: NEAP3delNLS, Primer_FN3dCC2a

```
Query  611  ATACTCCAAAGAATTCTGAAAGAATCAACAAACTTTTGACGGCTAAAGATGATGAAATTG  670
           ||||||| ||||||||||||||||||||||||||||||||||||||||||||||||||||||
Sbjct  31   ATACTCCNAAGAATTCTGAAAGAATCAACAAACTTTTGACGGCTAAAGATGATGAAATTG  90

Query  671  CAAGACTGAGAGATGAACTGAAGATTATATCGGCTCACTGGAGGTTTAACGATGTGGCAA  730
           ||||||||||||||||||||||||||||||||||||||||||||||||||||||||||||||
Sbjct  91   CAAGACTGAGAGATGAACTGAAGATTATATCGGCTCACTGGAGGTTTAACGATGTGGCAA  150

Query  731  TACAAGAACTCAAGGAGCAATTGGCTGCaaaaaaaCAGCATGAAGCTGATCATTCTAGCA  790
           ||||||||||||||||||||||||||||||||||||||||||||||||||||||||||||||
Sbjct  151  TACAAGAACTCAAGGAGCAATTGGCTGCAAAAAAACAGCATGAAGCTGATCATTCTAGCA  210

Query  791  ACCAAAACTTGTGGGACAAATCAGGTTTCAAGATTGTTGTCTCCATGTCAATGCTGATAT  850
           ||||||||||||||||||||||||||||||||||||||||||||||||||||||||||||||
Sbjct  211  ACCAAAACTTGTGGGACAAATCAGGTTTCAAGATTGTTGTCTCCATGTCAATGCTGATAT  270

Query  851  TAGTTGCGTTTTCTAGGCGT  870
           ||||||||||||||||||||
Sbjct  271  TAGTTGCGTTTTCTAGGCGT  290
```

Conclusions: Reverse primer reads cleanly from start to 660bp on query, forward primer starts clean read at 620bp onwards till the end of NEAP3delNLS. No mutations.

Query: NEAP3delTM, Primer_RN3dNLSa

```
Query  4    CCAACTTCTGTTAGTCTAAGAGAGGATGATCCTTTGTTGAAGGATTTGAGTGAGAAGAAG  63
            ||||||||||||||||||||||||||||||||||||||||||||||||||||||||||||||
Sbjct  690  CCAACTTCTGTTAGTCTAAGAGAGGATGATCCTTTGTTGAAGGATTTGAGTGAGAAGAAG  631

Query  64   CAGAGTTTCAGGAGAAATGTGGTGTCTTTGGCCACTGAGTTGAAAGAAGCGAGGACTCGT  123
            ||||||||||||||||||||||||||||||||||||||||||||||||||||||||||||||
Sbjct  630  CAGAGTTTCAGGAGAAATGTGGTGTCTTTGGCCACTGAGTTGAAAGAAGCGAGGACTCGT  571

Query  124  CTTGCGGAACAGGAGCGGTCGTGTTCAAAAGAAGCTATGTCCAGGCAGGAGGCAGAAACA  183
            ||||||||||||||||||||||||||||||||||||||||||||||||||||||||||||||
Sbjct  570  CTTGCGGAACAGGAGCGGTCGTGTTCAAAAGAAGCTATGTCCAGGCAGGAGGCAGAAACA  511

Query  184  AGAGTTAAGAGAATGGAAGATGAAATGCATGAACTTGCCAAGGAACTAAACGAGAAAGTT  243
            ||||||||||||||||||||||||||||||||||||||||||||||||||||||||||||||
Sbjct  510  AGAGTTAAGAGAATGGAAGATGAAATGCATGAACTTGCCAAGGAACTAAACGAGAAAGTT  451

Query  244  GAGCAGATTCGTGCTTCGGATGTTGCTACTGAGAAGTTTGTGAAGGAATTGGCTGATATC  303
            ||||||||||||||||||||||||||||||||||||||||||||||||||||||||||||||
Sbjct  450  GAGCAGATTCGTGCTTCGGATGTTGCTACTGAGAAGTTTGTGAAGGAATTGGCTGATATC  391

Query  304  AAATCACAGCTAGCAGCAACACATGCAACTGCAGAGGCAAGTGCTTTGTCAGCTGAATCA  363
            ||||||||||||||||||||||||||||||||||||||||||||||||||||||||||||||
Sbjct  390  AAATCACAGCTAGCAGCAACACATGCAACTGCAGAGGCAAGTGCTTTGTCAGCTGAATCA  331

Query  364  GCACATTCTCATTGTAGAGTGCTTTCGAAACAATTGCATGAGAGGACCGGTTCTTTGAAA  423
            ||||||||||||||||||||||||||||||||||||||||||||||||||||||||||||||
Sbjct  330  GCACATTCTCATTGTAGAGTGCTTTCGAAACAATTGCATGAGAGGACCGGTTCTTTGAAA  271

Query  424  GAGCATGAGGACCAAGTAACTAGACTTGGTGAGCAGCTAGAGAATCTAAGAAAGGAGCTG  483
            ||||||||||||||||||||||||||||||||||||||||||||||||||||||||||||||
Sbjct  270  GAGCATGAGGACCAAGTAACTAGACTTGGTGAGCAGCTAGAGAATCTAAGAAAGGAGCTG  211

Query  484  CGAGTTAGAGAATCTTCACAGAAGCAGCTAAGAGATGAGCTTTTGAAAGTTGAAGGTGAC  543
            ||||||||||||||||||||||||||||||||||||||||||||||||||||||||||||||
Sbjct  210  CGAGTTAGAGAATCTTCACAGAAGCAGCTAAGAGATGAGCTTTTGAAAGTTGAAGGTGAC  151

Query  544  ATTATGCGGGCTGTATCAGTGGTCAAGACCAAGGAGAACTCTGAGGTGCGGAACATGCTA  603
            ||||||||||||||||||||||||||||||||||||||||||||||||||||||||||||||
Sbjct  150  ATTATGCGGGCTGTATCAGTGGTCAAGACCAAGGAGAACTCTGAGGTGCGGAACATGCTA  91

Query  604  AATGAAGATACTCCAAAGAATTCTGAAAGAATCAACAAACTTTTGACGGCTAAAGATGAT  663
            |||||||| ||||||||||||||||||||||||||||||||||||||||||||||||||||
Sbjct  90   AATGAAGATGCTCCAAAGAATTCTGAAAGAATCAACAAACTTTTGACGGCTAAAGATGA-  32

Query  664  GAAATTGCAAGACTGAGA  681
            ||||| ||||||| ||||
Sbjct  31   GAAAT-GCAAGAC-GAGA  16
```

Query_NEAP3delTM, Primer_FN3dCC2a

```
Query  598  ATGCTAAATGAAGATACTCCAAAGAATTCTGAAAGAATCAACAAACTTTTGACGGCTAAA  657
            |||||  ||||  ||||||||||||||||||||||||||||||||||||||||||||||
Sbjct  19   ATGCT-AATG-AGATACTCCAAAGAATTCTGAAAGAATCAACAAACTTTTGACGGCTAAA  76

Query  658  GATGATGAAATTGCAAGACTGAGAGATGAACTGAAGATTATATCGGCTCACTGGAGGTTT  717
            ||  ||||||||||||||||||||||||||||||||||||||||||||||||||||||||
Sbjct  77   GACGATGAAATTGCAAGACTGAGAGATGAACTGAAGATTATATCGGCTCACTGGAGGTTT  136

Query  718  AAGACCAAGGAATTAGAAGATCAGGTGGAGAATCAAAGGAGAATTGATCAGGAGCTGAAG  777
            ||||||||||||||||||||||||||||||||||||||||||||||||||||||||||||
Sbjct  137  AAGACCAAGGAATTAGAAGATCAGGTGGAGAATCAAAGGAGAATTGATCAGGAGCTGAAG  196

Query  778  AAGAAGGTGCTGAAGTTAGAATTTTGCCTACGAGAAACACGCATCCAAACTCGAAAACTT  837
            ||||||||||||||||||||||||||||||||||||||||||||||||||||||||||||
Sbjct  197  AAGAAGGTGCTGAAGTTAGAATTTTGCCTACGAGAAACACGCATCCAAACTCGAAAACTT  256

Query  838  CAAAAGATGGGAGAGCGAAACGATGTGGCAATACAAGAACTCAAGGAGCAATTGGCTGCa  897
            ||||||||||||||||||||||||||||||||||||||||||||||||||||||||||||
Sbjct  257  CAAAAGATGGGAGAGCGAAACGATGTGGCAATACAAGAACTCAAGGAGCAATTGGCTGCA  316

Query  898  aaaaaaCAGCATGAAGCTGATCATTCTAGCAACCAATTTTCTAGGCGT  945
            ||||||||||||||||||||||||||||||||||||||||||||||||
Sbjct  317  AAAAAACAGCATGAAGCTGATCATTCTAGCAACCAATTTTCTAGGCGT  364
```

Conclusion:

Reverse primers starts clean read from bp 4, so start codon is missing: need to repeat with another reverse primer. clean sequencing upto 611. Forward primer reads cleanly from 610bp so only a bp overlap but is un-mutated.